University of Hertfordshire
School of Engineering and Technology

OPTIMISATION AND CHARACTERISATION OF A CURVED BIMETALLIC BLADE AND ITS PERFORMANCE WITHIN A THERMAL MOTOR

GEOFFREY DENNIS ANGEL

A thesis in fulfilment of the requirements of the University of Hertfordshire for the degree of Doctor of Philosophy

The programme of research was carried out in the School of Engineering and Technology, University of Hertfordshire

May 2014

ABSTRACT

In most flat bimetallic strip applications, the bending is employed in the transverse direction, that is, upon the application of uniform heating to the entire strip, the initially straight strip bends transversely up from the flat plane. This study is concerned with a pre-curved bimetallic strip that upon heating up from the ambient, straightens up along the chord line tending to become flatter. The initial ambient radius of curvature of the strip is smaller, and upon heating, the radius of curvature becomes larger. By mounting the curved bimetallic strip with a rotational degree of freedom at each end, and fixing one end against displacement, a chord line displacement of the free end of the strip occurs when the strip is uniformly heated. It is this chord line case that this work investigates and characterises. This work provides a way of evaluating the net combined axial loading case whereby an external load is applied to the free end of the strip as it uniformly heated. The main application of this work is for the characterisation of a curved bimetallic blade within a thermal motor. This is a novel device for converting renewable heat energy into mechanical energy and power as part of a larger energy harvesting network.

The curved bimetallic strip with minor modifications, functions as a curved bimetallic blade within the thermal motor. The application of this work has a wider impact, in that it can be used in any other temperature induced force and displacement applications. Thus as a result of this investigation, a new form of linear actuator has been created that can utilise an input heat differential, and produce an output axial force and displacement. The displacements and forces generated by the axial case can be quite large, and as a result of this work, relatively easy to calculate, when designing a thermally driven linear actuator.

The thermal motor, which possesses the curved bimetallic strip at the heart of its mechanism, can also be powered by other secondary heating sources such exhaust, or waste heat, that would otherwise be lost to the surroundings.

DEDICATION

I would not have been able to complete this project without the unstinting support of my family who have endured my passion for this work over many years, and without their support and selfless understanding, I would never have completed it.
This is for you, Judy, Tammy, Dani, Dylan, and Pippa, who have made this possible.

ACKNOWLEDGEMENTS

The author wishes to thank the following persons who volunteered unconditional help throughout this project.

Dr George Haritos	Principal Project Supervisor
Professor Andreas Chrysanthou	Second Project Supervisor
Mr Ian Campbell	Test support

I have to extend a very special thank you to Miss Anna Kennett for her unstinting support and reading of the document.

This work was only made possible with the guidance and support of Dr George Haritos, Professor Andreas Chrysanthou, who offered their advice and generous cooperation throughout this work.

Thanks must be extended to the School of Engineering and Technology at the University of Hertfordshire for the financial support and research facilities that they afforded me throughout the project.

TABLE OF CONTENTS

LIST OF FIGURES

PAGE

LIST OF TABLES

PAGE

NOMENCLATURE

		UNITS	PAGE
$\alpha_2\ \alpha_1$	Coefficients of linear thermal expansion (CTE) of a material	$\frac{10^{-6}}{\text{K}}$	2
BS	British Standard	-	3
NASA	National Aeronautics and Space Administration	-	5
°C	Celsius degree ; unit of temperature measurement	°C	5
K	Kelvin ; absolute temperature scale	K	7
DIN	Deutsches Institut für Normung eV – German Standard	-	28
ASTM	American Society for Testing and Materials	-	28
k	Flexivity or specific curvature of bimetal	-	34
R_T	Radius of curvature at any temperature T	mm	34
R_0	Radius of curvature at ambient temperature T_O	mm	34
s	Total thickness of the bimetallic strip	mm	34
a	Specific deflection definition	-	35
A	Deflection from flat at the end of the cantilever beam	mm	35
L	Length of the cantilever beam	mm	39
ASME	American Society of Mechanical Engineers	-	37
ρ	Radius of curvature of the bimetallic strip (Timoshenko)	mm	46
m	Ratio of coefficients of thermal expansion (Timoshenko)	mm	46
n	Ratio of Young/s Modulus (Timoshenko)	-	46
h	Total thickness of the bimetallic strip (Timoshenko)	mm	46
T	Temperature above or below ambient (Timoshenko)	K	46
T_O	Temperature at ambient temperature (Timoshenko)	K	46
L_c	Chord length at cold or at ambient temperature	mm	47
R_c	Radius of curvature cold or at ambient temperature	mm	47
L_h	Chord length at hot or above ambient temperature	mm	48
R_h	Radius of curvature hot temperature	mm	48
A_c	Arc length of bimetallic strip cold	mm	48
A_h	Arc length of bimetallic strip hot	mm	48
A_b	Arc length of bimetallic strip	mm	48
θ	Angle of arc subtending chord length	radian	49
L	General chord length	mm	49
R	General radius of curvature	mm	49

ASME	American Society of Mechanical Engineers	-	42
x_d	Unloaded chord or axial displacement of a curved	mm	50
y	Vertical ordinate distance from chord line	mm	51
x	Distance along chord line axis to y ordinate	mm	51
τ	Line at angle β degrees to chord line axis	mm	51
β	Angle between line τ and the chord line axis	radian	51
ω	Angle of arc subtending chord length	radian	51
θ	Angle to y intercept with line τ	radian	51
μ	Portion of arc length to y intercept with line τ	mm	51
δ	Deflection in direction of force *P (or F)*	mm	53
P	Applied force	N	53
$\frac{\partial u}{\partial P'}\ \frac{\partial u}{\partial M}$	Partial derivatives of internal strain energy w.r.t. P & M	-	53
M	Applied bending moment	N mm	53
σ	bending stress	$\frac{N}{mm^2}$	53
y	Distance from the neutral axis to the outer fibres of the material	mm	53
E	Young,s modulus of the material	$\frac{N}{mm^2}$	53
R	Radius of curvature of a beam	mm	53
I	Second moment of area	mm^4	53
ds	Small incremental element along the beam	mm	53
$d\delta$	Small displacement	mm	53
S	Portion of arc length	mm	53
F	Applied force	N	54
ω	Total angle of the entire arc length A_b.	radians	56
E_a	Averaged Young's module of both metals in bimetallic strip	$\frac{N}{mm^2}$	56
F_δ	Force resulting in δ displacement	N	56
F_h	Temperature induced force	N	56
ω_h	Total angle of the entire arc length A_b *above ambient*	radians	56
ω_c	Angle of arc subtending chord length *at ambient*	radian	57
X	Net loaded displacement	mm	58
$x_{\sigma b}$	Safe chord line displacement before reaching elastic limit	mm	60

F_a	Axial load acting along the chord line of a near flat bimetallic strip	N	60
σ	Permissible bending stress specified by manufacturer	$\frac{N}{mm^2}$	60
$R_{\sigma b}$	Stress limited radius of curvature subjected to an axial load and displacement	mm	60
y	Equal to half the thickness of the strip	mm	60
t	Total thickness of bimetallic strip	mm	60
R_d	Radius of curvature as a results of a displacement	mm	61
$L_{\sigma b}$	Safe stress limited chord length from flat strip	mm	61
L_d	Safe stress limited chord length from pre-curved strip	mm	61
R_a	Chord line reaction to force F_a	N	61
R_d	Modified radius of curvature from safe bend radius $R_{\sigma b}$	mm	61
R_e	Stress limited modified radius of curvature larger than R_c from safe bend radius $R_{\sigma b}$	mm	62
$x_{\sigma d}$	Chord line displacement limited by permissible bending stress	mm	63
$\eta_{\sigma b}$	Stress limited angle as a function of $R_{\sigma b}$	radians	63
$h_{\sigma b}$	Internal height at midpoint to stress limited arc of radius $R_{\sigma b}$	mm	63
h_c	Internal height at midpoint of L_c to arc of radius R_c	mm	63
η_b	Internal angle of pre-curved arc to height h_c	radians	63
η_a	General internal angle	radians	63
t_p	Proportionally adjusted thickness of bimetallic strip	mm	64
t_i	Thickness of the Invar 36 side of bimetallic strip	mm	64
t_m	Thickness of the other material side of bimetallic strip	mm	64
E_i	Young's modulus of the Invar 36 metal of the strip	mm	64
E_m	Young's modulus of the other mating metal of the strip	mm	64
E_p	Proportionally expression for combined Young's modulus	$\frac{N}{mm^2}$	64
F_i	Temperature induced internal force developed by strip	N	66
ΔT	Temperature change of the metal from ambient	K or °C	66
C_a	Cross-sectional area of the bar or strip	mm^2	66
ς	Ratio of coefficients of linear thermal expansion	-	68
ϕ	Unity minus the ratio of coefficients of thermal expansion	$\frac{10^{-6}}{\mathrm{K}}$	68

ν	Sum of coefficients of linear thermal expansion	$\frac{10^{-6}}{\mathrm{K}}$	68
CTE	Coefficients of linear thermal expansion	$\frac{10^{-6}}{\mathrm{K}}$	68
φ	Difference of quotients of CTE modifier	-	68
κ	Intermediate quotient ratio of CTE squared modifier	-	68
∇	Intermediate quotient ratio of CTE modifier	-	68
R_{φ}	Modified radius of curvature using φ as the modifier	mm	69
$R_{\kappa.}$	Modified radius of curvature using κ as the modifier	mm	69
Ω	Correction factor multiple of $\varphi\ \kappa$	$\frac{10^{-6}}{\mathrm{K}}$	69
γ	Internal angle of triangle opposite angle ω_h	radians	71
$\varkappa$	Internal angle of triangle opposite angle θ	radians	71
χ	Angle of free hot end of bimetallic strip with original axis	radians	71
R_f	Radius of curvature of free end of strip under combined loading	mm	72
R_b	Radius of bend from flat as a result of applied input force F_a	mm	73
F_n	Normal resolved force applied to free end of bimetallic strip	N	73
f	Point at which the end of bimetallic deflects under load F_a	N	73
R_σ	Maximum radius of curvature from a flat strip limited by stress	mm	74
σ_a	Stress value evaluated as a function of the applied load F_n	$\frac{N}{mm^2}$	74
σ_{bp}	Manufacturer recommended permissible stress value	$\frac{N}{mm^2}$	74
$R_{d\sigma}$	Stress limited radius of curvature from hot free position R_h	mm	74
x_n, y_n	Spatial coordinates of the free end of the strip under combined loads	mm	75
L_f	Chord length as function of radius of curvature R_f	mm	75
h_{dia}	Height at midpoint of chord to arc at full diameter	mm	77
R_{dia}	Radius of full diameter- *half diameter*	mm	77
a, b, c, d	Coefficients in cubic equation	-	78
γ_k, γ_2	Intermediate parameters in cubic equation	-	78
u_1, u_2, u_3	Three cube roots of unity in cubic equation	-	78
L_d	Displaced chord line length as a function of R_v and x_d	mm	78

i	Imaginary root parameter of the cubic equation	-	79
Δ_0, Δ_1	Constants within cubic equation	-	79
R_v	Radius of curvature as a function of distance x_d	mm	80
$f(\Delta T)$	Function of change in temperature	K or °C	81
$f(t)$	Function of time	seconds	81
q	Energy required to raise the temperature in a body with mass	Joules	81
$c_{p,} c_{p1}, c_{p2}$	Specific heat capacity of the material, for metal 1, 2	$\frac{J}{kg\ K}$	81
T_c	Ambient temperature state	K or °C	81
T_h	Heated temperature state	K or °C	81
F_h	Forced convective hot air flow	$\frac{m^3}{sec}$	81
Q	Power consumed to heat up section	Watts	82
k	Thermal conductivity of the material	$\frac{W}{m\ K}$	82
t_b	Depth of the body being heated	mm	82
q_1, q_2	Energy required to heat a material side of a bimetallic strip	Joules	82
A	cross-sectional area of the heat flow through the body	mm^2	82
q_t	Sum of energies of material 1 and material 2	Joules	82
t_{m1}, t_{m2}	Time heat through material 1, material 2	seconds	82
R_t	Radius from flat of a straight bimetallic strip as a function of time	mm	82
v_1, v_2	Volume of metal for material 1, material 2	mm^3	83
w	Width of the bimetallic strip	mm	83
t_{b1}, t_{b2}	Thickness of the material 1, 2 forming the bimetallic strip	mm	84
$\rho_{1,}\ \rho_2$	Density of the material 1, 2 forming the bimetallic strip	$\frac{kg}{mm^3}$	84
m_1, m_2	Mass of material 1, mass of material 2	kg	84
t_t	total time to heat through the bimetallic strip	seconds	84
$\omega_{\sigma b}$	Angle of stress limited arc	radians	87
F_c	Equilibrium force to maintain radius of curvature R_c	N	106
M_d, M_c	Bending moments displaced, and initial radius of curvature	N m (J)	106
F_d	Force to deflect an arc by a distance of x_d	N	107
h_d	Height at mid-span of displaced arc due to load F_d	mm	108
F_{cast}	Castigliano derived quadrant of circle force equation	N	108

F_{cd}	Castigliano derived non-linear force equation	N	108
UH	University of Hertfordshire	-	117
PEEK	Polyether ether ketone	-	121
CNC	Computer Numerical Controlled		137
w	chord length L	mm	140
r'	averaged measures diameter	mm	140
x	vertical height from the flat plate	mm	140
PTFE	Polytetrafluoroethylene		147
$h_{1,}\ h_2$	General ambient state, heated state of height to arc at mid-span	mm	177
θ_1, θ_2	General angle of an arc in ambient, heated states	radians	177
R_1, R_2	General radius of curvature in ambient, heated states	mm	177
η_1, η_2	General internal angle to mid-point of arc in ambient, heated states	radians	177
L_1, L_2	General chord length in ambient, heated states	mm	177
ξ	Angle equal to twice the difference of angle $\eta_1 - \eta_2$	radians	177
ϱ_1, ϱ_2	Line at angle η_1, η_2 to chord line axis	mm	177
ψ_1, ψ_2	Short chord lengths of intersecting arcs of the same length	mm	179
k	ratio of short chord lengths	-	179
β	half the difference of angle (ω -θ)	Radian	180
C_n	Angle between tangent to arc and internal line to mid-span of arc	Radian	183
k_n	Ratio of C_n divided by ΔT	-	183
ε	Ratio of input displacements for finding constants of a parabola	-	186
a, b	Constants of a parabola	-	186
F_1, F_2	Low and high force inputted for finding constants of a parabola	N	187
$x_{1,}x_2$	Low and high displacement for finding constants of a parabola	mm	187
X	New inputted displacement of the parabola	mm	187
F	New output force of the parabola	N	187

CHAPTER 1 Introduction

Summary

This chapter provides the aims and rationale for this work plus an outline of the thesis. The chapter introduces the thermal motor concept.

1.1 Background

With the ever dwindling supplies of easily obtainable fossil fuels, and as the world's demand for energy continues to increase, the cost of extracting and converting the carbon based energy into useable fuels, grows yearly. The aim of this work is to propose a new way of harnessing renewable, sustainable energies, such as solar or geothermal. The world is bombarded with an almost limitless supply of free solar energy according to an online industrial report by a collection of solar energy companies, (Solar Thermal, 2008). To date, solar energy has been exploited in a relatively small way when compared to the astronomical amounts of free radiative energy that our sun emits. According to the report, our sun emits 400 x 10^{24} Joules of energy per second. To increase the harnessing of this free energy, it is incumbent upon mankind to strive to find new alternative methods of translating that freely available solar energy into useable power.

This investigation shows how existing bimetallic strip technology can be used to produce usable power from any heat source. Additionally, the scope of this work provides new knowledge that can be applied to other applications such as heat activated linear actuators and heat driven timing mechanisms. The bimetallic strip is a thermal mechanical device that is composed of two metals of differing coefficients of linear thermal expansion denoted here by α_1 & α_2. The two metals are intimately and permanently joined together at a common material interface, see Fig.1-1a. Upon the uniform application of a heat differential along the entire length of the strip, in this case, an increase in temperature from the ambient, the bimetallic strip will bend from the initially flat state to the curved state shown in Fig.1-1b. The curvature will remain for as long as the heat differential to the strip is applied. Upon removal of the heat, the strip will recover to its initial flat state, Fig.1-1a. If material side 1 has a coefficient of linear thermal expansion denoted by α_1, which is numerically higher than that of material side 2, then the bending will occur in the direction shown in Fig.1-1b.

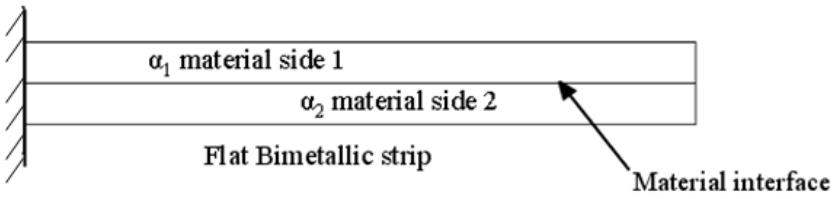

Fig. 1-1a

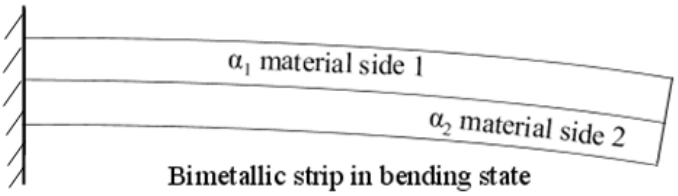

Fig. 1-1b

Fig.1-1 Flat and curved bimetallic strip edge view

Bimetallic strip is traditionally and primarily used as part of a sensing unit, whereby the heat differential from a set temperature point is used as a trigger to initiate or close an electrical circuit, or mechanically to open or close a valve. Such a sensor configuration is shown by a patent by Fraisse (1998), and one of the most common applications of the bimetallic strip, is as a failsafe sensor in the domestic central heating boiler which is generally covered by BS EN 14597, (2012).

In this application see Fig.1-2, the bimetallic strip is permanently being heated by the pilot flame of the boiler. If the pilot flame of the boiler was to extinguish for any reason, the heat differential would be removed from the bimetallic strip and it would bend back to a preheated state. The pre-heated state closes the pilot gas supply valve. This fail to safe mechanism prevents further flow of gas to the exit pilot. In this specific application, the material side with the larger coefficient of linear thermal expansion lies on the outside of the "U" shaped bimetallic strip. In normal operating mode the "U" shaped bimetallic strip bends inwards and pushes down against the spring, thus opening the valve from its seat and allowing the gas to flow. If the heat is removed from the "U "shaped strip, the downward force is removed, and the spring lifts the valve against its valve seat, thus closing the gas supply to an unlit pilot.

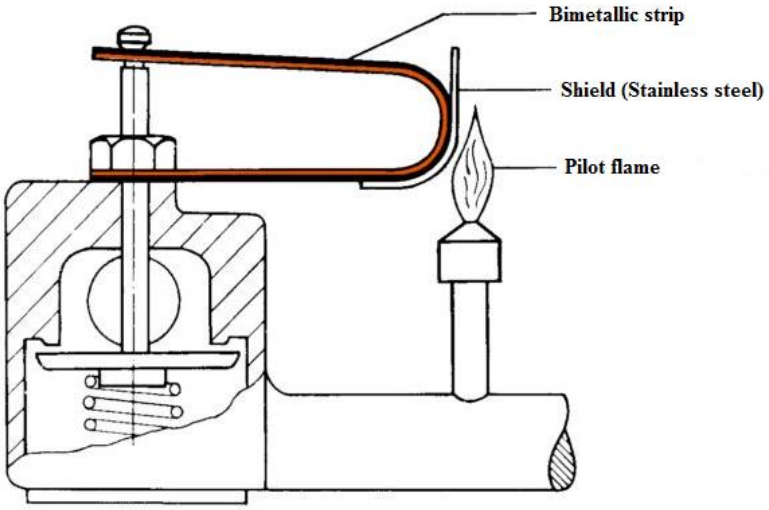

Fig.1-2 Reproduced with kind permission (Kanthal, 2002)

A bimetallic strip room sensor is used in central heating systems to regulate the temperature of the room. Other well-known applications include flasher indicator units for cars, thermometers, domestic household kettles and water boiler units. Bimetallic strip is used as general thermal trip sensor in a multitude of applications acting as a safe guard to prevent the overheating of a component within a system.

This project investigates the use of a bimetallic strip as the major component in a novel application, the thermal motor, an invention of the author, Angel (2013).

In this application, the bending qualities of the bimetallic strip are used to produce an axial force and displacement when the curved strip is mechanically mounted with a rotational degree of freedom at each end; this is referred to as the chord line, or axial case. When simply supported in a manner as shown in Fig.1.3, with one end of the strip fixed against linear displacement, then a chord line displacement of the free end can be obtained. Fig.1-3 shows the pre-curved bimetallic strip mounted in a chord line axial orientation for potential force generation and displacement. Upon heating the bimetallic strip, the chord line force and displacement can then be converted into rotary motion and power within a thermal motor.

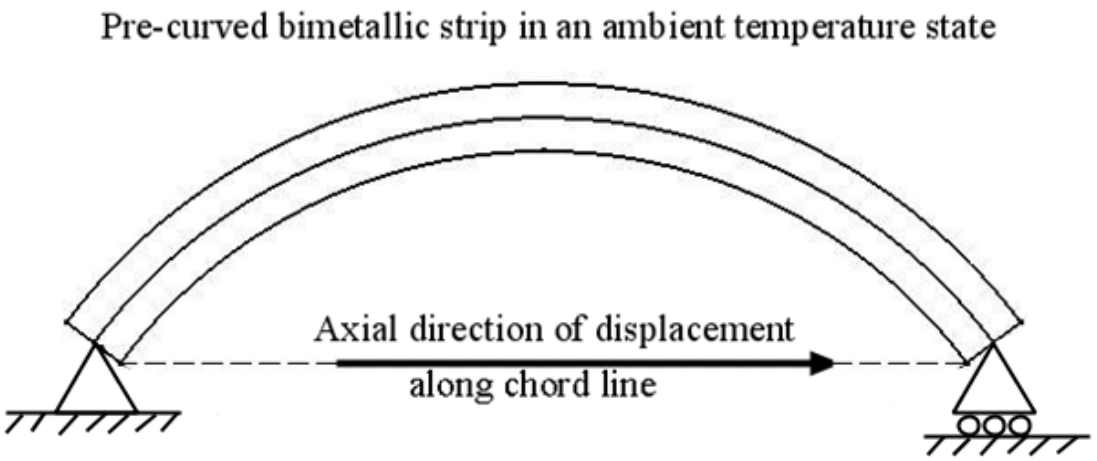

Fig.1-3 Mounting of simply supported curved bimetallic strip "axial case"

If the primary power for driving the bimetallic "blade" within the motor comes from a renewable energy source such as solar or geothermal or waste exhaust heat, then the thermal motor can provide an alternative energy converter that does not rely on dwindling carbon based fuel supplies. For certain applications and environments, the thermal motor can provide a clean, non-polluting alternative energy harvesting machine. For places or remote regions where harsh conditions exist, the thermal motor could be used as a power generator. A major application of the thermal motor is to generate power in space. In the space environment, all fuel to power spacecraft, space stations and satellites must be brought at great cost from Earth. A thermal motor driven by bimetallic strip blades, could produce an endless, "fuel -less", power supply simply by presenting the blades to direct sunlight or shade. In low earth orbit space, a temperature difference of up to 135 °C (NASA, 2012) can exist between an object in direct sunlight and shade. Some bare metals can reach temperatures above 260°C when exposed to direct sunlight. Thus the potential for driving the thermal motor in a space application is high, when considering the naturally occurring high temperature differences that can be obtained.

The rationale for this investigation therefore stems from the application of the pre-curved bimetallic strip within the thermal motor device. As part of the development of the thermal motor, the curved bimetallic strip functions as the major component. This work sets out to identify, mathematically model and measure the parameters of the pre-curved bimetallic strip when applied in an axial loading case already described by Fig.1-3. The main thrust of this work will therefore concentrate on the characterisation of the

pre-curved bimetallic strip, and the thermal motor is included in this work as the main driving force for the investigation.

1.2 Aims and Objectives of this Research

Aim 1: to characterise the behaviour of a pre-curved bimetallic strip that is configured and mounted so that it can be displaced along the chord displacement axis as shown in Fig.1.4.

Aim 2: to derive the load vs. displacement vs. temperature relationships of the pre-curved bimetallic strip that is subjected to a combination of heating and external loading.

Objectives: to undertake a series of experiments that will enable a better understanding of the relationships of objectives 1 to 5.

Objective 1: Load vs. Displacement.

Objective 2: Temperature vs. Displacement.

Objective 3: Load vs. Temperature.

Objective 4: Spatial Position End Point Position.

Objective 5: Time vs. Displacement.

Objective 6: Produce theoretical derivations to predict the objectives 1 to 5.

Objective 7: Run a series of experimental tests to meet the objectives 1 to 5.

Objective 8: Comparison of theoretical derivations to experimental test data.

Objective 9: Development of a thermal motor prototype.

Objective 10: Produce new geometric arc related relationships and formulae.

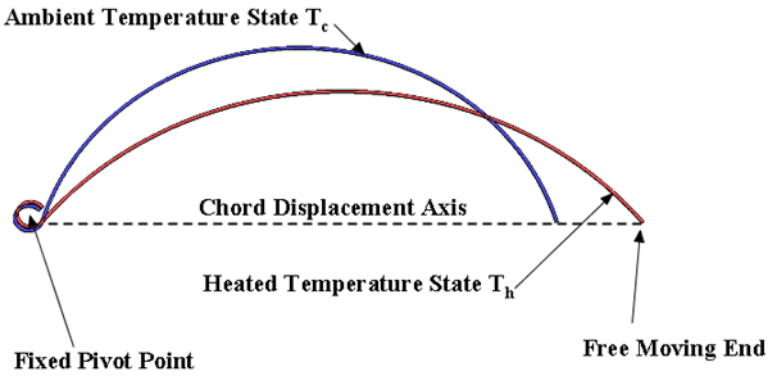

Fig.1-4 Pre-curved bimetallic blade in ambient and heated states.

1.3 Thermal Motor – Rationale for this Research

The thermal motor is not a new invention; there are many patents for devices that are powered by a heat differential that utilise the bimetallic strip as the means for converting a heat energy source into mechanical power O'Hare (1985) and Sandoval (1977) have both submitted patents for thermal engines that are powered by bimetallic strip. There are also patents for thermal motors or thermal engines that use a heated media or fluid, as a means of converting heat energy into mechanical movement and power. The Sterling engine is one such device that converts a heated fluid into mechanical movement and power. This device was invented by the Reverend Dr Robert Stirling in 1816. The Sterling engine can also work as a cryogenic cooler when used in reverse. When used as a cooler the Sterling engine is supplied by mechanical power and the internal working fluid, pure Helium, is pumped from the hot end to the cold end and back, thereby extracting heat. The sterling engine when used as a cooler can reach extremely low temperatures in the region of 80K Riabzev (2002).

Churchill (1968), patented a device that uses the expansion of a heated fluid that exerts pressure on an internal piston to develop displacement and power. Many patents are for devices or contraptions that are quite complex in their nature, and are elaborate machines that comprise of many components parts. The patent application by Slonneger (1970) is for a complex thermal motor device with many components. In the thermal motor proposed here, there is just one moving component which is the rotational output shaft. The original idea and brief, was to make a device that would convert a heat differential into mechanical movement in the most direct and simplest way, with the minimum of complexity and components parts. This was the most important requirement of the thermal motor design concept.

The pre-curved bimetallic strip that this work investigates, when used in an axial chord line orientation, affords the thermal motor with a simple force generator mechanism. Furthermore, the simplicity of the pre-curved bimetallic strip also enables a flexible motor configuration from a conceptual design viewpoint, allowing the thermal motor design to be tailored to the individual end application. Two thermal motor prototypes were developed to be used as a test bed for further bimetallic blade characterisation.

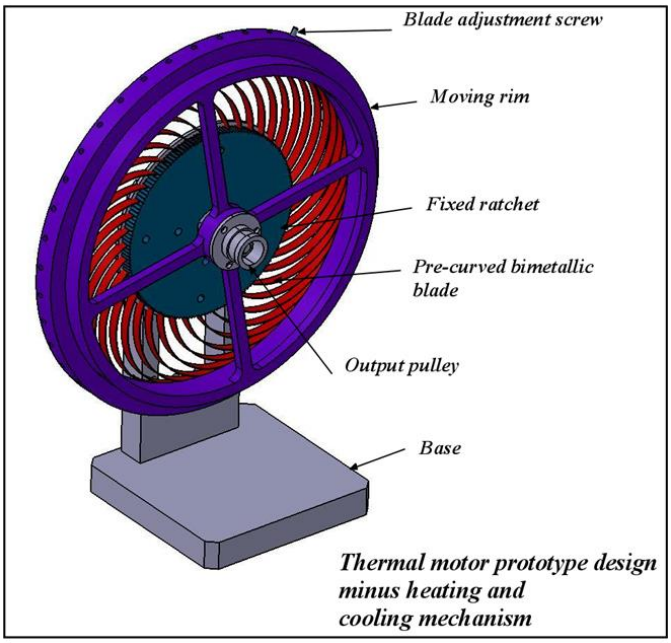

Fig.1-5 Thermal motor Mark I prototype as designed

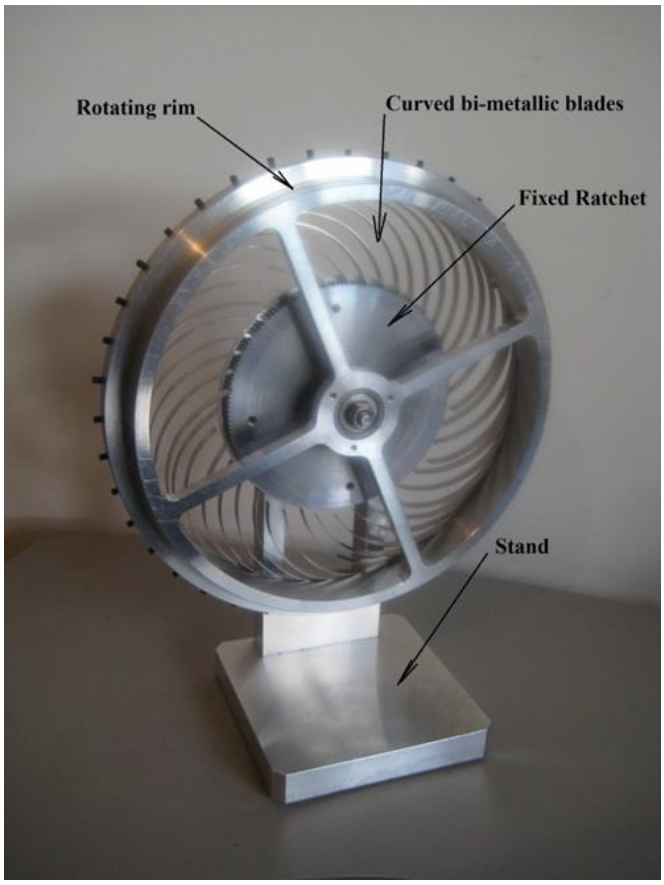

Fig.1-6 Thermal motor, Mark I prototype as realised

Fig.1-5 shows the Mark I thermal motor as designed and Fig.1-6 shows the motor as it was made for part of this study. The motor works on the simple principle of action and reaction of the pre-curved bimetallic blades. Each blade at one end is freely pivoted on

the moving/rotating rim, and the other end lies within the ratchet teeth on the fixed central ratchet. As the pre-curved bimetallic blade is heated, it straightens up along its chord line due to the rotational freedom of each end of the strip. As a consequence of the straightening action, one end of the strip catches in the teeth of fixed ratchet. The other end of the strip forces an angular displacement of the rotating rim. An output pulley attaches to the rotating rim by the three central screw holes in the rim as shown in Fig.1-5. Fig. 1-7 depicts the detail of a single pre-curved bimetallic blade within the thermal motor whereby the rest of the blades have been removed for clarity.

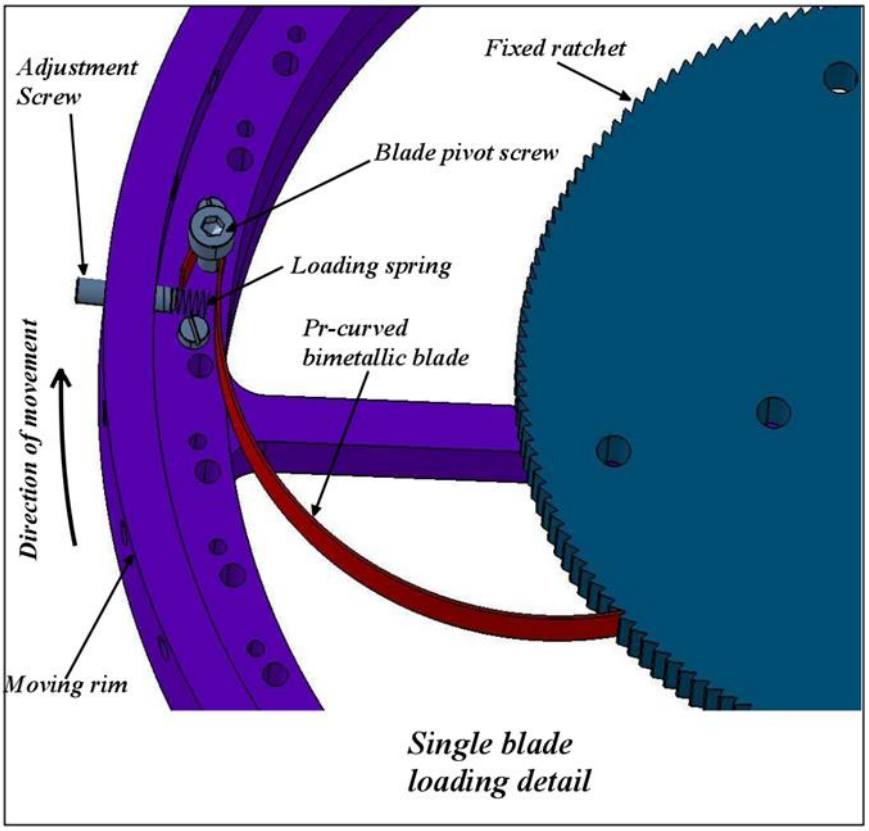

Fig.1-7 Bimetallic blade mounting within the thermal motor

The simple Mark I mechanism requires a heating and cooling cycle to allow each bimetallic blade in turn to expand, do work and recover when cooled. In the Mark I prototype as shown in Fig.1-6, and as detailed in Fig.1-7, there was no means to enable cyclic heating and cooling. An additional heating and cooling mechanism was added to the Mark I thermal motor to enable the cyclic heating and cooling of the bimetallic blades. Fig.1-8 shows the Mark I thermal motor with the additional heating and cooling mechanism attached. The flexibility of the thermal motor concept has been confirmed by comparison of the single to a six-stack prototype. The stack refers to the number of rows of bimetallic blades within a thermal motor. The Mark I prototype has only one

stack of blades, the Mark II has six stacks, or six rows of blades. In the Mark I prototype of Fig.1-6, the outer rim is the output shaft that rotates, contrasting with the six-stack Mark II prototype in Fig.1-9 whereby the outer rim is a fixed internal ratchet, and the central shaft is the component that rotates. Fig.1-8 depicts the Mark I thermal motor which operates by using an externally driven heating and cooling mechanism

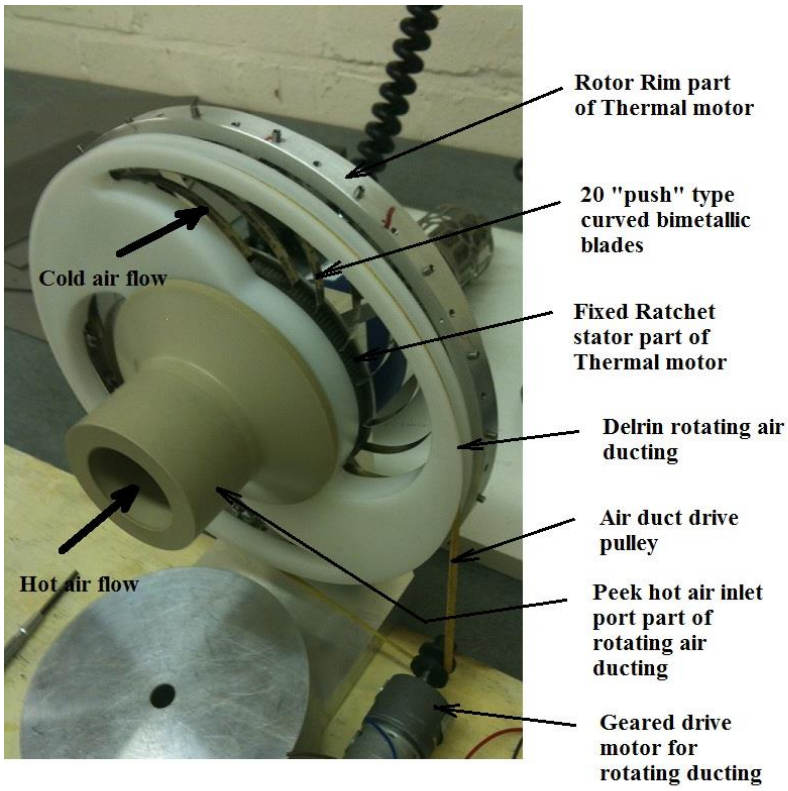

Fig.1-8 Mark I thermal motor with a heating & cooling mechanism.

Although continuous rotation was achieved by this additional mechanism, the original simplicity of the thermal motor was heavily compromised. To maintain the philosophy and ideal of a simple design, the six-stack prototype thermal motor was developed. The six-stack thermal motor Mark II achieves continuity of motion by the “built in” heating and cooling cycle that relies on a staggered blade overlap system. The staggered overlap concept requires that the all bimetallic blades are attached to the central rotor that is the moving part, see Fig.1-9, Fig.1-10 and Fig.1-11. This ensures that all the blades ”self-drive”, or move in and out of the fixed internal heating and cooling zones. This concept was realised in a Mark II prototype thermal motor that included six stacks of nine blades. As a single blade enters the fixed heating zone, blades from other stacks are brought into the heating zone by virtue of being attached to same central rotor.

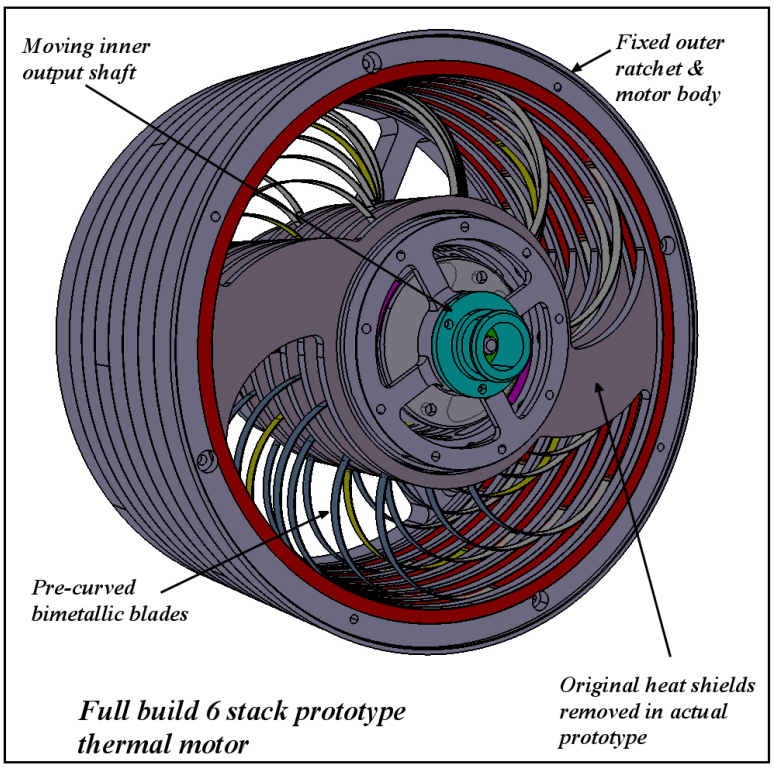

Fig.1-9 6-stack thermal motor design with heat shields

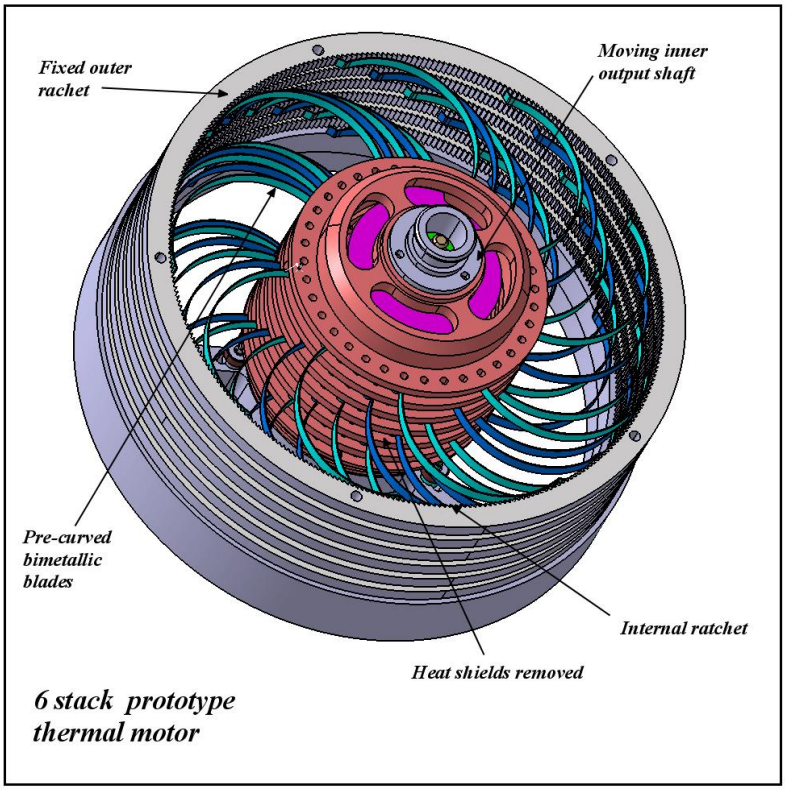

Fig.1-10 6-stack thermal motor design without heat shields

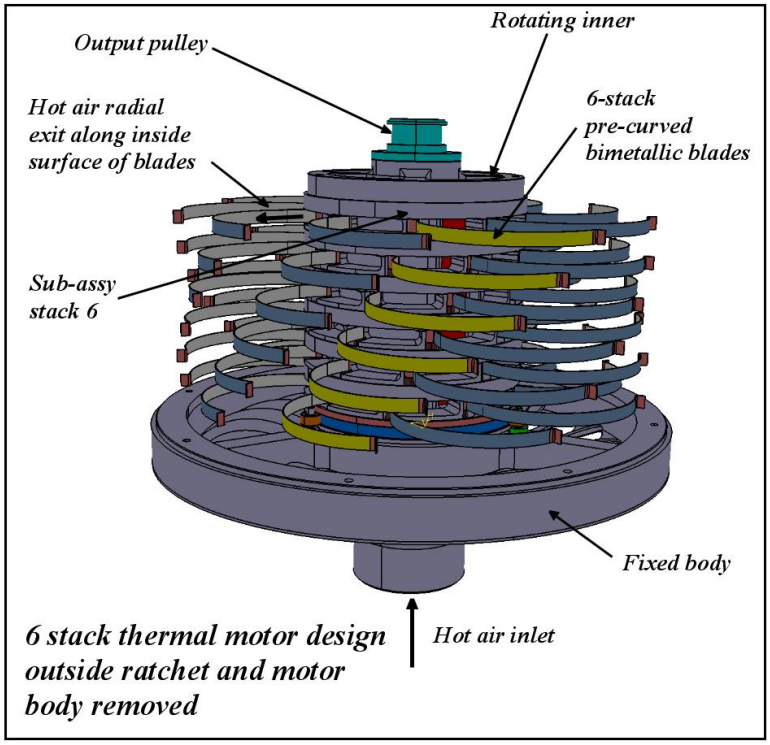

Fig.1-11 6-stack thermal motor design with outer fixed ratchets removed

The 6-stack thermal motor design works on the same principle as the Mark I design, except for the way the blades are heated and cooled. In the 6-stack design, hot air is pumped into the central rotating chamber to exit radially along the inside of the blades in two fixed heating zones. As the air exits along the inside of the blade, the blade changes shape and as before, the straightening effect is translated into chord line movement resulting in an angular rotation of the central rotor assembly. Fig.1-9 and Fig.1-10 depict the 6-stack thermal motor design with and without heat shields respectively. The heat shields were removed in the physical prototype due to the clashing of the blades against the shields. Although the heat shields were removed in the build, the role of the heated shield remains valid. The heat shields enable the containment of the heat during the heating part of the cycle. Fig. 1-11 shows the 6-stack thermal motor design with the external fixed ratchets removed for clarity.

In the realised Mark II 6-stack prototype, a rotational movement of the central rotor was achieved without an additional heating and cooling mechanism. In the first test of the Mark II prototype, the motor when heated, accelerated from a stationary position. The rotor maintained a 1° / sec unloaded steady state rotational speed at an average 200°C change in temperature from an average ambient temperature of 23°C. Forced cooling air was pumped axially across all the radial blades outside of the two fixed heating zones.

During one of the early performance tests, a thermal runaway occurred in the central rotating shaft causing the motor to stall and permanent damage was sustained to the internal components. From the post strip-down analysis, the Peek rotor component had melted which suggests that the thermal runaway had peaked at over 500℃ as a minimum. As part of a future work, the 6-stack motor concept could be successfully realised if the heating and cooling directions were reversed; i.e. cooling air is pumped into the central rotating component , and the heating of the blades is confined to the gap between the rotor and the fixed outer ratchet. If the change in applied heating is adopted then it is possible to eliminate the internal thermal runaway experienced in the Mark II prototype.

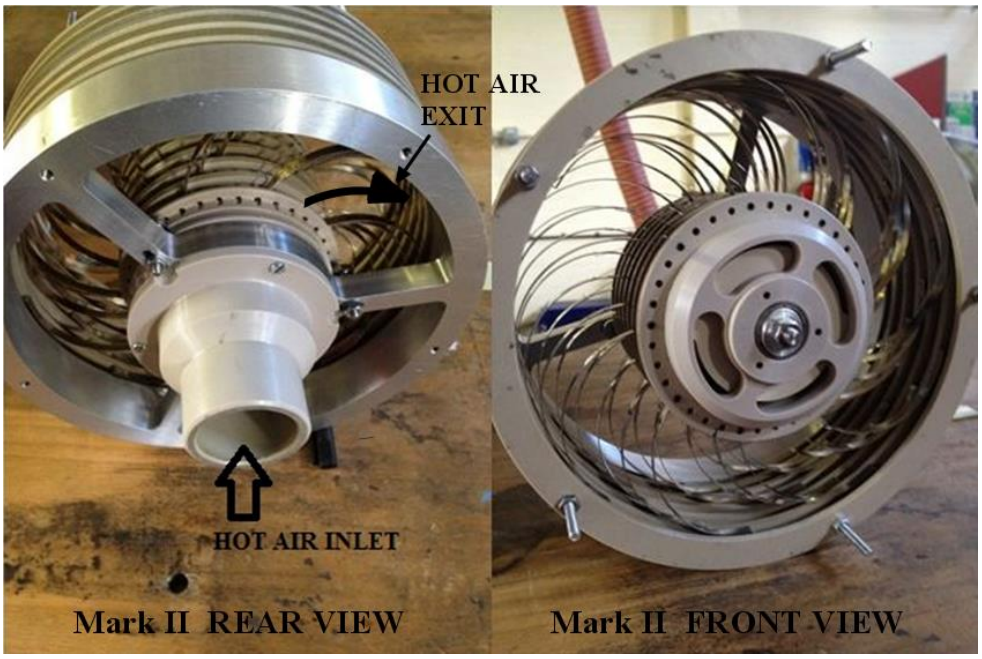

Fig.1-12(a) Mark II rear view Fig.1-12(b) Mark II front view

Fig.1-12a and Fig.1.12b depicts the rear and front view of the Mark II thermal motor respectively. The Mark II thermal motor is a direct application for the work presented here. However, the characterisation of the curved bimetallic strip in the chord line, or axial case is the main thrust of this investigation, and not a treatise of the thermal motor. The thermal motor is a research project in its own right that is being developed at the Sustainable Energy Technologies Centre at the University of Hertfordshire. Mark I and Mark II thermal motor technical drawings are shown in the Appendices.

1.4 Outline of the Thesis

The thesis is set out to address the aims and objectives as described in section 1.2. To achieve those aims and objectives the thesis is set out as follows:

Chapter 2 provides a literary review as part of the background knowledge. The literary review looks at the historical and modern methods of fabricating bimetal components through the ages and reviews the current standards, theory, and methods of manufacture of modern bimetallic strip.

Chapter 3 provides an investigation into the underlying theory required to characterise and optimise a pre-curved bimetallic strip. The characterisation and optimisation of the bimetallic strip is achieved by the application and modification of both Timoshenko and Castigliano formulae.

Chapter 4
Provides verification of formulae by simulation and calculated comparison methods.
This chapter provides correlation to theory for simulated data.

Chapter 5 sets out the test equipment, test set up and methods used to generate test data for the validation of the theory as described in chapter 3. As part of the validation process, the methods of manufacture of the test samples are included. An overall test regime is introduced that covers both bespoke and fabricated bimetallic test samples.

Chapter 6 presents the results of the performance of the bimetallic strip test samples. The tests are performed for the validation process of the theory as highlighted in chapter 3. The test results and the theory are displayed in graphical form with 5% error bars as a means to evaluate the correlation between the test data and the theory.

Chapter 7 provides the new knowledge introduced by this investigation. New geometric relationships and formulae concerned with arcs of circles are presented.
Discussions and concludes the body of work and provides suggestions for future work.

CHAPTER 2 Literature Review

Summary

This chapter provides a comprehensive literature review of the area of bimetallic strip history and production techniques. The review covers the technology development of the bimetallic strip and its applications.

2.1 Aim of the Literature Review

The object of this review was to examine prior work in the field of energy generation by bimetallic strip technology, and to specifically analyse and compare similar work pertaining to the current investigation: *pre-curved bimetallic strip that is mounted and configured to produce a chord line axial force and displacement*. The review investigates existing devices that have been patented and produce a linear displacement as a function of a heat differential. As part of the review, bimetal technologies past and present are reviewed. The review contrasts the different technologies and includes and discusses the historical viewpoint, metal joining technologies, technical standards, theory of bimetallic strip and force displacement mechanisms.

2.2 Historical Viewpoint

Many of the ancient civilisations became masters of forging and smelting iron ores into useful implements. Spurred on by the need to protect their own nations or the desire to conquer neighbouring nations, the search for stronger metals and thus weapons, was the driving force for ancient alchemists to experiment in the "black" art of metal making. As time progressed, and the techniques of manufacture were refined, iron swords became steel swords and further embellishments were found by secondary casting methods.

Secondary casting is the very old process of casting around or over an existing metal object to produce a bimetallic artefact that combines the best structural qualities of the original object, plus the benefits of the secondary cast material. The reason for the casting process was to imbue a single metal structure with a second metal that enhances the original metal's properties. The secondary casting process was also used to embellish the original object. A report by Aftandilyants (2007) on the classification of modern techniques of bimetallic casting, outlines the traditional methods used to produce bimetallic components and artefacts thousands of years ago. These ancient techniques are still very much in demand as modern manufacturing processes of bimetallic engineered components.

In this report, the two main methods of secondary casting are contrasted. According to Aftandilyants, there are two distinct mechanisms to produce a bimetallic component by secondary casting. One method is by the successive casting of molten metals into a mould by the mechanism of separate pouring gates. The second method is to cast the

liquid metal onto or around a solid blank, or billet, that is already loaded into the mould. The report is a snapshot or overview of the secondary casting processes and is only intended as such.

An archaeological find in China by Chen et al. (2009) revealed some early samples of bimetallic implements. At around 800 BC, artefacts such as swords with iron blades were found to be secondary cast with bronze, silver and gold handles. The paper, which reports the finding of the bronze-iron bimetallic objects in the Liangdaician M27 archaeological dig site in China, provides a rich insight into the iron casting techniques that were mastered by the ancient Chinese. The report Chen et al. (2009) delves into the scientific analysis of the artefacts, and via carbon dating techniques, were able to ascertain with reasonable certainty, the chemical make-up and age of the objects. The rigour applied to the analysis techniques and the resulting data, yield conclusive proof of one of the earliest bimetallic finds and the state of the art of metal production techniques at that historic point in time.

In addition to the Chinese, other civilisations were manufacturing multi-layered swords by the hot forging of separate layers of both brittle and tough steel during the forge weld process. This process produced a laminated cross structure which was significantly more robust and tougher than a blade forged out of a single homogenous material. One such steel that is discussed by Uhlig (2007) was called Damascene steel, this steel was layered, twisted, and hot forge welded. However according to Brown (2012) in his short online article, there was a distinct difference between what is known as Damascene steel and Damascus steel.

Brown states that "*Damascus steel is not to be confused with damascene, which is a process of inlaying gold leaf onto the surface of steel for the purpose of decoration".* This seems to contradict with Uhlig's findings. However, Sherby and Wadsworth (2001), seem to agree with Uhlig, stating that on Damascus swords, the" *pattern is achieved by a complex forging procedure".* The paper by Sherby and Wadsworth (2001) is a more in depth treatise of ancient sword making, and provides a greater insight to the hot forging weld techniques of very early composite metal production.

Additionally in the Far East, the Japanese throughout the last millennium have been famous for the production of the Samurai steel sword edge, which again, is formed by folding layers of semi-molten steel over and over sometimes the number of folds can

reach several hundred. The process of folded steel resulted in a laminated forge welded structure that was extremely tough against shock, and possessed a hard, patterned surface structure as well. Samurai blades, due to the method of manufacture, have exhibited the keenest edges of any sword blade.

A report by Bluhm (1946), provides an in-depth analysis into the structural properties of a particular Japanese Samurai sword just after world war two. The conclusions from a forensic review of the material properties, via various testing techniques such as Brinel indentation tests and Rockwell hardness tests Freudenberger (2009), chemical analysis, and microscopic microstructural analysis, yielded poor results. The findings of the Bluhm report are less than enthusiastic and favourable with respect to the actual structural properties of the Japanese blade.

It should be noted that Bluhm had only tested a single blade and thus was at a disadvantage when considering an important aspect of the Samurai steel blade, and that is, that each Samurai blade is uniquely manufactured. The structural properties of Samurai steel are heavily influenced by the methods of production, material composition and techniques used to manually forged the blade. Henceforth, no two Samurai swords would necessarily yield the same structural properties. Japanese master sword makers have always used their own individual methods of manufacture that have been handed down over the centuries and contain closely guarded secret techniques. Therefore, another sword could have provided a different set of structural results, possibly more favourable from a structural viewpoint. In support of the variation of Japanese sword characteristics, there is a brief example of how the variations in Japanese sword steels were obtained. According to the online article by Davistown (2013), reference is made to "Yaki-ire" which is the rapid cooling of the blade after heating to the critical temperature of 723°C. The reference then states that,"*In the case of Japanese sword production, the thickness of the clay enclosure covering the steel sword during the quenching process determined the cooling rate and thus the microstructure of the steel sword".*

The article by Davistown further discusses "Yaki-modoshi" which is the further heat treatment of the hard sword blades by tempering and further re-quenching to relieve internal stresses, it goes on to state that "*Sword edges covered by a thin layer of clay cooled more quickly and were thus harder than the softer and more flexible sword bodies*.". Both the methods employed in the forensic analysis of the blade by (Bluhm,

1946) and the techniques and rigour shown by the archaeological objects that were analysed in the report of Chen et al. (2009) were shown to be comparable and thorough, using the same basic scientific techniques. It is interesting to note the timing of the Bluhm report, for the analysis of the Samurai blade, took place just one year after the end of world war two. As the war with Japan came to a close in 1945, the American army captured many Japanese weapons. The Samurai sword was a feared close combat weapon due to its keen edge. The report by Bluhm was commissioned by the Ordinance Department of the USA which provided the evaluation of the Samurai blade from a technical viewpoint. It is possible to infer that the report by Bluhm, was for reasons far more immediate, than the archaeological report by Chen that was reviewing ancient implements. The Samurai sword manufacturing methods of hot forging and controlled quenching followed by tempering were techniques that were copied and refined by the manufacturers of modern bimetallic strip.

The origins of what is considered to be the first "modern" functional bimetallic strip application goes back to the late seventeenth century when John Harrison, Sobel (1995), is credited with inventing the bimetallic strip in or around 1759. This was the first bimetallic strip that utilised the bending characteristics of a bimetal as a function of temperature change. Harrison an English, self-taught carpenter and later clockmaker, invented the bimetallic strip to act as a temperature and humidity compensation mechanism in his H3 Marine chronometer that calculates longitude at sea. Harrison found that to achieve the time accuracy required for a marine clock, he needed a mechanism that could compensate for the changes in length of the balance spring that was occurring due to changing humidity and temperature. Harrison had surmised that just a minute out, time wise, could mean in longitude terms, that the ship's navigator could miss the ship's destination by hundreds of miles. Harrison's first bimetallic strip was made out of two metals that were mechanically fastened together by rivets. Harrison, in addition to inventing the first fabricated bimetallic strip, for his last time piece the H5, had perfected a way of joining brass onto a steel substrate, by directly fusing the molten brass onto the steel. This was the method that was subsequently adopted by clockmakers and early bimetallic strip thermometers from then on. As a consequence of Harrison's invention of the bimetallic strip, one of the earliest bimetallic strip temperature sensor thermometers was manufactured. An original sample of this thermometer that was reviewed by Holbrook and can be found as one of the engineering and science exhibits in the Hunterian Museum, Holbrook (1992). This very early

thermometer, according to the information supplied, was manufactured by James Crichton circa 1804 of Charlotte Street, Glasgow, Scotland. However, the design for this very early device, according to the information supplied by the Holbrook, dates the thermometer design to David Rittenhouse in 1767 of Philadephia, United States of America.

The Hunterian Museum thermometer was a domestic Fahrenheit thermometer which posessed a scale ranging from -10 °F to 100°F (-23.3°C to 37.7°C). According to the data supplied by Hunterian Museum, the thermometer was a lower temperature version of a type already invented by Crichton in 1803. The Critchton thermometer was "*designed to measure the freezing points of lead tin alloys*". The bimetallic mechanism comprised of a brass-steel bimetallic strip, attached directly to a pointer/ hand which was pivoted at its lower end. Additionally, as a means of recording the maximum and minimum temperatures experienced by the device, two wire indicators that were attached to the same pivot point as the main indicating hand, were free to move and record the extremes of temperature. This device was most likely the earliest application of a bimetallic strip used to differentiate temperatures, and thus a most important device in the history of, and development of bimetallic technology.

Harrison's bimetallic compensation idea was carried through to the 19th century design of clocks, and was adopted by American clockmakers and watchmakers who used a "*temperature compensating bimetallic balance with timing poising screws*" in a clock movement mechanism that was described as being both complex and precise. A paper by Hoke (1989), reviewed the design of 19th century products. Hoke reviewed the technological developments of that time that focussed on design and manufacture of three traditional products, wooden movement clocks, watches and typewriters. Hoke looked into specific products and reviewed the case studies from a design, cost, and manufacturing viewpoint. There was a desire of the 19th century engineers to design in adjustment to the complex mechanisms where possible, since as was stated in the article, *"watches were routinely adjusted as an integral part of their manufacture"*. As a historical reference to the inclusion of the Harrison bimetallic compensation mechanism in a clock application, Hoke covers this detail well, and gives a detailed insight into the design for manufacture techniques that were gaining ground during this evolutionary engineering period.

One of the many modern day applications of Harrisons historic bimetallic strip invention is found in a medical apparatus for the administration of anaesthetic vapours to patients. According to an article by Mclaren (1994), "*in nearly all modem temperature-compensated vaporisers a bimetallic strip is used to regulate the gas flow into the vaporising chamber".* Additionally, Mclaren gives an in depth history of Harrison and his lifelong trials and tribulations in developing his marine clocks, and how eventually he was financially rewarded and honoured for his life's work. Harrison's invention of the bimetallic strip is contributing to saving lives in ways that could never have dreamed of.

2.3 Modern Metal Joining Technology

With the introduction of practical electricity to the masses in the late 19th century, a rapid requirement for electrical engineering equipment arose over a very short time. With domestic demands for the conveying of, and controlling of the electrical appliances, the mechanisms to govern the many uses of electricity lagged behind the variety of newly invented electrical applications. Electrically heated rooms were temperature controlled by the first practical use of a bimetallic strip to control an electrical switch. The first practical thermostatic device to control the temperature of an electrically heated room was invented by Johnson (1883). Johnson's patented device used a delicately coiled bimetallic strip to push a finely balance switch to either make or break an electrical contact depending on the bimetallic disposition about a neutral balance point. The sensitively of the device, and thus the room temperature, could be adjusted by increasing or decreasing the sensitively of the bimetallic coil. From the turn of the 20th century to the 1940's there is very little recorded information on the wholesale bimetal production methods used during this period. It is reasonable to assume that the methods that were tried and tested since Harrison, included fabrication using rivets, hot forge welding, secondary casting, fusion, or brazing. However according to Howard (1942), the state of the art in producing bimetallic strip was by "*into a large bar which is subsequently hot and cold rolled to sheet. Most bimetal depends on final cold rolling to finish size for its physical properties."* At some point during the late 1800's to the early 1940's, hot rolling followed by cold rolling was introduced and established as the method to manufacture bimetallic strip.

As the need for more sensing and controlling of electrical devices increased, attention again focussed on the properties of the bimetallic strip and ways to economically

manufacture bimetallic strip on an industrial scale. An early patent for the method of manufacturing of bimetallic sheet and strip was granted to Goulding (1947), for the hot rolling method and welding method of joining two separate metals and forming them into a single bimetallic sheet. For the hot rolling process, Goulding's patent describes the process of manufacture in general terms, providing a detailed sequence of the process starting with, as the patent refers to it "*a slab*" of metal, which is placed on a similar "*slab*" of metal, and both are heated until the they become plastic enough to be welded together. According to the process, the assembled "*slab*" of metal is then passed through "*pressure rolls*" which exert huge shape changing forces on the now conjoined metals. The process of heating and rolling the initially assembled slab dramatically reduces the cross-sectional thickness of the original slab, and at the same time the initial slab's width and length have increased by the same degree. The process is repeated until the desired thickness or gauge of sheet is obtained. The detail of the patent then describes the finishing operations such as the surface cleaning of the faces of the bimetallic sheet, grinding of the surfaces and edges to render the sheets smooth and burr free. The final process of manufacture described in the patent involves cleaning of the bimetallic strip by a "pickling" process and the subsequent washing off of the pickling material. For the process of joining the "*slabs*" of metal using the welding method, as opposed to the hot or pressure rolling, Goulding describes containing the slabs within a special box that allows for lengthwise extension. The walls of the box are insulated to prevent the edges of the slabs welding to the box. The whole assembly is both heated and then passed through the rolling mills. The box serves to hermetically seal the slabs during the weld process. This process is more complex and drawn out than the hot rolling process also as described by Goulding.

The "*pressure roll*" or hot rolling process was adopted universally by the late 1940's as the main method of manufacturing bimetallic strip and is still used today in many mainstream bimetallic strip producing companies. However, the process has been refined since 1947 and all hot rolling processes of bimetallic strip, or material production in general, are normally followed by a sequence of stress relieving annealing cycles.

As the applications and requirements for specific bimetallic strip diversified, research into tailored bending characteristics of bimetallic strip was undertaken and a patent was granted to Aisaka (1980) for a specific bimetal composition and make up. Aisaka's

invention was to provide a novel bimetallic composition that was attributed to having a high rapid deflection rate over a specified temperature range. Aisaka's patent and its included research, was for an overhung cantilever beam that possessed a quicker rate of curvature change due to the above-average iron-manganese composition with the manganese constituting between 15 to 30% by weight.

The patent by Goulding refers to the "*bimetallic samples… thermal forged into thick plates….were bonded together by rolling at a temperature of 900°C to 950°C",* Aisaka's patent further describes that subsequent to hot rolling, the samples were "*further subjected to cold rolling"* and then*"annealing was repeated at 1050°C"*. The cycle of cold rolling and then annealing was repeated until the desired sample thickness was achieved. Additionally Aisaka's patent details the nescessity for the annealing process to "*eliminate accumulated work strains"*. According to the patent claims, the elimination of the work induced strains, suppresses the production of the "*harmful (a' phase)*", which is responsible for preventing the rapid change in the thermal expansion of bimetallic strip, over the specified temperature range. Although not fully explained in Aisaka's patent, the harmful (a' phase**) ,** refers to the alpha iron phase, which according to Dossett (2006), in pure iron exists at or below 910°C. The particular metal structure obtained by the Aisaka's research has been tailored via the specific proportions of alloying elements e.g. Manganese, Chromium, Cobalt in varying amounts to achieve the higher coefficient of thermal expansion of the bimetallic strip. This patent and the findings of the research therein, are therefore very pertinant to the current investigation, which aims to produce rotational movement from a rapidly changing bimetallic strip.

As previously shown by Goulding's patent, from around the 1950's onwards, innovations in bimetals have resulted in the present day techniques of bimetallic strip production. Around this time, Boessenkool (1954) was granted a patented for the invention of solid phase bonding of metals. Boessenkool's patent was for the invention of a joining technique of two separate metals that could be joined together without the aid of an additional interface material. Furthermore, the patent introduced a method to dispense with the need to heat the metals to a liquid phase to facilitate a join between the two separate metals. This was a ground breaking invention in that the fundamental technology established is still used in present day manufacturing of commercial bimetallic strip. The main thrust of this patent meticulously spells out the sequence of events and precautions to take. As part of the prior art part of the patent, Boessenkool

refers to cold welding as a process that essentially affects the bonding of two metals by pressing "*localised areas under extremely heavy pressure at room temperature, so as to cause great local deformation and welded spots. There is no attempt to improve the weld strength of these localised spots by a subsequent treatment in the process"*. Boessenkool further contrasts the prior art of cold welding with the multi-stage bonding process of his own patent. The claims of the Boessenkool patent are for a process that has universal application with the ability to bond all malleable metals at cold working temperatures. Boessenkool further clarifies that cold working temperature is considered to be up to the minimum recrystallization temperature of the softest or metal with the lowest recrystallization temperature of the metals to be joined. Boessenkool then goes on to state the basic steps involved and the importance of the first step of the process, which is the metal preparation of the surfaces to be joined as to "*adapt them to the bonding"*. Durst.G (1955), a co-author of the Boessenkool patent, had invented an "*apparatus for cleaning metal strips*". The patent for apparatus for cleaning the metal strips by Durst was referenced in Boessenkool's patent as part of the equipment in the preparation process. The established prior cleaning methods used *"scratch brushing"* which establishes a "*continuous film of molecular dimensions, effective in preventing atoms of the metals from coming within the field of attracting atoms of the other metal, a condition necessary for bonding".* Boessenkool further claims that if just one of the mating surfaces was wiped with alcohol as a cleaning agent prior to joining, this would not enable the bond to take place by his process, until the alcohol had been removed. However wiping a surface clean with pure alcohol was the accepted prior art up to this date and it is this fact, that Boessenkool emphasises as one of the differences of his process. Boessenkool then elaborates via test cases why the "*barrier films"* due to oxide build up, prevent the successful joining of metals with his process. After the initial cleaning, which effectively was just blowing the dust off the surfaces and drying, the next step was to remove the barrier film by "pickling". After the "pickling", the surfaces of the strips were subjected to heating to remove the film caused by the immersion in the pickling fluid, which is normally Hydrochloric acid. Mention was made via instructions in the patent, that care must be taken not to allow oxidation to reform after the pickling process, and Boessenkool suggests that steps are made to prevent this before the cold rolling joining process takes place. After the preparation process, Boessenkool states that the temperature of the metals at the time of entering the squeezing phase of the process, should lie below recrystallization temperature of the

softest metal. Boessenkool states that the squeezing process affords the formation of a multitude of discrete bonds. After the joining stage, the instructions of the patent recommends heat treatment to the adjoined metals to effect growth of the bonds, thereby increasing the overall bond strength. In additional to the cold rolling processes to affect joint, hot rolling processes are also included in the patent. In reviewing this patent of process of joining dissimilar metals, it should be noted that for the cold rolling process outlined in the patent, the process starts with solid metals already pre-processed in rolling mills. The patent's scope does not attempt to encompass the entire process from a hot cast billet, but concentrates on the role of a secondary manufacturing operation. Boessenkool does acknowledge existing hot weld forging processes as prior art. In conclusion, the processes and equipment defined by Boessenkol's patent for the solid formation of bimetallic strip and all types of clad metals is an important step in the modern manufacture of bimetallic strip. Even though some of the processes and equipment may have improved or changed since this patent, overall, the process remains essentially the same today as when it was patented in 1954.

In 1963 a patent was granted to Morrison (1963) for the manufacture of bimetallic strip for the application of bearings. Hitherto this invention, according to the patent, the joining of Aluminium alloy to a base Steel with a strong metallurgical bond had not been a success. According to Morrison, attempting to join Aluminium alloy to a base of steel normally resulted in a low strength interface that was unsatisfactory for a bearing application in the automotive field. In his patent, Morrison elaborates that the prior art of bonding an aluminium alloy to a steel part required heating the aluminium alloy above its melting point, and then applying pressure to the aluminium /steel assembly to affect a joint. According to the patent claims, this invariably resulted in a weak bimetallic interface joint, due to the heated and now softened aluminium "*squirting and dislocating*" during the process. Morrison maintained that his invention overcame the earlier joining problems, by the discovery that the addition of of between 5% and 25% of tin to the aluminium alloy, afforded the aluminium alloy with a 5% lower melting point that resulted in a stronger more ductile bond. According to Morrison, the lowering of the melting point of the aluminium results in a bimetallic bond strength that can easily be cold pressed and formed into curved shapes via the aid of presses, without delamination of the bimetallic occurring. It is interesting to note that as with the patent by Goulding (1947) who elaborated on a "special box" to maintain a hermetical seal of the plates during the hot rolling process, Morrison also describes of a similar facility in

his process "*of the layers through a furnace having a controlled atmosphere and temperature suitable to avoid dislocation of the low melting point constituents".*

The bimetallic production process that Morrison (1963) describes in his patent is specified in minute detail. The preparation of the metal sheets are vapour degreased using Trichloroethylene followed by a subjecting the sheets to a rotating brush apparatus that abrades the mating adjoining surfaces. Morrison then describes the temperature range and time through the gas tight furnace, and the requirement to be in a non-oxidizing atmosphere. Morrison highlights the importance of the rolling mill temperatures, in that if they are too high or too low, the resulting bimetallic joint could become compromised. Morrison further provides a range of temperatures found to produce the strongest joint. The recommended temperature being 100° to 250° F (38°C to 121°C) lower than the melting point of the lower melting point constituent, in this example, the Aluminium alloy. The process concludes with a reference to stress relieving by low temperature annealing and makes claims that the process as described, enhances the annealing process. In summary, Morrison provides highly detailed data of the processes and the conditions required to manufacture bimetallic strip of dissimilar metals to a peel strength sufficient for subsequent cold forming operations. Around the time of the patent by Morrison, an American company started to produce bimetallic bearings that seemed to incorporate the technology being developed by Morrison.

A technical paper by Kopellovich (2012), demonstrated the bimetallic bearing technology for automotive applications. This paper although not intended as a scientific paper as such, discusses the technical ability of the company to reliably produce successful bimetallic shell type bearings that are found in car engines. Kopellovich discusses various alloying elements to augment the properties of bimetallic bearing. Kopellovich suggests that the varying of the alloying elements enables the tuning of the lower temperature material constituent of the bimetal to provide the most suitable bearing surface for the operational loading, environment, and bearing life. In the article, Kopellovich states that bimetals invariably possess a hard steel back which provides the rigidity and structure of the bearing shell. He further states that the actual side of the bimetallic that serves as the bearing material is very thin when compared to the steel backing. In the article, Kopellovich refers to aluminium bearing linings that are made up of an aluminium alloy containing between 6-20% of tin, which was shown by the patent of Morrison to result in a reliable intermetallic bond. Kopellovich also suggests

that the addition of 2 to 4% of silicon dispersed in the aluminium in the form of fine particles further strengthens the resulting alloy and serves as an abrasive polishing of the journal surface.

Hence it is possible to summarise that as far back as the late 1950's, the technology of permanently joining dissimilar metals successfully on an industrial basis was established. Moreover, the paper by Kopellovich demonstrates the reliablity of the high peel strength that can be achieved when procedures such as stated by Morrison, are adhered to in the production of bimetallic metals. The constant driving force to research into new ways of joining metals which is the ever present, is the need to reduce costs and manufacturing cycles times.

The ancient techniques of joining metals by forging were rediscovered in the late twentieth century and updated and refined with modern production equipment to be used successfully today. However, some of these updated processes are not the most cost-efficient way of producing bimetals. However cost alone, is not the only driving force for the research into bimetal technology. New, more demanding and specific applications require very special bimetals with exacting characteristics. It is these highly critical components that require very specific bimetal compositions and a performance that can only be obtained by research and development.

One of the most common bimetallic strip production techniques used today is called continuous roll bonding, or cladding, and this is a cold or solid phase joining process exclusively. This can be a separate, secondary manufacturing process in its own right, in that the material is cast and rolled into strip in a primary smelting process at the rolling mills, and then shipped as raw material strip in large rolls to the secondary processing plant.

Shivalik Bimetal Controls, Shivalik (2013), is one of those secondary processes plants that employ the continuous cold rolling, or bonding process. Shivalik an Indian manufacturer of bimetallic strip, use the continuous roll bond method for the fabricating of their bimetallic strip. The process starts with the raw material that is scrubbed cleaned and dried. Then the two separate strips of raw metal are fed into the high pressure rolls at a temperature that is below the re-crystallisation temperature of the two metals. The intense pressure of the high pressure rolling mill, forces the atoms of the two materials to inter-diffuse at the interface, and a strong intermetallic bond is formed.

After primary bonding under intense pressure, the newly joined bimetallic strip is now annealed to relieve the internal stresses of the roll bond process and to encourage the growth of further atomic bonds at the material interface. Subsequent to the annealing process, the strips are then rolled again and then annealed once more. The bimetal sheet is then etched with the part number and cut into strips by the slitting process. The final steps of the cold bonding process are the flattening and de-burring operation, to straighten and remove the burrs from the slitting process. The bimetallic strip is coiled and sent to be stamped into the final shapes and sizes ready for packing and distribution.

The secondary process of continuous roll bonding is a less elaborate method of manufacture, involving less steps and operations than the full primary and secondary process of manufacturing bimetallic strip. The full process includes the smelting of the iron ores, hot casting, hot rolling, cold rolling, and annealing. However, the continuous roll bonding for the manufacturing stages of production of the strip is still a lengthy process, and usually only possible in a large scale manufacturing plant. Because the basic manufacturing process is lengthy with many intermediate operations e.g., hot casting, forging, hot rolling, cold rolling, annealing, cleaning, stamping, slitting, the setup cost for the manufacture of a special run of bimetallic strip can only become cost viable on a large quantity order, or long continuous run.

Modern bimetallic strip is made to conform to German DIN 1715-2 (1984-01), American standards ASTM Standard B388-06 (2006), and ASTM Standard B106-08 (2008). Each manufacturer of bimetallic strip usually provides certificates of conformity with each order. Modern bimetallic strip can be formed into many different geometry types to accommodate the multitude of applications. The most common geometric configurations are flat strip, although many configurations and shapes such as spiral shaped strip, and circular domed shaped strip are possible, see Fig.2.1. Bimetallic strip is usually designed to order and manufactured specifically for each application; however, most bimetallic strip manufacturers offer a stock range of flat strip as a minimum. A special coiled bimetallic shape is shown in Fig. 2-1. The coiled helix type bimetallic strip enables a spring like action when heated, which could be a type of bimetallic configuration that could be exploited for a linear displacement actuator.

Fig.2-1 Reproduced with kind permission Kanthal (2002)

During the latter part of the 20th century, research activity into materials made a step change driven by the need for those materials to meet the exacting requirements of more demanding applications. The new forming technologies and applications such as space flight, supersonic air travel, lighter faster ships and more fuel efficient cars, has been the impetus to evolve many ways to permanently join similar and dissimilar metals. The outcome of this research and development has resulted in making lighter more robust bimetal hybrid structures. Many different joining techniques have been investigated in recent times, and from the 1980's onwards, new techniques have been employed that have resulted in new ways of permanently joining similar and dissimilar metals.

Furthermore, awareness of the energy required for the production of metals from raw materials, and the primary and secondary manufacturing operations that use huge amounts of electricity, there has been a continuous drive to refine and reduce the core manufacturing processes to save money. From the work of Goulding (1947) who was granted a patent for the hot cast and cold roll process of bimetallic strip production, Poloni (2006) was granted a patent for a machine that enables a process known as twin roll casting. Twin roll casting is a continuous casting process. In this process, a special machine that enables the two different molten metals of different melt temperatures, to come together just prior to the rolling stage, each in a crystalized state that is, the machine enables each material to cool sufficiently to obtain a clear separation interface, which creates a more controlled bond interface. Fig.2-2 shows the principal of the Twin roll cast method.

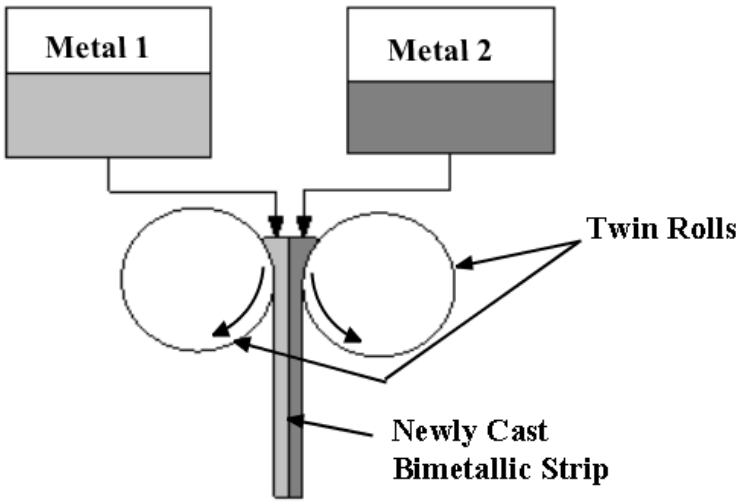

Fig.2-2 Twin cast rolling method

This modern method of producing bimetallic strip enables a reduction of energy processing costs. A paper by Haga (2009) confirms the rationale for the twin roll cast method, and confirms that "*The aim of the use of the twin roll caster to make clad strip was in the reduction of the production-energy of the clad strip".* In addition to bimetallic strip by hot casting and subsequent cold rolling methods there are other methods that have come to be accepted as ways of manufacturing bimetallic strip or clad components.

Explosive welding is a method of joining two dissimilar metals permanently together that was discovered by accident in world war two. It was observed that pieces of shrapnel that had become embedded in armour plating were also fused to the armour plate. The mechanism that affects the weld, was down to the force of the impact of the shrapnel with the armour plate. This discovery led to a new form of metal joining known as the explosive welding process. According to Young (2004), in 1962, DuPont first patented the explosion welding technique after developing it during the 1950s. Today it is a widely used method of joining a variety of dissimilar metals and the process has found a particular usefulness in making aluminium steel joints for naval applications, and is used to tackle marine corrosion problems of the US Navy.

Diffusion bonding as described by Shirzadi (2004), is another advanced solid state method of joining two dissimilar metals. In this process, the parts to be joined are held in an inert gaseous environment, or in some cases, within a vacuum chamber. The metals to be joined are carefully cleaned, then subjected to high temperatures usually within 50% to 70 % of their melting points. In the case of a copper-steel bimetallic

joint, copper melts at 1084°C and steel at an average temperature of 1483°C Engineeringtoolbox (2014). Thus assuming 60% of the melt temperature gives 650°C for the copper and 890°C for the steel. Then under intense pressure, atomic bonding at the bond interface occurs. This is a highly specialised process of joining dissimilar metals, and not a cost viable option for the production of bimetallic strip on a large scale basis. The technology of joining metals is still an emerging technology as new materials and composites are created, and as research expands the new metal forming techniques.

As such this review can only provide a snapshot of the current state of the art in the field of metal joining, and whilst this is not a truly exhaustive review of every single joining process, it does cover the main methods employed in the wholesale production of bimetal metals up to the time of print.

2.4 Technical Standards

As the wholesale manufacture of bimetallic strip became prevalent in the early part of the twentieth century, then the control and standardisation became necessary to guarantee repeatable, and predictable bimetallic strip characteristics irrespective of the manufacturing source. Today there are only a handful of large companies actively manufacturing bimetallic strip around the world, and all of them produce bimetallic strip in accordance with one or more of the following internationally agreed standards as shown in Table 1.

A Swedish manufacturing company, Kanthal (2002), ironically was one of, if not, the best suppliers of bimetallic strip in the world. The company no longer manufacture bimetallic strip, however Kanthal set the standard when it came to all things bimetallic. Their bimetallic handbook has become the definitive bible of bimetallic information with an extremely useful technical section that enables the designer to calculate the correct bimetallic strip for his or her own application.

In the technical section of the Kanthal handbook, differences are made between the American ASTM Standard B106-08 (2008) method of calculating the “flexivity” of a bimetallic strip, and the German Uhlig (2007) standard of measuring the “specific curvature” of the same.

Another very useful bimetallic handbook is produced by Auerhammer Metallwerk of Germany, Uhlig (2007). This handbook affords a high level of technical data for bimetallic strip manufacture and applications. The handbook provides a highly detailed section on the processes involved in the manufacture of their bimetallic strip.

Additionally, the handbook possesses a world bimetallic strip standard comparison table from page 126 to page 134 that enables the user to find equivalent bimetallic strip for all the major manufacturing brands. Moreover, it details the different manufacturing standards associated with each manufacture's brand of bimetallic strip.

In summary both the Kanthal and Auerhammer Metallwerk thermostatic handbooks are an extremely useful for engineers in the field of bimetallic strip design. Both books provide a wealth of highly detailed information pertinent to the knowledge and application of bimetallic strip. It should be noted however, that although both books provide a large range of applications with a variety of bimetallic strip geometries and configurations, the application and specific geometry of this investigation is not covered or provided for in either book.

Table 1 includes the major bimetallic strip manufacturing standards that cover the production requirements, technical specifications, testing methods and technical delivery of bimetallic strip. All major bimetallic brands are manufactured and controlled according to one of more of the standards, and thus an equivalent bimetallic strip from a different manufacturer is easily obtained.

Table 1 World-wide bimetallic manufacturing standards

Germany :

DIN 1715-1 (1983-01)

Thermostat metals: technical delivery conditions.

Uhlig (2007)

Testing the specific thermal curvature.

USA:

ASTM Standard B106-08 (2008)

Standard Test Methods for Flexivity of Thermostat Metals

Dossett (2006)

Standard Specification for Thermostat Metal Sheet and Strip

ASTM Standard B753-07 (2007)

Standard Specification for Thermostat Component Alloys

Japan:

JIS C 2530 referred to by Boessenkool (1954)

Thermostat metals for electric apparatus

Russia:

GOST 10533 referred to by Boessenkool (1954)

Cold – rolled thermostatic bimetallic strip . Specifications

GOST 10994 referred to by Boessenkool (1954)

Precision alloys. Grades

China:

GB/T 4461 referred to by Boessenkool (1954)

Thermostatic bimetal strip

2.5 Theory of Bimetallic Strip

At the time that Harrison was developing his marine clocks, it is improbable because metallurgy was still in its infancy, that a mathematical method of evaluating the radius of curvature of a bimetallic strip as function of temperature would have been known. However, at the time of Harrison, and there afterwards, it is almost certain that an empirical method, or other means, to evaluate the radius of curvature, would have been devised by the early 17th century clockmakers. It is possible that someone through the 17th, 18th and 19th centuries did work out how to calculate the bend radius of a bimetallic strip. Furthermore, it is most likely that the person was a clockmaker, however, that clockmaker would also have had a strong business incentive for keeping that information secret.

Therefore no scientific treatise on the calculation of bimetallic strip was published until the seminal paper by Timoshenko (1925). This paper was the first paper that provided a mathematical proof, using modern understanding of the behaviour of metals under heating, to formally describe the relationship between temperature and the radius of curvature.

The main formula that Timoshenko propounded is the fundamental formulae that were adopted by the American ASTM Standard B106-08 (2008) for evaluating the flexivity which is a constant of the bimetal. The flexivity which is defined as" *the change of curvature of a bimetal strip per temperature change times thickness"*, is after certain simplifying assumptions have been made to the original Timoshenko formula, equal to the contant:

$$\frac{3}{2}(\propto_2 - \propto_1)$$

Where $\propto_2, \propto_1$ are then coefficients of linear thermal expansion of the metals within the bimetallic strip.

The full flexivity is given on page 4 of the Kanthal handbook by;

$$k = \frac{\left(\frac{1}{R_T} - \frac{1}{R_O}\right) * s}{(T - T_O)} \qquad \text{Kanthal (2008)}$$

where s is the thickness of bimetallic strip.

R_T is the radius of curvature at any temperature *T*.

R_0 is the radius of curvature at ambient temperature T_O.

The European standard uses a different approach based on the geometry of a cantilever beam in bending, for the derivation of the formula for the calculation of the specific curvature k, of the bimetal. The European specific deflection is defined as :

$$a = \frac{A*s}{(T-T_O)(L^2+A^2)} \quad \text{Uhlig (2007)}$$

where A is the deflection from flat at the end of the cantilever beam in (mm).

L is the length of the cantilever beam to the point of deflection at A in (mm).

s is the total thickness of the bimetal.

According to Kanthal, the newer DIN specification, which is similar to the ASTM standard, differs in the understanding that bimetals components "*often elongate in a nonlinear way as a function of the temperature of the specific curvature or flexivity, which depends upon the temperature between which it has been measured"* this is the reason that the newer DIN specification has been slightly redefined.

From reviewing both standards of specifying the flexivity or specific curvature k of the bimetal, the drawbacks of using the DIN method is in the limitation of the assumption that in most calculations ," *A is smaller than 10% of L*" which is not the case in the application of this research. It is therefore more reliable to use the original Timoshenko formula for the work described here since in its original form, it accomodates all geometries without limitations.

2.6 Linear Force Displacement Mechanisms – Steam Onwards

This part of the review investigates the bimetal technologies and other technologies that utilise heat energy to produce a linear force displacement. Man, has for thousands of years sought to employ the power of heat in some way to produce mechanical movement and thus power. A research paper by Keyser (1992), reviews the Heron steam engine. This article benefits by having original Greek translations of the description of the device that is common also known as the "Hero" steam engine.

In the article by Keyser, the author explores the early variants and ancient developments of the steam engine. Keyser explores how in, or before the first century BC, the development and experience of dabbling in primitive steam engines was gaining ground. As a result of this early experimentation, the worlds first steam engine was devised that heated by a fire, boiled water into steam, and used that steam in a reaction turbine to produce a small output power. This primitive machine is most commonly

known as the Hero steam engine, but in the paper by Keyser, he authoritively refers the Hero invention to that of being the invention by Heron.

Because of a Greek translation, the commonly known Hero is indeed the Heron engine and the article is most persuasive in the level of detail and many literal translations from Greek. What is most important, is the acknowledgment that a thousand years ago or more, mankind was dabbling in the heating of a fluid to extract mechanical movement and thus power. Another source which describes the Hero steam engine is an article by Petroski (1996), who refers to the Hero machine as being acknowledged as the first steam engine, and accordingly he refers to Hero of Alexandria, as being credited with inventing the first steam engine.

Petroski further provides a quick overview of the historic milestones in the development of the steam engine right through to the 18th century. Both papers by Keyser and Petroski agree on the commonly held belief that the Hero, or Heron engine, was in it's time, considered to be merely a novel toy. It would seem that no one of that ancient time thought to use the invention to produce useful power. Petroski looks into that aspect and explains why it was not taken seriously as a useful machine, putting it down to the lack of engineering materials around at the time that could withstand the pressures required for it to be used as a reliable useful machine.

Therefore exploitation of the Heron steam engine could not have taken place until the materials technology had matured to a point that enabled the production of structural steels capable of withstanding boiler pressures, and this coincided with the understanding and devlopment of fastening and sealing techniques in the late 17th century.

Petroski mentions the major inventors, or the grandfathers of the steam engine, such as being Hero, Thomas Newcomens, Otto von Guericke, Thomas Savery, Christian Huygens, and James Watts. He further illustrates how the idea of using steam to produce power was refined as each inventor solved the problems that arose in the then, infant steam technology period of the 17th and 18th century.

It is interesting to note that in early industrial steam engines, the boilers frequently blew up killing workers. Until the intervention of the pressure relief valve that was invented almost by accident. Legend has it, that because of the build up of steam in the early boilers, the owners of the industrial steam engines would employ a young child to vent the build up of excessive steam pressure in the boiler, by pulling a lever at certain timed intervals. On one occasion, one enterprising lad who wanted to be somewhere else,

possibly to play, contrived a simple weighted mechanism that would automatically be lifted upon an overpressure condition of the boiler, thus the automatic press relief valve for the steam boiler was invented.

Even with the invention of the pressure relief valve, early steam boilers were notoriously unreliable and dangerous. Petroski reviews a tragic marine accident that occurred in 1865, that was attributed to a boiler explosion. The explosion took place onboard the steamboat *Sultana* which resulted in the death of 1500 people. At the time, this was the worst marine disaster in American histrory, and as a result of this tragic loss of life, new safety laws and standards were introduced resulting in a code of practice named" *Standard Method for Steam Boiler Trials*" which was instigated by the ASME in 1884.

Hence it has been shown that the application of heat to a fluid will generate, via steam, substantial power to motivate machines, and the great golden age of steam railways around the world started in earnest with Stevenson "Rocket" train. In the application of using steam, the gas pressure of the steam times the area of the piston, results in a linear force and displacement of the piston. The piston is coupled to a mechanism that converts linear to rotational motion at the wheel of the train, or in the case of a paddle steamer, to the paddle wheel which propels the vessel through the water.

In addition to heating water into steam to produce pressure to generate a linear force displacement of a piston, as mentioned earlier, Dr Robert Sterling in 1816 was granted a patent for a hot air engine. Stirling's invention worked on the closed thermodynamic Carnot heating and cooling cycle.

Riabzev (2002) in his presentation, refers to the original Sterling engine concept as being unchanged in almost 200 years, and affirms that the engine has been refined by advances in materials and sealing technology in modern times. Riabzev describes the first sterling engine as a large affair, of large proportions and of being very reliable, which contrasts with the first steam engines of that time which were both unreliable and sometimes deadly.

The Stirling cycle is included in this review because of the thermodynamic similarity with the heating and cooling cycle of a bimetallic blade within the thermal motor.

The basic Sterling cycle is realised by machines that possess the means to shunt a working internal gas between a hot and cold volume. It is the displacement of this gas or

working fluid, with the pressure - volume relationship, that enables the work to be done by the machine. The original Sterling engine possessed a piston and a displacer that are held within a single long cylinder and are out of phase in operation. Both the piston and displacer are mechanical linked to a rotating crankshaft or flywheel, in a similar arrangement to that of a conventional 4 stroke internal combustion engine. The Sterling cycle functions as follows, heat is applied to the hot end of the cylinder; this increases the gas temperature and pressure of the volume of air at the hot end, resulting in the piston being displaced. Work is being done by the air expanding resulting in the turning of the crankshaft; this is known as the *expansion* phase of the cycle. The momentum of the crankshaft displaces the displacer piston which is a smaller diameter than the cylinder bore, this action displaces, or ”*shunts*” most of the hot air from the hot end of the cylinder to the cold end of the cylinder, this is the *transfer* phase of the cycle. The majority of the hot gas has now transferred to the cool end of the cylinder and now, by the out of phase of the piston to the displacer, the volume of the hot gas increases and the gas cools by the heat loss to the surroundings, thus contracting and drawing the piston backwards, this is the *contraction* phase of the cycle.

The momentum of the crankshaft moves the displacer so that the cooled air is now transferred to the hot end of the cylinder for the cycle to repeat, this is also a *transfer* phase of the cycle. The Stirling cycle therefore inputs heat energy at a hot temperature, it does work in the cylinder, and the output is a lower heat energy that is loss to the surroundings, plus mechanical work done by the machine.

Contrasting the thermal cycle of the Stirling engine to that of the Mark II thermal motor introduced earlier. As with the Stirling engine, the thermal motor is based upon the Carnot heating and cooling cycle in which heat is applied to a single bimetallic blade, the blade expands and does work which rotates the rotor bringing other blades into the “hot zone”. The heated blade is then cooled, heat is rejected to the surroundings, work is done by the machine, and the cycle repeats for the other bimetallic blades. This cycle closely mimics the Stirling engine heat “shunting” mechanism.

The Sterling Engine can also be operated in reverse as a heat pump that enables cryogenic cooling, Riabzev describes the Sterling cycle in minute detail outlying the various configurations and types that have been developed. The Stirling cycle although exhibits a vast number of advantages over the internal combustion engine, the ability to be heated by sustainable energy heat sources such as Solar power, Geothermal, or any

type of combustible carbon based or organically grown fuel, it has however, never been a direct threat to the internal combustion engine as an automobile power plant.

This is despite those now very important nasty side effects that mass internal combustion engines produce, ie toxic exhaust fumes and noise pollution. The sterling engine is used in special applications such as in submarines or in space applications whereby polluting either by exhaust gases or by noise, cannot be tolerated. A NASA derived space manual entitled Stirling Engine Design Manual by Martini (1978), provides an in-depth treatise on the design detail parameters of the piston and displacer units within the Sterling Engine, and includes a summary of work done to ascertain the usefulness of the Sterling engine as a possible alternative to the internal combustion engine.

Martini compares and contrasts the major types of Sterling engines and looks at quantifying the most successful types, whilst providing a collective snapshot of the current Sterling Engine technology.

In addition to steam engines and hot air engines that heat a fluid to expand and do work in a cyclic fashion, there are other various types of machines that exploit a temperature difference to expand a solid material under elastic tension to produce an output displacement and force. One such device patented by Hein (1976) uses the expansion and contraction of a spiral tube that is periodically heated and cooled to impart a cyclic rotatory oscillation in the device, this rotary displacement is coupled to a linear piston to pump fluids.

The patent by Hein and another by Clark (1973) exploits the expansion and contraction of a single solid material to provide displacement and force as a function of a temperature difference. In the patent by Clark, the inventor refers to having two *"linearly heat-expansible bands stretched"* and being cyclically heated and cooled by exposing or shielding from a radiated heat source, thus enabling the housing containing the bands to rotate.

Another device invented by Churchill (1968) uses a sealed fluid to expand in a piston actuator. This device employs an electrically heated element, wound around a shaft immersed in a thermally responsive liquid, the type of liquid is not disclosed in the patent. The inventor refers to the device as a thermal transducer that upon the heating of

the element causes the liquid to expand, thus displacing the piston and associated output shaft. The application of this device is to provide feedback as a heat sensor.

A thermal motor invented by Sandoval (1977), was granted a patent in 1977. In Sandoval's patent, the invention purports to convert thermal energy into mechanical motion in a device resembling two pulley wheels joined by a continuous belt. The smaller pulley wheel is in air and is subjected to a heating source, the larger pulley wheel is immersed in a liquid that is assumed to be the heat sink or cooling source. The pulley belt material is not published, but the claim is that some metals such as nickel-titanium alloys change their shape when heated or cooled and that with the absence of heat are pliable, but upon the application of heat become rigid. It is this effect that the inventor is exploiting to generate movement of the belt, and thus convert heat energy into mechanical movement.

There are many patents for bimetallic machines, also sometimes known as thermal motors, Whitney (1945), O'Hare (1985), Low (1972) to name a but a few, and they all work on the same principal, that is, that heat is cyclically applied and removed from the bimetallic strip. The bimetallic strip has been prior fashioned to work either by bending from flat, or from a spiral shape, or a disc shape or "U" shape. In most of the patents, the machines could be made to work, however some of the thermal motor concepts and patents reviewed so far, are too complex and costly to be manufacture as a viable practical product.

However, the bimetallic solution to produce a force and linear or rotational displacement, offers similar advantages as an environmentally friendly machine, as the aforementioned Stirling engine discussed earlier. For the bimetallic arrangement or thermal motor to be fully realised, the concept on how the bimetals are efficiently heated and cooled in a cyclic manner, with the minimum of complexity and components is of paramount importance.

It is interesting to note, that the first patent for a device that uses a bimetallic strip to perform the function of generating a force or torque, was as recent as 1951. Dayton (1951) was granted a patent for a device that used a bimetallic strip to provide the impetus for a slow acting egg timer, or toaster application.

A much more complex contraption received a patent for the thermal motor for a rotisserie shaft by Cole (1965). This device was an elaborate device that used the

bending of the flat bimetallic strip to produce a linear reciprocating motion that was converted to rotary motion at the shaft of the spit. Although devices discussed so far, seem trivial and crude by today's standards, they were the start of inventors seeking to make use of the special properties of a bimetallic strip. In 1972 an interesting patent was granted to Low (1972) for the sole purpose of generating power to a solar powered heliotrope. In this invention the bimetallic strip is used to drive and maintain the orientation of the device to track the suns path across the sky. This device utilises a bimetallic sensor that performs a feed forward function of sensing the suns orientation in the sky, and correcting the mismatch between the solar array and the sensor.

The application of Low is a much more meaningful role for a bimetal in a sensing and activation application.

O'Hare (1985), was granted a patent for a bimetallic solar engine for the purpose of generating useful power more than the patents previously reviewed. In the patent by O'Hare, heat is cyclically applied to a series of stacked "U" shaped bimetallic strips that are attached to a common output shaft. The device contains a Solar collector and a heat sink. The media for heating the bimetallic strip is hot air collected from the suns ray. The hot air is allowed to flow into a sealed chamber to heat the stacked bimetallic strip. The output shaft is connected to flaps in such a way, as to control the charge of hot air to the "U" shaped bimetallic strips, and then to allow the venting and cooling of the stacks of bimetallic strips in a cyclic fashion. Although this may seem a very crude mechanism, it is very similar to the Sterling engine in that it employs a heating and cooling cycle to process the heat to and from the bimetallic strips. The two major differences between this concept and the Sterling engine is, one, the frequency of operation of a bimetallic engine is much slower than that of a Sterling engine, and two, in a bimetallic strip powered motor, the heating and cooling cycle is effectively a "two stroke" whereas the Sterling engine is a "4 stroke" in operation.

At the time of writing, the research into energy harvesting and power generation by bimetallic strip technology is continuing to grow. A paper on thermal energy harvesting by Boisseau.S. (2012) reveals a method to harvest potential re-new able energy by heating a straight bimetallic strip cyclically. Boisseau suggests that as the bimetallic strip oscillates, the force and displacement produces a change in capacitance of two adjoining electrodes, thus directly generating electrical power.

It is important to note that bimetallic thermal motor or engine is in its infancy as a technology for the generator of power in the field of energy harvesting. This contrasts with Sterling engine technology that has been around and continually developed since 1816. Potentially, the thermal motor can provide the same desirable features as found in the Sterling Engine, clean power, non-polluting, silent, with the additional advantage of being a simpler machine with less components. Additionally, bimetallic technology can provide a wide range of different configurations, thus enhancing the ways that the bimetallic effect can be exploited in the field of energy harvesting.

2.7 Discussions on the Literary Review Findings

From the review on prior bimetal technology, it is clear that for thousands of years dating back to very early civilisations, there has always been a need to produce bimetal implements, such as swords, axes, to benefit from the enhanced structural properties that a bimetal composition has to offer. It was shown that the smelting and forging and layering of different metals such as in the Samurai sword blade, or the Damascus steel, enabled early metal workers to enhance the keenest of the cutting edge of the sword, and at the same time provide a harder and tougher steel.

The review also has revealed that the cladding of one metal with another metal was perfected many hundreds of years BC by ancient civilisations, and that recent archaeological digs have revealed exquisite objects that have been clad in various metals such as gold and silver for the embellishment of the artefact.

It was shown that although bimetal implements existed over this long time frame, from about 600BC to 1700AD, the properties of bimetal objects were only exploited as a single composite metal yielding structural or cosmetic advantages. The review has shown that the first recorded use of a bimetal to cause a displacement as a function of a heat differential was by Harrison, Sobel (1995), in the mid seventeenth century. Shortly after Harrison's application of a bimetal in a functional role, the review illustrates that a very early Thermometer Holbrook (1992) was invented using the idea of Harrisons bimetallic strip. Harrison's invention, showed the world another useful side to a bimetal, other than enhancing the structural properties of a single structure, his invention enabled the bimetal to act as a sensing activator. However, it took until the twentieth century that the scientific analysis of a bimetal performing as a temperature dependant displacement mechanism was published, Timoshenko (1925).

The review has illustrated that since the early part of the 20th century, much progress had been made in the manufacturing processes for the production of bimetallic strip. The hot forge bonding processes that hitherto had been the most prevalent method of joining two metals together were slowly replaced by the roll or cold bonding processes because this enabled the secondary operation of manufacturing bimetallic strip to be produced in plants away from the primary process of smelting and hot casting in steel foundries.

In the review, the standardisation of the way bimetallic strip is controlled and mathematically evaluated was highlighted by Dossett (2006) and ASTM Standard B106-08 (2008), and European standards becoming the basis for bimetallic strip specification Uhlig (2007). With the controlled production of repeatable bimetallic producing from the 1950's onwards, a greater diversity of applications of bimetal was highlighted, Kopellovich (2012).

The diverse method of fabricating bimetallic strip was reviewed, and exotic processes or more advanced special processes such as explosive welding DMC (2013) and diffusion bonding methods Shirzadi (2004) were briefly reviewed. From the review, it became evident that from the 1930s onwards inventors have successfully patented many devices that exploit the functional aspect, or by-product of the bimetal, namely, force and displacement as a function of temperature differential.

The functional aspects of the bimetallic strip were highlighted by patents granted for a sun aligning mechanism Low (1972) and by a patent for the rotation of a rotisserie spit, Cole (1965). Moreover, the review has shown that from these simple ideas for applications for exploiting the bimetallic effect, inventors have considered energy harvesting in patents by O'Hare (1985), who put forward his bimetallic solar engine as a means to harness the suns energy to generate power. Boisseau.S. (2012) illustrated in his article, that the field of bimetallic research into energy harnessing is actively being pursued. The review has shown that the application of a heat differential as the mechanism to provide mechanical power, has evolved over the ages as the need to find cleaner ways of generating electrical power production is being sought.

2.8 Conclusions of the Literature Review

The review has shown that throughout the ages of mankind, the development of artefacts, weapons were enhanced by the coupling of two different materials and their separate metallic properties. The review has demonstrated that as late as the 17th century, the main application for bimetallic structures were either for enhancing the laminated metal for structural or cosmetic purposes, as in cladding metals with gold and silver.

It was shown that Harrison was the father of functional bimetallic technology, when he used the bimetallic strip as a temperature compensating sensor in his marine clock application. It was also demonstrated, that for hundreds of years after Harrison, clocks made good use of his initial invention, but it waited until the early 20th century before the seminal treatise on the mathematical analysis of a bimetal was produced by Timoshenko.

During the 20th century, manufacturing and production technique of bimetallic strip became standardised, and application of bimetallic strip as a sensor became widespread. Research into bimetals in the latter part of the 20th century became a field of study in its own right, and ideas and patents to use the bimetal effect to harness clean renewable energy is now being considered as another alternative option to best conserve the earth's natural resources.

The over reliance on fossil fuel generated energy and power, and the consequences of burning those fossil fuels with the release of toxins and pollutants, is the driving force for the Sterling engine resurgence, and now for the thermal motor, or solar powered bimetallic engine to come of age.

CHAPTER 3 Theory and Simulation

Summary

This chapter introduces the application of Timoshenko and Castigliano formulae, and additional correction formulae to modify the formulae for this study.

3.1 Introduction

For the characterization of a pre- curved bimetallic strip functioning as a bimetallic blade in a thermal motor, it is necessary to understand how the bimetallic strip behaves in the specific chord line orientation and loading axis. The literature does not hold current information of a bimetallic strip configured in the specific axial case as shown in Figure 3-1. The chord displacement axis is the theoretical axis or path, that the free end of the bimetallic strip displaces along, when mounted as depicted in Figure 3-1. This chapter develops equations that enable the evaluation of the non-loaded chord line extension of a pre-curved bimetallic strip as a function of a temperature change by the application of Timoshenko's temperature induced radius of curvature formula.

The fundamental Timoshenko formula that defines the radius of curvature for a bimetal strip as a function of temperature is given by:

$$\frac{1}{\rho} = \frac{6(\propto_2 - \propto_1)(1+m)^2(T-T_O)}{h(3(1+m)^2+(1+m.n)\left(m^2+\frac{1}{m.n}\right))}$$ Eqn. 1 Timoshenko (1925)

where ρ is the radius of curvature of the bimetallic strip.

$\propto_2, \propto_1$ are the coefficients of thermal expansion of the two metals and $\propto_2$ is considered to be numerical greater than $\propto_1$.

$m = \frac{\propto_1}{\propto_2}$ ratios of the coefficients of thermal expansion of the two metals.

$n = \frac{E_1}{E_2}$ ratios of the Young's Modulus. Matthews (2005).

h is the total thickness of the bimetallic strip.

T is the temperature of the strip at above or below ambient temperature.

T_O is the temperature of the strip at ambient temperature.

It should be noted that T_O is highly dependent on the local ambient temperature, and that the bimetallic strip must be in a steady state ambient temperature condition, before the addition or subtraction of heat to the strip, produces a temperature difference and thus a change in the radius of curvature.

Timoshenko enables the evaluation of the radius of curvature from an initially flat bimetallic strip that has being uniformly heated. To obtain the radius of curvature from a pre-curved bimetallic strip, the present study has added a correction formula to Timoshenko. To evaluate the chord line axial force generated by the displacement of the free end of the strip, Castigliano's energy theorem, Egelhoff (2010), is applied along the pre-curved bimetallic strip. Castigliano's energy theorem applies to a homogenous

pre-curved beam, and thus when applied to a bimetallic strip, the bimetallic strip is assumed to be a homogeneous beam.

This section provides the theoretical formulae and linking equations to obtain a way of calculating the net chord line axial displacement of the free end of a pre-curved bimetallic strip, subjected to uniformly applied heating, and at the same time, subjected to an externally applied resisting opposing load.

It is important to note that Castigliano's energy theorem that is used to evaluate the force vs. deflection theory of the pre-curved bimetallic strip in the up-coming sections, is limited to relatively small and linear displacements, but as a first approximation, the linear theory fits reasonably well for small chord line displacements.

In later sections, as part of the new knowledge, non-linear expressions are introduced that more closely match the test data for force vs. deflection in the pre-curved bimetallic strip loaded along the chord line.

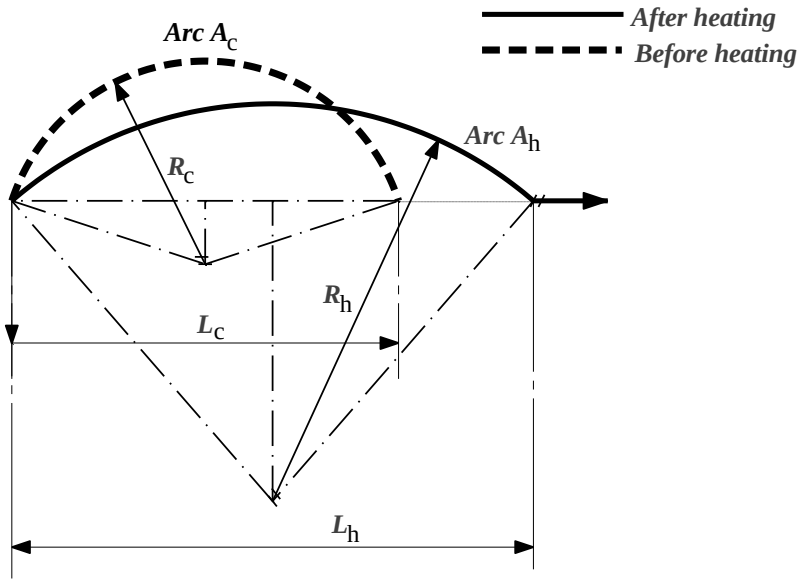

Fig.3-1 Idealized pre-curved bimetallic strip in two states of heating.

In Fig.3-1, L_c represents the chord length of the curved bimetallic strip at cold or ambient temperature, and the strip's corresponding radius of curvature is R_c. The bimetallic strip is cold-formed by a gentle bending process to produce the initial, permanent radius of curvature R_c . The suffixes "*c*" and "*h*" are cold and hot states respectively, and assuming hereafter, that the thickness of the bimetallic strip is very

small as compared with the radius of curvature of the strip, and the thickness to radius of curvature ratio is approximately 1:100.

As the strip is uniformly heated above ambient temperature, it begins to straighten up and extends to L_h, and now the radius of curvature is R_h. In order to obtain the chord line axial displacement from L_c to L_h **,** a free rotational pivot condition must exist at each end of the strip. It is this degree of rotational freedom at each end of the strip that produces the chord line axial extension, or straightening effect of the strip during the heating process. Since the strip is subjected to heating, its radius of curvature changes, whilst the arc length of the strip essentially remains the same and thus $A_h = A_c = A_b$, since the arc lengths are equal throughout the heating and cooling cycle. It is therefore easier to refer to the arc length of a pre-curved bimetallic strip in general terms as A_b.

The application of Timoshenko (1925) for the calculation of unloaded "hot" distance L_h now follows:

Assumptions that were made;

- the pre-curved bimetallic strip is simply supported at each end with a rotational degree of freedom.
- the strip is uniformly heated along the entire length of strip, and the strip remains approximately circular.
- no external loads are applied during heating
- the material with the higher coefficient of thermal expansion α_2 is on the inside radius R, see Fig.3-2.
- that the strip has sufficient time to cool down back to ambient temperature.

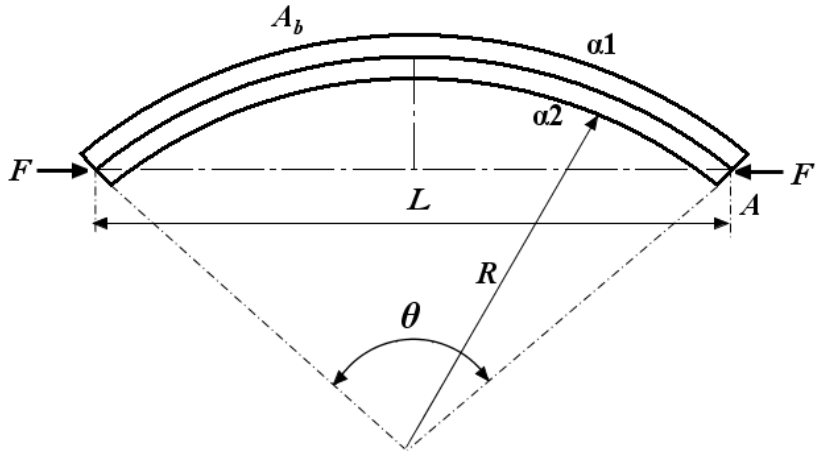

Fig.3-2 α_2 & α_1 for a strip of a material with α_2 is on the inside.

The Timoshenko equation shown earlier, provides the radius of curvature from an initially straight flat bimetallic strip. It can be shown that for a strip which is required to straighten up from a pre-curved condition R_c, that the Timoshenko equation can still be used with the following empirically derived correction formula that evaluates the new hot radius of curvature R_h from the bend radius of curvature ρ by the Timoshenko equation. The empirically derived R_h correction equation evaluates the radius of curvature of a heated bimetallic strip from an initially pre-curved radius of curvature R_c. The empirical correction works by subtracting the reciprocals of both radii $\frac{1}{R_c} - \frac{1}{\rho}$ together, and inverting.

Thus:

$$R_h = \frac{\rho R_c}{\rho - R_c} \quad \text{Eqn. 2}$$

where R_c is the initial pre-curved radius of curvature at ambient temperature.

ρ is the Timoshenko radius of curvature formula defined earlier, Eqn.1.

R_h is the un-loaded hot radius of curvature.

It is important to note that Eqn.5 is based upon the fact that ρ which is the heat induced radius of curvature of a bimetallic strip as defined by Timoshenko, obeys the linear elastic properties of the bimetallic strip. Therefore at no time can the strip due to heating alone, exceed the yield point of the material and not recover, or return to its original form or shape, upon cooling down to ambient temperature. This is the main assumption that Timoshenko makes in the derivation of the bending formula.

The extension L_h will be the maximum the strip can extend for any given temperature differential.

With the R_h value established by the application of the Timoshenko formula, the corresponding "hot" chord length L_h can now be found.

The general chord length of any arc is generally published as being;

$$L = 2Rsin\left(\frac{\theta}{2}\right) \quad \text{Eqn. 3}$$

Where: L is the general chord length

R is the general radius of curvature

A_b is the general arc length (in radians) part of a true circle

θ is the angle subtending the portion of arc A_b over distance L.

By using the established relationship: arc = radius x angle (in radians) $A_b = R\ \theta$ and substituting for $\theta = \frac{A_b}{R}$ into Eqn.4, angle θ can be eliminated and it is possible to obtain the length of a chord as a function of arc length A_b and radius of curvature ***R.***

Thus, the general length of a chord of any arc is:

$$L = 2R\ sin\left(\frac{A_b}{2R}\right) \quad \text{Eqn. 4}$$

Thus it is possible to evaluate the chord length L as a function of the radius of curvature R and the length of arc A_b, which is normally fixed for any given application. Rewriting the general chord equation in terms of hot and ambient states of the bimetallic strip:

Thus;

$$L_h = 2R_h \sin\left(\frac{A_b}{2R_h}\right) \quad \text{Eqn.5}$$

where L_h is the new "hot" chord length of the straightened strip.

$$L_c = 2R_c \sin\left(\frac{A_b}{2R_c}\right) \quad \text{Eqn. 6}$$

and L_c is the initial "cold" or chord length at ambient temperature of the strip,

whereby A_b, R_h & R_c were all defined previously.

Hence, using Timoshenko's radius of curvature formula with the chord formulae, it is possible to evaluate the hot length of bimetallic strip L_h. Given that L_c can be easily evaluated if the pre-curved radius of curvature is R_c is known, then the unloaded chord displacementx_d, from L_c to L_h can be evaluated by simple subtraction.

$$x_d = L_h - L_c \qquad \text{Eqn. 7}$$

And the full expression with substitution of R_h becomes:

$$x_d = 2\left(\frac{\rho R_c}{\rho - R_c}\right)\sin\left(\frac{A_b(\rho - R_c)}{2\rho R_c}\right) - 2R_c \sin\left(\frac{A_b}{2R_c}\right) \quad \text{Eqn. 8}$$

Where x_d is the unloaded chord line axial displacement of a curved bimetallic strip as a function of a temperature differential T - T_O.

L_h & $L_c, \rho, A_b, R_h, T, T_O$ and R_c were all defined previously.

Thus Eqn.11 provides the unloaded chord line axial displacement x_d of the free end of a pre-curved bimetallic strip, subjected to uniform heating. x_d is found by knowing initial arc length A_b, the initial radius of curvature R_c, and evaluating ρ, as provided by the Timoshenko formula. It is important to note that Eqn.8 is for the free end point chord line displacement of a pre-curved bimetallic strip that is not subjected to any external axial load.

3.2 General Integration Geometry for Evaluation of the Castigliano

To enable the evaluation of Castigliano's theorem, Egelhoff (2010), it is first necessary to find a relationship between y as a function of angle θ. Fig.3-3 shows an arc portion which is part of a true circle, with a chord line *ab* equal in length to chord length *L*, which was described in the previous section. It should be noted that the chord line *ab* for this segment does not necessarily coincide with the circle centre line, or the circle diameter, and that it is a relatively shallow arc.

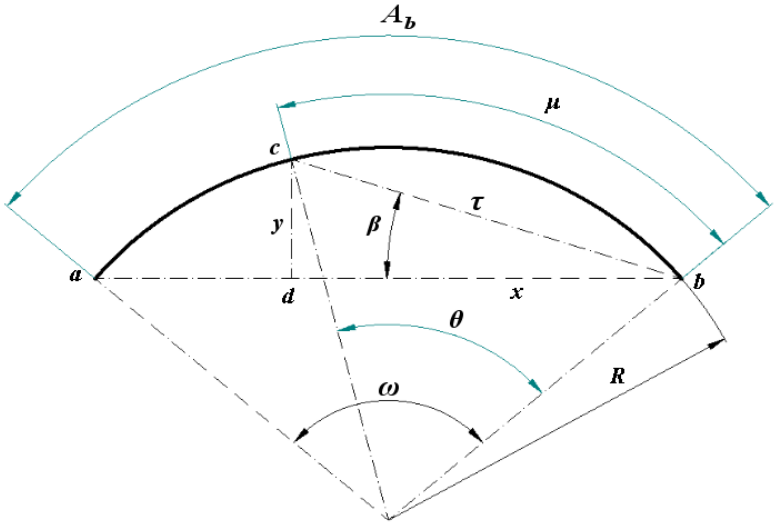

Fig.3-3 General geometry of a strip for *y* as a function of *R*, θ and ω.

From Fig.3-3, it can be seen that vertical line *cd* equates to length y which is given by:

$$y = \tau \ sin\beta \quad \text{Eqn. 9}$$

Using Catia, Dassault (2014), in the design sketcher environment, a relationship was established that links angle β to angle θ and total angle ω. This relationship was tested for a variety of values of arc $A_{b,}$ angle β, and angle ω, and was found to hold true for all values tested that in general:

$$\beta = \frac{(\omega - \theta)}{2} \quad \text{Eqn. 10}$$

where β is the angle between line τ and the *ab* axis.

A relationship between line τ and angle θ is now required.

From Fig.3-3, the general chord line length *a* to *b* was previously described by length $L = 2Rsin(\frac{\omega}{2})$; therefore equally, for chord line length *cb*, over arc length μ, the chord length $\boldsymbol{\tau}$ can be written as:

$$\tau = 2R\ sin(\frac{\theta}{2}) \quad \text{Eqn. 11}$$

From the standard trigonometric identity for half-angles relationships, Davies (1982)

$(\sin x)^2 = \frac{1}{2}(\cos 2x)$ and using $(\sin x)^2 + (\cos x)^2 = 1$

It can be shown that by rearrangement and substitution with $x = \frac{\theta}{2}$ that

$$sin\left(\frac{\theta}{2}\right) = \sqrt{\frac{1-\cos\theta}{2}} \qquad \text{Eqn.12}$$

Squaring each side, and multiplying each side by 2,

$2\ sin^2(\frac{\theta}{2}) = (1 - cos\ \theta)$, and by multiplying both sides by $2R^2$ the expression becomes $4R^2\ sin^2\left(\frac{\theta}{2}\right) = 2R^2(1 - cos\ \theta)$.

If $\tau^2 = 4\,R^2\ sin^2(\frac{\theta}{2})$, this becomes $\tau^2 = 2R^2(1 - cos\ \theta)$

or $$\tau = \sqrt{2R^2\big(1 - cos(\theta)\big)} \qquad \text{Eqn.13}$$

where; R is the radius of curvature of the segment of arc μ subtended by angle θ in radians.

Substituting equations Eqn.10 and Eqn. 13 into Eqn.9, therefore:

$$y = \sqrt{(2R^2\big(1 - cos(\theta)\big)}\ .\ \sin\left(\frac{\omega-\theta}{2}\right) \qquad \text{Eqn. 14}$$

which presents the general perpendicular height ordinate y to arc μ as a function R and angles θ and ω.

Similarly:

$$x = \sqrt{(2R^2\big(1 - \cos(\theta)\big)}\ .\ \cos\left(\frac{\omega-\theta}{2}\right) \qquad \text{Eqn. 15}$$

where x is the general distance along the chord ab to the y perpendicular.

and θ is the angle of the sector which intersects the y perpendicular.

ω is the total angle of the arc length A_b.

R is the general radius of curvature of the arc.

It should be noted that Eqn.14 and Eqn.15 are equations that have been proven to hold true for all radii of curvature and not just for shallow arcs and thus are new general formulae.

The y variable just derived, is dependent only on the angles θ, ω, and radius R, and is used in the next section to evaluate Castigliano's theorem to establish the force deflection relationships of the pre-curved bimetallic strip.

3.3 Castigliano's Theorem - Derivation using Simple Bending Theory

Castigliano's theorem for beams is also referred to by Hibbeler (2006), is used for the evaluation of the deflection of the pre-curved bimetallic beam subjected to axial loading along the chord line. The deflection is along the line of action of the applied external force. Because the chord line of the arc does not coincide with the diameter of a circle, the integration becomes more complex than for integrating the full semi-circle quadrant loading case.

The following assumptions were made:

- The bimetallic strip behaves the same as a solid curved beam of a single material under bending.
- The bimetallic strip's radius of curvature is large as compared with the total thickness of the strip a ratio of 100:1 or greater, is assumed.
- As a result of the high ratio of curvature to the strip cross section, the cross section stresses are considered negligible and only the bending strain is significant.

The Castigliano energy theorem states that: $\delta = \frac{\partial u}{\partial P}$ likewise $\theta = \frac{\partial u}{\partial M}$

Where δ is the deflection as a result of force *P* along the line of action of *P*.

θ is the angular deflection as a result of a moment M.

$\frac{\partial u}{\partial P}, \frac{\partial u}{\partial M}$ are the partial derivatives of the internal strain energy u of the system with respect to P and M.

For a linear elastic system, where Hooke's law applies, Freudenberger (2009), for any curved beam using the established relationship: arc = radius x angle (in radians), thus

$S = R\theta$.

where *S* is the arc length of the beam.

R is the radius of curvature.

θ is the angle subtending length *S*.

From the well-recognised and established simple bending theory equation;

$\frac{\sigma}{y} = \frac{E}{R} = \frac{M}{I}$, just using the last two terms, re-arranging $\frac{1}{R} = \frac{M}{EI}$ and considering small elements and substituting $ds = Rd\theta$ or $\frac{ds}{d\theta} = R$ then

$\frac{d\theta}{ds} = \frac{M}{EI}$; and re-arranging this becomes; $d\theta = \frac{M}{EI} ds$.

Manipulating the partial fractions $\frac{\partial u}{\partial P}, \frac{\partial u}{\partial M}$ to obtain $\frac{\partial M}{\partial P}$

$\frac{\partial M}{\partial P} = \frac{\partial M}{\partial u} * \frac{\partial u}{\partial P}$ or $\frac{\partial M}{\partial P} = \frac{1}{\theta} * \delta$ and considering small displacements and elements $d\delta$ and $d\theta$, re-arranging this becomes:

$d\delta = \frac{\partial M}{\partial P} * d\theta$ then substituting for $d\theta = \frac{M}{EI} ds$ derived previously,

which becomes $d\delta = \frac{\partial M}{\partial P} * \frac{M}{EI} ds$ tidying up and integrating both sides,

$\int d\delta = \frac{1}{EI} \int \frac{\partial M}{\partial P} M * ds$ after integrating both sides this becomes:

$$\delta = \frac{1}{EI} \int_0^L \left(\frac{\partial M}{\partial F} \right) . M . ds \quad \text{Eqn.16 Hibbeler (2006) (Wright, 2013)}$$

This is the general form of Castigliano's energy theorem for deflection in beams.
When substituting *F* for *P*. Eqn.16 provides the general deflection δ of a beam for an applied load *F*, assuming *EI* is constant along the entire length of beam.

where E is the Modulus of the beam material, average of two bimetallic strips.

I is the Moment of inertia of the beam section.

$\frac{\partial M}{\partial F}$ is the partial derivative of *M* to applied load *F* in the direction of the load.

M is the applied moment to the beam.

ds is the incremental element along the beam.

δ is the deflection due to applied force *F* in direction of that load.

3.4 Application of Castigliano Theorem to obtain Loaded Displacement

In Fig.3-4, the bimetallic strip is assumed to have an in plane rotational degrees of freedom at each end, and is externally loaded along the chord line by force *F*. The general Castigliano expression previously derived is used to evaluate the chord line deflection δ as a result of the axial load force *F*. A free body diagram of the bending moment at any section *x* distance along the chord line, is shown Fig. 3-5. From the free body diagram, the moment equation necessary for the evaluation of the integral of Castigliano's formula is obtained. It should be noted that the application of force *F* is along the chord line of an arc of a circle that is not necessarily at the diameter of a circle, thus the need for deriving the general *y* vs. θ relationship previously.

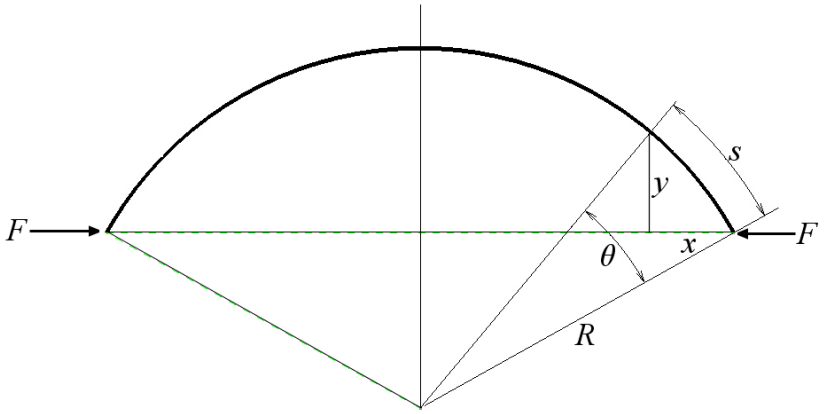

Fig.3-4 Geometry of bimetallic strip subjected to axial load F

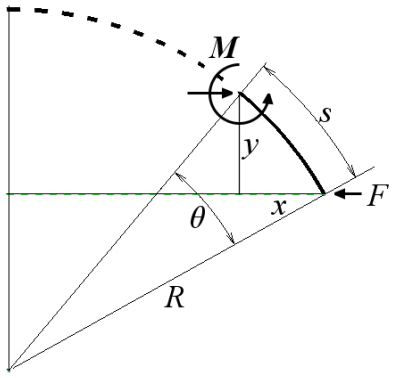

Fig.3-5 Free body diagram of the curved strip under external load F.

From Fig.3-5, the equilibrium moment M equals; $M = F.y$

For any circle, arc = radius x angle, considering the section at y; $S = R * \theta$ and thus by ratio it follows, for a small element, $ds = R\,d\theta$

Taking the partial derivative of the moment , $\frac{\partial M}{\partial F} = y$,

Thus; $\delta = \frac{1}{EI}\int_0^L \left(\frac{\partial M}{\partial F}\right).M.ds$ is substituted with $\frac{\partial M}{\partial F} = y$; $M = F.y$; and $ds = R\,d\theta$, to become:

$\delta = \frac{1}{EI}\int_0^L y.(F.y).R.d\theta$ and then changing the length of beam L in terms of angle of arc θ;

This reduces to $\delta = \frac{FR}{EI}\int_0^\theta y^2\,d\theta$ and remembering that the general relationship of y as a function of angle θ was derived previously, i.e.;

$y = \sqrt{(2R^2(1 - cos(\theta))}\,.\,sin\,(\frac{\omega-\theta}{2})$

Therefore the integral becomes:

$$\delta = \frac{FR}{EI}\int_0^{\theta}[\sqrt{2R^2(1-cos(\theta))}.sin\left(\frac{\omega-\theta}{2}\right)]^2 \ d\theta$$

Simplifying the integral and re-arranging:

$$\delta = \frac{2FR^3}{EI}\int_0^{\omega}(1-cos(\theta)).sin\left(\frac{\omega-\theta}{2}\right)^2 \quad \text{Eqn. 17}$$

After integrating Eqn.17, Eqn.18 is the ambient temperature deflection formula as a function of F, R, E, I and ω. Replacing Young's modulus *E* of a homogenous beam, with the average value in a bimetallic strip, E_a, thus:

$$\delta = \frac{2FR^3}{E_a I}\left[\frac{\omega}{2} - \frac{3\sin(\omega)}{4} + \frac{\omega*\cos(\omega)}{4}\right] \quad \text{Eqn. 18}$$

where

δ is the total displacement due to load *F*, in the direction of *F*

E_a is the averaged modulus of both metals of the bimetallic strip

F is an externally applied axial load along the chord line.

I is the Moment of Inertia of section of strip.

R is the radius of curvature of the bimetallic strip at ambient temperature.

$A_{b,}$ is the total arc length of the bimetallic strip.

$\omega = \frac{A_{b,}}{R}$ total angle of the entire arc length A_b.

By re-arranging Eqn.18 in terms of *F*, two values of force can be obtained.

The equilibrium force to maintain the displaced radius of curvature at ambient temperature is given by:

$$F_\delta = \frac{E_a I\,\delta}{2R^3[\frac{\omega}{2}+\frac{1}{4}(\omega\,cos(\omega)-3\,sin(\omega)]} \quad \text{Eqn. 19}$$

where F_δ is the equilibrium force at displacement δ. See Fig. 3-6

All other variables were previously stated.

The force developed by a pre-curved bimetallic strip subjected to heating is obtained as a function of the displacement x_d which was provided earlier. As this force is developed by the heating of the bimetallic strip, and is a function of a temperature difference, the radius of curvature used must reflect the change in temperature from the ambient, thus here, *R* must be replaced by $R_{h.}$. Also note that for the force as a function of temperature, x_d replaces δ in the temperature induced force expression.

Thus:

$$F_h = \frac{EIx_d}{2\,{R_h}^3[\frac{\omega_h}{2}+\frac{1}{4}(\omega_h cos(\omega_h)-3\,sin(\omega_h)]} \quad \text{Eqn.20}$$

where F_h is the temperature induced force generated by the bimetallic strip.

x_d was evaluated by Timoshenko previously.

R_h is the radius of curvature from heating above ambient temperature.

$\omega_h = \frac{A_{b,}}{R_h}$. total angle of the entire arc length A_b due to R_h.

It is important to note that the displacements for Eqn.19 and Eqn. 20 are obtained from the pre-curved position. The pre-curved geometry of the bimetallic strip is defined as a bimetallic strip that is permanently deformed into a radius of curvature equal to R_c with an angle subtending the arc $A_{b,}$ denoted by ω_c. The corresponding chord length is equal to L_c, see Fig. 3-6. A further point to note is that the ambient displaced radius of curvature R changes in value from R_c as it is displaced by the distance δ. In later sections, new formulae are introduced that compensate for the change in radius of curvature as a function of displacement δ. For this reason, the Castigliano derived formulae of Eqn.19 is only applicable and useful for relatively small displacements of δ.

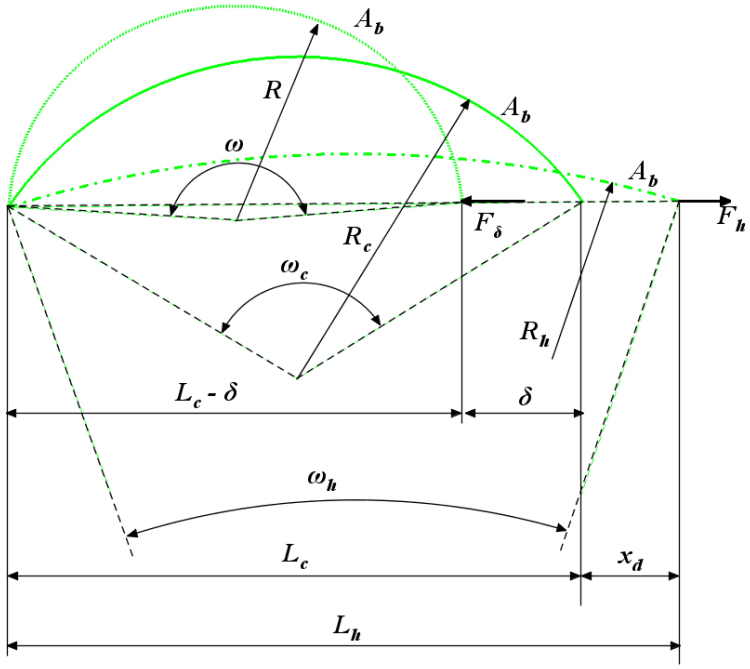

Fig.3-6 Force vs. displacement geometry from pre-curved position

3.5 Net Loaded Displacement - Combined Heating and Loading Case

To find the net loaded displacement of the strip when being subjected to uniform heating requires the application of the principle of superposition. The derivation of the axial force versus deflection by the curved bimetallic strip is dependent on the following assumptions:

- the curved bimetallic strip is freely pivoted at both ends, i.e. not a cantilever beam.
- the strip is uniformly heated along its total length.
- the radius of curvature of the strip is very large when compared to its thickness.
- the strip's radius of curvature remains approximately circular throughout the heating process.

By the principle of superposition, the bimetallic strip is considered to be subjected independently to an external force, and then to an applied heat load. By the superposition mechanism, both loading effects are added to produce the effects of the combined loading case. From this case, it is possible to ascertain the net loaded displacement *X* of the strip whilst being subjected to combined heating and an applied load *F***.**

In Fig.3-7 at position *1***,** the initial unheated pre-formed curved strip is shown.
At position *2***,** the strip is loaded by an external force, *F***,** and the strip deflects by a distance δ.
At position *3,* heat is uniformly added to the strip and it extends to distance L_h.
At position *4,* the loaded distance δ , is subtracted from distance L_h , to obtain the net loaded displacement *X*. Displacement *X* is the result of a combined load *F* and heat applied to the strip.
See Fig.3-7 for the superposition geometry:

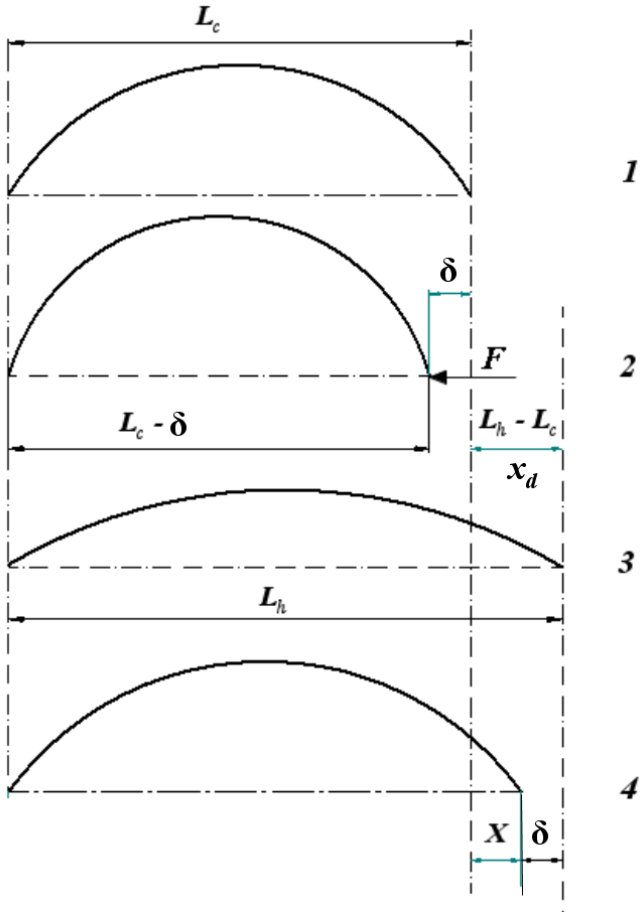

Fig.3-7 Net displacement *X* of strip loaded by force *F* & heating combined

Thus for any externally applied static load F, the net loaded displacement X for any temperature differential ΔT experienced by the strip is given by:

$$X = x_d - \delta \qquad \text{Eqn. 21}$$

Rewriting the full expression to include all the terms, thus:

$$X = \{2\left(\frac{\rho R_c}{\rho - R_c}\right) sin\left(\frac{A_b(\rho - R_c)}{2\rho R_c}\right) - 2R_c\, sin\left(\frac{A_b}{2R_c}\right)\} - \{\frac{2FR^3}{E_a\, I}\left[\frac{\omega}{2} - \frac{3sin(\omega)}{4} + \frac{\omega * cos(\omega)}{4}\right]\}$$

Eqn. 22

where X is the net displacement from initial ambient position L_c .

For any application of Eqn. 22, it is normal to know initial values of R_c, A_b, E_a, I, α_2 & α_1 , T, T_0 , ω, from which other values such as ρ and R_h can be calculated.

Therefore, using Eqn. 22, it is possible to evaluate the net loaded displacement *X* of a curved bimetallic strip subjected to a combined axial load *F* and a heat differential equal to (T – T_0).

A simulation of the formulae derived is provided in Chapter 4, section 4.1

3.6 Calculation of the Permissible Displacement of a Pre-curved Strip

In order to prevent the over-straining of a pre-curved bimetallic strip when axially loaded and deflected along its chord line, calculation to determine the safe chord line displacement is required. The value of the permissible displacement is the maximum the strip can be displaced along its chord line without causing plastic or permanent deformation damage to the strip. The derivation takes the form of two parts, the first part establishes the safe chord line displacement $x_{\sigma b}$ when compressing the initially flat and nearly straight bimetallic strip, to form a shallow arc of a large radius of curvature, see Figure 3-8 case 1. The second part of the derivation, case 2, is the maximum permissible displacement from the pre-curved position.

Case 1

The assumption for case 1 is that the bimetallic strip is very thin with a high ratio of length to thickness greater than 100:1. Case 1 assumes that the strip is slightly pre-curved with a very large radius of curvature to thickness ratio, again 100:1 or over. This initial configuration therefore, is not a case for applying Euler's Munday (1982) buckling equation for instability of slender columns. With the application of a force F_a, the strip is inclined to bend into an arc of a circle $R_{\sigma b}$. The first derivation for case 1, enables the calculation of the amount of displacement that the strip can be displaced to, i.e., $x_{\sigma b}$, before reaching the elastic limit of the material of the strip.

For case 1, the bending from nearly flat is shown in Figure 3-8, at 1, from simple bending theory;

$\frac{\sigma}{y} = \frac{E}{R} = \frac{M}{I}$ shown previously, using the first two terms thus:

$$R_{\sigma b} = \frac{t\, E_a}{2\, \sigma} \quad \text{Eqn. 23}$$

where

$R_{\sigma b}$ is the radius of curvature limited by the permissible stress of the bimetallic strip and is taken from an initially flat straight strip.

σ is the permissible bending stress as specified by the bimetallic strip manufacture. This stress value is normally supplied by the manufacture of the bimetallic strip.

$y = \frac{t}{2}$ where t is the total thickness of the bimetallic strip.

E_a the average value of Young's modulus of both metals in the strip.

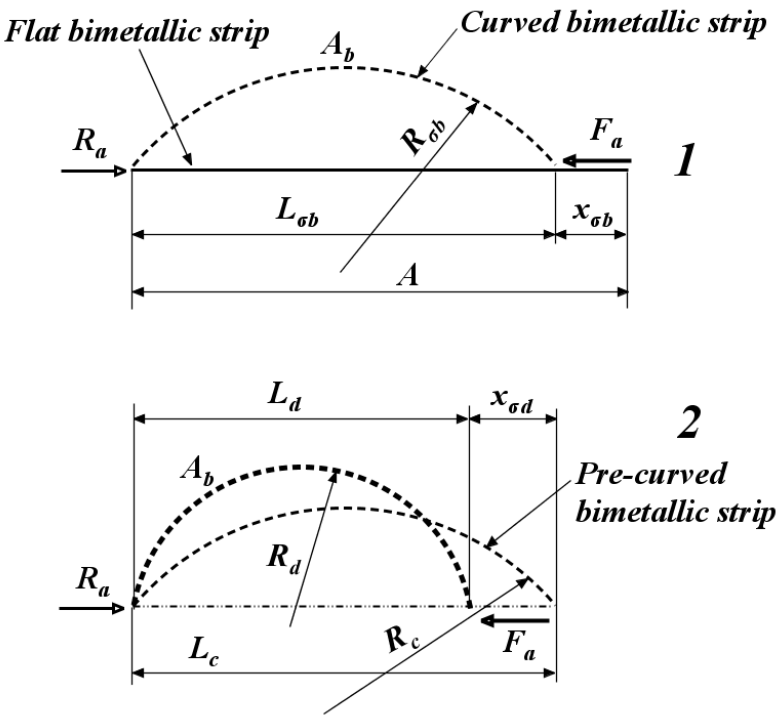

Fig.3-8 Permissible bending as a function of chord line displacement

Previously the general chord length of pre-curved strip was given by:

$$L = 2R\ sin\left(\frac{A_b}{2R}\right)$$

Therefore writing the chord length in terms of permissible bending stress σ:

Hence: $L_{\sigma b} = \frac{t\,E_a}{\sigma}\ \ sin\left(\frac{\sigma\,A_b}{t\,E_a}\right)$ thus:

$$x_{\sigma b} = A - [\frac{t\,E_a}{\sigma}\ \ sin\left(\frac{\sigma\,A_b}{t\,E_a}\right)] \quad \text{Eqn. 24 case 1}$$

Here the assumption is that $A = A_b$, that is the flat length of strip A equals the arc length A_b.

Eqn.24, case 1, evaluates the permissible displacement $x_{\sigma b}$ that avoids over stressing the bimetallic strip as it forms into a radius of curvature equal to $R_{\sigma b}$ coming from an initially, near straight, bimetallic strip.

Case 2

The second derivation, case 2, assumes that the bimetallic strip is already permanently formed into a radius of curvature R_c after having been worked plastically to achieve the pre-curved condition, (see Figure 3-8, case 2). Starting from the pre-curved radius of curvature R_c and applying a chord line force F_a which is reacted at the fixed end of the

strip by R_a, the second formula establishes the maximum safe displacement $x_{\sigma d}$ from the pre-curved state, before reaching the yield point of the material.

For the second case, where the maximum chord line displacement is required from a pre-curved bimetallic strip, it is necessary to use the initial theoretical bend from flat, stress limited radius of curvature $R_{\sigma b}$, as the starting point for the bend from the pre-curved condition.

It is important to note that there are two entirely different expressions that can be used to obtain the new radius of curvature $R_{d.}$. The first formula has been previously stated in the subtraction form, i.e. $R_h = \frac{\rho R_c}{\rho - R_c}$ from shown in an earlier section.

For the new radius of curvature R_d, limited by permissible the stress is given by:

$$R_d = \frac{R_{\sigma b} R_c}{R_{\sigma b} + R_c} \quad \text{Eqn. 25}$$

Equation 25 is formed by adding the reciprocals of the radii of curvature, thus $R_d = \frac{1}{R_{\sigma b}} + \frac{1}{R_c}$. It is important to note that by re-arranging the order and subtracting the reciprocals as stated earlier, a larger radius of curvature from the initial R_c, can also be obtained, i.e. $\frac{1}{R_e} = \frac{1}{R_c} - \frac{1}{R_{\sigma b}}$ or

$$R_e = \frac{R_{\sigma b} R_c}{R_{\sigma b} - R_c} \quad \text{Eqn.26}$$

where

R_e is the new stress limited radius of curvature as a result of an axial extension.

Eqn.26 is used if the direction of the applied force F_a was reversed, i.e. extending the pre-curved bimetallic strip by distance $x_{\sigma d}$ along the chord line axis.

The second method to evaluate R_d is more complicated since it requires the evaluation of additional intermediate formulae as a function of the geometry of the strip. The second method is included as verification of the first method, see Fig.3-9.

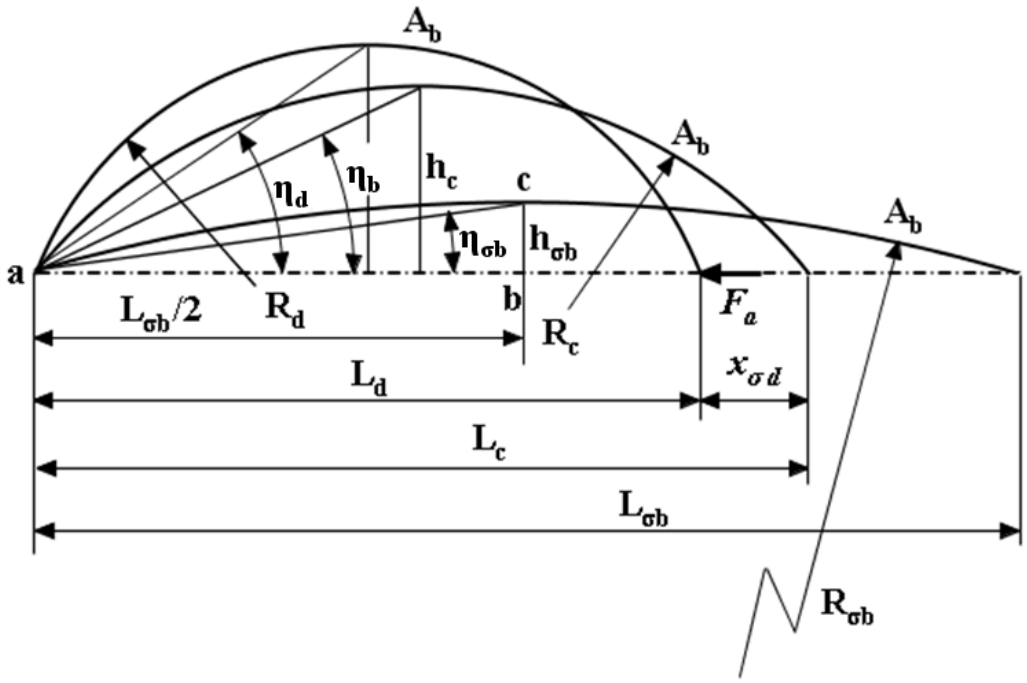

Fig.3-9 Geometry for the evaluation of R_d as function of $R_{\sigma b}$ and R_c

The second method relies on the fact that the arc geometry formed as a function of the stress limited radius of curvature, $R_{\sigma b}$, is the maximum bend geometry that can safely be achieved within the elastic limits of the material, this was stated previously in an earlier section. Therefore considering Δabc in Fig.3-9, angle $\eta_{\sigma b}$, given that $R_{\sigma b}$ was evaluated previously, thus:

$$\eta_{\sigma b} = \tan^{-1}\left(\frac{2\,h_{\sigma b}}{L_{\sigma b}}\right) \quad \text{Eqn. 27}$$

where $h_{\sigma b} = R_{\sigma b}\left(1 - \cos\left(\frac{A_b}{2R_{\sigma b}}\right)\right)$ and $L_{\sigma b} = 2R_{\sigma b}\sin\left(\frac{A_b}{2R_{\sigma b}}\right)$.

Hence angle $\eta_{\sigma b}$ is the stress limited angle as a function of $R_{\sigma b}$.

Likewise angle η_b can be expressed as:

$\eta_b = \tan^{-1}\left(\frac{2\,h_c}{L_c}\right)$ where it follows that: $h_c = R_c\left(1 - \cos\left(\frac{A_b}{2R_c}\right)\right)$ and

$L_c = 2R_c\sin\left(\frac{A_b}{2R_c}\right)$ was shown previously.

The new angle η_d is obtained by adding the stress limited angle $\eta_{\sigma b}$ to η_b.

Thus: $\eta_d = \eta_b + \eta_{\sigma b}$.

It can be shown that in general: $\eta_a = \frac{A_b}{4\,R}$ in radians.

Thus the new radius of curvature is:

$$R_d = \frac{A_b}{4(\eta_b + \eta_{\sigma b})} \quad \text{Eqn. 28}$$

where:

$\eta_{\sigma b}$ as per Eqn.27.

η_b, as per shown earlier .

η_a is the general internal angle to the chord height from chord line axis.

A_b , has been stated previously.

Either Eqn.25 or Eqn.28 can be used for the value of R_d, but Eqn. 25 is quicker to use since there are less equations to evaluate on the way.

A simulation and verification of the formulae follows in Chapter 4, section 4.2.

3.7 Modification to Young's Modulus for Bimetallic Strip

Timoshenko in the derivation of the bimetallic bend radius formula, assumes that the Young's modulus of a bimetallic strip is taken as the average of the individual modulus of each metal making up the strip.

This is a fair assumption if each thickness of strip is equal e.g. Invar 36 = 0.2mm thick and Copper = 0.2mm thick. However if the two metals within the strip are of different thicknesses, a more accurate way of accessing the combined Young's modulus of the bimetallic strip must take into account the value of each Young's modulus combined with the thickness of each strip as a ratio.

Let $t_p = t_i + t_m$ the sum of the thicknesses of the bimetallic strip

and t_i is the thickness of the Invar 36 side.

t_m is the thickness of the other mating material side.

E_i is the Young's modulus of the Invar 36 metal of the strip, while

E_m is the Young's modulus of the other metal of the strip.

Then by thickness ratio :

$$E_p = \frac{t_m}{t_p} E_m + \frac{t_i}{t_p} E_i \quad \text{Eqn. 29}$$

where E_p is the ratio modified combined Young's modulus.

Note that because Invar 36 possesses a very low coefficient of linear thermal expansion as compared with all other engineering materials, it is predominantly used as one half of virtually all industrially produced bimetallic strip, since per degree change of temperature, it affords the best bimetallic bending performance.

The other material that is commonly mated with the Invar 36, is Nickel steel.

3.8 An Immediate Bimetallic Radius of Curvature Formula

An alternative formula has been derived to enable a close prediction of the radius of curvature of a thin bimetallic strip that at its initial ambient temperature, is both flat and straight, but at above ambient temperature, forms into an arc of a circle. The formula enables the evaluation of the radius of curvature of the strip as a function of heating or cooling. A formula for calculating the radius of curvature of a bimetallic strip already exists, and was produced by Timoshenko. The formula by Timoshenko has been vigorously proven, tried and tested and accepted by others, Krulevitch P (1998), Prasad (1993), the Thermostatic Metal handbook, Uhlig (2007) and the Kanthal handbook Kanthal (2002).The formula introduced by this work, closely approximates to the Timoshenko formula for equal thicknesses of the two mating metals within the bimetallic. The disadvantages of Timoshenko's formula are that it requires many sub-calculations in its application, and also requires the Young's modulus of the two metals making up the bimetallic strip, to enable its evaluation. The formulae put forward in this section are both simple and quick to use, making it more immediate in the evaluation of the radius of curvature as a function of temperature change. For the correlation of the new formula, Timoshenko's formula is used as a datum, or benchmark. From the upcoming simulation an excellent correlation was shown to exist between the Timoshenko generated values and the values generated by the new formula from this section. The limitations of the simplified theory proposed here are that one metal making up the bimetallic strip requires a very low coefficient of linear thermal expansion, e.g. Invar 36, and that both metals are of equal thickness. Invar 36 enables the best bend performance per degree change when coupled with any other engineering metal in the bimetallic strip, and thus this theory is relevant and useful for the majority of applications.

When a bimetallic strip is uniformly heated along its entire length, it will bend or deform into an arc of a circle with a radius of curvature, the value of which, is dependent on the geometry and metal components making up the strip. As will be seen later on, the nature of the bend as a function of temperature change from ambient is characteristically asymptotic.

For the derivation, Fig. 3-10 shows a bimetallic strip in two states of heating, at state *1*, at ambient temperature, the strip will be flat with no discernible radius of curvature *R*. At state *2*, uniformly distributed heating will cause the strip to form into a radius of

curvature. Note that α_2 has a numerically higher coefficient of linear thermal expansion and thus naturally wants to extend further than the side with α_1. The clash between the amounts that each metal can freely extend, leads to internal stresses, forces and bending moments at the material interface, resulting in the bending as shown at state *2*.

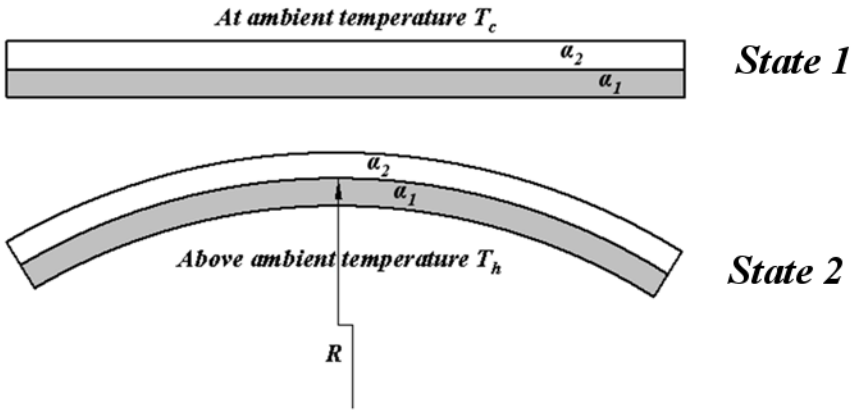

Fig.3-10 Bimetallic strip in two states of of thermal conditions

The derivation is based upon the amalgamation of two well established formulae, with the addition of new correction relationships that are a combination of the ratios, sums, and quotients of the coefficient of linear expansion of the metals.

Where possible, the nomenclature employed in the Timoshenko formula will be used in the new formula.

It is commonly known that the internal force developed within a metal bar by heating or cooling, can be written as follows:

$$F_i = \alpha\ \Delta T\ C_a\ E \qquad \text{Eqn. 30}$$

where; F_i is the force *(N)*

α is the coefficient of linear thermal expansion of the metal ($\frac{10^{-6}}{K}$).

ΔT is the temperature change of the metal from ambient (*K*).

C_a is the cross-sectional area of the bar(m^2).

E is the Youngs modulus of the material of the bar ($\frac{N}{m^2}$).

Eqn.30 can be re-written in terms of the stress, since $\sigma = \frac{F_i}{C_a}$

Thus the internal stress due to heating: $\sigma = \alpha\ \Delta T\ E$

By substitution of $y = \frac{t}{2}$ where y is assumed to be the distance from bi- metal interface to the outer edge, this is also equal to half the total thickness of the bimetallic strip.

From the simple bending equation $\frac{\sigma}{y} = \frac{E}{R} = \frac{M}{I}$ substituting and re-arranging using the first two terms of the simple bending equation, thus ;

$$R = \frac{t}{2\,\alpha\,\Delta T}$$

where R is the radius of curvature of the bimetallic strip to the bimetallic joint center line (mm).

t is the total thickness of the bimetallic strip (mm).

with $\alpha = \frac{\alpha_2 + \alpha_1}{2}$ the average coefficient of linear expansion of both metals $\frac{10^{-6}}{K}$.

Thus

$$R = \frac{\boldsymbol{t}}{(\boldsymbol{\alpha_2 + \alpha_1})\boldsymbol{\Delta T}} \quad \text{Eqn. 31}$$

This is a first order equivalent estimate of the radius of curvature of the strip as a function of change in temperature that approximates to the Timoshenko formula. See Fig.3-11 for the results of plotting the new formula with the same data, next to the Timoshenko formula. The Timoshenko formula is the continous line, and the new theory is shown as the dotted curved.

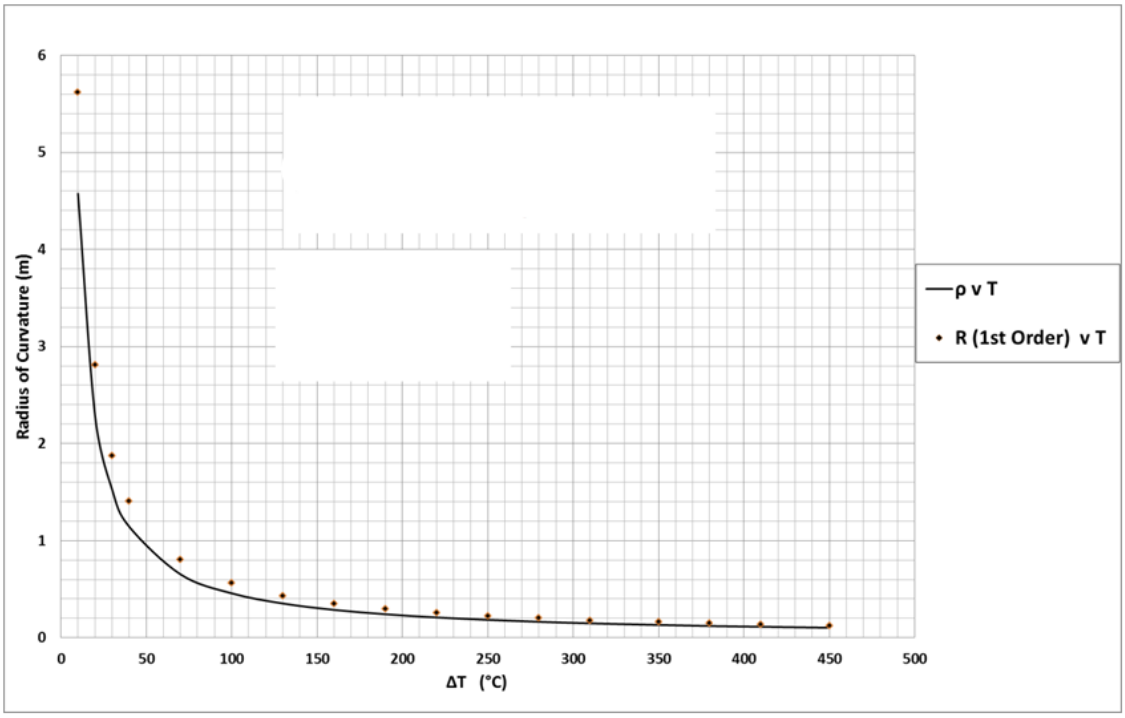

Fig.3-11 Comparison of present study with Timoshenko formula

The simple derivation resulting in Eqn.31 and shown in Fig.3-11, provides a rough or first order estimate of the radius of curvature as a function of temperature change in the strip. It should be noted that although this is a first order approximation to the

Timoshenko formula, the accuracy tends to improve as the temperature increases, or as the expression becomes more asymptotic. Furthermore, the nature the first order derivation, closes resembles the Timoshenko formula and follows a similar trajectory, that of an asymptotic curve.

Using a similar approach to Timoshenko in the original Timoshenko derivation, where the ratios of the thicknesses of the metals and the sum of the thicknesses in the metals, play an influential part of the derivation. In the derivation put forward here, the ratios of the coefficients of linear thermal expansions, sum and differences are used as a correction factor with similar effect that ultimately modifies the first order expression to a close approximation of the Timoshenko formula. The rationale for using the coefficients of linear thermal expansions to correct the first order curve, is based upon the fact that in this derivation, the thicknesses of the two constitute metals are assumed equal for reasons explained earlier.

From Fig.3-11, it can be seen that the radius of curvature of the approximate curve *R*, is slightly larger numerically, than the Timoshenko line. Thus a useful correction factor needs to multiply *R* by a number slightly less than one. Introducing a proportional correction factor reduces the value of *R* to a close approximation of Timoshenko ρ.

Thus letting $\varsigma = \frac{\alpha_1}{\alpha_2}$ and $\phi = 1 - \varsigma$ this provides an initial lowering of *R*.

and also letting $\nu = \alpha_2 + \alpha_1$, and $\varphi = \frac{\alpha_2}{\nu} - \frac{\alpha_1}{\nu}$ be the proportional difference in the coefficients of linear thermal expansions, then the proportional correction influence on *R* is:

$$\varphi = \frac{\alpha_2 - \alpha_1}{\alpha_2 + \alpha_1} \qquad \text{Eqn. 32}$$

Eqn.32 is a very effective modifier when multiplied by the Eqn.31 see Fig.3-12 for the close approximation R_φ.

At the same time, the correction must take into account the rapid change of curvature in the lower temperature range of 20°C to 80°C. A further correction factor is achieved if the ratios of the sums and differences are considered, thus letting:

$$\kappa = \frac{\phi}{\nabla} \text{ and } \nabla = \frac{\varphi}{\phi} \quad \text{combining the ratios.}$$

Thus $\kappa = \frac{\phi^2}{\varphi}$ which expands to $\kappa = \frac{\frac{(\alpha_2 - \alpha_1)^2}{{\alpha_2}^2}}{\frac{(\alpha_2 - \alpha_1)}{(\alpha_2 + \alpha_1)}}$

Combining and re-arranging and reducing, thus:

$$\kappa = \frac{(\alpha_2 + \alpha_1)(\alpha_2 - \alpha_1)}{{\alpha_2}^2} \qquad \text{Eqn. 33}$$

The first order expression for R was independently multiplied by correction factors, or coefficients $\kappa, \& \varphi$, the results were plotted in Fig.3-12, which shows the region of the relationship that possesses the greatest rate of change of radius of curvature against change in temperature.

From Fig.3-12, it can be seen that the most effective modifier is when R is multiplied by φ , which is shown as the curve R_{φ}, and that κ only slightly improves on the first order derivation curve, this is shown in Fig. 3-12 as the curve $R_{\kappa.}$

However, when R, Eqn.31, is multiplied by both correction factors $\kappa, \& \varphi$, the resulting curve is an almost perfect fit to Timoshenko's formula as seen in Fig.3-12, the R vs T set of plotted points.

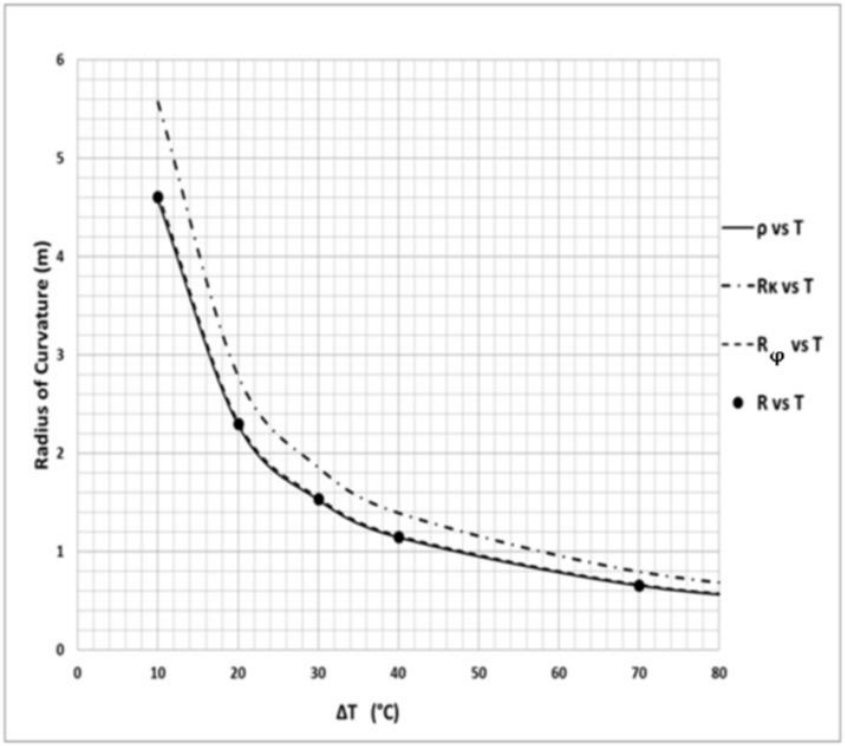

Fig.3-12 Influence of the correction coefficients on R

Therefore adding derived components, φ , κ, to Eqn.31 enhances the accuracy of to that of Timoshenko. Thus the radius of curvature R, as a function of temperature is given by:

$$R = \frac{t\,\varphi\kappa}{(\alpha_2 + \alpha_1)\,\Delta T} \qquad \text{Eqn. 34}$$

From Eqn.34, it can be seen that in this derivation, there is no requirement to know E, the Young's modulus of the two separate metals of the bimetallic strip.

Also Eqn.34 can be also be expressed as:

$$R = \frac{t(\alpha_2 - \alpha_1)^2}{\Delta T(\alpha_2 + \alpha_1)\,\alpha_2^2} \qquad \text{Eqn. 35}$$

The absence of Young's modulus E, limits this theory to having equal thicknesses of the

metals making up the bimetallic strip, and for a close approximation to Timoshenko, the ratio of the values of $\alpha_{2,}$ to α_1 , must be very large. This is the case when one metal is Invar 36 with a very low, α_1 ; thus for good results, you need to ensure that $\alpha_2 \gg \alpha_1$. Thus if $\Omega = \frac{(\alpha_2 - \alpha_1)^2}{(\alpha_2 + \alpha_1)\alpha_2^2}$ this need only be calculated once for any strip as it will be a constant, and finally the formula reduces to just;

$$R = \frac{t\Omega}{\Delta T} \qquad \text{Eqn. 36}$$

where t is the total thickness of the bimetallic strip (m).

ΔT is the change in temperature of the strip from ambient ($^\circ C$).

R is the radius of curvature of the strip (m).

Ω is the correction factors $\varphi, \kappa,$ multiplied by $(\alpha_{2+}\alpha_1)$ ($^\circ C$).

A simulation comparison to Timoshenko is provided in Chapter 4, section 4.3.

3.9 Bimetallic Arc Endpoint Locus Prediction

In addition to the derivation of the theory for the chord line force and displacement case, this research also looks at establishing relationships and formulae to enable the prediction of the free endpoint of a pre-curved bimetallic strip as a function of uniform heating. In this case, the bimetallic strip is fixed against displacement and rotation at one end of the strip whilst the other end is free to move, see Fig.3-13. This work is useful for applications whereby the bimetallic strip is used to touch a sensor in a switching circuit as a function of reaching a specific temperature.

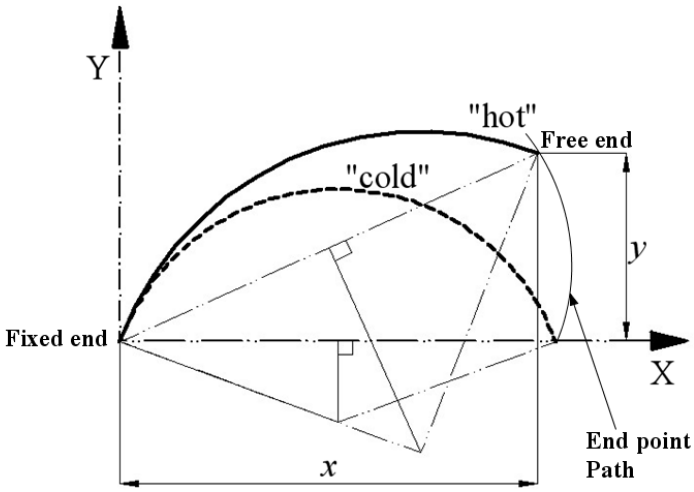

Fig.3-13 x, y, position of heated bimetallic strip

This section enables the derivation of relationships that prediction of the free end point position of a bimetallic strip as a function of heating from the ambient. The output relationships are defined in terms of a Cartesian coordinate system Fig. 3-14 show free endpoint "a" as described within a Cartesian axis system by *x* & y coordinates, and endpoint "o" is rigidly fixed. The relationship required is *x* & y as a function of R_h which is a function of the Timoshenko temperature bending formula.

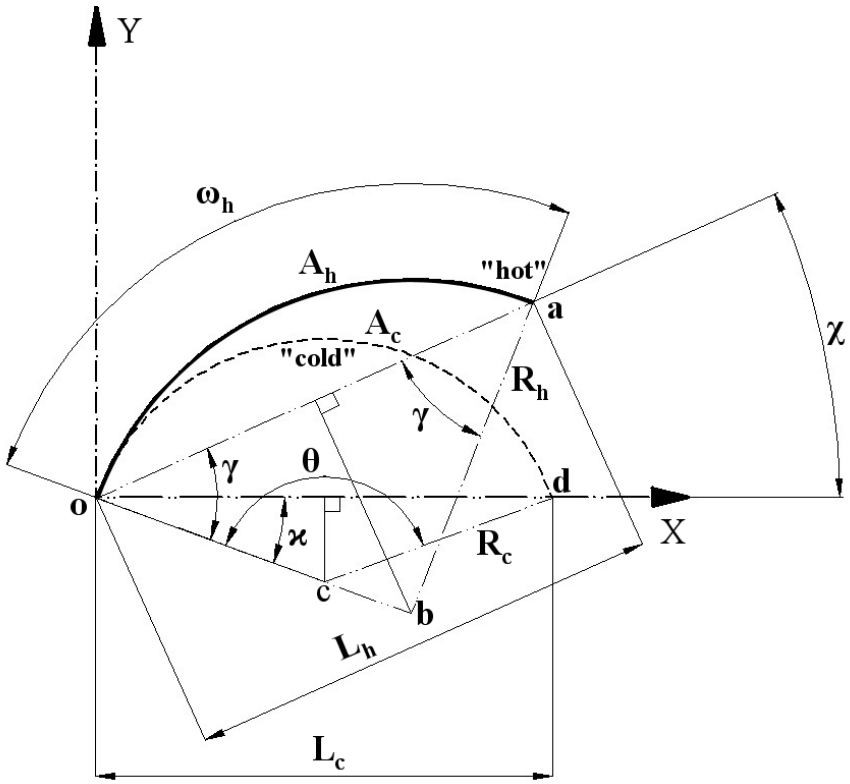

Fig.3-14 End point "a" as function of R_h

From Fig.3-14, two isosceles triangles exist, Δoab and Δodc. From both triangles, the angles up to 180°: $2\gamma + \omega_h = 180°$ and $2\varkappa + \theta = 180$. The third relationship is $\chi = \gamma - \omega_h$.

The previous equation can be re-arranged in terms of $\gamma = 90° - \frac{\omega_h}{2}$ and similarly can be re-arranged in terms of $\varkappa = 90° - \frac{\theta}{2}$.

Substituting this becomes:

Angle $$\chi = \frac{\boldsymbol{\theta}}{\mathbf{2}} - \frac{\boldsymbol{\omega_h}}{\mathbf{2}}$$ Eqn. 37

By substituting the following equations $\theta = \frac{A_c}{R_c}$ and $\omega_h = \frac{A_h}{R_h}$ this becomes:

$$\chi = \frac{A_c}{2}\left(\frac{1}{R_c} - \frac{1}{R_h}\right)$$ Eqn. 38

And thus finally:

$$x = L_h \cos\left(\frac{A_c}{2}\left(\frac{1}{R_c} - \frac{1}{R_h}\right)\right) \quad \text{Eqn. 39}$$

$$y = L_h \sin\left(\frac{A_c}{2}\left(\frac{1}{R_c} - \frac{1}{R_h}\right)\right) \quad \text{Eqn. 40}$$

where $A_c = A_h$ is the arc length of the curved bimetallic strip in (mm).

R_c is the ambient radius of curvature stated previously and initially known.

R_h is the hot radius of curvature calculated by Timoshenko equation.

and where $L_h = 2R_h \sin\left(\frac{A}{2R_h}\right)$ was defined earlier.

When re-arranged, Eqn.42 can be expressed in terms of R_h:

Thus: $$R_h = \frac{A_c * R_c}{A_c - 2\,R_c\,\chi} \quad \text{Eqn. 41}$$

The new R_h formula evaluates the hot radius of curvature as function of the cold radius of curvature R_c when the length of arc A_c and the angle of χ are already known. The geometry and formula introduced predict the unloaded free end of a pre-curved bimetallic strip, however to be more practical as a lifting or switching mechanism, the loaded case is later described in the next section.

3.10 Spatial Prediction of a Bimetal Strip under Combined Loading

The preceding case of section 3.9, enabled the prediction of the free end of the pre-curved bimetallic strip as a function of temperature change from ambient. The output of the calculation was the x and y coordinates of the end point of the free end of the strip. Although this will facilitate the position of the end the of the strip quite accurately, if the function of the free endpoint of the strip is to activate a micro-switch or other tripping device, then the reaction load from the switch or tripping device, must be taken into account. Therefore it is important to be able to evaluate the net loaded spatial position of the end of the strip. When the endpoint of the bimetallic strip is loaded by an external force, the strip will behave as a straight beam and bend accordingly. The following theory describes the combined loading case whereby the pre-curved bimetallic strip is fixed at "*o*" and is free to move at point "*d*", see Fig.3-15. Initially the ambient radius of curvature is R_c, and as the strip is uniformly heated along its entire arc length, it will straighten up as shown previously to reach position "*a*" with a "hot" radius of curvature R_h. With the application of an externally applied load F_a exerting a force in an orientation that is perpendicular to the radius of curvature R_h, the strip will

bend back downwards in accordance with simple beam bending theory. The deflection from point "*a*" to point "*f*" changes the radius of curvature from R_h to R_f. To observe the elastic properties of the strip under loading, simple bending theory is employed to evaluate the maximum deflection of the curved beam along "*oa*". Beam "*oa*" is being subjected to force vector F_n that is acting upon the displaced strip, perpendicular to its chord line "*oa*", see Fig.3-15.

From the simple bending equation, the radius of curvature of a flat bimetallic strip is given as:

$$R_b = \frac{E_a\, I}{F_n\ L_h} \quad \text{Eqn. 42}$$

where:

R_b is the bend from flat as a result of applied input force F_a.

E_a is the averaged Young's Modulus of both metals making up the bimetallic strip.

I is the second moment of area of the strip.

F_n is the normal force to the chord line of the strip and $F_n = F_a \sin(\gamma)$.

and angle $\gamma = \frac{\pi - \omega_h}{2}$.

F_a is the applied input load, normal to the strip (N) at point "a".

$L_h = 2\, R_h \sin(\frac{A}{2\, R_h})$ chord length of hot free strip defined earlier.

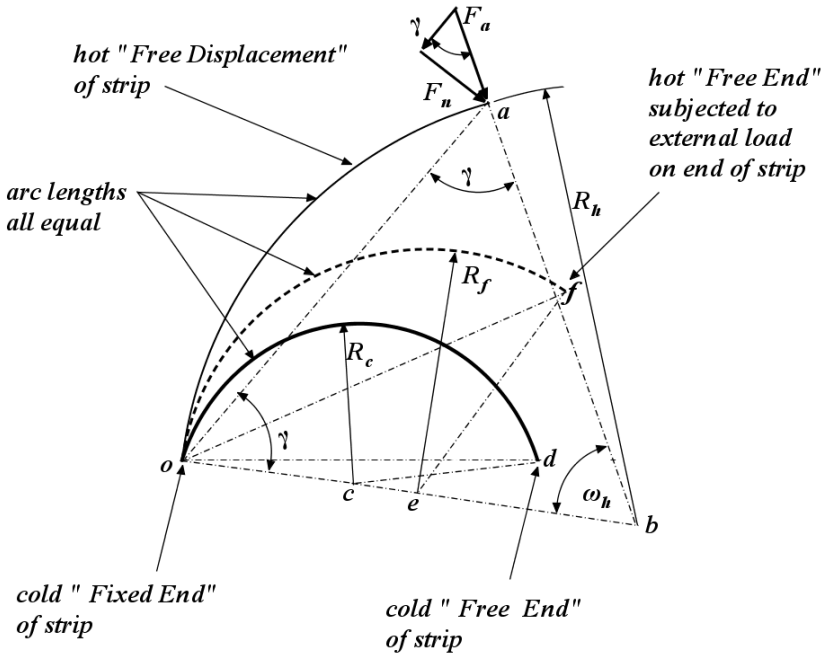

Fig.3-15 Combined loading case of fixed pre-curved bimetallic strip

It is important to note that R_b is the bend from flat as a function of a normal load F_n as considered to be applied to a straight, flat strip.

But the load F_a is applied to a pre-curved beam with radius of curvature R_h, thus a modifier is required to find the radius of curvature R_f which is the loaded radius of curvature from the already pre-curved hot strip R_h .

The modified radius of curvature R_f is found by adding the reciprocals of the bend from flat R_b, to the bend from hot radius of curvature R_h;

Thus from earlier: $$R_f = \frac{R_b R_h}{R_b + R_h} \quad \text{Eqn. 43}$$

Eqn. 43 is the radius of curvature as a function of external load F_a, see Fig.3-15.

As shown previously in the chord line case, as in this case, it is very possible to breach the elastic limit of the bimetallic strip by applying an external load that exceeds the permissible bending stress of the strip.

It is normal to get the permissible bending stress value for most mass produced bimetallic strip from the manufacture's Thermostatic Metal handbook and the Kanthal handbook.

Assume that σ_{bp} is the maximum permissible bend stress value as supplied by the manufacturer.

The maximum radius of curvature from a flat strip limited by stress is defined as:

$$R_\sigma = \frac{tE_a}{2\sigma_{bp}} \quad \text{Eqn. 44}$$

Eqn. 48 is similar to Eqn. 46, but here, the radius of curvature is stress limited.

The stress value evaluated as a function of the applied load F_n is given by:

$$\sigma_a = \frac{F_n L_h t}{2 I} \quad \text{Eqn. 45}$$

where $\frac{t}{2}$ equals half the thickness of the strip, all other values have been stated.

If as a function of the applied load F_n, the calculated value of $\sigma_a < \sigma_{bp}$, the manufacturer recommended permissible stress value, then the strip under the external load F_n will remain within the elastic limit region, or within the limit of proportionality, as defined by Hooke's law Freudenberger (2009).

Therefore if R_σ, the radius of curvature as a function of the maximum permissible bending stress, is substituted for R_b, then the stress limited radius of curvature $R_{d\sigma}$ from the hot free position R_h can be calculated.

Therefore :

$$R_{d\sigma} = \frac{R_\sigma R_h}{R_\sigma + R_h} \quad \text{Eqn. 46}$$

Eqn. 46 enables the calculation of the maximum radius of curvature limited by stress from the pre-curved radius of curvature R_h.

If as a function of an external load F_a, the radius of curvature $R_f < R_{d\sigma}$, then the strip has deformed into a radius of curvature tighter than the permissible limited stress radius of curvature $R_{d\sigma}$. In this case, the strip could exceed the elastic limit of the strip, thus becoming permanently deformed at radius of curvature R_f .

Eqn.46 calculates the combined loading case whereby the pre-curved bimetallic strip is heated and straightens up to end point "*a*" the free hot radius of curvature R_h, then it is externally loaded by load F_a that bends the end point back down to point "*f*". The net loaded, or displaced radius of curvature R_f is then used to find the *x* and *y* ordinates as shown previously for the unloaded case.

A check between the calculated stress σ_a coming from the applied load F_n, and the recommended stress level by the manufacture σ_{bp} must be performed to ensure that the applied load and its associated stress level stays within the elastic limits of the bimetallic strip.

Note if the condition $\sigma_a > \sigma_{bp}$ for an applied loading F_n, then a possible non elastic event may occur, resulting in a permanently deformed strip. If the stresses are higher than the recommend values, the geometry of the strip can be modified to reduce the stresses to within the elastic limit of the bimetallic material.

The new chord length as a function of $R_{f,}$ is given by:

$$L_f = 2\,R_f \sin\left(\frac{A_b}{2\,R_f}\right) \quad \text{Eqn. 47}$$

The net loaded position of the end of the strip at point *f* is given by:

$$x_n = L_f \cos\left(\frac{A_b}{2}\left(\frac{1}{R_c} - \frac{1}{R_f}\right)\right) \quad \text{Eqn. 48}$$

$$y_n = L_f \sin\left(\frac{A_b}{2}\left(\frac{1}{R_c} - \frac{1}{R_f}\right)\right) \quad \text{Eqn. 49}$$

where:

x_n & y_n are the spatial Cartesian ordinates of the end of a loaded pre-curved bimetallic strip that is subjected to combined heating and external loading.

R_f, $R_{c,}$ $A_{b,}$ L_f were all defined earlier.

A simulation verification of the formulae is provided in Chapter 4, section 4.5.

3.11 An Alternative Force vs. Displacement Theory to Castigliano Theorem

The new formulae and relationships introduced in this section are concerned with a pre-curved bimetallic strip that is applied with a force in an axial orientation, that is, along its chord line. A bimetallic strip loaded in this specific orientation, exhibits nonlinear force displacement characteristics. For thin bimetallic strips, whereby the radius of curvature is large compared to the thickness of the strip, the non-linearity tends to be tangent related. The formula put forward in this section enables the evaluation of large chord line displacements but is limited to the permissible stress limits of the material. This work can also be directly applied to thin shallow arc beams of a single, homogeneous material.

The formulae derived in this section are aimed at providing an alternative method of evaluating the force displacement in the shallow arc beam. There are other traditional methods of evaluating the chord line force deflection in thin beams such as covered by Timoshenko (1945) and traditional Euler-Bernoulli beam theory Bauchau and Craig (2009). Additionally, numerical methods can be used that use the finite element mechanism as discussed by Kinyanjui (2007). For the chord line displacement of a pre-curved beam, Castigliano second energy theorem, according to Dalhlberg.T (2004) can be used for shallow arcs, but only for small displacements, due to the inherent limitations of the simple bending theory assumed within its integration.

The underlying geometry of the pre-curved bimetallic strip is shown in Fig.3-16, where the three important radii of curvature are defined. It should be noted that all three arcs are the same length A_b.

The derivation in the following section facilitates the calculation of the radius of curvature to displacement relationship that is crucial in evaluating the force displacement formula shown in later sections.

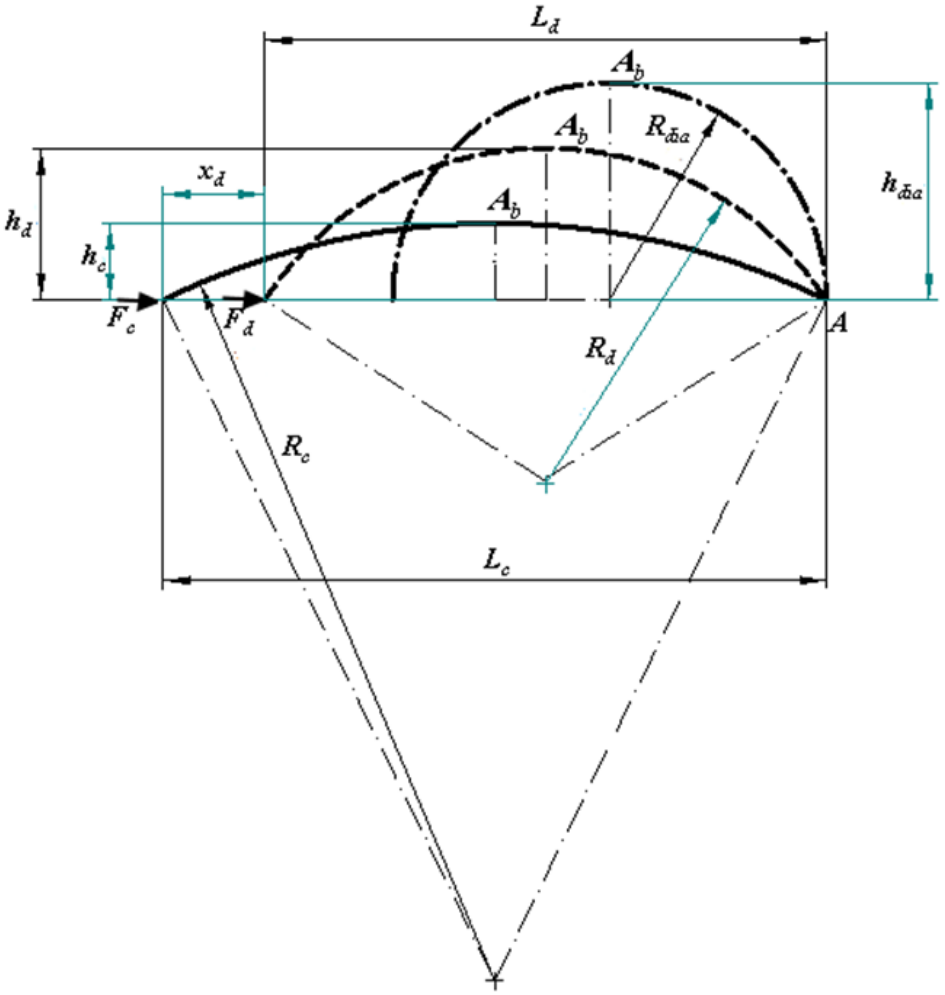

Fig.3-16 Defining force displacement geometry

Castigliano theorem that was mentioned previously, enables the calculations of force vs. displacement, but is limited to small displacements of 1mm or 2mm. This section introduces a mechanism that can cope with much larger displacements, and enables an accurate prediction of the forces when non-linear displacements are found.

From before, the general chord length previously defined in this work as:

$$L = 2Rsin\ (\frac{\theta}{2})$$

where: L is the chord length (mm).

R is the radius of curvature (mm).

θ is the angle subtending the portion of arc A over distance L (radian).

By using the established relationship: arc = radius x angle (in radians), $A = R\,\theta$ and substituting for $\theta = \frac{A}{R}$, angle θ can be eliminated and the length of a chord L as a function of arc length A and radius of curvature R, can be obtained. Denoting the lengths by suffixes, c and d :

Thus; $L_c = 2R_c \sin(\frac{A_b}{2R_c})$

And thus; $L_d = 2R_d \sin\left(\frac{A_b}{2R_d}\right)$

where L_c is the initial pre-curved ambient chord length in (mm).

L_d is the displaced chord length in (mm) as a function of an externally applied load *F*.

From Fig. 3-16, it follows that $x_d = L_c - L_d$ similarly defined previously.

Where x_d is the displacement from the initial position L_c as a result of an applied load *F* (N).

For the evaluation of the force vs displacement relationship, the relationship between displaced radius of curvature R_d and displacement x_d first needs to be established.

Combining the formulae and by substitution:

$$L_c - x_d = 2R_d \sin\left(\frac{A_b}{2R_d}\right) \quad \text{Eqn. 50}$$

But what is actually required is R_d as function of x_d, which is the non-linear influence on the force displacement relationship. From Eqn.50, it can be seen that it is not possible to explicitly express R_d as a function of x_d. The "$\sin(\frac{A_b}{2R_d})$" term can be expanded in the Taylor series:

The general published rule for a sine expansion using Taylor series is published as:

$$sin(x) \approx \sum_{n=0}^{\to\infty} \frac{(-1)^n}{(2n+1)!} x^{(2n+1)} \quad \text{Eqn. 51 Abramowitz (1964)}$$

And thus applying for x:

$$sin(x) \approx x - \frac{x^3}{6} + \frac{x^5}{120} - \frac{x^7}{5040} \quad \text{Eqn. 52 Abramowitz (1964)}$$

Now substituting $\frac{A_b}{2R_d}$ into x and expanding until the 4th term, this becomes:

$$L_c - x_d \approx 2R_d(\frac{A_b}{2R_d} - \frac{1}{6*8}\frac{A_b^3}{R_d^3} + \frac{1}{120*32}\frac{A_b^5}{R_d^5} - \frac{1}{5040*128}\frac{A_b^7}{R_d^7}) \quad \text{Eqn. 53}$$

Terms larger than to the 4th term are ignored due to a negligible change in the accuracy of the solution for this application.

Using the substitution of $\gamma = \frac{1}{R_d^2}$ into Eqn. 53 then simplifying and rearranging it becomes:

$$\frac{A_b^6}{5040*64}\gamma^3 - \frac{A_b^4}{120*16}\gamma^2 + \frac{A_b^2}{6*4}\gamma + \frac{L_c - x_d - A_b}{A_b} = 0 \quad \text{Eqn. 54}$$

Eqn.54 is a cubic equation of the general form :

$$a\,\gamma^3 + b\gamma^2 + c\gamma + d = 0 \qquad \text{Eqn. 55}$$

Eqn. 67 can be solved by finding the discriminant and coefficients in the equation.

The discriminant for a cubic equation is generally published as :

$$\Delta = 18abcd - 4b^3d + b^2c^2 - 4ac^3 - 27a^2d^2 \quad \text{Eqn. 56} \quad \text{Weisstein (2014)}$$

Where *a, b, c, d* are the coefficients and are equal to:

$$a = \frac{A_b^6}{5040*64} \qquad \text{Eqn. 57}$$

$$b = -\frac{A_b^4}{120*16} \qquad \text{Eqn. 58}$$

$$c = \frac{A_b^2}{6*4} \qquad \text{Eqn. 59}$$

$$d = \frac{L_c - x_d - A_b}{A_b} \qquad \text{Eqn. 60}$$

In this particular case we have the condition that $\Delta < 0$ which means that the equation has only one real root and also two complex conjugate roots. Due to physical nature of the results required, only the real root has significance in the required solution of the equation.

The roots of the equation in terms of the coefficients can be solved by the published general formula for solving cubic equations:

$$\gamma_k = -\frac{1}{3a}\left(b + u_k C + \frac{\Delta_0}{u_k C}\right) \qquad \text{Eqn. 61}$$

where

$$c = \sqrt[3]{\frac{\Delta_1 + \sqrt{\Delta_1^2 - 4\Delta_0^3}}{2}} \qquad \text{Eqn. 62}$$

with

$$\Delta_0 = b^2 - 3ac \qquad \text{Eqn. 63}$$

$$\Delta_1 = 2b^3 - 9abc + 27a^2d \qquad \text{Eqn. 64}$$

and

$$\Delta_1^2 - 4\Delta_0^3 = -27a^2\Delta \qquad \text{Eqn. 65}$$

And the three cube roots of unity are therefore:

$$u_1 = 1;\ u_2 = \frac{-1 + i\sqrt{3}}{2};\ u_3 = \frac{-1 - i\sqrt{3}}{2} \qquad \text{Eqn. 66}$$

with $k = 1,2,3$ substituted into Eqn.61.

From experimental test calculations the root γ_2 is the real root that best fits the application requirements. Thus from the earlier substitution of $\gamma = \frac{1}{R_d^2}$ into Eqn.53, by simple rearrangement in terms of radius of curvature, thus;

$$R_v = \frac{1}{\sqrt{\gamma_2}} \qquad \text{Eqn. 67}$$

A simulation follows in the Chapter 4, section 4.6.

3.12 Time vs. Displacement Theory

The time vs. displacement relationship of a single pre-curved bimetallic strip that is subject to uniform heating, is described in this section. It should be noted that the derivation involves many supporting formulae that would best be programmed into an electronic spread sheet such as Microsoft Excel. The fabricated bimetallic strip case will be considered since it encompasses the bespoke bimetallic strip.

Assumptions:

1) Initial heat flow to the internal face of the strip is by the forced convection mechanism normal to the chord line of the bimetallic strip, but acts normal to the surface of material side 1.
2) Boundary layer interactions of the directed heat flow onto the internal surface of the bimetallic strip are ignored.
3) The internal surface of material side 1, of the pre-curved bimetallic strip is entirely uniformly heated.
4) Unimpeded conduction of the heat flow from the first internal material side of the bimetallic to the second outer material[1].
5) Arc length of the strip is assumed to be at the material interface[2].
6) A one dimensional heat flow analysis is considered, with all other directions ignored. [3]

---

[1] this may not fully occur in fabricated bimetallic strip due to minute air gaps arising from manufacturing defects, however in bespoke bimetallic strip with interstitial atomic bonding at the material interface, full heat flow can be assumed.

[2] this may not be the case when the thicknesses of the two metals widely vary, but can be assumed for minute variations of metal thicknesses of a few percent difference.

[3] The accuracy of the theory could be improved, if a two dimensional theory is derived, see further work in chapter 7.

7) The heating of the bimetallic strip is constant irrespective of the radius of curvature of the strip.
8) Assuming no heat losses to the surroundings.

A one dimensional representation and conditions of the model are shown in Fig.3-17.
Previously, a simpler approximate way of defining the radius of curvature as a function a temperature change in a bimetallic strip was given by:

$R = \frac{t\Omega}{\Delta T}$, where $\Omega = \frac{(\alpha_2 - \alpha_1)^2}{(\alpha_2 + \alpha_1)\alpha_2^2}$, t = thickness of strip, ΔT temperature change.

The previously stated R equation will be used in the upcoming time vs. displacement derivation. Previously R as a $f(\Delta T)$ was obtained, so now what is required is ΔT as a $f(t)$, where t is time.
Newton's law of heating and Fourier's one dimensional conduction flow equation are used to formulate the temperature vs. time equation.
Using Newton's law of heating or cooling across the wall thickness of the bimetallic strip and assuming that the surface of material is impeded by forced convective heat flow F_h against side 1, see Fig.3-28.

$$q = m\, c_p\, \Delta T \quad \text{(J)} \quad \text{Eqn. 68}$$

Where:

q is the energy required to raise the temperature in a body with mass (m).

ΔT is the change of temperature between hot and cold states, i.e. $(T_h - T_c)$.

c_p is the specific heat capacity of the material, $(\frac{J}{kg\ K})$.

F_h is the forced convective hot air flow to the surface of material side 1,see Fig.3-17.

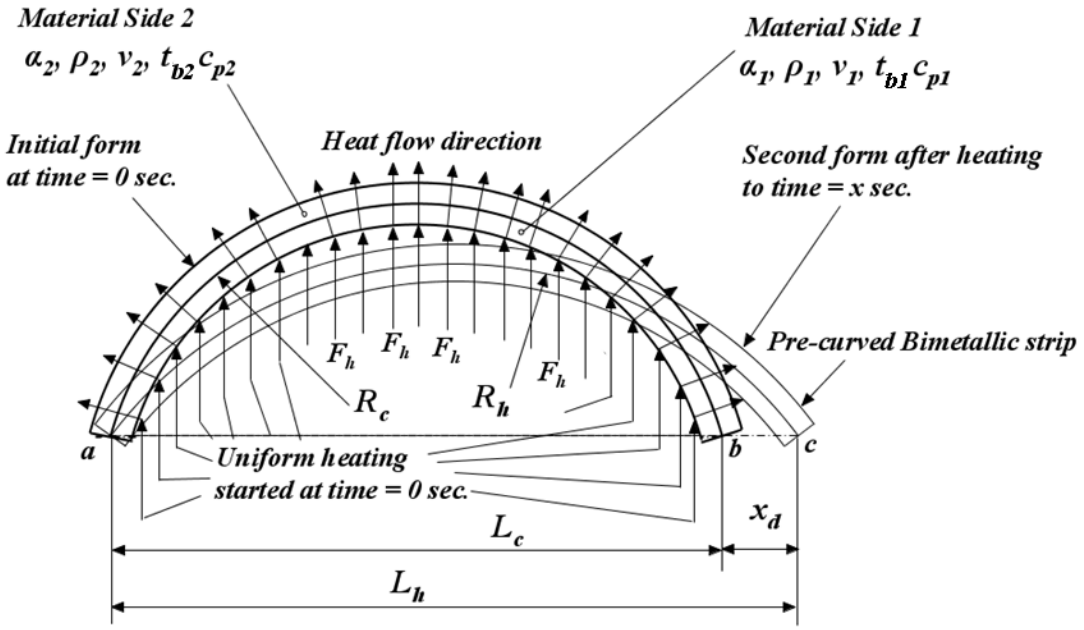

Fig.3-17 Time vs displacement geometry and conditions

The second expression that is used is Fourier's one dimensional flow conduction equation.

$$Q = -k\,A\frac{\Delta T}{t_b} \quad \text{Eqn. 69}$$

where :

Q is the power consumed to heat through area A to depth t_b mm.

k is the thermal conductivity of the material,$(\frac{W}{m\,K})$.

A is the cross-sectional area of the heat flow through the body, (m^2).

t_b is the depth of the body being heated (mm).

T_h, T_c temperatures hot and cold [4] respectively (K).

$\Delta T = T_h - T_c$ is the change in temperature across a discrete thickness of metal.

From Eqn.68, the energy required for each metal within the bimetallic strip can be evaluated, thus:

$q_1 = m_1\, c_{p1}\, \Delta T$ is the energy required to heat material side 1 of the bimetallic strip.

$q_2 = m_2\, c_{p2}\, \Delta T$ is the energy required to heat material side 2 of the bimetallic strip.

The total energy to heat the combined bimetallic strip is thus:

$$q_t = q_1 + q_2 \quad (\text{J}) \quad \text{Eqn. 70}$$

[4] Cold means at ambient temperature, hot means a temperature above ambient.

Since power is defined as work divided by time $\frac{J}{s}$, thus Eqn.69 can be re-written in terms of time with the individual energies for each material of the strip.

Hence from Fourier, the time can be extracted for each individual material side, thus:

$$t_{m1} = \frac{q_1\, t_{b1}}{(T_h - T_c)\, k_1\, A_1} \qquad \text{Eqn. 71}$$

and also:

$$t_{m2} = \frac{q_2\, t_{b2}}{(T_h - T_c)\, k_2\, A_2} \qquad \text{Eqn. 72}$$

Thus the total time to heat through the bimetallic strip is:

$$t_{tm} = t_{m1} + t_{m2} \quad (\text{s}) \qquad \text{Eqn. 73}$$

The power consumed by heating the strip is given by:

$$Q = \frac{(T_h - T_c)\,(m_1 + m_2)(c_{p1} + c_{p2})}{2\, t_{tm}} \text{ (W)} \qquad \text{Eqn. 74}$$

Now substituting for $R = \frac{t\Omega}{\Delta T}$ in Newton's equation:

Thus : $$R_t = \frac{(m_1 + m_2)(c_{p1} + c_{p2})\, t_b\, \Omega}{2Q\, t_{tm}} \quad (\text{mm}) \qquad \text{Eqn. 75}$$

Eqn.75 provides the bend from flat of a straight bimetallic strip as a function of time that is also a function of temperature change and the physical variables of the metal. Note that the average specific heat capacity value is used.

As previously shown, if the starting or pre-formed radius of curvature is R_c, then the strip will form into the new hot radius of curvature by using the aforementioned relationship: $\mathrm{R_h} = \frac{R_c R_t}{R_t - R_c}$ which then enables the hot chord length calculation. Thus from before, $L_h = 2R_h \sin\left(\frac{A_b}{2R_h}\right)$ and $L_c = 2R_c \sin\left(\frac{A_b}{2R_c}\right)$ that yields the displacement relationship as stated before: $x_d = L_h - L_c$. The difference now, is that the distance of chord line extension x_d, is now a function of time as well as a function of heating.

The symbols used in the specific derivations are as follows:

<u>Geometric considerations of material side 1, similar notation for material side 2</u>

$v_1 = w\, t_{b1}\, A_b$ and thus $m_1 = v_1 \rho_1$

where:

v_1 is the volume of metal on material side 1.

t_{b1} is the thickness of the material side 1 of the bimetallic strip.

ρ_1 is the density of the material side 1 of the bimetallic strip.

α_1 is the coefficient of linear thermal expansion of the material side 1 of the bimetallic strip.

m_1 is the mass of the material side 1 of the bimetallic strip.

w is the width of the bimetallic strip.

A_b is the arc length of the strip along the material 1 and 2 interface.

t_t total time to heat through the bimetallic strip.

t_{m1} is the time for the heat to penetrate through material side 1 and reach the material interface with material side 2 .

c_{p1} is the specific heat capacity of the material side 1 forming the bimetallic strip.

Similar variables exist for material side 2, without repeating in terms of side 2.

For material side 2, at time t_{m2} = 0 secs., T_c = ambient temperature. For material side 1 at time t_{m1} = 0 secs, T_c = ambient temperature. As heat is applied as shown in Fig.3-17, a temperature gradient must exist between the outside face of material side 1 that the heating is applied to, and the interface of material side 1 with material side 2. After t_{m1} seconds, heat from material side 1 is transferred to material side 2. After a further; t_{m2} seconds, the temperature of material side 2, assuming no losses, will equal material side 1. After t_t seconds, a homogenous or steady state temperature in the entire bimetallic strip has been reached. It is important to note, that although the bimetallic strip may be at a homogenous temperature, the bending actually starts prior to the steady state temperature being reached.

For the arrangement as shown in Fig.3-17, the coefficient of linear thermal expansion α_1, eg. Copper, is numerically higher than α_2 ,Invar 36. The ideal conditions for bending occur during the transient heating phase where initially, only material side 1 has increased in temperature, and thus the largest heat temperature differential will exist. In very thin bimetallic strip, the response to heating is almost instantaneous, or within a few seconds. The best performance in terms of rate of bending or changing shape of a bimetallic strip can be obtained when the Invar side is kept cool and the other side e.g. Copper is heated up. The theory put forward here, is used in the time vs. displacement correlation that is applied in the evaluations shown in Chapter 6 section 6.3.9.

CHAPTER 4 Verification of Theory and Simulation

Summary

This chapter verifies the theory by simulation techniques. Random sample calculations are part of the simulation techniques.

4.1 Net Loaded Displacement - Verification

The theory of the combined loading case of section 3.5 was subjected to the following simulation:

The bimetallic strip used in the generation of the theoretical data in Fig.4-1 was as follows:

Bimetallic strip length A_b = 80mm**,** thickness of strip: *t = 0.4 mm, 0.2mm* for each metal in the strip.

Radius of curvature at ambient temperature: $R_c = 40mm.$

Average Young's Modulus $E_a = 1.775 \text{ x } 10^{11}\ Pa.$

Moment of Inertia $I = 2.66 \text{ x } 10^{-14}\ m^4$,

Steel; *FeNi20 Mn6* coefficient of linear thermal expansion $\alpha_s = 20 \text{ x } 10^{-6}/K.$

Invar; *Fe64Ni36* coefficient of linear thermal expansion $\alpha_I = 1.85 \text{ x } 10^{-6}\ /K.$

From Fig.4-1 it can be seen that the temperature induced loaded displacements are non-linear in nature, and for a temperature of 200°K, and an external load of 1.6N, the net displacement X is approximately 5.2mm.

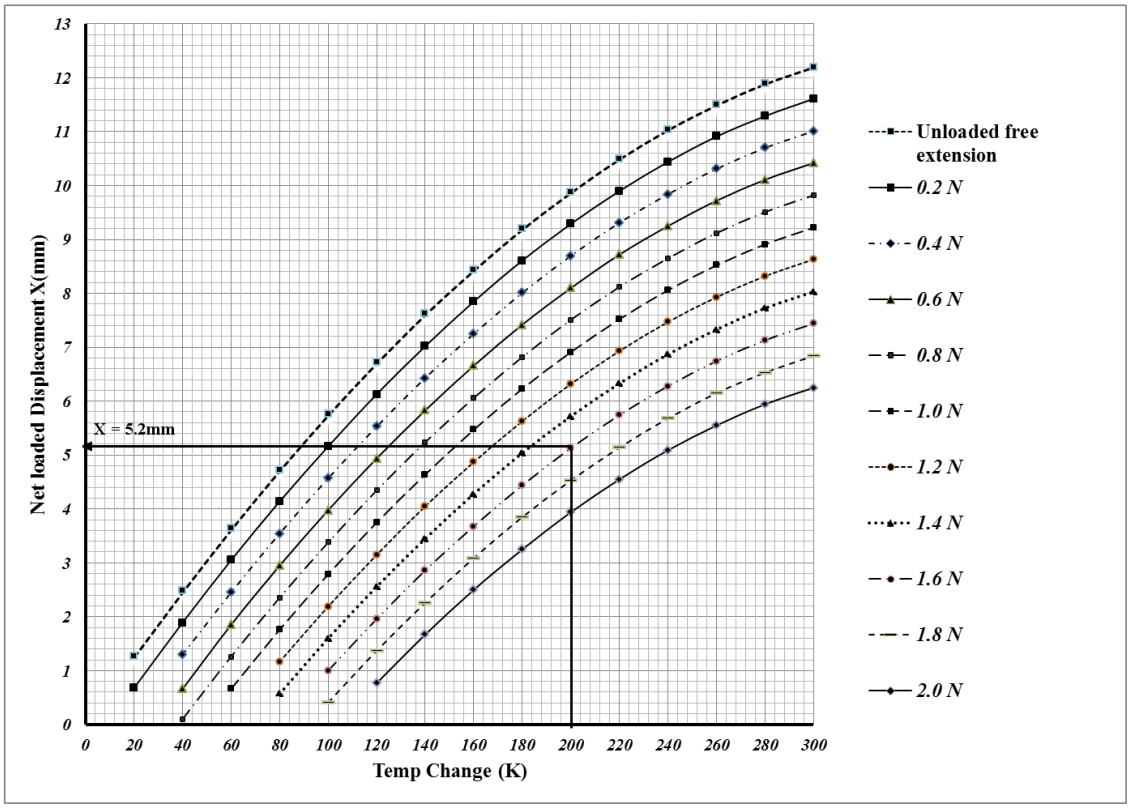

Fig.4-1 Net loaded displacement *X* of bimetallic strip

4.2 Permissible Displacement –Verification

A simulation proof of the permissible displacement now follows to demonstrate that $R_d = \frac{R_{\sigma b} R_c}{R_{\sigma b} + R_c}$ is equal to $R_d = \frac{A_b}{4(\eta_b + \eta_{\sigma b})}$.

The following data was used for the simulation:

$$R_c = 50mm\ ;\ A_b = 100mm\ ; t = 0.4mm;\ E_a = 175Gpa\ ;\ \sigma = 200\text{Mpa}$$

Note: values for E_a and σ are for a bespoke bimetallic strip from page 47 of the Thermostatic handbook Uhlig (2007).

The evaluation was ; $R_{\sigma b} = \frac{t\, E_a}{2\, \sigma}$ = 175 mm the bend from flat value.

$R_d = \frac{R_{\sigma b} R_c}{R_{\sigma b} + R_c}$ = 38.89 mm the stress limited bend from R_c.

For the second method R_d was evaluated as follows:

$h_{\sigma b} = R_{\sigma b}(1 - \cos(\frac{A_b}{2R_{\sigma b}}))$ = 7.094 mm and $L_{\sigma b} = 2R_{\sigma b} \sin\left(\frac{A_b}{2R_{\sigma b}}\right)$ = 98.64 mm

And thus: $\eta_{\sigma b} = \tan^{-1}(\frac{2\, h_{\sigma b}}{L_{\sigma b}})$ = 0.143 radians

$h_c = R_c(1 - \cos(\frac{A_b}{2R_c}))$ = 22.98 mm and $L_c = 2R_c \sin(\frac{A_b}{2R_c})$ = 84.15 mm

Hence $\eta_b = \tan^{-1}(\frac{2\, h_c}{L_c})$ = 0.5 radians

Therefore adding η_b and $\eta_{\sigma b}$: thus $\eta_d = \eta_b + \eta_{\sigma b}$ = 0.643 radians

Using the general relationship $\eta_a = \frac{A_b}{4\, R}$ re-arranging and substituting

Finally as shown earlier, with the alternative formula $R_d = \frac{A_b}{4(\eta_b + \eta_{\sigma b})}$ = 38.89 mm

Therefore the two formulae are equivalent expressions.

Summary of values evaluated in the simulation:

<u>Starting values:</u>

$$R_c = 50mm\ ;\ A_b = 100mm\ ; t = 0.4mm;\ E_a = 175Gpa\ ;\ \sigma = 200\text{Mpa}$$

$h_c = 22.98$ mm; $L_c = 84.15$ mm ; $\omega_b = 0.5$ radians

<u>Displaced values:</u>

$R_{\sigma b} =$ 175 mm ; $R_d =$ 38.89 mm ; $h_{\sigma b} = 7.094$ mm ; $L_{\sigma b} = 98.64$ mm

$\omega_{\sigma b} = 0.143$ radians ; $\omega_d = 0.643$ radians

From the simulation it can be observed that the maximum chord line displacement of the end of the strip, limited by permissible bending stress was $L_{\sigma b} - L_c = 14.49\ mm$. An important new relationship was established that by adding the internal angles $\eta_b + \eta_{\sigma b}$ of the arc geometry, the maximum stress related angle η_d could be evaluated.

Because the arc length of a pre-curved bimetallic strip must physically remain the same irrespective of the radius of curvature change, then due to the nature of the variability, consideration must be given to the possible various radiuses of curvature sizes to arc length sizes. It is important to note that value of R_d may be impossible to obtain if the radius of curvature is smaller than the radius of curvature equal to the diameter.

If $R_c \geq A_b$ then $R_d \geq R_{dia}$ and R_d can be used as the maximum radius of curvature limited by stress.

If $R_c < A_b$ and $R_d < R_{dia}$ and if the minimum radius of curvature to maintain the arc length is compromised, then the minimum radius of curvature must be equal to R_{dia}.

where

$R_{dia} = \frac{A_b}{\pi}$ is the full radius of a circle of arc length A_b.

Hence it is important to validate that $R_d \geq R_{dia}$ before using the new formulae, and if $R_d < R_{dia}$, then R_{dia} must be substituted for R_d.

Thus referring back to case 2, the chord line displacement that avoids overstressing the pre-curved bimetallic strip is given by:

$$x_{\sigma d} = 2R_c\ sin\left(\frac{A_b}{2R_c}\right) - 2R_d\ sin\left(\frac{A_b}{2R_d}\right) \quad \text{case 2}$$

Case 2 provides the maximum displacement of the free end of a pre-curved bimetallic strip of radius R_c, to form a tighter radius of curvature R_d, without the strip becoming overstrained that could result in the strip becoming permanently deformed.

where:

R_d is the radius of curvature modified and limited by $R_{\sigma b}$

$R_{\sigma b}$ is the permissible stress limited radius of curvature.

R_c is the permanently pre-formed radius of curvature at ambient temperature.

σ is the permissible stress value from the bimetallic strip manufacturer.

t, A_b, E_a, were all defined earlier.

For both calculation cases, the values for R_c, E, A_b are known, y equals the thickness of the strip $\frac{t}{2}$, and the value for the permissible stress σ can be found from bimetallic strip Thermostatic Metal handbook .

Using: SBC206-1 bimetallic strip as the datum strip, two separate calculation simulations were performed. The data for the simulation was taken from the Thermostatic Metal handbook Uhlig (2007), page 48. The calculations provide the permissible displacement $x_{\sigma d}$ as a function of radius of curvature R_c and also as a function of arc length A_b.

For the calculation the following values were used:

A_b = 80mm ; y = 0.2mm ; E_a = 175GPa ; $\sigma = 200\ MPa$; $R_c = 80mm$

From the data supplied $R_{\sigma b}$ was calculated to equal 0.175m. Remembering that this radius of curvature is from a nearly flat straight bimetallic strip, and is constant for the particular bimetallic strip under consideration.

Figure 4-2 shows the results of plotting $x_{\sigma d}$ as a function of R_c.

Thus if the radius of curvature for the bimetallic strip is $R_c = 80mm$, for an arc length A_b = 80mm, the recommended operational chord line displacement should be up to 3.6 mm. In practice it may be possible to deflect further, but the theoretical maximum is advised to prevent the strip from becoming overstrained.

From Fig.4-3 it can be seen that as the radius of curvature increases, i.e. as it becomes flatter, the less the pre-curved bimetallic strip can safely be displaced. The opposite is true in the other extreme, as the bimetallic tends to become closer to a semi-circle in shape, the further it can safely be deflected.

Thus for a radius of curvature $R_c = 50mm$, the safe chord line displacement increases by 5.114mm.

The second calculation bears out the argument just stated, see Fig.3-12.

Here the displacement $x_{\sigma d}$ is plotted against arc length A_b, with a constant radius of curvature $R_c = 80mm$. In this case, as the arc lengths increases, large displacements are possible before reaching the stress limited displacement.

In summary, from this research, generally it can be stated that as the radius of curvature tends to become more round, and closer to the semi-circle in shape, or as the arc length increases, the greater the chord line displacement can be obtained before reaching the permissible stress limit of the material.

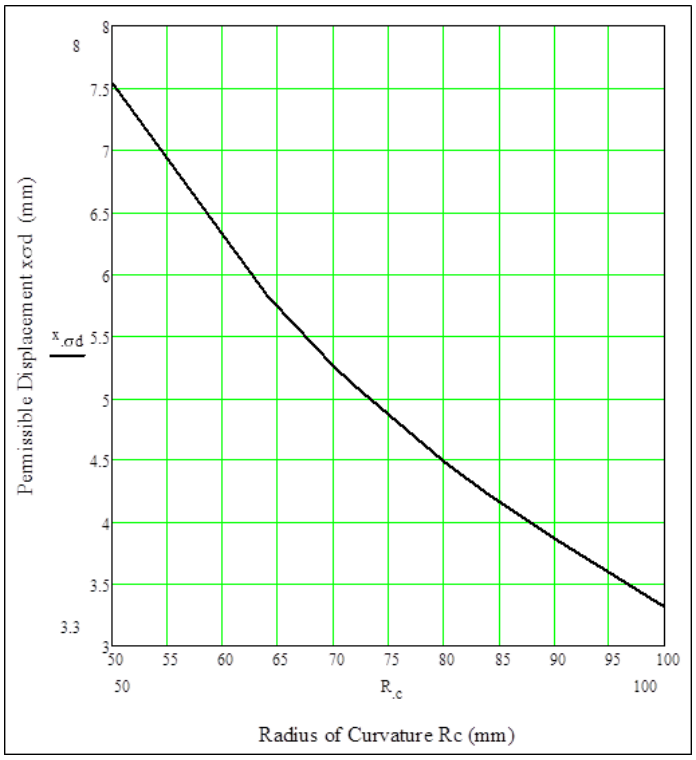

Fig.4-2 Permissible displacement as a function of curvature

Data used to generate plots shown in Figure's 4-2 and 4-3, were calculated by using Eqn. 29.

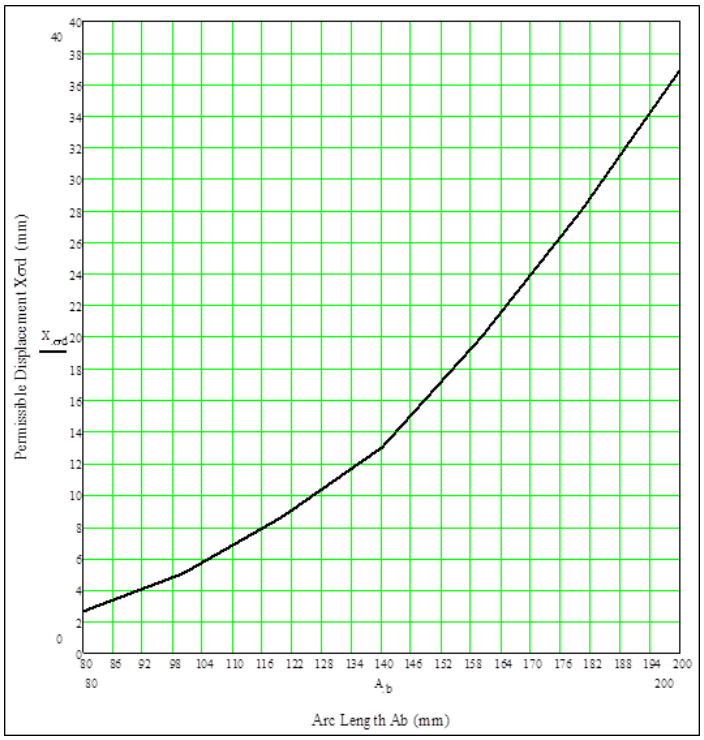

Fig.4-3 Permissible displacement as a function of arc length

Once the permissible displacement curves for a specific bimetallic strip have been generated using the formulae provided, it is possible to ensure that any intermediate specific arc length, or for any radius of curvature that is proposed in a design, for that design, the maximum safe chord line displacement can be read off the curves as shown in Fig.4-2 or Fig.4-3. The calculation of $x_{\sigma d}$ prevents the strip under operating conditions from becoming overstrained or in a worst case permanently deformed as a result of a chord line overload.

4.3 Immediate Radius of Curvature Formula-Verification

For the proof of the correlation between the new formula proposed in this research, and Timoshenko's original formula, two separate simulations were performed.

The first simulation, simulation set 1, was based around a bespoke Bimetallic strip SBC206-1 from Shivalik; 100*mm* long x 5*mm* wide x 0.4*mm* thick , these were the starting values of the first simulation.

For the generation of comparison data, parameters T_h , and t were varied in the simulation; t = 0.4, 0.8, 1.2, 1.6, 2, 4, 6, 8 and 10mm being the total thickness of strip. It should be noted that in most applications of bimetallic strip, the total thickness is usually quite thin, up to 1mm thick for switching applications see bimetallic handbook Kanthal (2002).

For simulation set 1, the following data was assumed;

The strip thickness *t,* was varied from 0.4mm thick to 10mm thick.

E_2 = 213 $\frac{GN}{m^2}$; Young's modulus of Steel side of the bimetallic strip.

E_1 = 145 $\frac{GN}{m^2}$; Young's modulus of Invar side of the bimetallic strip.

α_2 = $\frac{19.5\ 10^{-6}}{K}$ coefficient of linear thermal expansion for Steel side of the strip.

α_1 = $\frac{1.85\ 10^{-6}}{K}$ coefficient of linear thermal expansion for Invar 36 side of the strip.

t_1, t_2 both equal $t = t_1 + t_2$ total thickness of the strip.

T_c = 20 °C assumed ambient temperature constant throughout the simulation.

T_h = Input variable temperature °C.

ΔT = change in temperature $\Delta T = T_h - T_c$ in °C.

ρ = radius of curvature evaluated by the Timoshenko formula (m).
R = radius of curvature evaluated by the proposed new formula (m).

For the second simulation, simulation set 2, a combination of different materials within the bimetallic strip, and also a variety of thicknesses of strip were used. It should be noted that the material combinations put forward in the second simulation may not be practical for the manufacture of bimetallic strip by modern mass production methods of cold pressure rolling, but they can be produced by other, older fabrication methods such as by riveting the two metals together.

For the simulation set 2, the mixtures of bimetallic materials have been selected in a random fashion to test the robustness of the new formula.

Note that Invar 36 is used as the common mating material since it possesses a very low coefficient of linear thermal expansion as compared with all other engineering materials. For both simulations the ambient temperature is assumed to be T_c = 20 °C.

Timoshenko and the new formula proposed here, were used to generate the data values of ρ and R respectively for both simulations.

The radii of curvature were plotted against the change of temperature for each thickness of bimetallic strip, see Fig.4-4 for the results of the simulation set 1 on bespoke bimetallic strip, and see Fig.3-17 until Fig. 3-22 for simulation set 2.

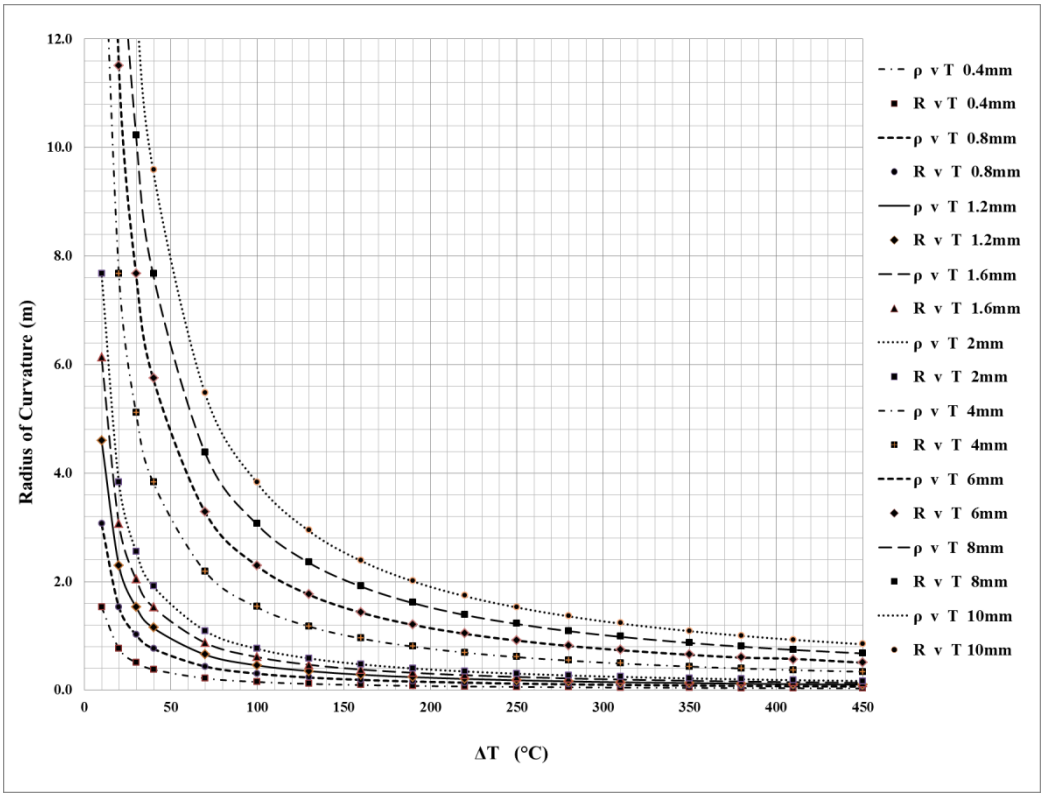

Fig.4-4 Timoshenko behaviour of Bimetallic accuracy for various ΔT

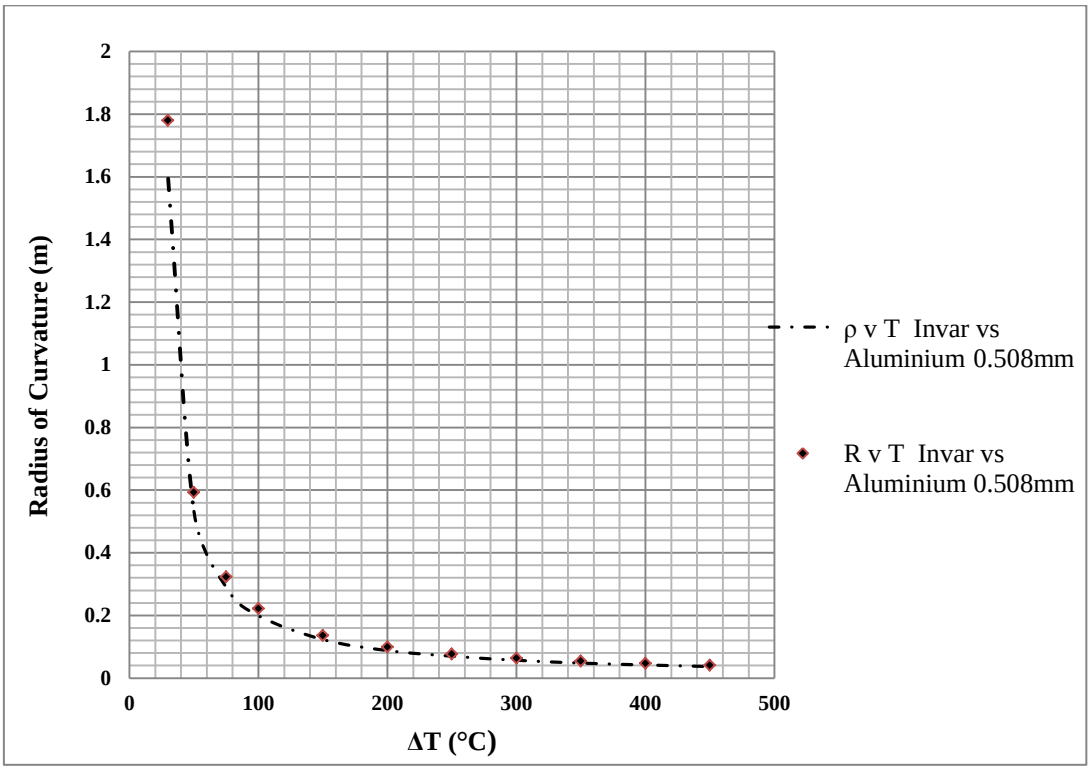

Fig.4-5 Timoshenko comparison to present study

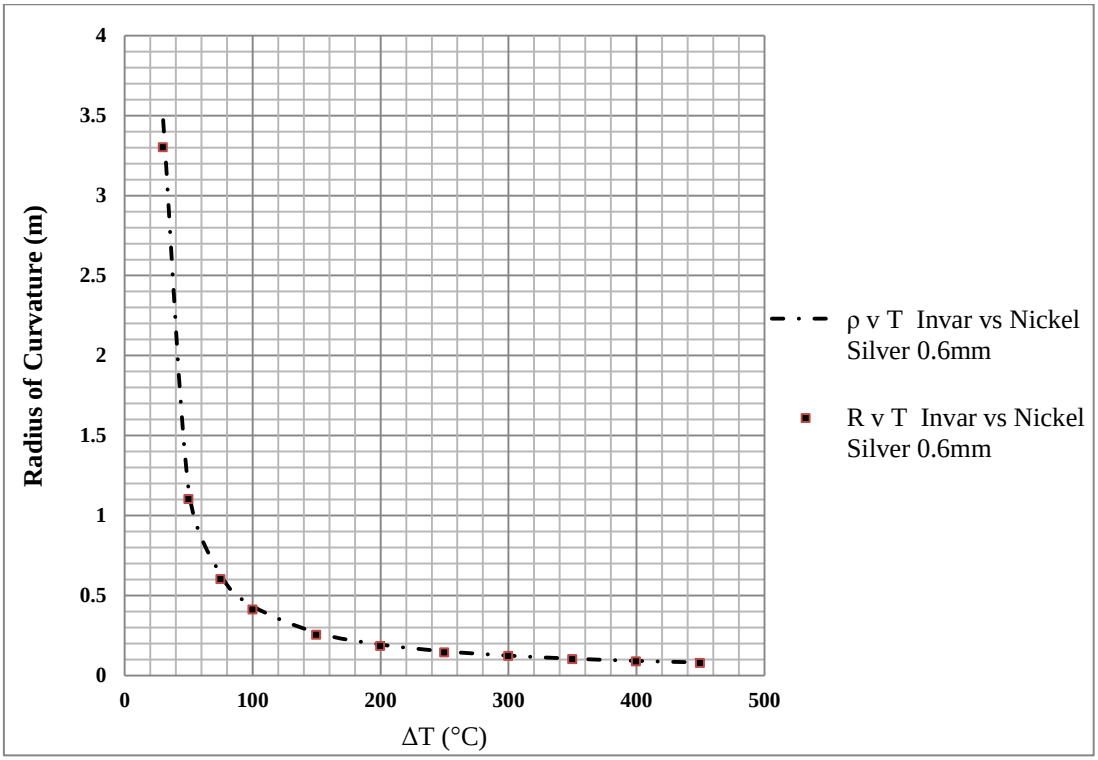

Fig.4-6 Timoshenko comparison to present study

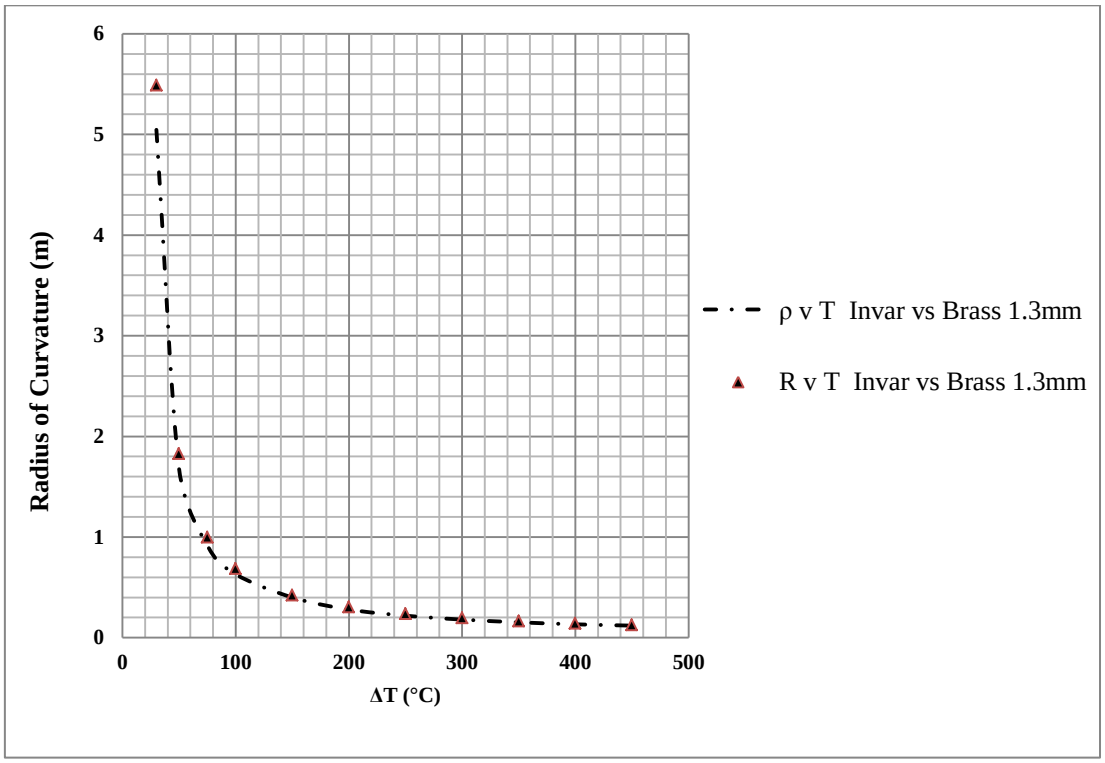

Fig.4-7 Timoshenko comparison to present study

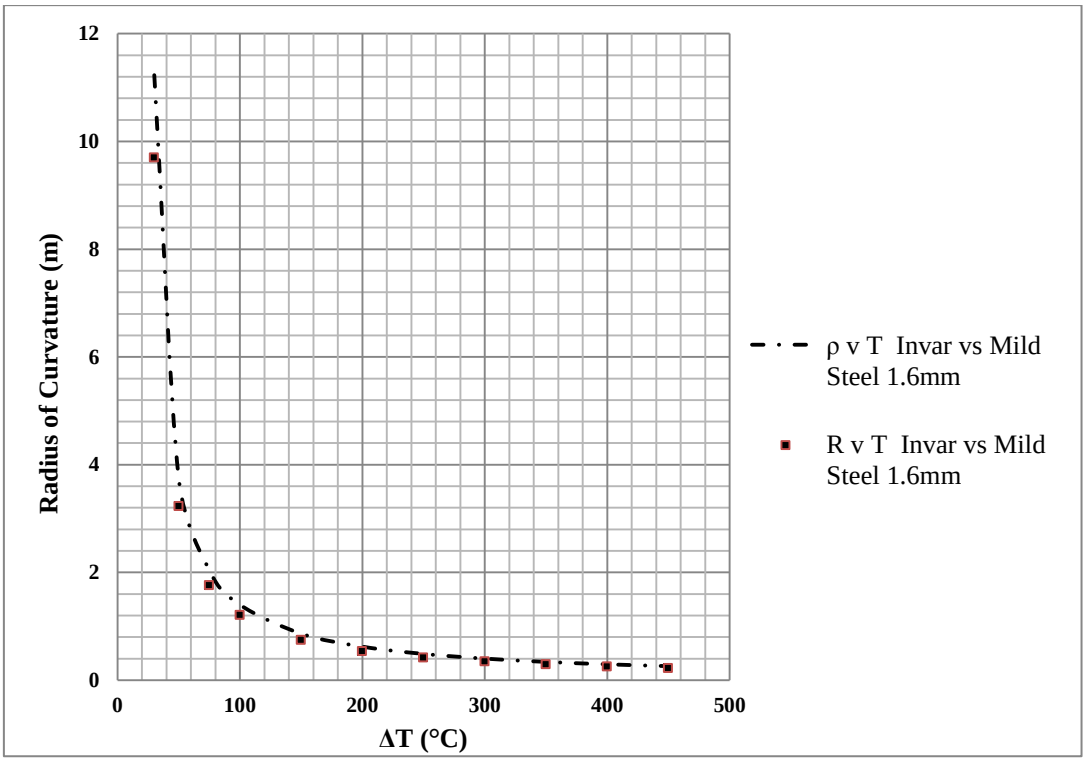

Fig.4-8 Timoshenko comparison to present study

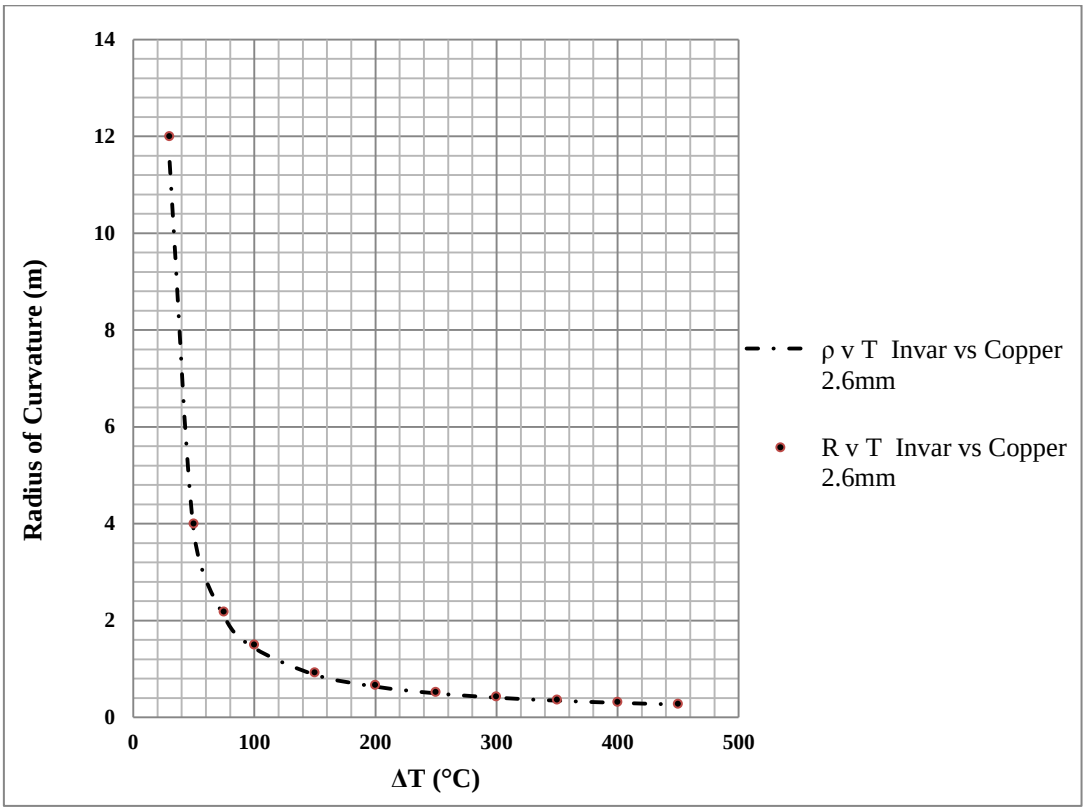

Fig.4-9 Timoshenko comparison to present study

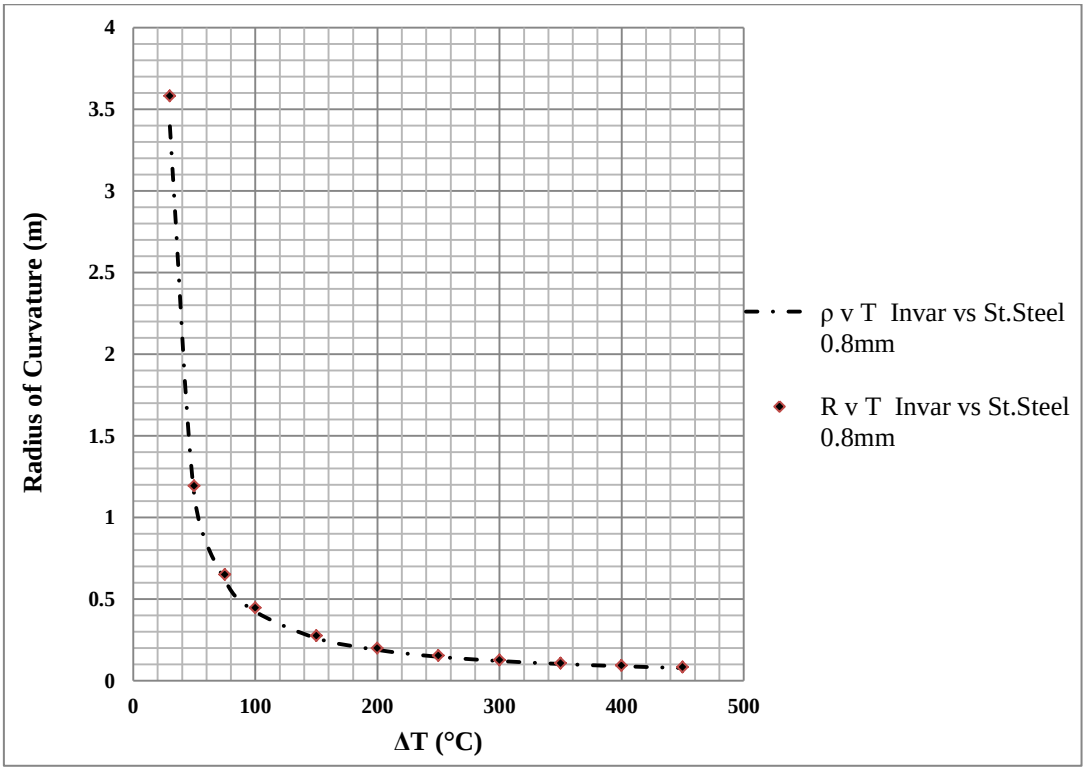

Fig.4-10 Timoshenko comparison to present study

From Fig.4-4 it is evident that for the 153 overall data points from simulation set 1, yielding nine different thicknesses of the strip, an excellent correlation between the two formulae has resulted.

From simulation set 2, Fig.'s 4-5 to 4-10, comparing the six different materials types and thickness combinations yielding 66 data points, a very good overall correlation between the new formula and Timoshenko was shown to exist.

From the analysis of the results from the nine data tables generated from simulation 1, the overall average error was 0.64%.

The break down in average error for each thickness was as follows:

0.4mm thick = 0.9927 average 0.73%.

0.8mm thick = 0.9938 average 0.62%.

1.2mm thick = 0.9949 average 0.51%.

1.6mm thick = 0.9936 average 0.64%.

2.0 mm thick = 0.9912 average 0.88%.

4.0mm thick = 0.9938 average 0.62%.

6.0mm thick = 0.9960 average 0.40%

8.0mm thick = 0.9940 average 0.60%

10mm thick = 0.9940 average 0.60%

The errors shown are the deviation from the Timoshenko formula in each case.

From the breakdown of average error it is evident that the error fluctuates slightly as a function of the thickness of the strip. The maximum fluctuation of error lies between the 2mm thick and 6mm thick test strips, was only 0.48%.

From simulation set 2, the error breakdown was as follows:

0.508mm thick = 0.899 average 1.01% Invar vs. Aluminium

0.6mm thick = 1.054 average 0.54% Invar vs. Nickel Silver

1.3mm thick = 0.925 average 0.75% Invar vs. Brass

1.6mm thick = 1.158 average1.58% Invar vs. Mild Steel

2.6mm thick = 0.956 average 0.4% Invar vs. Copper

0.8mm thick = 0.948 average 0.52% Invar vs. St. Steel

The maximum fluctuation of error of the function was 1.18% which occurred between the 1.6mm and 2.6mm simulation data. It should be noted that the second test was simultaneously subjecting the formula to all changes of the data, i.e. different thicknesses, different Young's modulus, and different coefficients of linear expansions.

The average error in simulation set 2 was 0.8% and the maximum fluctuation error was 1.18%.

From simulation set 1 the average error was 0.62% and the maximum fluctuation error was 0.48%.

The derivation has shown, and the correlation of the new formula to the Timoshenko formula has proven, that the values of Young's Modulus for each metal within the bimetallic strip are not required in the evaluation of the new formula. This is very useful since it is not always quick and easy to find the Young's modulus of the metals, and the value as used in the Timoshenko formula, takes the average of both Young's moduli which can only be an approximation at best. It should also be noted that this work assumes that Young's modulus for a bimetallic strip is the average of the two constitute metals making up the strip, as per the original Timoshenko formula.

The results prove an acceptable overall maximum error of 1.18%, and an overall average error of 0.64%. Thus it has been demonstrated that the formula put forward here can be a useful, quick, easier alternative to Timoshenko's radius of curvature formula for very close estimates of the radius of curvature as a function of temperature change. Furthermore, it has been shown that the new formula works without the requirement of first knowing the Young's moduli of the two metals within the bimetallic strip. Most usefully, the formula presented in this work can be evaluated without the need of an electronic spread sheet or program as is required with the more complex Timoshenko's formula, but can be easily used on a hand held calculator at a fraction of the time.

4.4 Bimetallic Arc Endpoint prediction - Verification

For the verification of the formulae proposed in section 3.9, a Catia 2D geometry simulation check now follows and the screenshot of the output is shown in Fig.4-11.

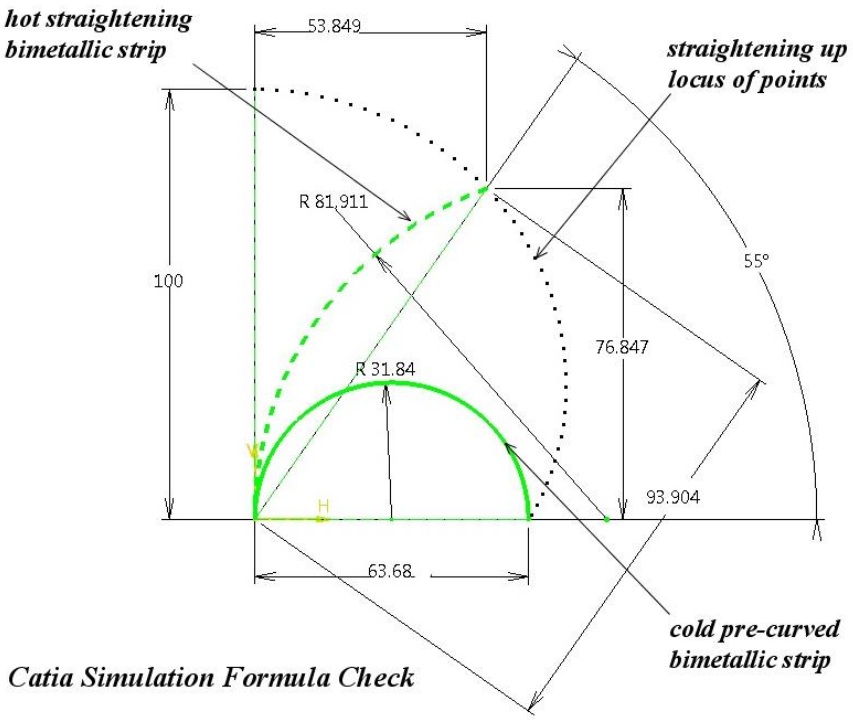

Fig.4-11 Catia simulation formula check screenshot

The simulation was performed as follows:

R_h for each locus point was calculated using Timoshenko heat induced radius of curvature formula, which was modified as previously shown.

The geometry was modified to accord to the R_h value and the endpoint of straightening bimetallic strip was recorded by inserting a point at each value of R_h.

For the simulation, the arc length A_c =100mm, the bimetallic strip with an ambient /cold initial radius of curvature was: $R_c = 31.84mm$.

Taking one random sample point from the Catia simulated locus of points, the radius of curvature extracted was;

$R_h = 81.911mm$

Thus from the calculation, the values were:

$L_h = 2R_h \sin(\frac{A}{2R_h})$ = 93.904mm

$x = L_h \cos(\frac{A_c}{2}(\frac{1}{R_c} - \frac{1}{R_h}))$ =53.849 mm, and from the formula $x = 53.861mm$

$y = L_h \sin(\frac{A_c}{2}(\frac{1}{R_c} - \frac{1}{R_h}))$ = 76.847mm, and from the formula $y = 76.922mm$

The discrepancy between the formula and the Catia simulation as shown in Fig. 4-11 is because of the approximate method of generating the locus path in Catia. It should be noted that the initial radius of curvature of the bimetallic strip used in the simulation is

virtually equal to the semi-circle in this case, which for any semi-circle, the radius of curvature is:

Radius of curvature of a circle where the radius is half the diameter is given by:

$R_{circle} = \frac{Arc\ length}{\pi}$, which equalled 31.83mm. The simulation used $31.84\ mm$ due to the limitations of Catia to provide an absolutely perfect vertical point in the sketcher environment. The simulation shown in Fig.4-11 was repeated for other points in the locus, and a good correlation between the theory and the Catia simulation was achieved.

4.5 Spatial Endpoint Prediction Verification

To verify the new spatial prediction equations put forward in section 3.10, this section validates the theory by a simulation.

It is normal practice to program the formulae into an electronic spread sheet so that the iterative process can zero in on a working solution that satisfies the combined loading and stress requirements.

For the validation of the new formulae, the following simulation to evaluate the following design criteria was performed:

Constraints :

Using bespoke bimetallic strip SBC-206-1 Shivalik (2013) with the following data:

Loaded by 0.35N applied load to the end of the pre-curved bimetallic strip that is being subjected to 150°C and the ambient temperature is 25°C. The limiting stress is 200MPa as defined by Shivalik.

The bimetallic strip geometry is as follows:

100mm long by 5mm wide by 0.4mm thick.

Initial radius of curvature $\mathrm{R_c} = 35\mathrm{mm}$.

Arc length A_b = 100mm.

E_s = 213 GPa ; Young' modulus of the steel within the bimetallic strip.

E_i = 145 GPa ; Young' modulus of the Invar 36 within the bimetallic strip.

t = 0.4mm thick equal thickness for the two metals within the strip.

$\alpha_s = \frac{17.3\ 10^{-6}}{K}$ coefficient of linear thermal expansion of the steel.

$\alpha_i = \frac{1.45\ 10^{-6}}{K}$ coefficient of linear thermal expansion of the Invar 36.

The object of the calculations is to find the net displacement x_{n} and $\mathrm{y_n}$ ordinate positions.

Assumptions

The bimetallic strip is heated uniformly along its entire length, and is rigidly fixed at one end, end "*o*", against displacement and rotation.

Applying Timoshenko formula to find the "bend from flat" radius of curvature.

From the simulation calculation:

Change in temperature = 125° C.

ρ = 135.85 mm bend from flat provided by the Timoshenko formula.

Thus: $R_h = \frac{R_c \rho}{\rho - R_c}$ free hot radius of curvature.

R_h = 47.15mm.

$L_h = 82.28$ mm.

$\chi = \frac{A_b}{2}(\frac{1}{R_c} - \frac{1}{R_h}) =$ 21.0871 ° angle to chord line supporting R_h

$x_h = 76.77$mm free x ordinate position.

$y_h = 29.60$mm free y ordinate position.

The values just worked out, evaluate the free unloaded end point position "a*"* shown previously. This is the starting position from which the loaded displacement is calculated.

Applying the 0.35N force which simulates a possible switch activation load;

Thus F_a = 0.35N

$\omega_h = \frac{A_b}{R_h}$ = 2.1208 radians.

Therefore $\gamma = \frac{\pi - \lambda}{2}$ = 0.5103 rad.

And $F_n = F_a \sin(\gamma)$ = 0.17094 N

From the manufacturer, $\sigma_{bp} = 200\ Mpa$ permissible stress limit.

Thus

$R_\sigma = \frac{tE}{2\sigma_{bp}}$ = 179 mm this is the maximum bend radius that can be tolerated to meet the stress limit requirement.

The bending stress from the applied load of F_n, $\sigma_a = \frac{F_n L_h t}{2 I}$ = 1.0549 x 10^8 Pa or 105.49 MPa, which is under the limit of 200MPa.

Therefore the load applied to the bimetallic strip in the hot orientation is acceptable from a stress viewpoint.

$R_b = \frac{E_a I}{F_n L_h}$ = 339.37 mm bend from flat as a function of normal force F_n.

Note here that R_σ is a tighter radius of curvature than R_b which means that R_b which is bending from an initially flat condition, is not bending as acutely as the stress limited R_σ value, meaning that the bend of the strip due to an external load is less than the critical stress limited radius of curvature R_σ.

Using R_b to find the displaced radius of curvature R_f

$R_f = \frac{R_b R_h}{R_b + R_h}$ = 41.395mm modified radius of curvature due to applied force.

Note that the initial cold radius of curvature was $R_c = 35mm$. and that under heating the radius of curvature flattened to R_h = 47.15mm, but under external loading was reduced back to $R_f = 41.395mm$.

Thus the net loaded position of the loaded endpoint is:

$L_f = 2\,R_f \sin(\frac{A}{2\,R_f})$ = 77.39 mm, the new chord line length.

Thus the net loaded Cartesian coordinate positions under combined heating and external loading is :

$x_n = L_f \cos(\frac{A_b}{2}(\frac{1}{R_c} - \frac{1}{R_f}))$ = 75.52mm

$y_n = L_f \sin(\frac{A_b}{2}(\frac{1}{R_c} - \frac{1}{R_f}))$ = 16.94 mm

See Fig.3-27 for the graphical depiction of the results of the calculation.

As introduced, the method enables the calculation of loaded special position of the free end of a pre-curved bimetallic strip when subjected to a combined heating and an externally applied load.

Care must be taken not to exceed the bending stress values as supplied by the manufacturer. It should be noted that the free radius of curvature R_h only requires the calculation up to the point where the load is applied. From the calculation with a change in temperature of 125° C, the bimetallic strip freely straightened up from an initial ambient radius of 35mm to 47.15mm at 150° C. The 0.35N load reduced the radius of curvature back down to 41.395 mm, see Fig.4-12. It should also be noted that if the applied load had exceeded the permissible bending stresses as advised by the manufacturer, the geometry of the strip would need to be changed to meet the input load requirements.

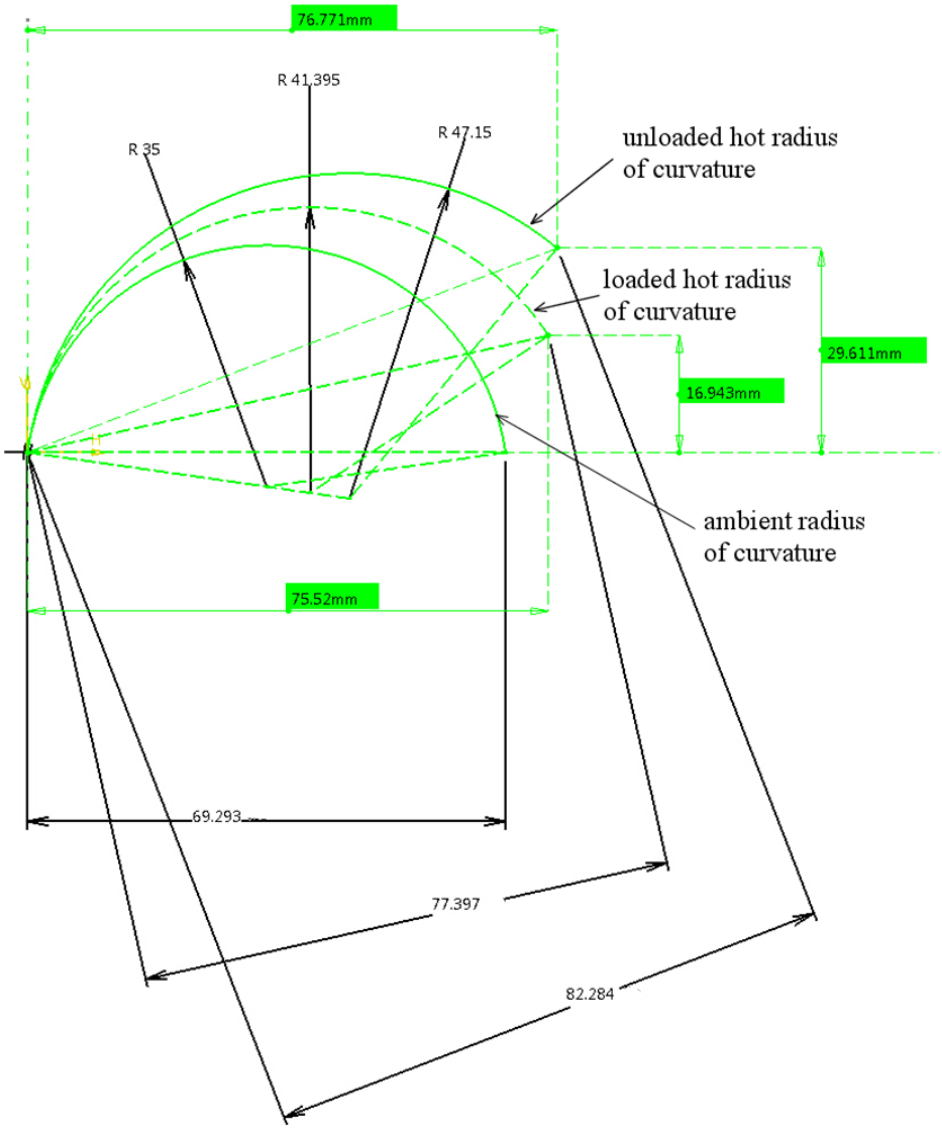

Fig.4-12 Catia verification sketch of the combined loading case

By lengthening the strip, the stresses can be reduced, also by increasing the cross-sectional area of the strip, and lastly, by changing the initial radius of curvature, this can also reduce the stresses.

Summary of calculation results

Unloaded spatial position of end point.

$x_h = 76.77\text{mm}$ from Timoshenko bending

$y_h = 29.61\text{mm}$

$\chi = 21.09°$

Change in temperature = 125° C

From 0.35N loading

Loaded spatial position of end point.

$x_n =$ 75.52mm net loaded position

$y_n =$ 16.943 mm net loaded position

Thus the load of 0.35 N reduces the free end of the bimetallic strip from a height of 29.611 mm to 16.943mm, a change of 12.668mm. The horizontal length reduces back by just by 1.25mm.

Formulae for the evaluation of the combined heating and loading of a pre-curved bimetallic strip were verified in this section. Permissible stress limited equations were introduced to enable the user to evaluate the safe loading conditions to prevent the bimetallic strip from becoming over strained due to an external load.

4.6 Alternative Force vs. Displacement Verification

The above equations were programmed into an Excel spread sheet and the formulae were found to hold true for a whole range of values and possible combinations of parameters. Catia V5 R19 solid modelling software, Dassault (2014), was used to exhaustively test the values which accorded to the theory with a very high degree of accuracy. It should be noted that the Catia part modeller sketcher environment was set to 8 decimal places of accuracy for the testing of the new theory.

The following values were drawn in Catia showing the initial radius of curvature: $R_c = 40mm.$

The length for both arcs was: $A_b = 100mm.$

The displaced distance inputted was $x_d = 7.8311649\ mm.$

A comparison of accuracy of the formulae was made between the output values shown in Fig. 3-30 and the values calculated by the Excel program, see Table 2.

For the purpose of evaluating the displaced chord line length L_d, R_v is made to equal R_d; thus $R_d = R_v$ and so from previously $L_d = 2R_d \sin\left(\frac{A_b}{2R_d}\right)$.

L_d is the modified chord length as a function of R_v which is a function of x_d.

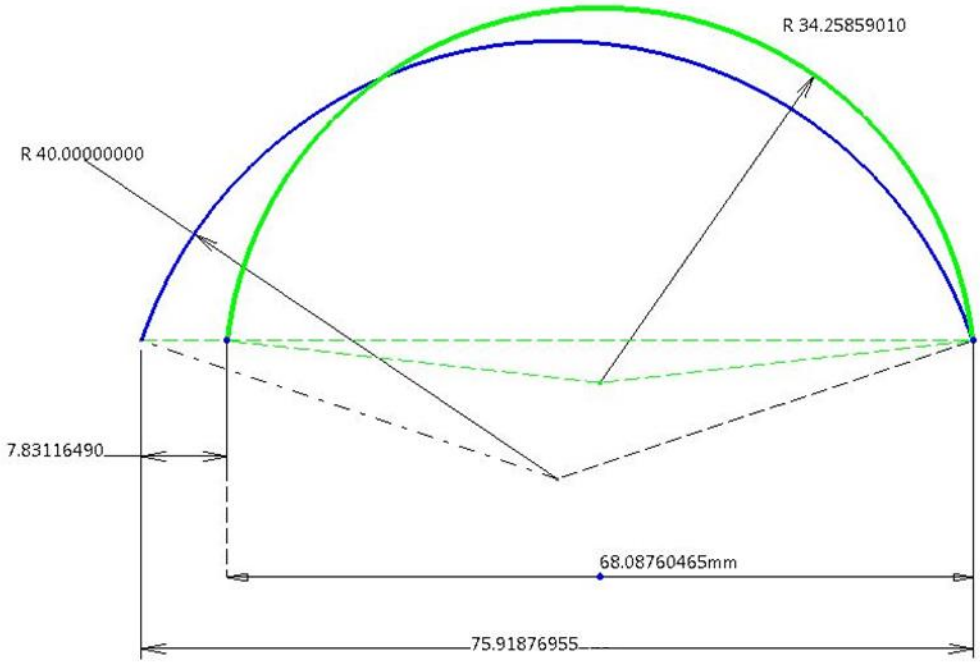

Fig.4-13 Catia sketcher verification of x_d vs R_v accuracy

Table 2 Excel program evaluating x_d vs R_v formulae

Excel Program		
Arc length	**Ab**	**100**
Initial Radius of curvature	**Rc**	**40**
Initial angle	**ϑc**	**2.5**
Initial chord length	**Lc**	**75.9187695**
Displaced distance	**xd**	**7.8311649**
chord height at mid chord span	**hc**	**27.3871**
Program		
variable	**a**	**3.100198.4**
variable	**b**	**-52083.333**
variable	**c**	**416.6666667**
variable	**d**	**-0.319124**
variable	**Δ**	**-2.46412E+14**
variable	**Δ0**	**-1162574400**
variable	**Δ1**	**2.40E+14**
variable	**Ca**	**62700.534**
variable	**ϒ1**	**0.000852042**
variable	**Rv**	**34.2585901**

The relationships just derived, enables the accommodation of the non-linear displacement characteristics by modifying the initial radius of curvature R_c to reflect the

changed radius of curvature R_d as a function of displacement x_d. R_d is used to evaluate the force displacement equation.

Using the formulae just derived, a $R_d\ vs\ x_d$ curve was plotted out using the following initial conditions:

$A_b = 100\ mm$ arc length
$R_c = 100mm$ initial radius of curvature of the arc

The results of the calculation are shown in Fig.3-31 which clearly indicates the nonlinear relationship.

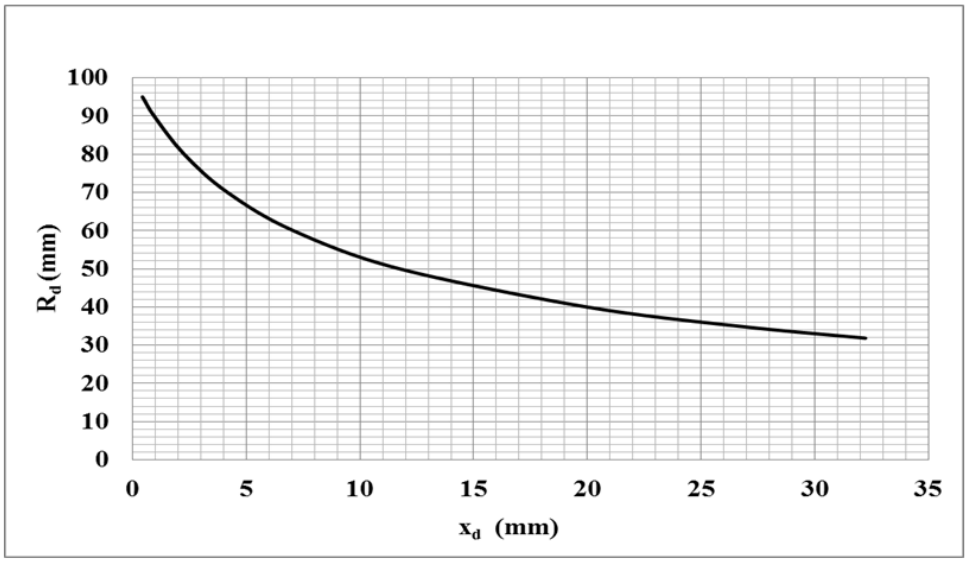

Fig.4-14 Non-linear relationship of the curvature varying with displacement

The derivation of the force displacement formula is based upon simple bending theory and the new evaluation of R_d as a function of displacement x_d. The method introduces a force F_c that is considered to be the equilibrium force required to hold the bimetallic strip at the initial radius of curvature R_c when F_c is applied to free end of the flat strip. The force F_c yields a moment M_c when multiplied by the distance h_c, The moment in simple bending terms is:

$$M_c = \frac{EI}{R_c} \qquad \text{Eqn. 76}$$

Likewise as result of applied force F_d

$$M_d = \frac{EI}{R_d} \qquad \text{Eqn. 77}$$

where M_d & M_c are bending moments (J).

E is the Young's Modulus for the bimetallic strip ($\frac{N}{mm^2}$), E is the average of both Young's Modulus for both metals within the strip.

I is the second moment of area of the cross section of the strip (mm^4).

The difference between the two energy states M_d & M_c are equated to the force F_d x h_d.

Thus the displaced force is given by:

$$F_d = \frac{M_d - M_c}{h_d} \qquad \text{Eqn. 78}$$

where h_d can easily be derived using the given geometry, thus:

$$h_d = \frac{L_d}{2} tan(\frac{A_b}{4R_d}) \quad \text{Eqn. 79}$$

But from previously $x_d = L_c - L_{d.}$

Thus Eqn. 82 can be written in terms of displacement x_d.

Hence $$F_d = \frac{M_d - M_c}{\frac{(L_c - x_d)}{2} tan(\frac{A_b}{4R_d})} \quad \text{Eqn. 80 displaced force.}$$

Thus the force F_d is evaluated as a function of the change in moments M_d & M_c divided by the height h_d which is a function of R_d, x_d, L_c, and arc length A_b.

Eqn.80 is the force vs displacement equation that overcomes the limitations of simple bending theory, and small displacements, via the introduction of R_d as a function of displacement $x_{d,}$ which accommodates the nonlinear characteristics of the thin pre-curved beam geometry.

In using Eqn.80, it is normal to know A_b, L_c and R_c as the initial pre-curved conditions of the bimetallic strip. By inputting a displacement x_d from the initial length L_c, F_d is evaluated.

In practice the amount of displacement x_d of the pre-curved bimetallic strip, is limited to the permissible bending stresses normally defined by the materials properties of the bimetallic, this was discussed earlier.

Comparison must be made with Castigliano's derived force displacement formulae with the same data. From Castigliano's starting formula $\delta = \frac{1}{EI}\int_0^L \left(\frac{\partial M}{\partial F}\right).M.ds$, it is possible to derive the force deflection expression of Eqn.81. The same Castigliano starting expression was used to derive Eqn.'s 82 and 83 but here, a new relationship was used in the integration; $y = \sqrt{(2R^2(1 - cos(\theta))}\ .\ sin\ (\frac{\omega - \theta}{2})$ which was introduced previously. From this additional relationship it is possible to establish Eqn.'s 82 and 83.

$$F_{cast} = \frac{2\,E\,I\,x_d}{R_{dia}^3\,[(\frac{A_b}{R_{dia}}) - \frac{1}{2}\sin\left(\frac{2A_b}{R_{dia}}\right)]} \qquad \text{Eqn. 81}$$

Eqn.81 is the unmodified quadrant derived formula for a semi-circle. This Castigliano derived expression cannot cope with shallow arcs, or large displacements, and is only useful for small displacements of a semi-circular arc.

$$F_c = \frac{E\,I\,x_d}{2R_c^3[\frac{\omega_c}{2} + \frac{1}{4}(\omega_c\,\cos(\omega_c) - 3\sin(\omega_c))]} \qquad \text{Eqn. 82}$$

Eqn.82 is Castigliano's theorem applied using x, y, coordinate geometry in the integration process, however it is limited to a non -varying R_c, and thus it is a linear expression that does not match well to the test data.

$$F_{cd} = \frac{E\,I\,x_d}{2R_d^3[\frac{\omega_d}{2} + \frac{1}{4}(\omega_d\,\cos(\omega_d) - 3\sin(\omega_d))]} \qquad \text{Eqn. 83}$$

Eqn.83 is the same derivation as Eqn.82, except here, the modified radius of curvature R_d replaces R_c. As can be seen from earlier work, that the application of the variable radius of curvature greatly improves the estimation of the force vs displacement when compared to the fixed radius of curvature R_c. And lastly, the newly introduced force displacement formula that most closely matches the test data.

$$F_d = \frac{M_d - M_c}{\frac{(L_c - x_d)}{2} tan(\frac{A_b}{4R_d})} \text{ introduced previously.}$$

It should be noted that the current formula evaluates the compressive deflections as a function of an external force. If the value of x_d in the part derivation; $d = \frac{L_c - x_d - A_b}{A_b}$ is positive,

i.e. $d = \frac{L_c + x_d - A_b}{A_b}$, then the preceding formulae with an inputted extension, enables the evaluation of an output force to the bimetallic strip along its chord line axis.

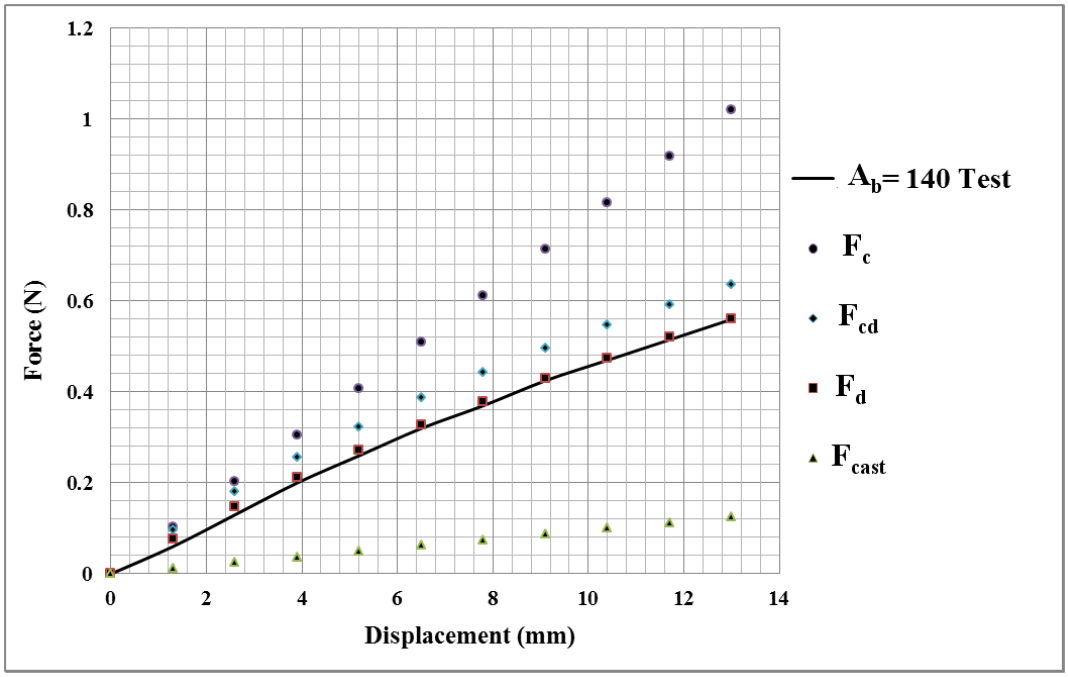

Fig.4-15 Comparison of Castigliano to new force displacement formulae F_d

By the principle of superposition in conjunction with Timoshenko's thermally induced bending equation, Eqn.1, it is possible to evaluate the extension force developed by a pre-curved bimetallic strip as a function of a temperature differential from ambient temperature. The known limitations of this theory applies to applications whereby the thickness of bimetallic strip to radius of curvature ratio is smaller than 1:100 over a 7mm deflection range with an approximate 5% error.

Summarising, a new method of obtaining the displaced radius of curvature $R_d \ vs \ x_d$ the displaced distance relationship, was introduced. This has resulted in a mechanism to evaluate the non-linearity that limits simple bending theory. The new $R_d \ vs \ x_d$ relationship was used in the force displacement derivation. The theoretical equations put forward in the previous sections were programmed into an electronic worksheet and theoretical values corresponding to test samples were generated. A comparison of the new force vs. displacement expression to Castigliano derived formulae was performed.

CHAPTER 5 Test Equipment, Setup and Test Procedures

Summary

This chapter outlines the tests, test equipment, test samples and test procedures used in the overall test methodology.

5.1 Introduction

To enable the validation and correlation of the theory put forward in chapter 3 to the objectives of this investigation see section 1.2, a comprehensive test regime was devised that used both fabricated and bespoke bimetallic strip. The test regime necessitated a mixture of test rigs to cope with the variable loading factors and loading orientations employed. It is important to note that the method of mounting and loading of the entire test samples on the test rigs was identical. The original mounting method was to be by coiling both ends of the bimetallic test piece to form a hole so that the test sample could be held by pins on the test rigs. Due to the difficulty in producing the coiled ends in the thicker fabricated test samples, a decision was made to change the mounting method to that of being simply supported for all test samples on all test rigs.

For the bespoke bimetallic test pieces, that were made from SBC-206-1 Shivalik (2013), the test samples were all 0.4mm thick and considered light duty. For the fabricated bimetallic strip test samples, the range varied from 0.4mm to 1.55mm thick, and these were considered to be heavy duty. Because of the different loading generated by the bimetallic test pieces, bespoke test samples were tested on the two lightly loaded test rigs whilst the fabricated test samples required a more heavy duty test rig to cope with the forces and loads applied to the rig. The reason for two different test rigs for the lightly loaded bespoke test pieces, was to improve the accuracy of the tests by using the Sauter test rig which was brought in at a later stage of the testing. The Sauter test rig was modified to allow for the same mounting and loading as in the Vertical lift and Magnetic coupling test rigs.

The rationale for having two types of bimetallic strip test samples, one fabricated, one bespoke, stems from the fact that it is not possible to obtain a variety of different thicknesses and different material combinations from bespoke bimetallic strip suppliers. To enable a wide range of dissimilar metal bimetallic strip and to satisfy academic rigour, the fabrication of the test samples was deemed the best way to provide a larger test data set. The testing of the bespoke bimetallic strip was also deemed necessary because the majority of bimetallic strip that is sold and used worldwide, is bespoke bimetallic strip, and the testing also needed to reflect that reality.

Thus the test set comprised of both fabricated bimetallic strip to test a wide variety of bimetallic material combinations and thicknesses, and bespoke test samples for the

commercially manufactured type of bimetallic strip. Having both fabricated and bespoke test samples, ensured that the tests reflected the majority of bimetallic strip that is sold, as well as special types with different material combinations.

To cater for both types of method of manufacture of the strip, specific test rigs were designed for the two types of bimetallic test samples.

5.2 Overall Test Regime

The test scheme comprised of a mixture of pre-fabricated test samples tests and bespoke test samples tests.

Additionally, as part of the theory, specific calculated simulations were performed in the Chapter 3.

Table 3 Overall test regime

Type of test	Conditions	Rig Used	Loading Attitude	Type of Bimetallic Strip
Load vs. Displacement	Ambient Temperature	Magnetic Assembly	Horizontal	Fabricated Bimetallic Strip
Load vs. Displacement	Ambient Temperature	Sauter Force Displacement	Horizontal	Bespoke Bimetallic Strip
Temperature vs. Displacement	Varying Temperature, No Load	Magnetic Assembly	Horizontal	Fabricated Bimetallic Strip
Temperature vs. Displacement	Varying Temperature, No Load	Sauter Force Displacement	Horizontal	Bespoke Bimetallic Strip
Combined Heating and Loading	Varying Mass Load & Temperature	Magnetic Assembly	Horizontal	Fabricated Bimetallic Strip
Combined Heating and Loading	Varying Mass Load & Temperature	Vertical Gravity	Vertical Lifting	Bespoke Bimetallic Strip
Straightening Test	Varying Temperature, No Load	Bench Fixed One End	Horizontal	Bespoke Bimetallic Strip
Time vs. Displacement	Temperature Constant, No Load	Magnetic Assembly	Horizontal	Fabricated Bimetallic Strip

The test scheme was realised by the design and manufacture of two specific test rigs, and the modification of a bought in test rig. The test rigs were designed to accommodating the test loading conditions that was a function of the type of test, and the method of manufacture of the test sample.

5.3 Test Methodology

The tests were arranged so that each bimetallic test piece was tested to meet the objectives as specified in section 1.2. The overall testing order was as follows:

1) Load vs. Displacement

   Fabricated test samples on magnetic coupling test rig
   Bespoke test samples on Sauter force-displacement test rig.

2) Temperature vs. Displacement

   Fabricated test samples on magnetic coupling test rig
   Bespoke test samples on Sauter force-displacement test rig.

3) Load vs. Temperature

   Fabricated test samples on magnetic coupling test rig
   Bespoke test samples on vertical gravity test rig.

4) Spatial Position of a Pre-curved Bimetallic strip

   Bespoke test samples on Bench fixed – test set up

5) Time vs. Displacement tests of a Pre-curved Bimetallic strip

   Fabricated test samples on magnetic coupling test rig.

5.4 Permissible Displacement Values for Test Samples

To ensure that the test samples were not tested beyond their elastic limits as defined previously by the theory put forward in section 3.6. The application of the theory of section 3.6 was used to evaluate the chord line displacement of the pre-curved test samples.

It is important to note that the displacement values are for force applied displacement and not for temperature induced displacement. Temperature induced values are included within the load displacement range of values, since the temperatures that were reached, were within the linear elastic properties of materials making up the bimetallic test pieces.

For the calculation of the fabricated test samples that comprised of both different material types and material thicknesses, the modified Young's modulus formula introduced in section 3.7 was used to evaluate a more representative average value. For

the bespoke bimetallic samples the permissible stress as supplied by the manufacturer, Shivalik was used. For the fabricated test samples the yield stress values were obtained for all the different material types from the online materials information resource MatWeb (2013). The average yield stress value of both metals making up the fabricated bimetallic was calculated and used to evaluate the maximum safe distance of displacement , see Table 4 for values of Young's modulus, Yield stress and coefficient of linear thermal expansion(LTE) for the fabricated test samples. See Table 5 for the calculated displacement values

Table 4 MatWeb values for yield stress, Young's modulus, CTE .

Material Mix	Specificaton	Thicknesses	Coefficient of LTE	Youngs Modulus	Yield stress
Invar 36	B388-06 2006	0.254mm	1.45 x 10-6m /m K	141 Gpa	276MPa
Aluminium	EN AW 1050A H14	0.254mm	21.8 x 10-6m /m K	69 GPa	103MPa
Invar 36	B388-06 2006	0.3mm	1.45 x 10-6m /m K	141 Gpa	276MPa
Nickel Silver	BS2870 NS103	0.3mm	13 x 10-6m /m K	120GPa	324MPa
Invar 36	B388-06 2006	0.65mm	1.45 x 10-6m /m K	141 Gpa	276MPa
Brass	BS 2870 CZ108	0.65mm	20.1x 10-6m /m K	106GPa	260MPa
Invar 36	B388-06 2006	0.8mm	1.45 x 10-6m /m K	141 Gpa	276MPa
Mild Steel	BS EN1 A	0.8mm	11 x 10-6m /m K	195 GPa	205MPa
Invar 36	B388-06 2006	1.3mm	1.45 x 10-6m /m K	141 Gpa	276MPa
Copper	BS 2879 C106	1.3mm	16.4 x 10-6m /m K	110 GPa	183MPa
Invar 36	B388-06 2006	0.4mm	1.45 x 10-6m /m K	141 Gpa	276MPa
Stainless Steel	AISI BS 304	0.4mm	17.3 x 10-6m /m K	200Gpa	215MPa

The values from Table 4 were used with the following formulae to evaluate the safe chord line displacements as shown in Table 5:

From section 3.6

$x_{\sigma d} = 2R_c \, sin\left(\frac{A_b}{2R_c}\right) - 2R_d \, sin\left(\frac{A_b}{2R_d}\right)$ case 2 stress limited displacement.

Supporting equations: $R_{\sigma b} = \frac{\boldsymbol{t\, E_a}}{\boldsymbol{2\, \sigma}}$: $R_d = \frac{R_{\sigma b} R_c}{R_{\sigma b} + R_c}$ where σ is provided by Table 5.

All other variables have been stated earlier.

Table 5 provides the calculated safe chord line displacements for each test sample using case 2 from section 3.7.

Table 5 Maximum displacements for test samples

Vertical gravity test set - bespoke bimetallic strip test samples

SBC206-1	
Ab=80mm	x
Rc=40mm	6mm

Sauter Force vs Displacement test set - bespoke bimetallic strip test samples

SBC206-1		SBC206-1	
Test 1		Test 2	
Rc=80mm constant	x	Ab=100mm constant	x
Ab=80mm	4mm	Rc=50mm	9.5mm
Ab=100mm	7mm	Rc=64mm	8.1mm
Ab=120mm	12mm	Rc=70mm	7.6mm
Ab=140mm	18mm	Rc=80mm	7.3mm
Ab=160mm	26mm	Rc=84mm	6.6mm
Ab=180mm	35mm		
Ab=200mm	45mm		

Magnetic Assembly test rig - fabricated bimetallic strip test samples

Test Num.	Test Sample	x	Test Num.	Test Sample	x	Test Num.	Test Sample	x
1	I/SS/0.25/0.25	16mm	7	I/A/0.25/0.2	21mm	13	I/C/0.25/0.3	20mm
2	I/SS/0.5/0.5	7.5mm	8	I/A/0.25/0.5	15mm	14	I/C/0.25/0.6	13mm
3	I/SS/0.25/0.51	9.4mm	9	I/A/0.5/0.5	9.5mm	15	I/C/0.5/0.6	9.5mm
4	I/SS/0.5/0.7	6.0mm	10	I/A/0.5/0.8	7.9mm	16	I/C/0.5/0.8	8.1mm
5	I/SS/0.75/0.5	6.2mm	11	I/A/0.75/0.5	7.0mm	17	I/C/0.75/0.6	7.4mm
6	I/SS/0.75/0.7	5.1mm	12	I/A/0.75/0.8	6.1mm	18	I/C/0.75/0.8	6.6mm

Test Num.	Test Sample	x	Test Num.	Test Sample	x
19	I/B/0.25/0.25	24mm	25	I/N/0.25/0.4	20mm
20	I/B/0.25/0.6	15mm	26	I/N/0.25/0.6	15mm
21	I/B/0.5/0.6	11mm	27	I/N/0.5/0.6	11mm
22	I/B/0.5/0.73	9.5mm	28	I/N/0.5/0.74	10mm
23	I/B/0.75/0.6	8.3mm	29	I/N/0.75/0.6	9mm
24	I/B/0.75/0.76	7.5mm	30	I/N/0.75/0.74	8mm

Key to test samples:

For the fabricated bimetallic strip test samples a unique identifier was applied to each test sample.

For test sample 1: I/SS/0.25/0.25 , this is an Invar 36 - Stainless Steel test sample with both metals equal to 0.25mm thick, its stress limited displacement was 16mm.

For test sample 11: I/A/0.75/0.5, this is an Invar 36 - Aluminium test sample with Invar 36 = 0.75mm thick and Aluminium = 0.5mm thick, its stress limited displacement was 7mm.

For test sample 30: I/N/0.75/0.74, this is an Invar 36 - Nickel test sample with Invar 36 = 0.75mm thick and Nickel = 0.74mm thick, its stress limited displacement was 8mm.

The next sections introduce the test rig type, test rig setup and equipment, followed by the set of test procedures for that test rig.

5.5 Vertical Gravity Test Rig – Bespoke Test Samples

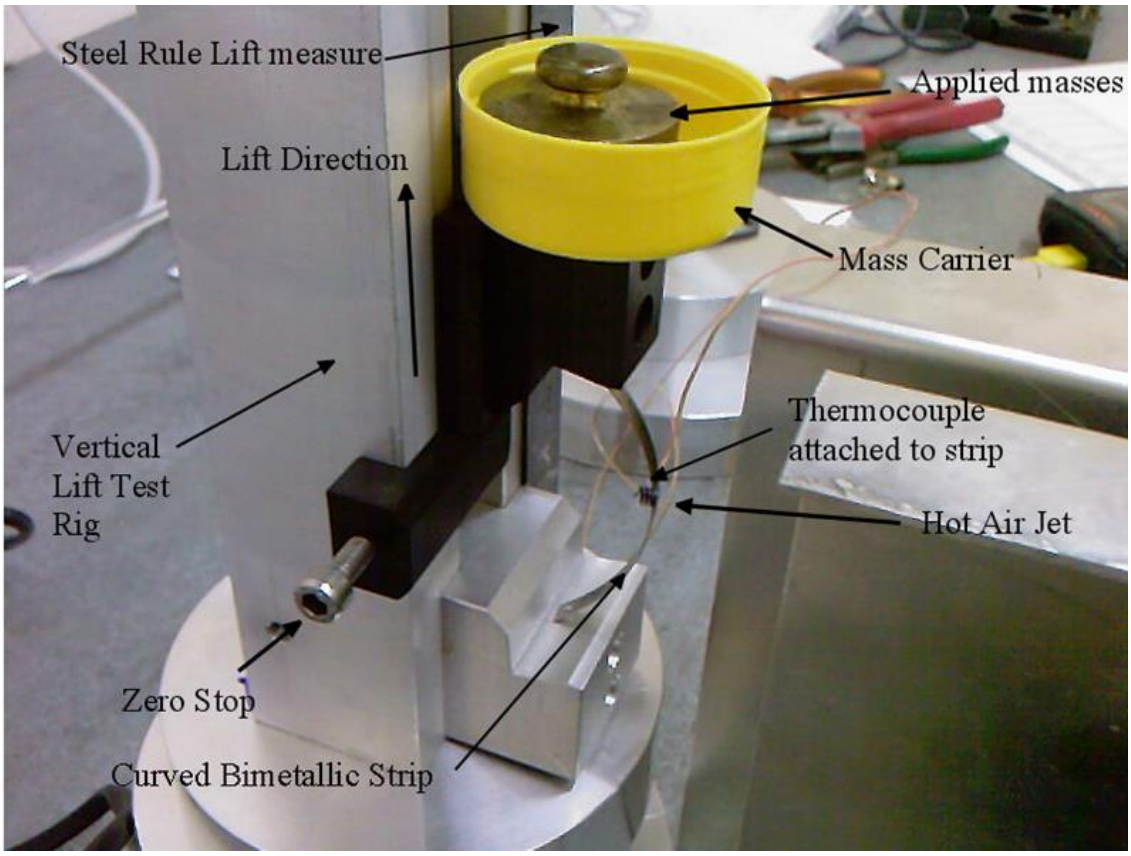

Fig.5-1 Vertical test rig for bespoke pre-curved bimetallic test samples

The test rig loaded the pre-curve test samples in the vertical plane. The rig was made from aluminium alloy with some generic plastic parts. The rig enabled the testing of the lightly loaded bespoke bimetallic strip test samples it was used in the vertical orientation in an attempt to reduce the dry friction of the moving parts. The rig was used to provide combined loading and heating "lift" tests.

5.5.1 Vertical Gravity Test Rig Equipment List – Bespoke Samples

Vertical Test Rig Capabilities:

Adjustable zero stop :

Fixed and moving test sample supports.

Plastic mass carrier.

Measurement

300 mm steel rule affixed to the rig.

Magnifying glass to view steel rule graduations

Heating and cooling

Hot air tunnel comprising of two 200mm bent aluminium sheets positioned to form 20mm wide tunnel of hot air flow.

Bosch Hot Air Gun; variable heat settings from 50°C to 600 °C in 50°C steps.

Wide nozzle 80mm x 15mm air flow cross section turned vertical for air tunnel

Solex St 4060 Digi-Thermometer Quarz.

K-Thermocouple (Dual Input) Hanna instruments (UH approved).

Hi 93532 plus thermocouple wire.

Cool Air Supply Remington model AC-5011 220- 240V 1850-2200W, serial no. 09411-SL with 80mm x 8mm cross sectional air flow distributor.

Test Samples

See Table 5 for vertical gravity test rig samples.

Masses used

Griffin and Tatlock Standard masses 0.5, 2, 5, 10, 20, 50, 100g masses.

All masses were calibrated Avery (2011) scales.

Sundry equipment

300 mm steel rule.

Fisher Brand- Laboratory Stands plus adjustable clamps

Paper recording sheets

Casio Scientific calculator Fx-82A

Pens, various permanent markers.

MacBook Air with Excel software for recording of data.

5.5.2 Load vs. Temperature Test Procedure - Bespoke Samples Tested on Vertical Gravity Test Rig:

A thermocouple was centrally attached to the blade on the outside face of the strip, protected from the direct air flow.

1) Test sample was simply mounted vertically into test rig as shown in Fig.5-1.
2) The zero stop adjusted so that the test sample was under no vertical loading.
3) Ambient and thermo-couple temperatures recorded.
4) A set mass was placed in the yellow plastic tray and vertical downward, and displacement was recorded by measuring the new position on the ruled scale.
5) Test sample was uniformly heated by hot air gun in 20° C steps.

6) Steps 1 to 4 were repeated 3 times for all the test samples. After the temperature gauge had stabilised, the new lifted position and corresponding temperature were recorded for each 20° C step.
7) Test sample was removed from rig and checked for roundness against former.

5.6 Sauter Force Displacement Test Rig – Bespoke Samples

The Sauter force and displacement gauge rig was used in the horizontal orientation, see Fig.5.2. The Sauter test force displacement test rig was purchased as a stand- alone rig and modified to provide the same mounting and loading conditions as on the magnetic coupling and vertical lift test rigs.

This test rig was only used to test bespoke bimetallic strip. It was used for force vs. displacement test samples and for testing temperature vs. displacement test samples. It had the advantage of a more precise loading and displacement reading over the vertical gravity test rig due to its digital readouts.

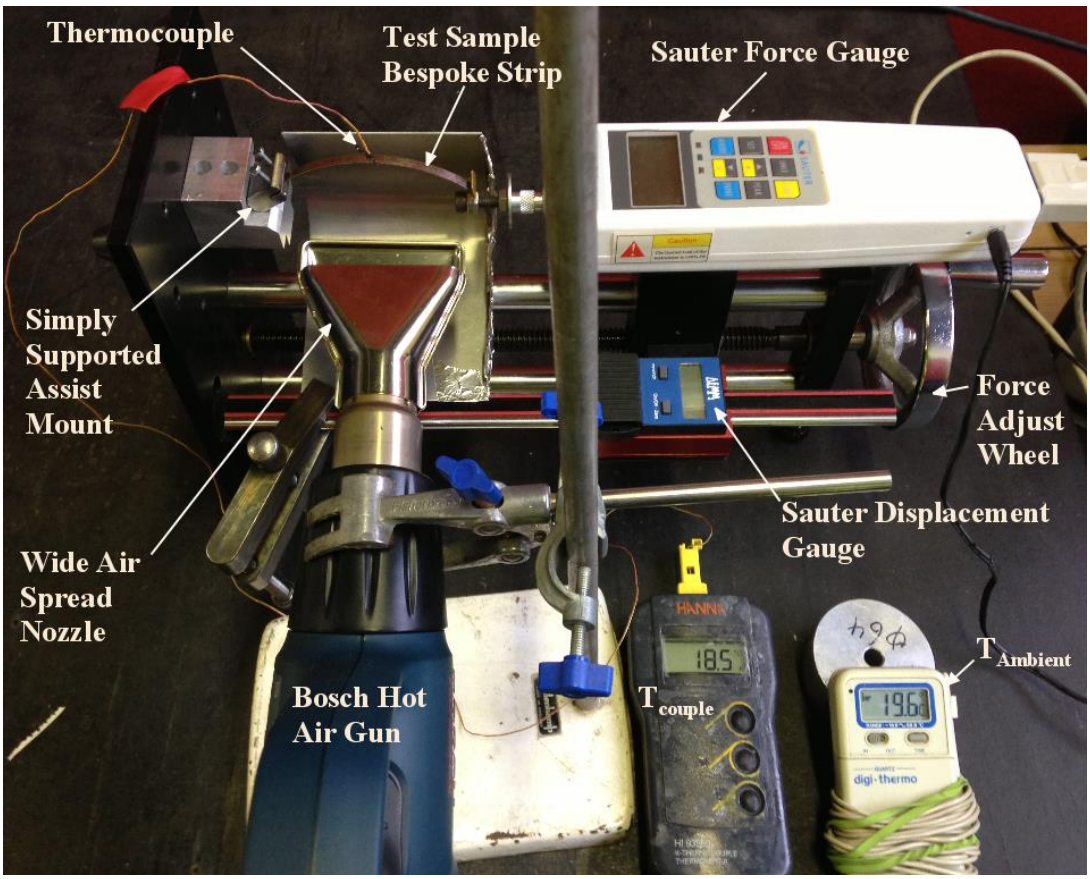

Fig.5-2 Sauter force displacement test rig in horizontal orientation

The Sauter force gauge was operated by a wheel which precisely enabled the accurate loading of the test samples and the displacement gauge recorded the displacements. The Sauter test rig was limited to 5N and thus was not suitable for the fabricated bimetallic test samples that required heavier loading.
The disadvantage of this test rig was the limited loading that could be applied via the loading wheel.

5.6.1 Sauter Force Displacement Equipment List – Bespoke Samples

Sauter Test rig capabilities:

Measurement

Variable force gauge: 0.001N to 5N

Displacement gauge: 0.001mm to 150mm

Heating and cooling

Bosch Hot Air Gun; variable heat settings from 50°C to 600 °C in 50°C steps.

Wide nozzle 80mm x 15mm air flow cross section.

Solex St 4060 Digi-Thermometer Quarz.

K-Thermocouple (Dual Input) Hanna instruments (UH approved).

Hi 93532 plus thermocouple wire.

Cool Air Supply Remington model AC-5011 220- 240V 1850-2200W, serial no. 09411-SL with 80mm x 8mm cross sectional air flow distributor.

Test samples

See Table 5 for Sauter bespoke test samples.

Sundry equipment

Fisher Brand- Laboratory Stands plus adjustable clamps.

Magnetic Clamp, plus adjustable posts.

Special simply supported test sample mounting aid 1 off to ensure stability during test.

Various light tools and Allen keys, 240v adjustable Spot light.

Paper recording sheets.

Casio Scientific calculator Fx-82A.

Pens and various permanent markers.

MacBook Air with Excel software for recording of data.

5.6.2 Load vs. Displacement Test Procedure – Bespoke Samples Tested on Sauter Force Displacement Test Rig:

1) Test sample mounted into test rig.
2) Force and displacement gauges set to zero.
3) Ambient and thermocouple temperatures were recorded.
4) Test sample displaced by the moving Sauter Force /displacement gauge.
5) Force and displacement values recorded until the maximum displacement was achieved**.**
6) Test sample removed from rig and checked for roundness against former.
7) Steps 1 to 5 were repeated for 3 runs [5] for all samples in test set.

5.6.3 Temperature vs. Displacement Test – Bespoke Samples Tested on Sauter Force Displacement Test Rig:

A thermocouple was centrally attached to the blade on the outside face of the strip, protected from the direct air flow.

1) Test sample was simply mounted into test rig as shown in Fig.5-2.
2) Force and displacement gauges set to zero.
3) Ambient and thermo-couple temperatures recorded.
4) Test sample uniformly heated by hot air gun, the displacement was recorded by unwinding the force adjust wheel see Fig.5-2, at the point where force gauge was zero.
5) Thermocouple and ambient temperatures and displacement were all recorded.
6) Steps 1 to 5 repeated for all the test set.
7) Test sample removed from rig and checked for roundness as in previous sets.

5.7 Magnetic Coupling Test Rig – Fabricated Samples

This test rig was designed specifically to cater for the testing of the heavy duty fabricated bimetallic strip test samples. The fabricated test samples were the most heavily loaded samples of all the test samples. The advantage of this test rig was that it

[5] Test set 2 only one test run per test sample.

had a central moving assembly on magnetic bearings that afforded near frictionless movement.

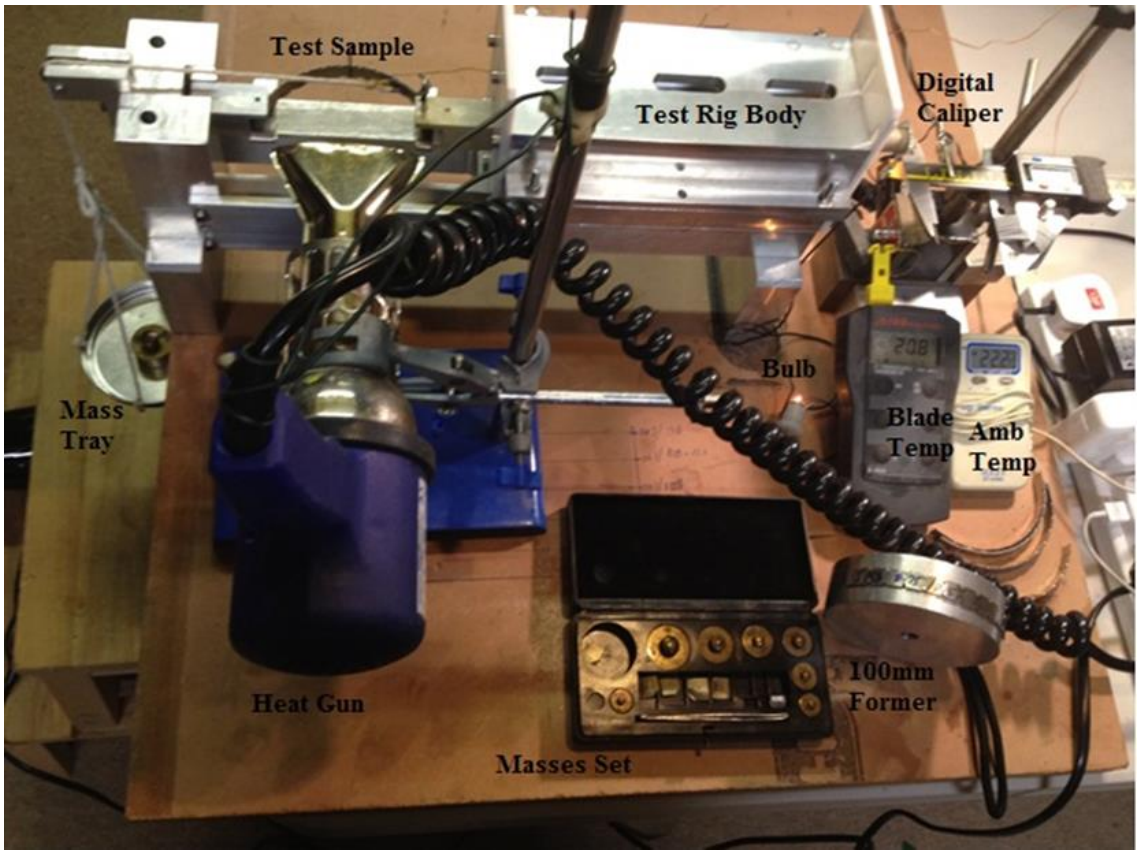

Fig.5-3 Magnetic coupling type test rig- used for fabricated test samples

Fig.5-3 shows the magnetic coupling type test rig. All the testing of the fabricated test samples was conducted on this test rig and as the main test rig, it was designed, it possessed a robust aluminium structure that coped well with the higher loading.

The test rig was designed for the specific test criteria and the design intent was to produce a totally frictionless moving floating centre that is “floating” in a magnetic field, thus offering no frictional load onto the test pieces. Due to certain minor manufacturing flaws, a true “floating” assembly could not be achieved, but a partial floating or very low friction moving centre was obtained. It should be noted that the original design intent was to pin mount the test samples, however due to a fabrication issues of the test samples, a simply supported test sample mounting and loading method was adopted which was same as on the other test rigs.

The major design requirement for the rig was that the measurement end of the rig should not be influenced by spurious heat emanating from the test strips at the hot test end of the rig. This was the rationale for using PEEK as the material for holding the

bimetallic strip, and another reason to stem the heat transfer along the rig by having a frictionless moving arm that minimised the heat transfer path. The magnetic coupling rig also possessed a specially designed heat gate. The heat gate was used to enable time vs. displacement tests to be performed on the fabricated test samples. This was the only test rig that it was possible to perform the timed tests.

5.7.1 Magnetic Coupling Test Equipment List – Fabricated Samples

The generic test equipment list is as follows:
Test Rig: as manufactured shown in Fig. 5-3.
Pulley rope and mass tray weighed 27.5g.
Counterbalance with thin thread weighed 18g.
Measurement
Contact Sensing feedback system including 9V battery and bulb for Digital Calliper.
Electronic Digital Calliper, 0.01mm accuracy, 0 -150 mm range, zeroing facility.
Solex St 4060 Digi-Thermometer Quarz.
K-Thermocouple (Dual Input) Hanna instruments (UH approved).
Hi 93532 plus thermocouple wire.
Stopwatch digital, application from Apple IPhone 4S.
Digital height gauge and plate, UH fabrication shop.
Heating and cooling
Hot air gun – Costech –Mar Equipment Ltd (UH approved). No. 03F13566 Ref: D200/400 V220/240
1100W Temp on 1, 200°C, on 2 400°C, with Wide nozzle 80mm x 15mm air flow cross section.
Bosch hot air gun; variable heat settings from 50°C to 600 °C in 50°C steps.
Cool Air Supply Remington model AC-5011 220- 240V 1850-2200W, serial no. 09411-SL with 80mm x 8mm cross sectional air flow distributor.
Test samples
See Table 5 for Magnetic coupling test rig fabricated test samples.
Masses used
Griffin and Tatlock Standard masses 0.5, 2, 5, 10, 20, 50, 100g masses.
Additional masses used and weighed on the UH Avery weighing scales
87.5g

281.1g

475.9g

560.2g

Note: all masses were weighed on weighing scales Avery (2011)

Test Sample Former used 100mm Dia. x 30mm thick +/- 0.25mm.

Sundry equipment

Fisher Brand-Laboratory Stands plus adjustable clamps.

Magnetic Clamp, plus adjustable posts.

Propan-2-OL: code: P/7490/17 Fischer Scientific.

300 mm steel rule.

9V battery, bulb, bulb holder, crocodile clips, electrical wire, black insulation tape.

Various light tools and Allen keys, 240V adjustable Spot light.

Paper recording sheets.

Casio Scientific calculator Fx-82A.

Pens, various permanent markers.

MacBook Air with excel for recording of data.

5.7.2 Load vs. Displacement Test Procedure – Fabricated Samples Tested on Magnetic Coupling Test Rig:

1) The test piece was checked for roundness and against a 100mm diameter round former, then checked for curvature according to section 5.13.
2) The test piece was placed in the test rig, the electronic digital calliper was set to zero, the light bulb illuminates, with no load applied to the curved bimetallic strip whilst the mass tray was supported.
3) The support for the empty tray was then gently removed and the displacement of the tray was measured on the calliper.
4) Masses were applied to the mass holding tray and the displacement from the zero point was recorded.
5) Step 4 was repeated for sufficient number of recorded points to enable the load vs. displacement graph for the test piece.
6) After each test the strip was checked again against the 100mm former, and as specified in section 5.13, for any permanent deformation.
7) The after test the condition of the strip was noted.
8) Each load vs. displacement test was repeated three times for every test piece.

9) Steps 1 to 6 were repeated for all the test samples.
10) The average of the three test runs for each test piece was plotted in an Excel spreadsheet.

5.7.3 Temperature vs. Displacement Test Procedure – Fabricated Samples Tested on Magnetic Coupling Test Rig:

A thermocouple was centrally attached to the bimetallic test sample on the outside face of the strip, protected from the direct air hot flow.

1) Each test piece was checked against the 100mm diameter round former and as specified in section 5.13
2) The test piece was loaded into the test rig with one end against the moving arm with no external loading, and checked that it was seated correctly on the fixed and moving arm of the rig.
3) The electronic digital calliper was set to zero when the light bulb was "on".
4) Ambient temperature was recorded
5) Strip temperature as measured by the thermocouple was recorded from the attached electronic thermometer.
6) The calliper was backed off approximately 0.5mm from the zero point; the light bulb was now "off". Note the backing off distance varied, depending on the permissible displacement value for the test sample.
7) Uniform heat was applied to the inside surface of the curved strip by a hot air gun.
8) When contact was made by the moving arm to the fixed calliper as shown by the light bulb illuminating again, the temperature of the thermocouple and the displacement from the zero point, were both recorded.
9) The calliper was backed off again and steps 7 and 8 were repeated until the strip provided sufficient points to enable a temperature vs. displacement graph.
10) The strip was cooled downed to ambient temperature and steps 1 to 9 were repeated for each test piece three of four times depending on strip results obtained.
11) The average of the three or four test runs for each test piece was plotted in an Excel spreadsheet.

5.7.4 Load vs. Temperature Test Procedure – Fabricated Samples Tested on Magnetic Coupling Test Rig:

1) The test piece roundness and size against 100mm diameter test former was checked and as specified in section 5.13.

2) The test piece was loaded into the test rig, and checked that it was seated correctly on the fixed and moving arm of the rig.
3) The thermal couple was checked and thermometer reading the strip temperature was recorded.
4) The ambient temperature was recorded.
5) The moving arm was moved back to touch the fixed calliper, which was then set to zero, upon contact the light bulb came on.
6) A test mass was added to the mass tray, and the displacement due to load alone, was recorded along with the strip temperature and ambient temperature the light bulb was now off.
7) Uniform heat was applied to the inside surface of the curved strip by a hot air gun.
8) Upon contact of the moving arm to the fixed calliper signalled by the illumination of the light bulb, the temperature and displacement and mass applied were all recorded.
9) The calliper arm was moved again to record another point.
10) Steps 5 to 11 were repeated until sufficient data had been collected.
11) Ambient temperature was checked again before and after each test.
12) All test data was recorded onto test sheets.
13) The average of the three or four test runs for each test piece was plotted in Excel spreadsheet.

5.7.5 Time vs. Displacement Test Procedure - Fabricated Samples Tested on Magnetic Coupling Test Rig:

Distance constant: approximately 1mm.

The aim of this test was to understand the influence of the bimetal component as a function of time, and to see how the different material thicknesses and combinations of materials affected the response time of strip to displace a short distance, typically 1mm. A thermocouple was centrally attached to the blade on the outside face of the strip. An illuminated touch sensor was used to detect when the moving arm had touched the calliper arm. For this specific setup see Fig.5-4.

Fig.5-4 Displacement vs. time test set up

The empty mass tray was used in this test set.

The test procedure is described below:

1) The test piece roundness was checked against 100mm diameter test former and as specified in section 5.13.
2) The test piece was loaded into the test rig, and checked that it was seated correctly on the fixed and moving centre arm of the rig.
3) The thermal couple was checked and for the thermometer reading the strip, the temperature was recorded.
4) The ambient temperature was recorded.
5) The centre moving arm was moved to touch the fixed calliper and was set to zero, the light bulb was on.
6) The heat gate was closed to prevent heat flow to the test sample.
7) The Bosch hot air gun was set 300 °C (repeat ably set for all test samples).
8) The calliper scale was moved back from the zero setting and the distance recorded, the light bulb was now off.
9) The heat gate was released, and the timer started.
10) At the point where the centre arm made contact, indicated by the light bulb now on, the timer was stopped.
11) Temperature, distance and time were recorded.

12) Steps 2 to 11 were repeated 5 times, for each test sample.

5.8 Bench Fixed – Clamped One End – Bespoke Samples

This was not a specific test rig but a method of enabling the "straightening up" tests. The straightening tests differed from the chord line displacement set-up by the way the bimetallic strip was constrained. As stated previously, the chord line displacement of a pre-curved bimetallic strip occurs due to the degree of rotational freedom at each end of the strip. In the straightening test, one end of the bimetallic strip was fully constrained against rotation and displacement, the other end was free to move. In this set-up, when heat was applied to the bimetallic strip, the strip simply straightened up at the free end. The pre-curved bimetallic strip was clamped parallel to the work bench surface.

This set up was only used for the end point locus prediction test for bespoke bimetallic strip, see Fig.5-5. To provide a consistent heat zone and maintain a temperature controlled heating environment, special heat shields were employed. The heat shields enhanced the capability of the set up to maintain a uniformly distributed temperature within the area.

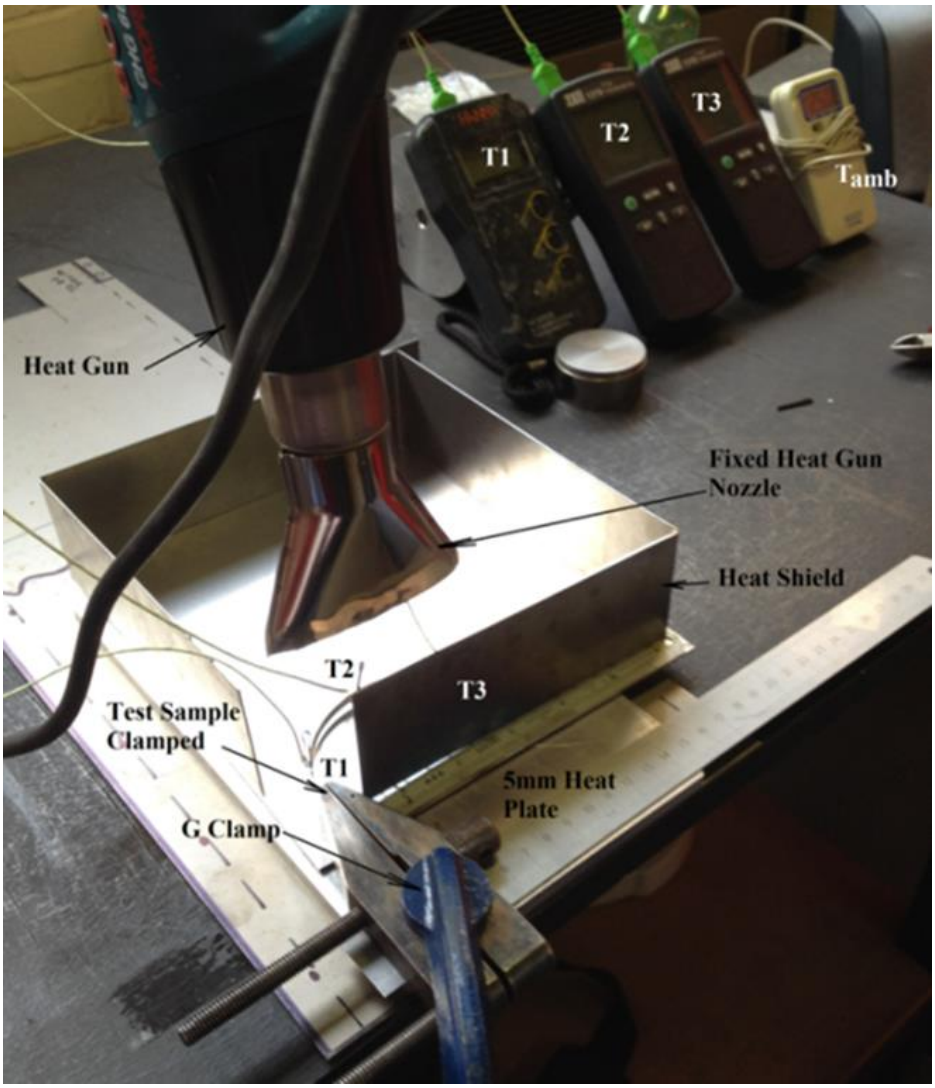

Fig.5-5 Bench fixed – clamped one end

5.8.1 Bench Fixed Test Equipment List

Test fixture comprising of:

1 - workshop “G” clamp steel medium size.

1 – small horizontal adjustable jaw clamp.

200 mm square x 1mm thick sheet aluminium base plate to record locus of data points during the tests.

200 mm square x 5mm thick aluminium heat stabilisation plate.

2 - 60mm x 1mm high “L” shaped aluminium heat shields.

Test set

4 - Curved bimetallic test samples, tagged as: D64, D80, D100, D128: Shivalik SBC-206-1. Thickness of each metal 0.2mm equal; total thickness = 0.4mm.

4 – Aluminium Round Formers D64, D80, D100, D128 mm nominal diameters.

Heating and cooling

1 - Hanna HI 93530 K-Thermocouple Thermometer Digital: Thermocouple: position T1. 2 - TES 1319 K-Type Thermometer: Thermocouple: position's T2 and T3.

1 - Solex, Digi-Thermo ST 4060 Digital Thermometer recording ambient temperature.

3 – Flexible thermocouple wires – at hot sensing end, soldered ends of the wires.

Bosch 2.3kW- GHG 660 LCD Professional variable flow hot air gun; adjustable heat settings in increments from 50 to 600 °C. Hot air gun outlet flow dimensions: 60mm long x 15mm wide.

Test Samples

See Table 5 for Bench fixed test samples.

Sundry equipment

1 set of fine black felt tip pen permanent ink type.

300 mm steel rule.

Test Stand generic scientific type with adjustable grip clamps.

3 – Lightly sprung clips.

5.8.2 Bench Fixed Test Procedure - Bespoke Samples Tested on the Bench Test Fixture

A thermocouple wire was affixed to each test sample by a spring clip on the outside surface and the sensing end of the thermocouple wire was shielded by the body of the test sample from direct hot air flow. The positioning pattern of the three thermocouples was the same for all test samples as presented in Fig 5-6.The hot air flow rate and position of the heat gun was fixed for all testing. The heat flow was perpendicular to the aluminium base plate for a constant uniform heating environment and the heat gun nozzle was 10mm from the aluminium surface. The 5mm heat stabilising plate was placed underneath the aluminium base plate. The heat stabilising shield was placed around the test pieces during testing, see Fig. 5-5. A 1mm thick sheet Aluminium base plate was used for recording the locus of points during the tests. The Test sample holder was clamped to the aluminium base plate using a workshop "G" clamp. The test samples were clamped in the test sample holder to 1mm depth for each strip. The test samples were measured to be 1mm parallel to, and clear of the aluminium base plate throughout all tests as shown in Fig.5-6. A black fine felt tip pen was used for recording

data points on the aluminium base plate. Each test sample was clamped parallel to the Aluminium base plate at a height of 1mm within the heat stabilised zone. One end of the bimetallic strip was rigidly fixed, the other end was free to move as can be observed in Fig.5-6. Each test sample was subjected to uniform heating and as the strip straightened up, the locus of the free end point was recorded on the aluminium base plate using a fine felt-tipped pen. At each individual point, the corresponding thermocouple temperature was recorded from reading the values of T1, T2 and T3 as shown in Figure 5-6. The heat from the gun was increased in steps of 20° C and an identifiable locus of points was produced for each test sample.

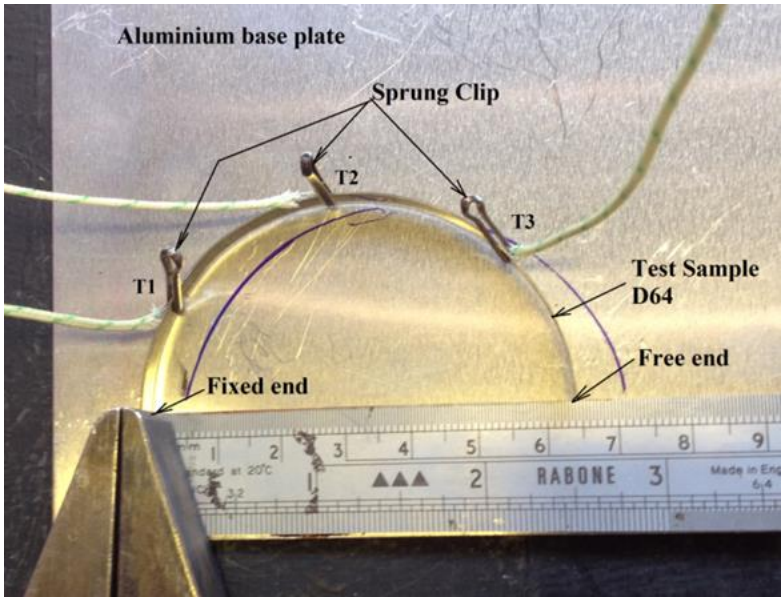

Fig.5-6 Test sample clamping and thermocouple

5.9 Test Sets –Fabricated Test Samples

All fabricated test samples were 120mm long by 10mm with an ambient temperature radius of curvature of $R_c = 50mm$. Samples were water jet cut with tabs "ears" formed over into "cut-outs", profile accurate to within + /- 0.25mm.

Test sample former used 100mm dia. x 30mm thick +/- 0.25mm. The fabricated test samples were also used in the time vs. displacement tests.

Table 6 Prefabricated test sample sets

No.	Invar/Stainless St.	No.	Invar/Alum.	No.	Invar/Copper	No.	Invar/Brass	No.	Invar/Nickel
1	I/SS/ 0.25/0.25	7	I/A/ 0.25/0.2	13	I/C/ 0.25/0.3	19	I/B/ 0.25/0.25	25	I/N/ 0.25/0.4
2	I/SS/ 0.5/0.5	8	I/A/ 0.25/0.5	14	I/C/ 0.25/0.6	20	I/B/ 0.25/0.6	26	I/N/ 0.25/0.6
3	I/SS/ 0.25/0.51	9	I/A/ 0.5/0.5	15	I/C/ 0.5/0.6	21	I/B/ 0.5/0.6	27	I/N/ 0.5/0.6
4	I/SS/ 0.5/0.7	10	I/A/ 0.5/0.8	16	I/C/ 0.5/0.8	22	I/B/ 0.5/0.73	28	I/N/ 0.5/0.74
5	I/SS/ 0.75/0.5	11	I/A/ 0.75/0.5	17	I/C/ 0.75/0.6	23	I/B/ 0.75/0.6	29	I/N/ 0.75/0.6
6	I/SS/ 0.75/0.7	12	I/A/ 0.75/0.8	18	I/C/ 0.75/0.8	24	I/B/ 0.75/0.76	30	I/N/ 0.75/0.74

I = Invar 36
N = Nickel
C = Copper
SS = Stainless Steel
B = Brass
A = Aluminium

A typical test sample may be described by the following code e.g. I/SS/0.25/0.2
This is an Ivar & Stainless steel test sample, with an Ivar thickness of 0.25mm and the Stainless steel is 0.2mm thick.
The dimensions of each sample is 120mm long x 10mm wide +/- 0.25mm

5.10 Test Sets - Bespoke Test Samples

5.10.1 Bespoke Bimetallic Strip Samples

For the bespoke bimetallic test samples, all were manufactured from Shivalik SBC206-1. The initial size of the raw strip was 200mm x 5mm x 0.4mm thick with an equal thicknesses of :

Steel FeNi20Mn6 - 0.2mm thick.

Invar FeNi36 - 0.2mm thick.

5.10.2 Vertical Gravity Bespoke Samples

For the vertical gravity tests, the bimetallic test sample strips were made with an arc length of: $A_b = 80mm$, with a radius of curvature of $R_c = 40mm$. 3 samples were used in this test. All test samples were made at ambient temperature of 21°C.

5.10.3 Sauter Force vs. Displacement Bespoke Samples

For the Sauter force vs. displacement tests, the test sample strips were made to a variety of sizes according to the following table:

Table 7 Sauter force vs. displacement test set

Test set 1 R_c= 80mm *constant*	Test set 2 $A_b = 100mm$ *constant*
$A_b = 80mm$	R_c = 50mm
$A_b = 100mm$	R_c = 64mm
$A_b = 120mm$	R_c = 70mm
$A_b = 140mm$	R_c = 80mm
$A_b = 160mm$	R_c = 84mm
$A_b = 180mm$	
$A_b = 200mm$	

5.10.4 Sauter Temperature vs. Displacement Bespoke Samples

The temperature vs. displacement test sample set is shown in Table 8. There were 4 test sets which were categorised initially by their arc length A_b which was constant for a set of varying radius of curvatures.

Table 8 Sauter temperature vs. displacement test set

Test set 1	Test set 2	Test set 3	Test set 4
Constant A_b = 75mm	*Constant* A_b= 80mm	*Constant* A_b= 85mm	*Constant* A_b= 90mm
R_c=30mm	R_c=30mm	R_c=30mm	R_c=30mm
R_c=35mm	R_c=35mm	R_c=35mm	R_c=35mm
R_c=40mm	R_c=40mm	R_c=40mm	R_c=40mm
R_c=45mm	R_c=45mm	R_c=45mm	R_c=45mm
R_c=50mm	R_c=50mm	R_c=50mm	R_c=50mm
R_c=55mm	R_c=55mm	R_c=55mm	R_c=55mm
R_c=60mm	R_c=60mm	R_c=60mm	R_c=60mm

5.10.5 Bench Fixed – Bespoke Samples

The Bimetallic strips used in the tests were purchased from Shivalik and were initially 202mm long x 5mm wide x 0.4 mm thick. Four bimetallic strip test samples were made by gently cold working the strips to form true arcs of a circle equal to D64mm, D80mm, D100mm, and D128mm. The bimetallic strips were formed with the material with the highest coefficient of linear expansion on the inner surface. To ensure that the curved bimetallic strips conformed to a true arc during cold working, special formers were produced to check the diameter and roundness see Fig.5-7. The formers were held to +/-

0.25mm tolerances. The length of each test sample was cut back to equal half the circumference of the former , i.e. 100.53mm,125.66mm,157.07mm, 200.06mm long respectively, within a tolerance of +/- 0.25mm. Each test sample was subjected to heat treatment according to the Kanthal Bimetal Handbook to 350 °C for a 3 hours before the actual testing took place. This was done in order to normalize the strips from any work-hardened induced stresses resulting from the cold forming process. In addition to the roundness formers for checking their roundness, each sample was also checked for accuracy using the bend checking procedure from section 5.13.

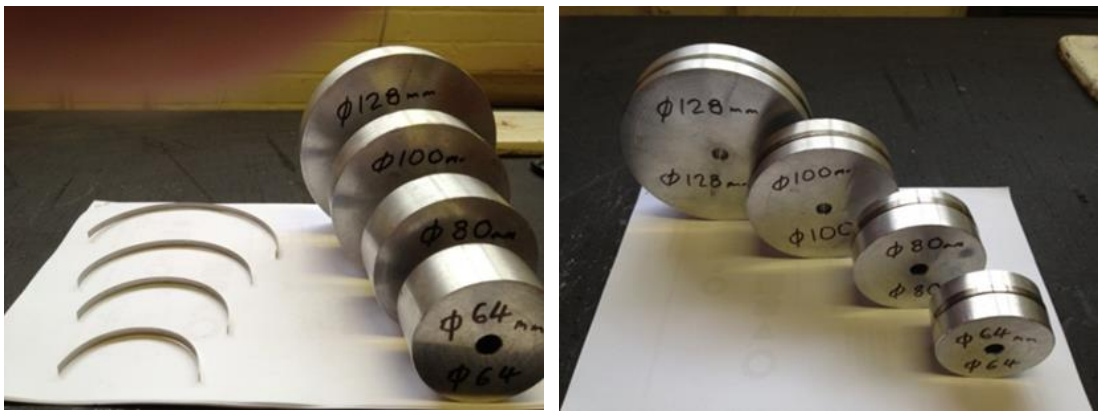

Fig.5-7 Test samples after forming and checking for roundness

5.11 Production of the Fabricated Bimetallic Strip Test Samples

To produce the test samples as specified in Table 6, a new fabrication process was introduced. In order to provide a large data test set, fabricated bimetallic strip test pieces in a variety of material combinations and material thicknesses were manufactured.

At the beginning of the investigation, bonding and riveting joining methods were both experimented with, but both methods were unsuitable due to rivet heads and peeling of the material layers at temperature in the bonding samples tested,

see Fig.5-8 and Fig.5.9.

Fig.5-8 Initial bi-metallic strip fabrication method using pop rivets

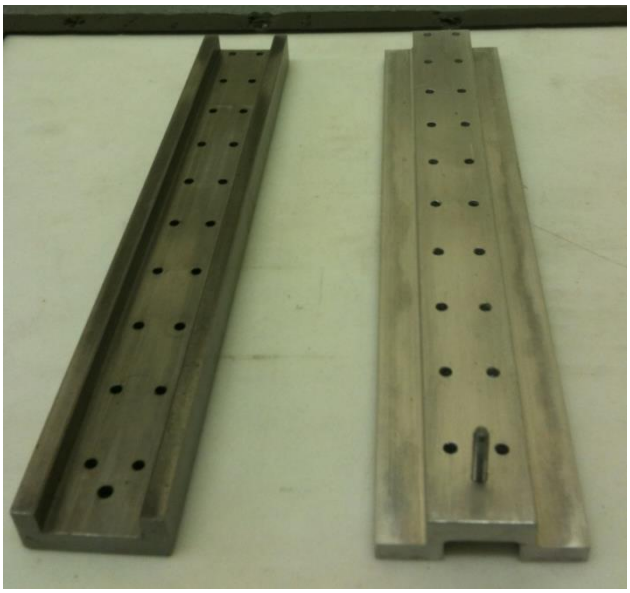

Fig.5-9 Hole drilling and assembly jig for pop riveted strips

Additionally, bonding of the two metal surfaces, using adhesives, creates a third material interface that is not found in bespoke roll bonded, or cold forged bimetallic strip. Riveting the strips, although sound, made it very difficult to bend or permanently form into curved strips because of the heads of the rivets, see Fig.5-8. The rivet heads could also cause a disruption of the even heat flow to the strip, again causing errors not found in commercially manufactured bespoke bimetallic strip.

One method of fabricating bimetallic strip that was investigated employed the “clinch” method of joining two thin metals together.

The clinch method, joins two thin sheets of material together by a punching action which pushes one material through the other in a controlled and limited fashion.The clinch method used by TOX (2013) uses no rivets, and the joints can be made suitable

on both sides for subsequent bending and secondary forming operation. Fig.5-10. shows the clinching steps starting at 1 through to the completed joint at 3.

However, after a few sample tests using the clinch tool, see Fig.5-11b, it became apparent that this method could not easily cater with the variety of thicknesses of test pieces required to be joined. Because the adjustment of the clinch tool for a specific thickness of join can require a large set up time, or a separate tool for each bimetallic test sample thickness, this method of joining was found unsuitable.

Fig.5-10 Courtesy of TOX (2013)

It should be noted that the clinch method produced a good joint that was comparable to a spot welded joint, and if the test regime required only one thickness of join throughout, then this would have been the preferred joining solution for the fabrication of the bimetallic strip.

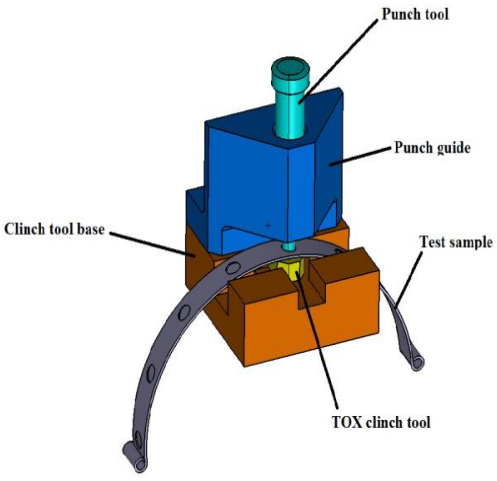

Fig.5-11(a) Tool concept

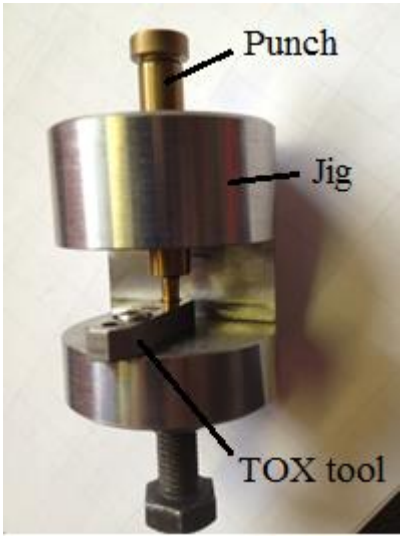

Fig.5-11(b) Test TOX (2013)

In practice the clinch joining method is set up for joining metal car panel sheets whereby there is no significant variability in either the materials to be joined, or their individual thicknesses.

In the fabrication of the test set as shown in Table 6, see section 5.9, the test pieces have a variety of thicknesses and material combinations and thus TOX PRESSOTECHNIK clinch method was not able to cater for this variety of joins, in just one tool. Therefore an alternative method of permanently joining two separate metals was sought.

The fabrication method required to meet the variable test set of Table 6 were as following:

1) Enable any combination of metal / plastic to be joined up to a combined 2mm thickness.
2) Enable the bimetallic strip after joining, to be cold formed into any radius of curvature.
3) Provide the production of repeatable and consistent test samples.
4) Not require a separate additional material/s to facilitate the permanent join of the fabricated strip

The joining solution that met all the requirements and was used to fabricate all the bimetallic strip test samples was as follows:

Each metal of the bi-metallic strip was provided with either a set of equi-spaced “ears” or “tabs”, or “cut-outs” along the entire length of the strip. To achieve these specific profiles out of the flat raw material sheet, the following methods of manufacture were considered:

A 2D router or CNC Vertical milling operation was considered to machine the profiles.

A punch tool was considered to stamp out the shapes.

A CNC guided laser cutting operation was considered.

Water jet cutting, CNC guided.

For a combination of costs and practical reasons, water jet cutting was the method adopted, and hence all the fabricated test samples profiles were cut out using this technology. See Fig.5-12 for the flat profiles of materials ready for the fabrication process.

It should be noted that this fabrication process was conceived and developed specifically to meet the fabricated test regime for this investigation.

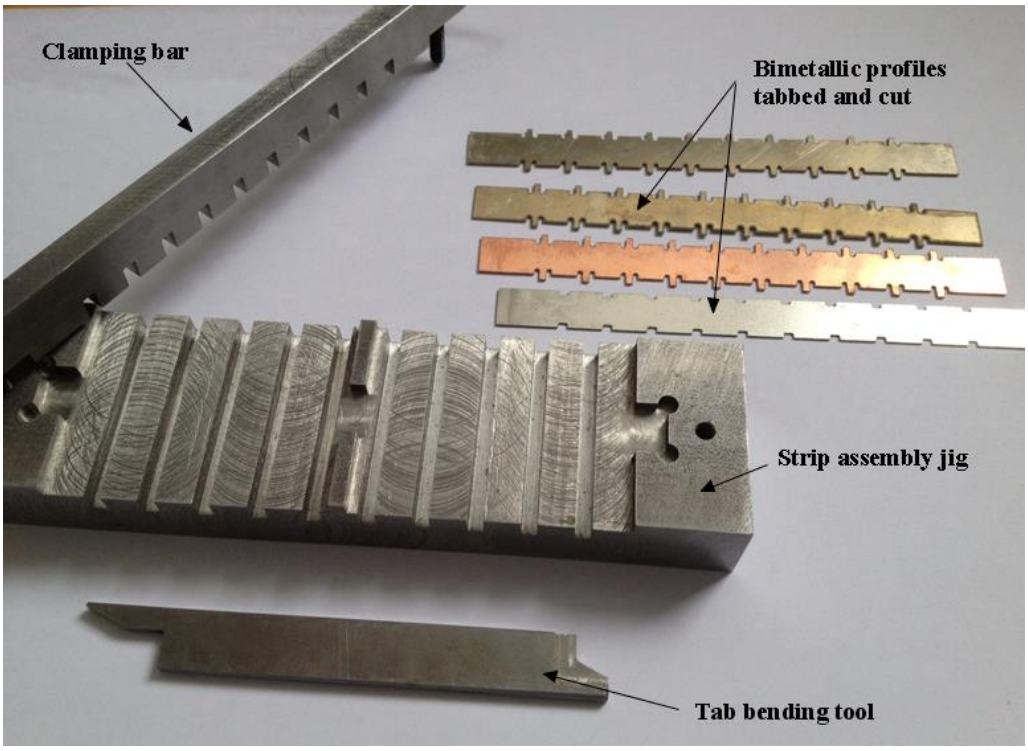

Fig.5-12 Water jet cut test samples prior to assembly in fabrication rig.

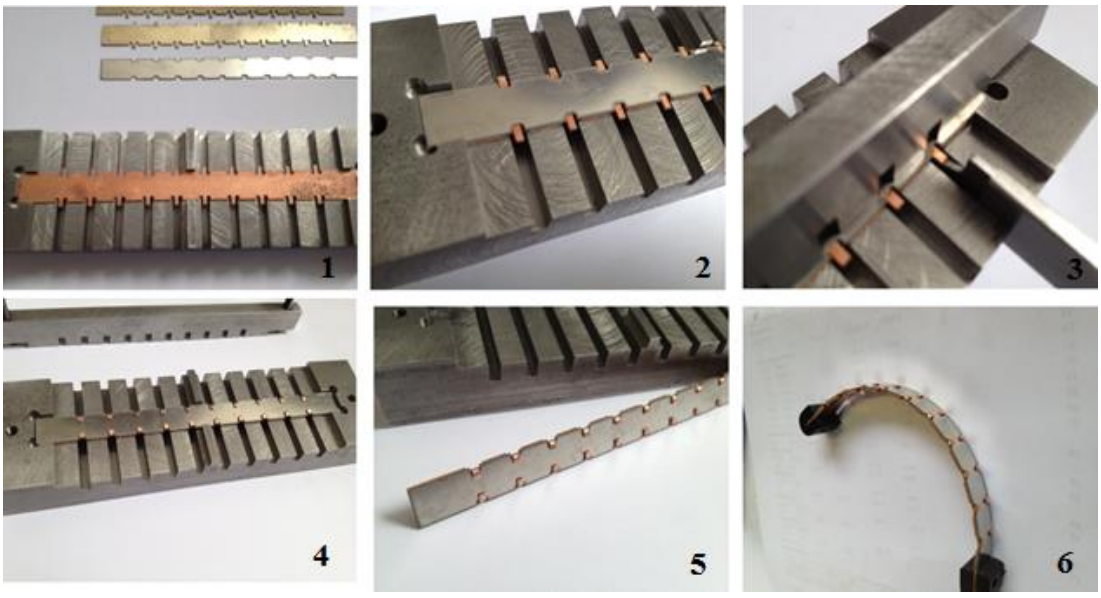

Fig.5-13 Test sample fabrication process

Water jet cutting of the test pieces, afforded complete flexibility in the mating up of different thicknesses of materials and material combinations. Fig.5-13, image 6, shows an early Steel /Copper bi-metallic strip of equal 0.5mm thicknesses. The black end pieces were used to protect the ends of the strip during the fabrication process.

It should be noted that where possible, the more malleable side of the bimetallic strip possessed the “ears” or tabs so that forming over into the material with the “cut-outs” would be more successful.

Using the water jet cutting process required specific design requirements of the test pieces to be cut:

1) Ensure that the minimum radius used on the test samples to be cut was 0.4mm; this was the due to the water jet being 0.8mm diameter.
2) The minimum gap between the samples on the raw sheet was to be 5mm.
3) When cutting through stacked sheets of mixed metals, each sheet had to be bonded together.
4) The thinnest, softest material sheet to be sandwiched between thicker sheets.
5) A gap of 10mm all-round the sheet border to enable clamping of the sheet in the water jet cutting machine.

Design of the test pieces was performed on CatiaV5 CAD software Dassault (2014). The fabrication jig, see Fig.5-13, was manufactured in-house at the UH machine shop.

The water jet cutting was outsourced to a company called Creative water jet (2012) who profile cut all the samples in a stacked configuration to protect the thinner sheets during cutting process.

The bimetallic test strips fabrication process was as follows:

See Fig.5-12 and Fig.5-13.

1) The individual strips were removed from the mixed stack sheets by cutting the remaining joining pips to the main sheet.
2) The strips were ultrasonically cleaned in a bath of Propan-2- OL for 2 hours until the surfaces were clean and free from adhesive or grease.
3) The strips were fully dried and inspected for burrs or sharp edges
4) According to Table 6, two separate flat metal strips were selected and assembled onto the assembly jig, see Fig.5-13 image1, with the metal, with the cut-out piece (Invar 36) without the tabs always assembled on top, image 2.
5) The assembled profiles were then clamped by the bar & two screws, image 3.
6) The tab bending tool was used to bend the tabs or “ears” over into the cut-outs of the mating metal profile by pushing in and peening over, image 3.
7) The clamping bar was removed, image 4.
8) The straight flat bimetallic strip was removed from the jig, image 5

9) Using a generic bending rig and the ϕ100mm test sample former, the flat strip was gently cold formed into a radius of curvature.
10) After the bending and forming operations, all the test pieces were heat-treated for 3 hours at a temperature of 260°C in accordance with Kanthal (2002).

5.12 Production of the Bespoke Bimetallic Strip Test Samples

According to the specific test sets, the test samples were cut to their required arc lengths, then formed using the generic bend rig see. Fig 5-14. After cold forming to the required radius of curvature, each test sample was checked for size using the bending checking procedure described in section 5.13. After validating the radius of curvature, each test sample was subjected to an annealing heat treatment process to reduce the cold worked induced stresses within the material. The annealing process involved heat treating each test sample for 3 hours at a temperature of 350°C in accordance with the Kanthal handbook .

5.13 Bending Check Process – Measurement of the Radius of Curvature

The bending process was achieved on a specially designed bend rig, see Fig 5-14.
The bend rig used a roller on a swinging arm to bend the strip around a former, to ultimately achieve the correct radius of curvature.
The process involved gently cold-forming the strip on a succession of increasing size formers until the final size was the required diameter. The process of bending the strip on a tighter radius of curvature and then relaxing back was to ensure that any naturally occurring spring back of the strip was compensated for and relieved.
Although the forming process of the test pieces was not by the punching method as described in British Standard BS ISO 24213 (2008), the validation of the radius of curvature was checked by this standard, in annex C. The ambient temperature conditions at the time of forming conformed to standard Sherby and Wadsworth (2001) were in the range of 21-23°C.

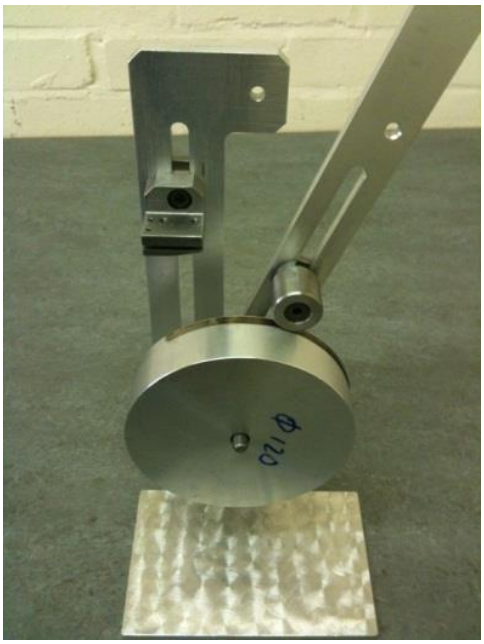

Fig.5-14 Generic hand operated bimetallic strip bending rig

Note: Fig. 5-14 depicts a sample former and sample bimetallic strip, it is important to note that both the pre-fabricated and bespoke bimetallic strip test samples were formed using the same bending rig. The ϕ100mm curvature test former was measured using a digital calliper to find its actual diameter at 22.3°C. Points around the circumference of the former were measured and the average of 4 readings gave the diameter of the former to be ϕ99.92mm. This former was used as the standard bending former for all the test pieces requiring a radius of curvature of $R_c = 50m$.Other formers were manufactured for other specific test samples sizes.

From the standard, annex C, the radius of curvature is defined for measuring purposes as:

$$\boldsymbol{r' = \frac{x}{2} + \frac{w^2}{8x}} \qquad \text{Eqn.84}$$

where :

w was assumed to be the chord length L when resting on a rigid flat metal plate.

r' was the averaged measured diameter of the former ϕ99.92 / 2 = R 49.96mm.

x was assumed to be the vertical height from the flat plate to the maximum arc.

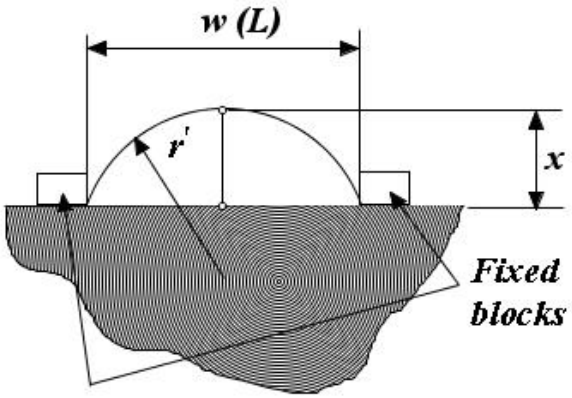

Fig.5-15 Curvature test setup accord to annex C

The distance between the blocks was set to the following dimension evaluated by the chord length equation previously described as:

$$L = 2R\ sin\left(\frac{A_b}{2R}\right)$$

Thus A_b= 120mm +/- 0. 25mm

R = 49.96 mm measured at 22.3°C.

Hence *w* (*L*) was calculated to have a maximum value of 93.254mm and minimum 93,155mm.

The distance between the blocks *w* (*L*) was set to an average position of 93.2 mm and checked by a digital calliper.

The vertical height of each strip ***x*** from the flat surface was calculated by the formula:

$$x = r'\left(1 - \cos\left(\frac{A}{2r'}\right)\right) \quad \text{Eqn. 85}$$

Thus height *x* was calculated to be: maximum 34.557mm and minimum 34.314mm

The average height was 34.44 mm, the height gauge was set to this value.

Thus x = 34.44mm and all test pieces were checked throughout the testing program to conform to (Sherby and Wadsworth, 2001), annex C.

After achieving the correct radius of curvature for the test piece former, the next step was to form the end mounting bends. The original design intent was to pin mount the bimetallic strips on the test rig through end mounting holes.

All the profiles were cut with equi-spaced “ears and cut outs” to within 15mm of each end of the strip so that a mounting hole bend could be formed. A special hardened tool was designed and manufactured to facilitate the end mounting hole bends, see Fig.5-17.

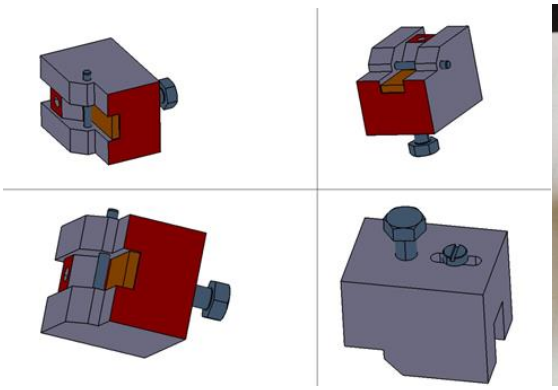

Fig.5-16 As designed

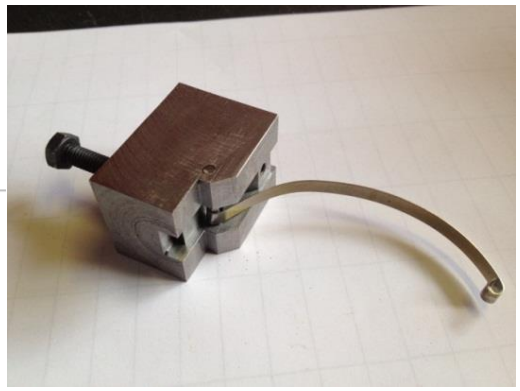

Fig.5-17 As manufactured

Some initial tests had demonstrated the feasibility of producing coiled ends in the thin bespoke bimetallic strip. However, for the fabricated test samples, which were much thicker, it was not possible to successfully form the end coil in strip using the tool. It was found that it was not feasible to form the end coil mounts in any combined strip thicknesses of greater than 0.5 mm. Fig.5-18 shows an early bend test sample with the thinnest fabricated test strip combination, note how the ends are incorrectly formed, this is due to the different spring-back properties of the two metals. This was a major setback to the testing planned for, and a reluctant decision was made that either all the test samples were formed at the both ends, or none would be. Hence all test pieces both pre-fabricated and bespoke would be mounted by the same simply supported method.

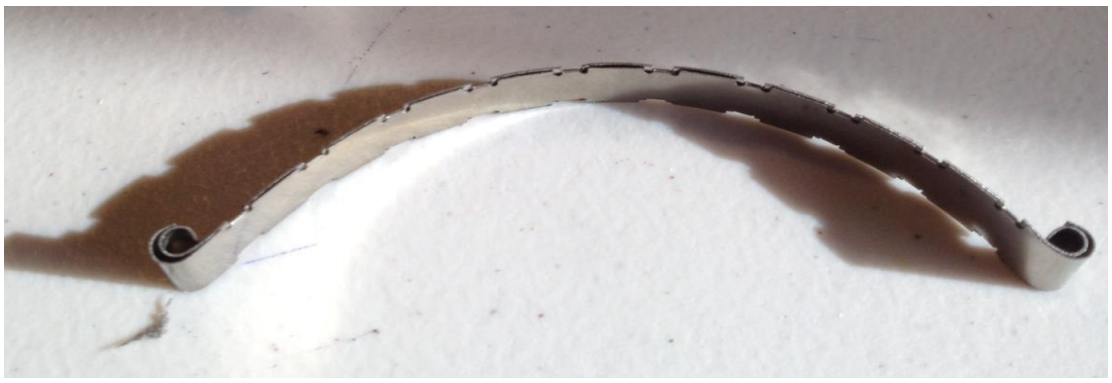

Fig.5-18 0.5mm maximum thickness strip with incorrectly formed coils.

For the pre-fabricated test samples with both ends of the test pieces not formed, this meant that each bimetallic strip was not fully secured along its entire length, see Fig.5-19. Another impact of not having pin mounting holes, was that the test rig required an alternative method to mount the test pieces; this was achieved by adding special “V” notched attachments into the rig which provided for a simply supported type of mounting for all the test samples.

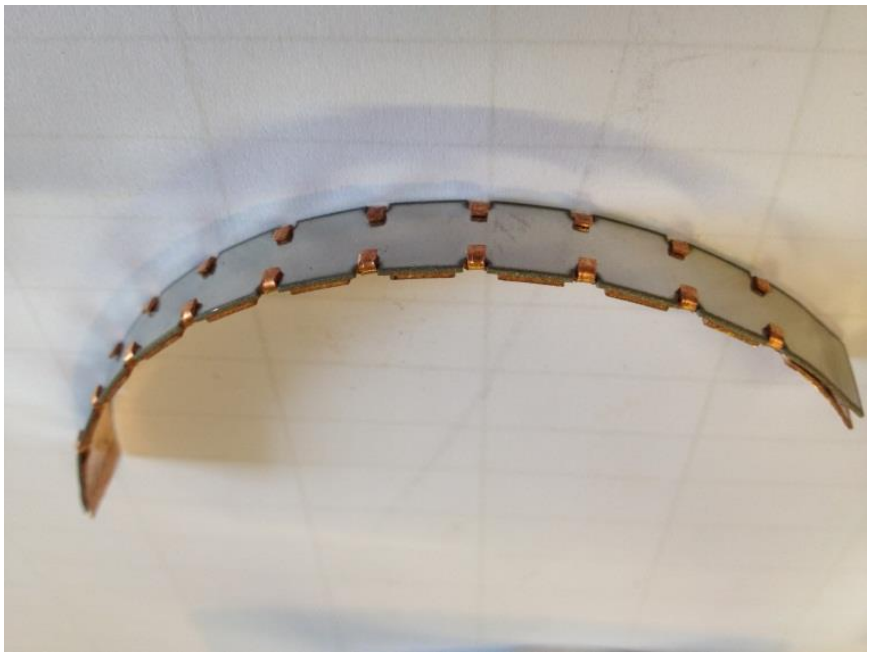

Fig.5-19 Showing the curved bimetallic strip test piece.

In Fig.5-19, note that the last 15mm of each end of the strip was not intimately secured as a bimetallic strip, and thus the effective "bimetallic length" was reduced to approximately 90 mm.

5.14 Conclusions of Test Equipment, Setup and Test Procedures

The objectives were set out to enable the validation of the theory put forward in chapter 3. The rationale for not just using bespoke bimetallic strip manufactured by bimetallic strip companies became apparent due to the scope and the wide variety of test samples required. Thus the decision to fabricate the test pieces was taken and implemented. Because the majority of bimetallic strip manufactured and sold around the world is bespoke bimetallic strip, it was necessary to reflect this fact by having tests of bespoke bimetallic test samples as well as pre-fabricated samples.

The design and manufacture of the test rigs for the purposes of extensive testing of curved bimetallic blades had been achieved. The Magnetic coupling type test rig did not meet its initial design criteria of an entirely frictionless moving centre arm. The fabrication of the bimetallic strip using the TOX clinch method, using a tool kindly supplied by TOX (2013), was eventually not chosen as the preferred method of fabrication, and an alternative method was successfully introduced and employed.

The bending of the coiled end rounds for mounting could not be achieved for all the test samples and thus reluctantly, all fabricated test samples were tested without being

formed in the last 15mm of each end of the strip. This had serious repercussions when it came to testing as a new simply supported mounting system was required, and the non formed ends heavily influenced the test results. To ensure conformity of testing throughout, a decison was made that the bespoke bimetallic test samples should be mounted and loaded in the same way as the fabricated test samples, that is, simply supported instead of pinned at each end. Thus, both the fabricated test samples and the bespoke test samples were tested by the same test piece mounting method. To prevent overstraining the bimetallic test samples during experimental testing, calculation of the maximum safe displacements were performed on all test samples.

CHAPTER 6 Test Results and Correlation to Theory

Summary

This chapter reviews the test results and correlates the test to theory. The influencing factors that produced the deviation from the theory are provided.

6.1 Introduction

This chapter provides an analysis of all the test results, starting with a section that discusses the factors affecting the test data and concluding with comparisons and analysis of the test data to the theory put forward in this investigation. The factors affecting the test results section, provides a list of all the possible spurious inputs that have been considered to influence the accuracy of the test results. In understanding and quantifying the test results, the physical constraints of the test sample sets, test set ups, and the methodology used, must be taken into account and considered.

As has been documented in the previous sections, for the fabricated test set, the fabrication process of the bimetallic strip produced test samples by the water jet process, which were repeatable profiles that were closely controlled with respect to size and shape, but early fabricate problems forced a change of mounting of all the bimetallic test samples, which again heavily influenced the test data outcomes. An illustration of the fabrication problem, was that the ends of the thicker bimetallic strips combinations could not successfully be formed into rounded ends for pin mounting in the magnetic coupling type test rig.

As a consequent, out of the 120mm arc length of the strip, approximately 90 mm was "clamped" by the tabs and the last 30mm, 15mm each side, was not joined together at all, see Fig.6-1. This figure shows the I/C/0.5/0.6 test sample in the background with its tabs hammered down and in the foreground a fabrication sample with tabs only bent over, and note the separation of the two metals in the last 15 mm of each end of the test sample.

Fig.6-1 Initial fabricated bimetallic strip, modified in background

6.2 Factors Affecting the Test Results

There were many factors that have contributed to the deviation from theory, the following is an overall list of those factors in no particular order:

1) Friction at the pulley wheel on the magnetic coupling test rig.
2) The magnetic coupling centre mass.
3) Friction of the rig centre floating arm assembly onto the PTFE guide plates.
4) Friction in the simple supported mounting system on all test rigs.
5) Setting accuracy and ensuring that the test sample was at zero loading.
6) Recording errors of the data from the digital readout displays.
7) Recording delay of light sensor activation.
8) Re-setting of the test samples after each test run.
9) Timer reading error, reading error due to human response time.
10) Thermocouple measuring temperature, spurious heat signals.
11) In fabricated test samples, only fixed together intermittently along the length.
12) In fabricated test samples, 15mm at each end of strip not fixed together.
13) Test samples physically changing properties during the tests.
14) Human data processing errors.
15) Humidity and ambient temperature fluctuations during the tests.
16) Tolerance of the test samples to theoretical values.
17) Theory error calculation by the large variance in the physical and mechanical properties assumed in the metals used.
18) The backlash in the Sauter test rig screw thread.

6.3 Correlation of Test Results vs. Theory

6.3.1 Introduction

This section compares the test results against the new theory proposed by this investigation. For the analysis, 5% error bars are used to measure the test result values to the theoretically generated values by the formulae introduced in chapter 3. For an overall rating system of how the theory measured up to the results, a count of the number of 5% cross bars that touch both the theoretical plotted points and the full test lines was performed for each graph. The 5% cross bars were added up and presented as ratio of the number of plotted points for that curve.

6.3.2 Load vs. Displacement: Correlation – Fabricated Samples

For the load vs displacement test set, equation $\delta = \frac{2FR^3}{E_a I}\left[\frac{\omega}{2} - \frac{3\sin(\omega)}{4} + \frac{\omega * \cos(\omega)}{4}\right]$ from section 3.3 was used for the generation of theoretical points.

For Fig.6-2 - 36 points hit 5% of 41 points, 87.8 % of points are accurate within 5%.
For Fig.6-3 - 9 points hit 5% of 36 points, 25 % of points are accurate within 5%.
For Fig.6-4 - 9 points hit 5% of 36 points, 25 % of points are accurate within 5%.
For Fig.6-5 - 19 points hit 5% of 36 points, 53 % of points are accurate within 5%.
For Fig.6-6 - 20 points hit 5% of 36 points, 56 % of points are accurate within 5%.
The average of all the results from Fig. 6-2 to Fig. 6-6 was that 49.36% of all points were within 5%.
The overall result was affected by the very poor performing aluminium samples that were tested in a soft condition, but the values used were standard values for normal aluminium alloy. Despite the average value of 49% of all the points being within 5%, there were many points that fell within 10%.
Note that the units for all displacements of the test samples are in millimetres, and all loads are in Newtons.

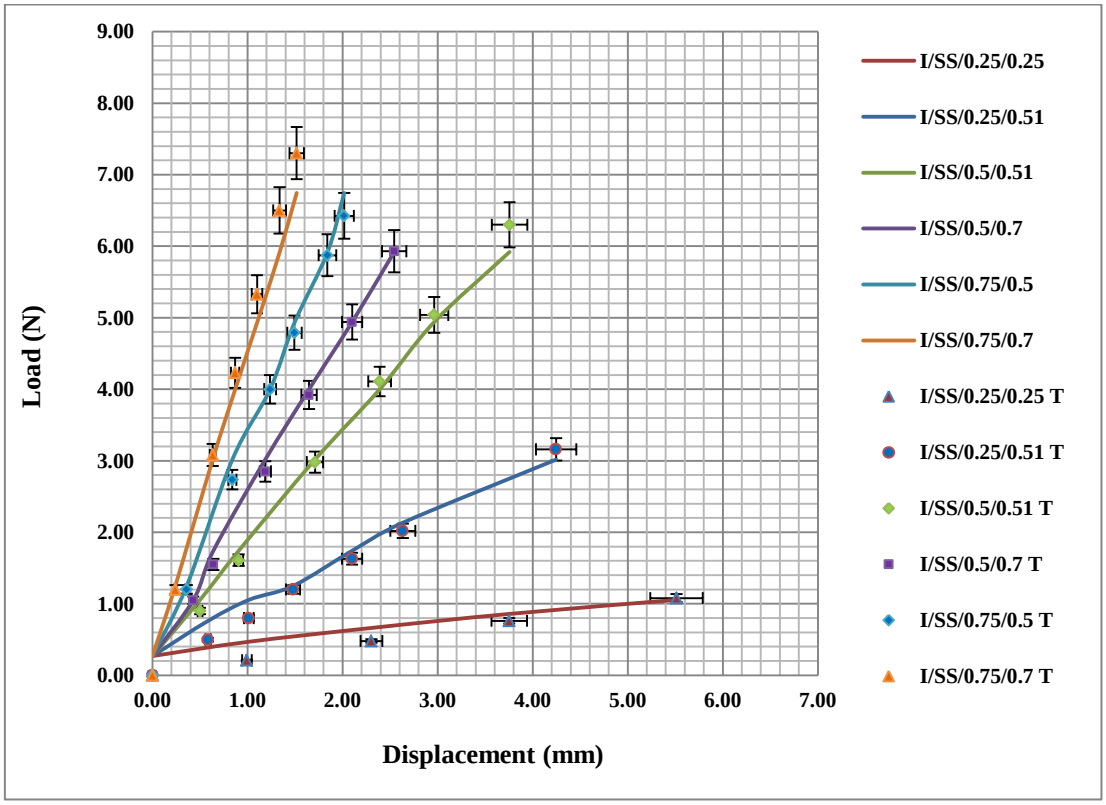

Fig.6-2 Verification of Load with Displacement for fabricated St. Steel

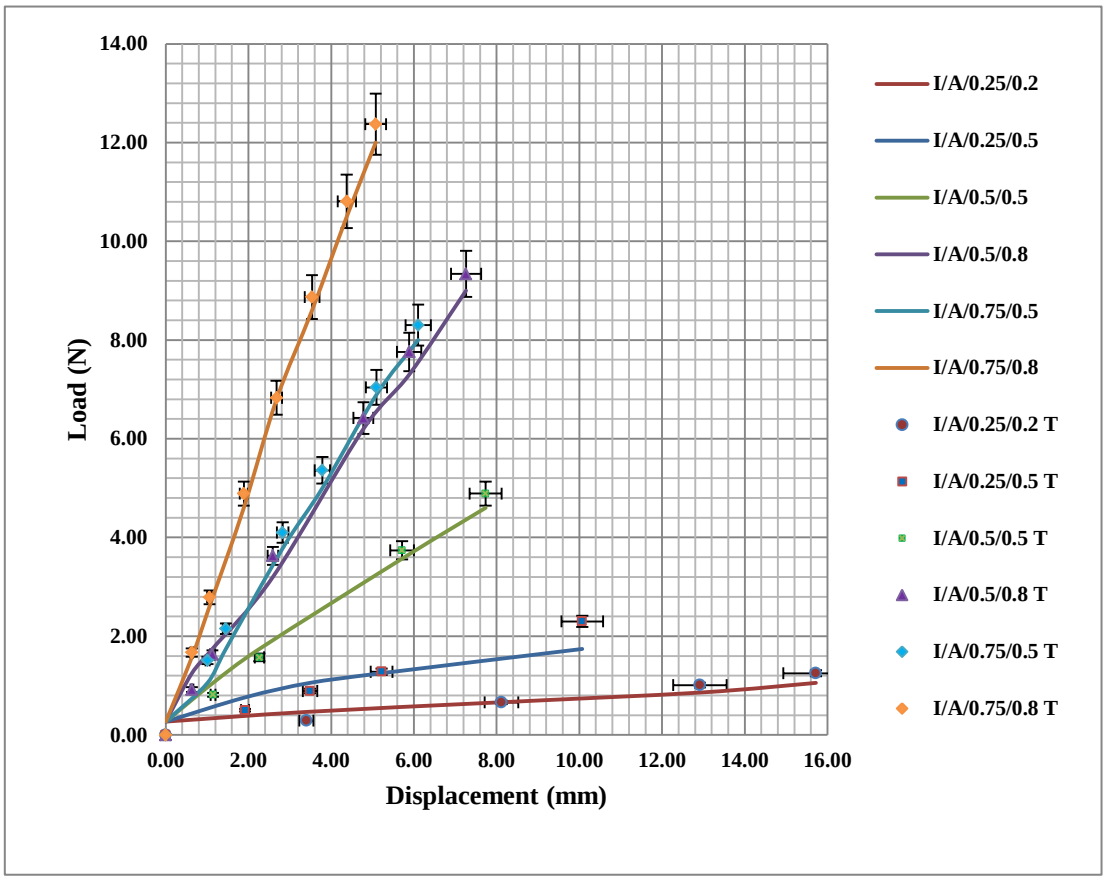

Fig.6-3 Verification of Load with Displacement for fabricated Aluminium

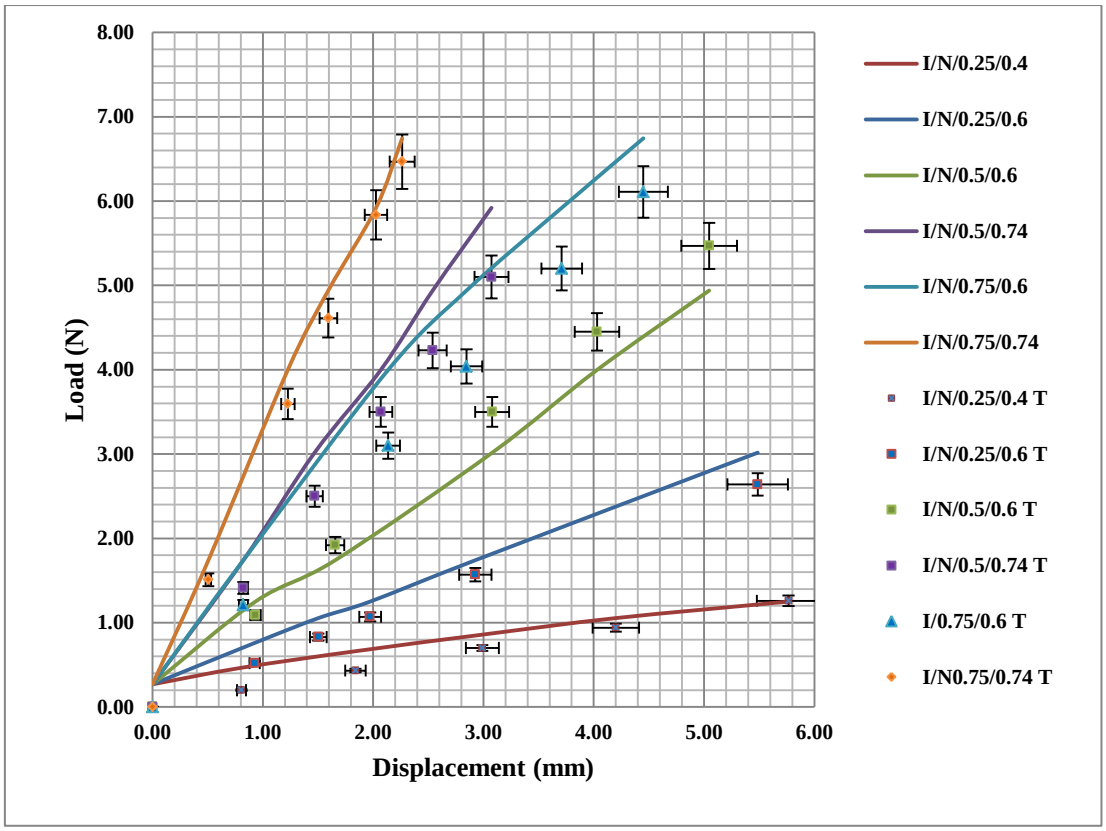

Fig.6-4 Verification of Load with Displacement for fabricated Nickel

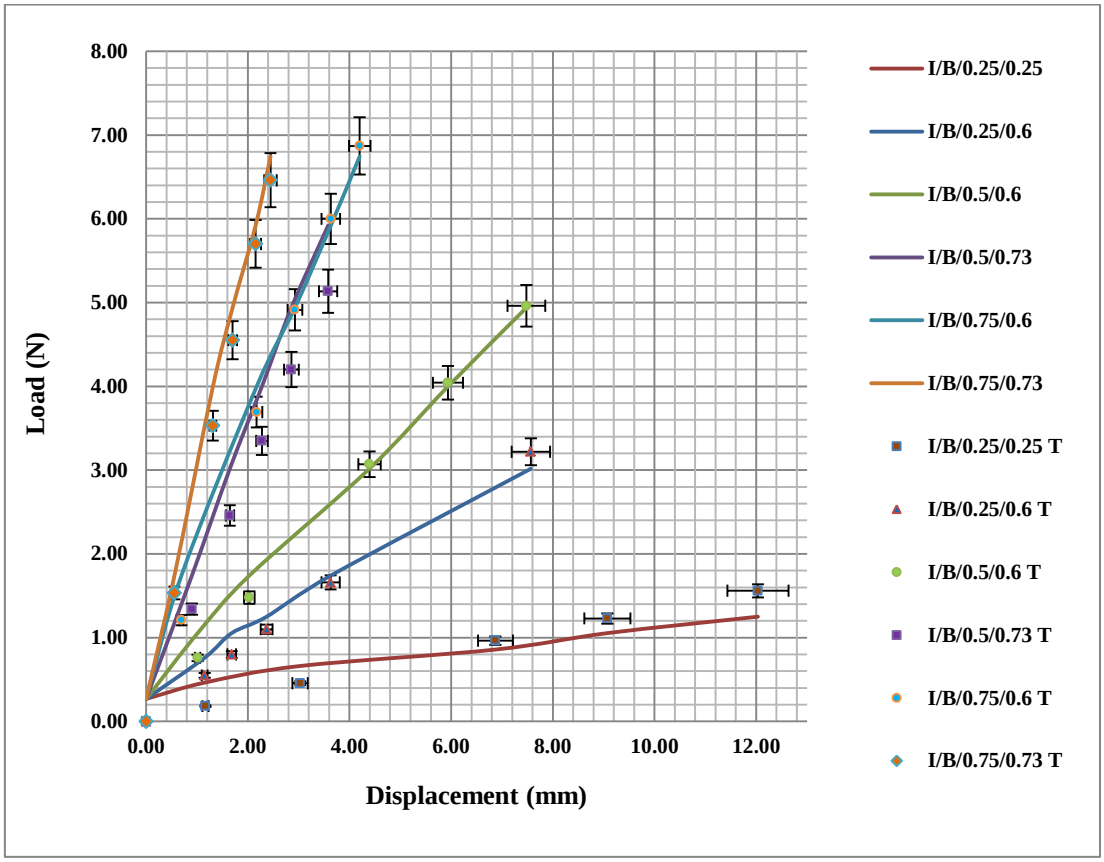

Fig.6-5 Verification of Load with Displacement for fabricated Brass

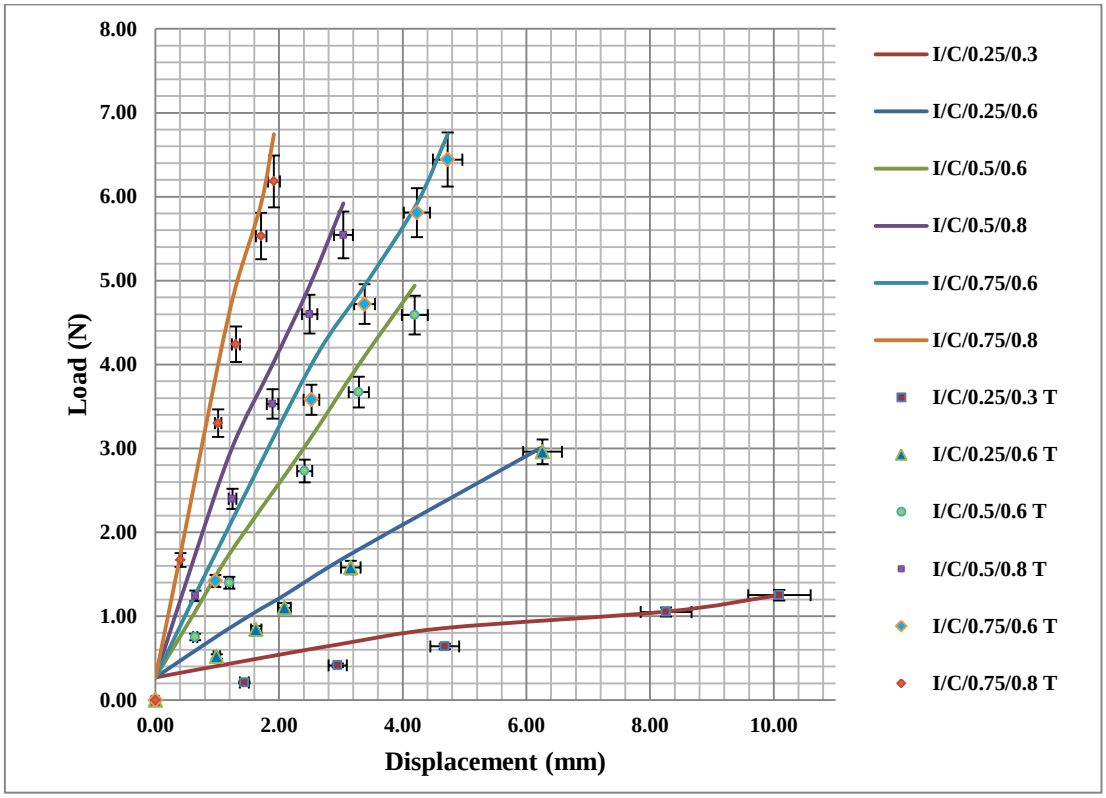

Fig.6-6 Verification of Load with Displacement for fabricated Copper

It is noted that the theory for this test set was based on the Castigliano derived linear equation from section 3.3 without the modification to cater for the non-linearity. For this specific range of values, the linear theory adequately approximates to the test data. Despite the low 41% of all points being within 5% of the theory, there were many factors contributing to this low correlation. The most salient factor was the condition of the Aluminium and Nickel fabricated bimetallic samples that did not perform well or produce reliable test data. Another important factor for the wide variance of the data from the theory was the assumed length of the bimetallic was 120mm, where in fact only 90 mm was secured as a bimetallic strip. A further factor that influenced the deviation of the theory to test was the variance in values assumed in the calculations. If the 10% correlation is considered, then for Fig.6-2, nearly all 41 points were within 10%, for 2, about 15 points were within 10%, for 3, 22 points were within about 10% and for 4, about 30 points were within 10%, and lastly for 5, about 33 points were within 10% accuracy. Thus for a 10% correlation translates into 100%, 42%, 61%, 83%, 92% and averages at 75.6% for all points within 10% of the theory. It should also be noted that the test data possessed very little scatter and nearly all the curves were of a very reasonable consistent shape. For the fabricated load vs displacement results, a good overall correlation between the theory and the test was proven with a high 75.6% correlation within 10%, and a low 41% correlation within 5% accuracy.

6.3.3 Load vs. Displacement: Correlation – Bespoke Samples

For the load vs displacement test set, equation $F_d = \frac{M_d - M_c}{\frac{(L_c - x_d)}{2} tan(\frac{A_b}{4R_d})}$ from section 3.13 was used for the generation of theoretical points. This section continues the correlation of load vs. displacement for the bespoke test samples. As before, 5% error bars were used for the correlation and T denotes theory.

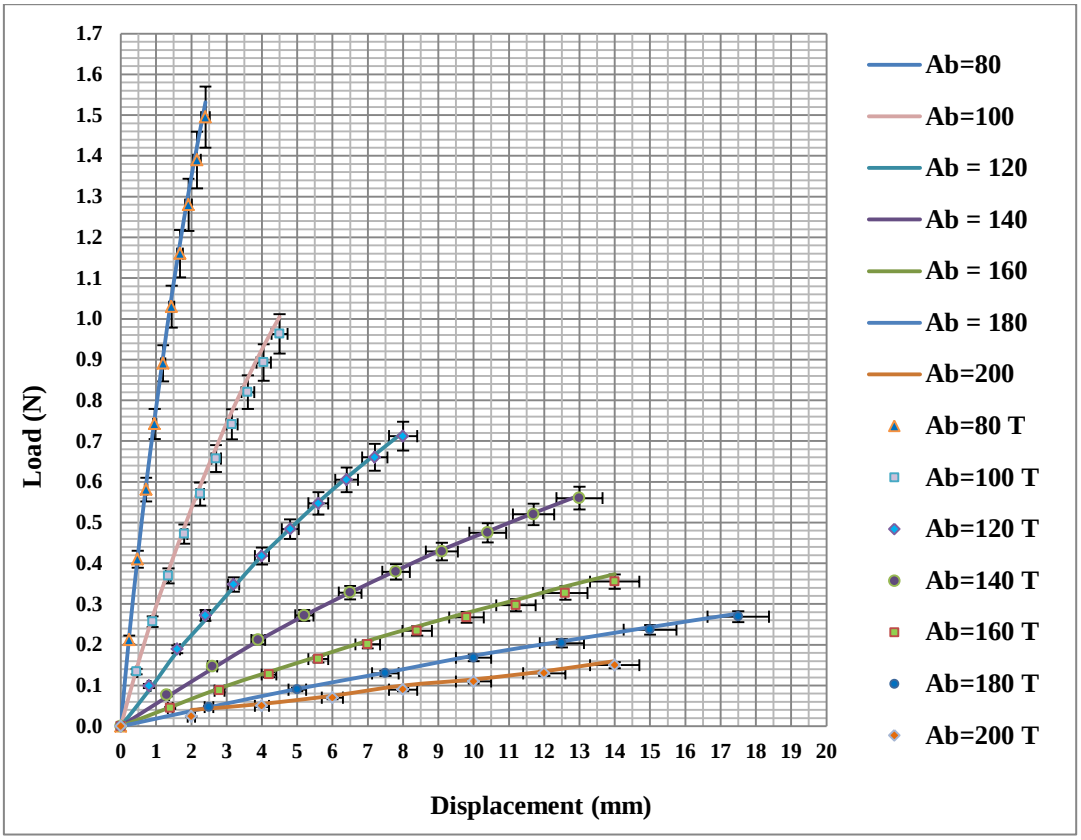

Fig.6-7 Verification of Load with Displacement for Rc = 80mm constant

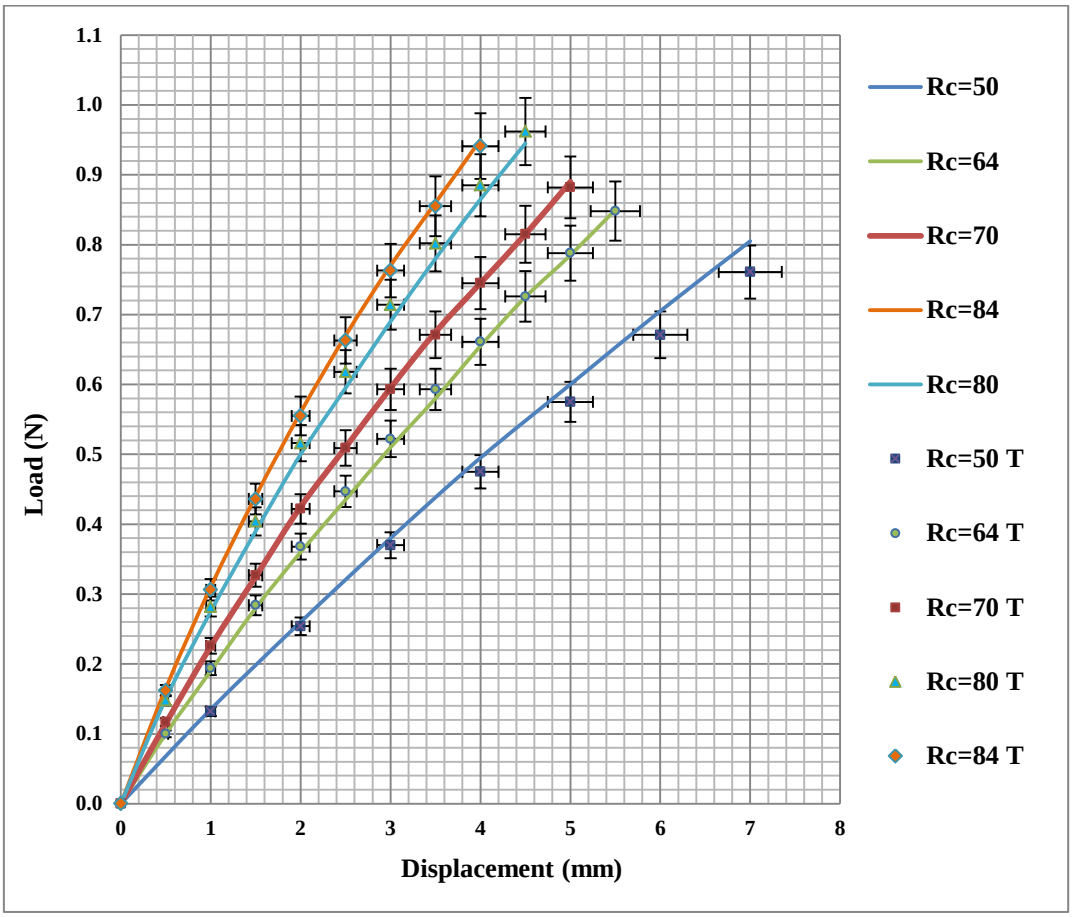

Fig.6-8 Verification of Load with Displacement for Ab =100mm constant

For the seven plots of Fig.6-7 - all points plotted hit the 5% error or less for 72 points, thus 100 % of the points are accurate within 5%, with a strong majority of points being less than 5% accurate to the theory.

For Fig.6-8 - 48 points hit 5% of 50 points, thus 96 % of the points were accurate to within 5% of the theory.

The overall average percentage accurate was therefore, 98% of all bespoke samples were accurate to within 5% of the theory.

The bespoke bimetallic test samples performed much more reliably on the bought in Sauter test rig with experimental scatter next to none and an extremely close correlation for the majority of points in graph 6. However in Fig.6-8, the tighter the radius of curvature, the more the deviation from the test results was observed. Thus whilst overall the correlation was very good, the limitation of the theory occurred on the tighter radii of curvature test samples, where the deviation to the theory increased with displacement, see Rc =50 in Fig.6-8. The shape of the test curves were consistent with that of a large parabola, and despite the larger scatter on the fabricated test results, it can be seen that the shape of the more consistent results closely match the bespoke samples.

For the bespoke load vs displacement results, an overall 98% of the test data correlates to the theory within 5%. The high correlation of the theory to test data provides confidence in accepting the theory put forward in section 3.13. That concludes the load vs. displacement correlation.

6.3.4 Temperature vs. Displacement: Correlation - Fabricated Samples

For the temperature vs displacement test set, equation

$x_d = 2(\frac{\rho R_c}{\rho - R_c}) \sin\left(\frac{A_b(\rho - R_c)}{2\rho R_c}\right) - 2R_c \sin\left(\frac{A_b}{2R_c}\right)$ from section 3.2 was used for the generation of theoretical points.

These test results were produced on the magnetic coupling test rig as described in the section 4.7. As before, 5% error bars were used to identify the level of correlation achieved between the theories introduced in section 3.2 to the test results. And as before, T denotes theory derived points. Due the amount of test data on each graph and the difficulty of distinguishing the error bars, additional plots were produced from the same data and each graph shows just three plots of the test results and three plots of the theory points. The thinnest, medium and the thickest samples were chosen. It should be noted that the correlations therefore were performed on a limited set of data. Up to 5% error is considered for each theory point that the error bar touches a test line.

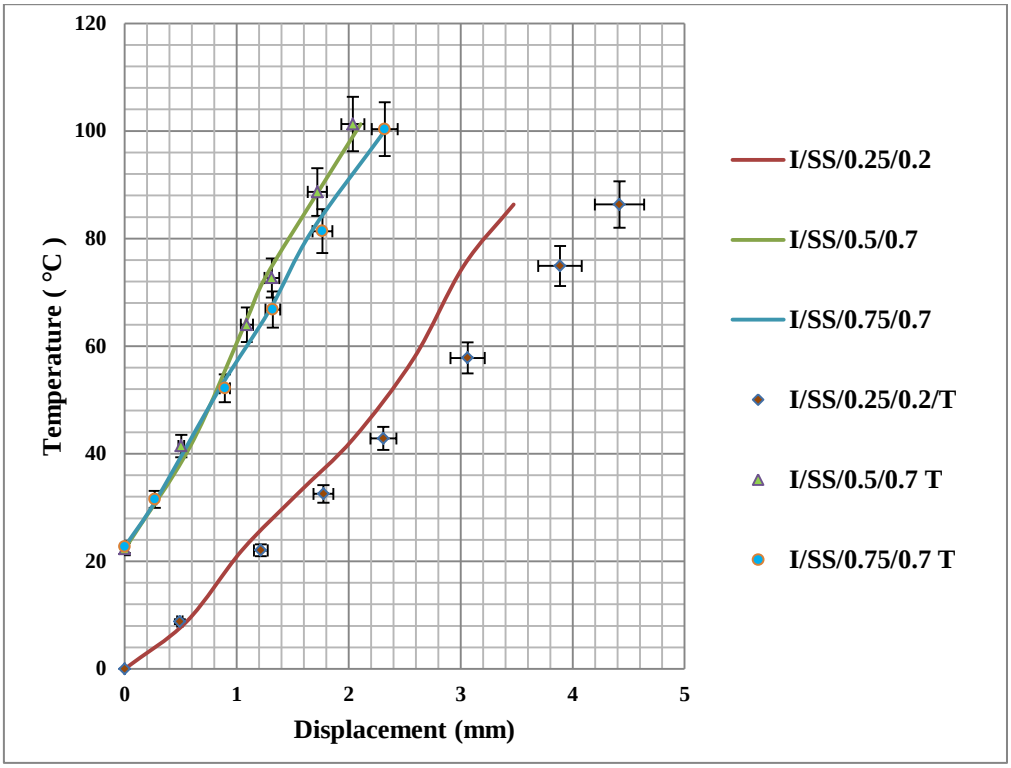

Fig.6-9 Verification of Temperaturewith Displacement for fabricated

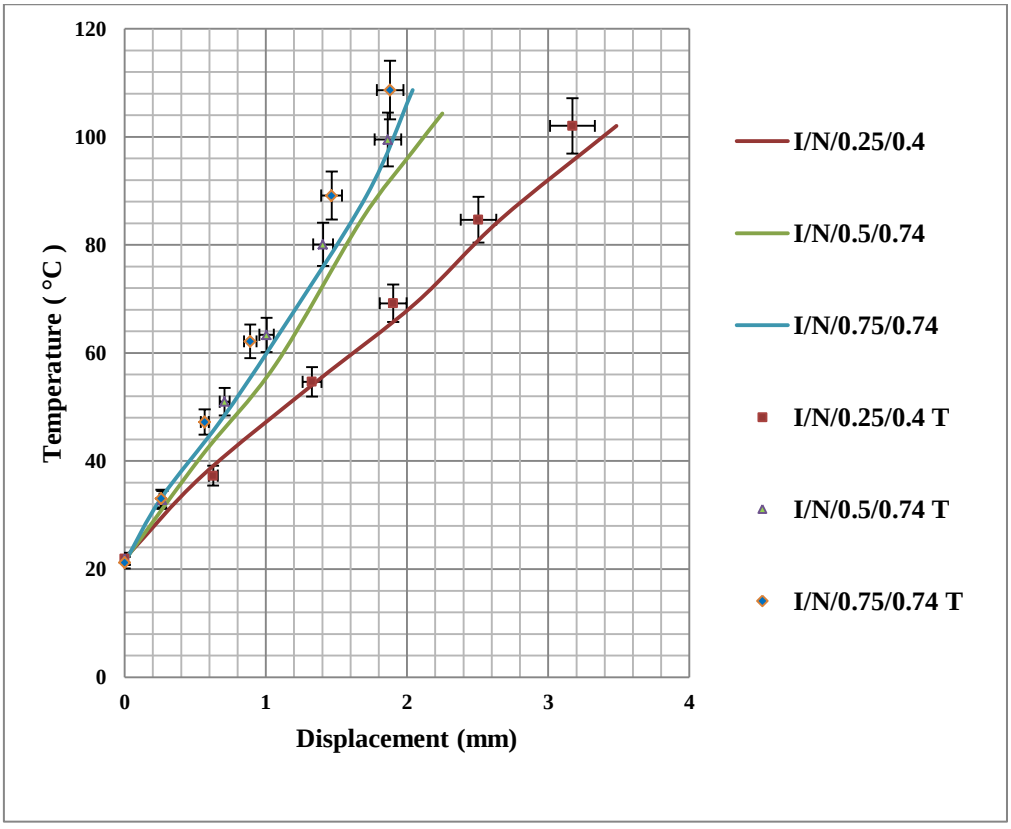

Fig.6-10 Verification of Temperature with Displacement for fabricated

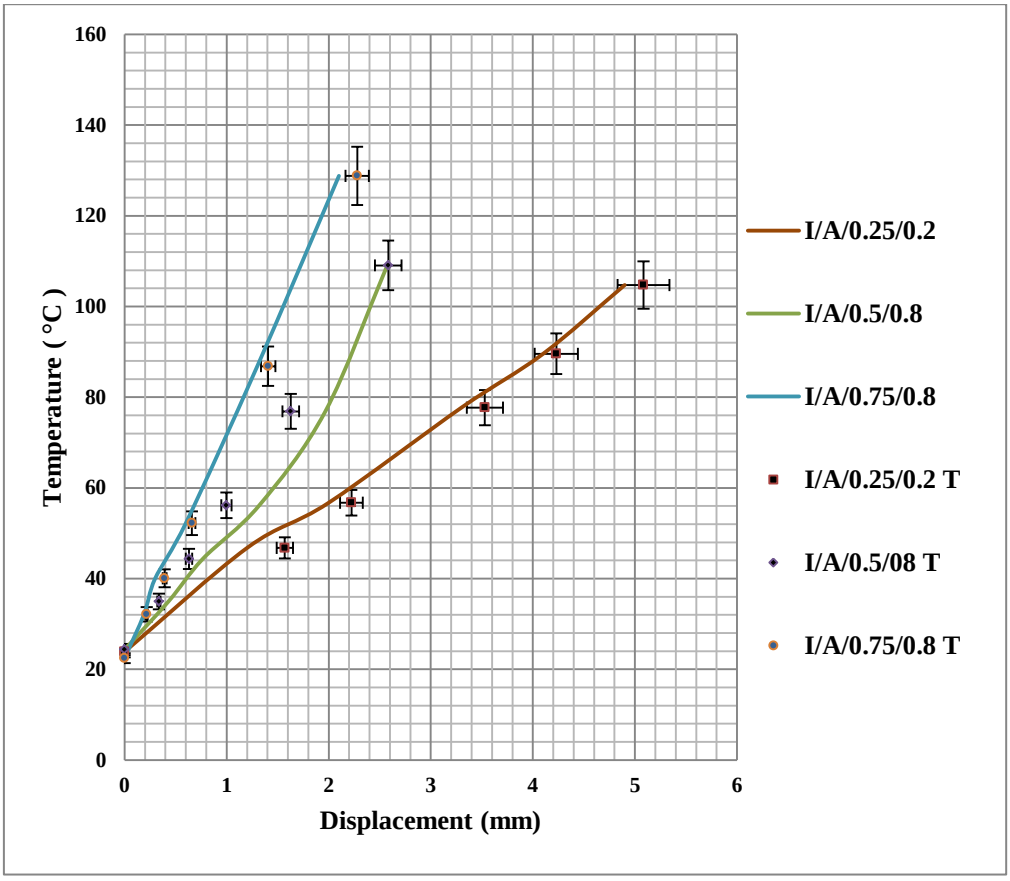

Fig.6-11 Verification of Temperaturewith Displacement for fabricated

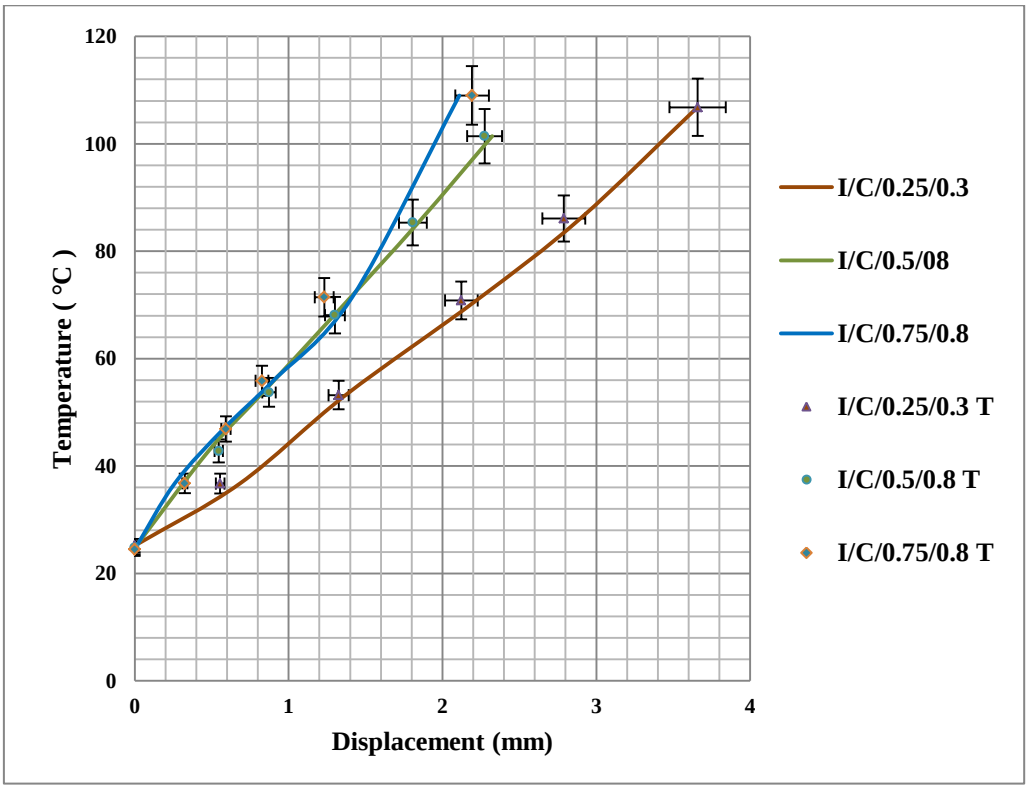

Fig.6-12 Verification of Temperature with Displacement for fabricated

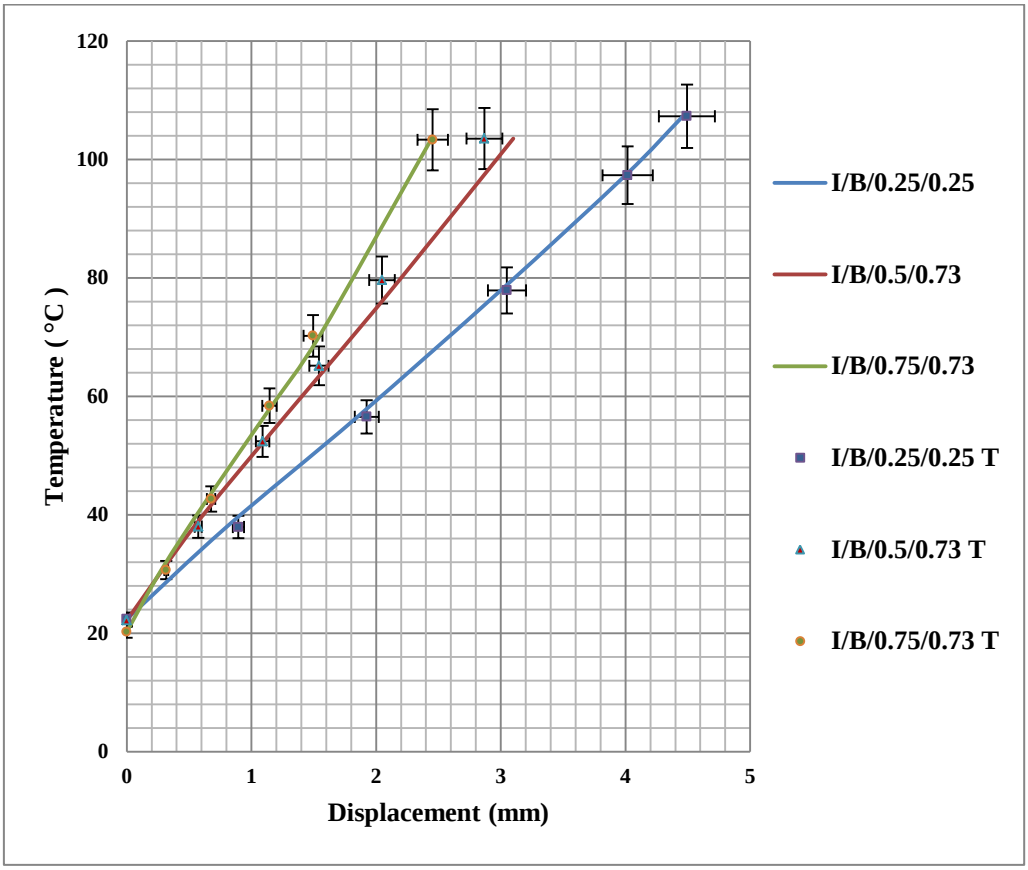

Fig.6-13 Verification of Temperature with Displacement for fabricated

For Fig.6-9 - 14 points hit 5% of 20 points, 70 % of points are accurate within 5%.
For Fig.6-10 - 9 points hit 5% of 18 points, 50 % of points are accurate within 5%.
For Fig.6-11 - 7 points hit 5% of 18 points, 4 % of points are accurate within 5%.
For Fig.6-12 - 17 points hit 5% of 18 points, 94 % of points are accurate within 5%.
For Fig.6-13 - 13 points hit 5% of 18 points, 72 % of points are accurate within 5%.
Thus the overall accuracy was that 58 % of all the points were within 5% of the theory.

As can be seen the set of aluminium test samples has drastically reduced the overall accuracy to that of 58% for an error of 5%. If the aluminium test samples were ignored, then the overall accuracy rises to 71.5 %, meaning that 72% of all the data points were within 5% of the theory. Whilst this was a reduced data set, a good overall correlation was achieved if the faulty aluminium test sample contribution was ignored.

Despite the many contributing factors that have introduced errors, the correlation between the theory and the test results was reasonably good. For the aluminium samples, 58% of the test points were within 5% of the theory, without the aluminium

test points this rose to a confidence level of 72% in the theory put forward in this investigation.

6.3.5 Temperature vs. Displacement: Correlation – Bespoke Samples

For the temperature vs displacement test set, equation $x_d = 2(\frac{\rho R_c}{\rho - R_c}) \sin\left(\frac{A_b(\rho - R_c)}{2\rho R_c}\right) - 2R_c \sin\left(\frac{A_b}{2R_c}\right)$ from section 3.2 was used for the generation of theoretical points.

Due the amount of test data on each graph and the difficulty of distinguishing the error bars, additional plots were produced from the same data and each graph shows just three plots of the test results and three plots of the theory points. The thinnest, medium and the thickest samples were chosen. It is important to note that unlike the fabricated test samples, these test results were produced on the Sauter test rig as described in the section 5.6.3. The Sauter test rig was proven to provide excellent test results for the load vs. displacement tests at ambient temperature, where the load was increased by adjusting the handle against the resisting force of the bimetallic strip. In the heated tests the handle was backed off to allow displacement. The backing off of the thread, resulted in looseness of the loading screw thread. The looseness of the thread, or "backlash", was significant and greatly contributed to the wide scatter of the test results. As before, 5% error bars were used to identify the level of correlation achieved between the theories introduced in 3.2 to the test results. And as before, T denotes theory derived points. A 5% error is considered for each theory point that the error bar touches a test line. It should also be noted that the correlations were performed on a limited set of data.

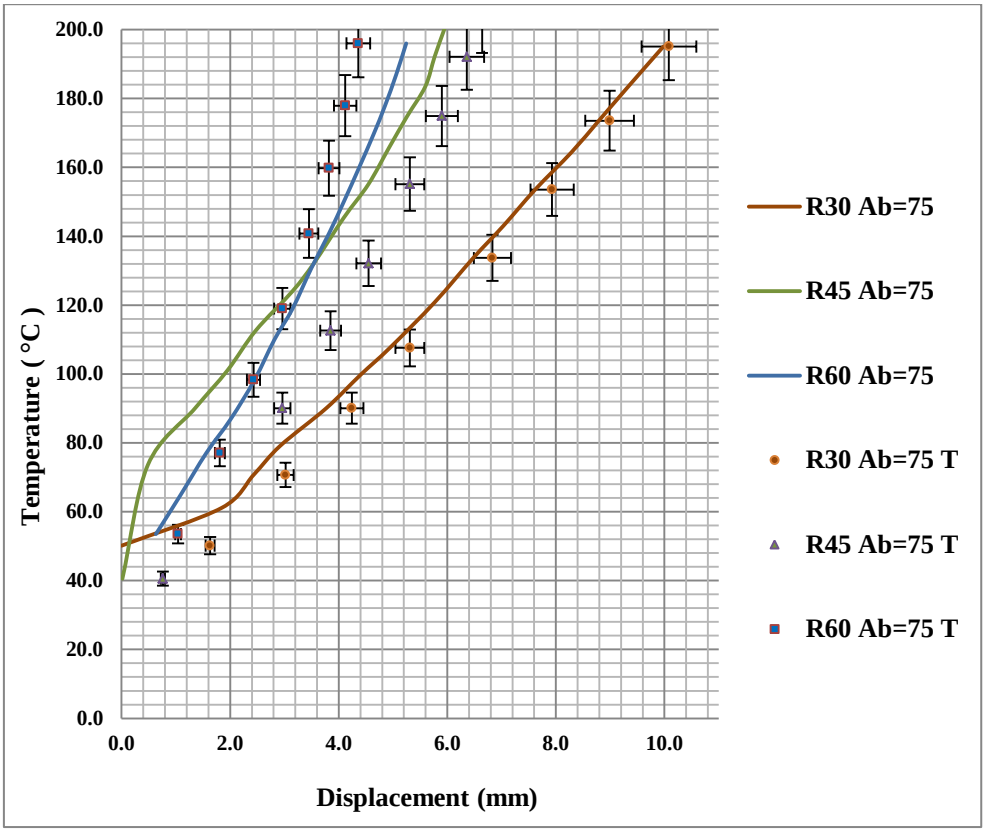

Fig.6-14 Verification of Temperature with Displacement for Ab =75mm

For Fig.6-14 - 8 points hit 5% of 24 points, 33.3 % of points are accurate within 5%.
For Fig.6-15 - 2 points hit 5% of 24 points, 8.33 % of points are accurate within 5%.
For Fig.6-16 - 7 points hit 5% of 24 points, 29 % of points are accurate within 5%.
For Fig.6-17 - 8 points hit 5% of 24 points, 33.3 % of points are accurate within 5%.
Thus overall, 26% of the points hit the 5% error.

Although a low percentage 26% of all the points hit the 5% error band, a good estimate from the closeness of the 5% error band to the test lines was that about 60 -70% of the theory points or higher was within a 10% error band. It should be noted that the shape of the theory points, which is a function of Timoshenko formula, provided non- linear curves and that in general, the theory points accorded to test lines. As was stated at the outset, the backlash or looseness of the screw thread of the handle heavily influenced the position of the test curves with respect to theory points. From Fig.6-14, it can clearly be seen that the theory points are out of synchronisation with the test curve by about 0.5 to 1mm displacement depending on the radius of curvature and length of the test sample. The R30 Ab= 80 curve of Fig.6-15, illustrates the relative displacement between the theory and test line, but the general slope and angle accord well. It was very

possible to have at least 1mm to 2mm looseness in the screw thread on the Sauter test rig due to backlash that contributed to the displacement shift.

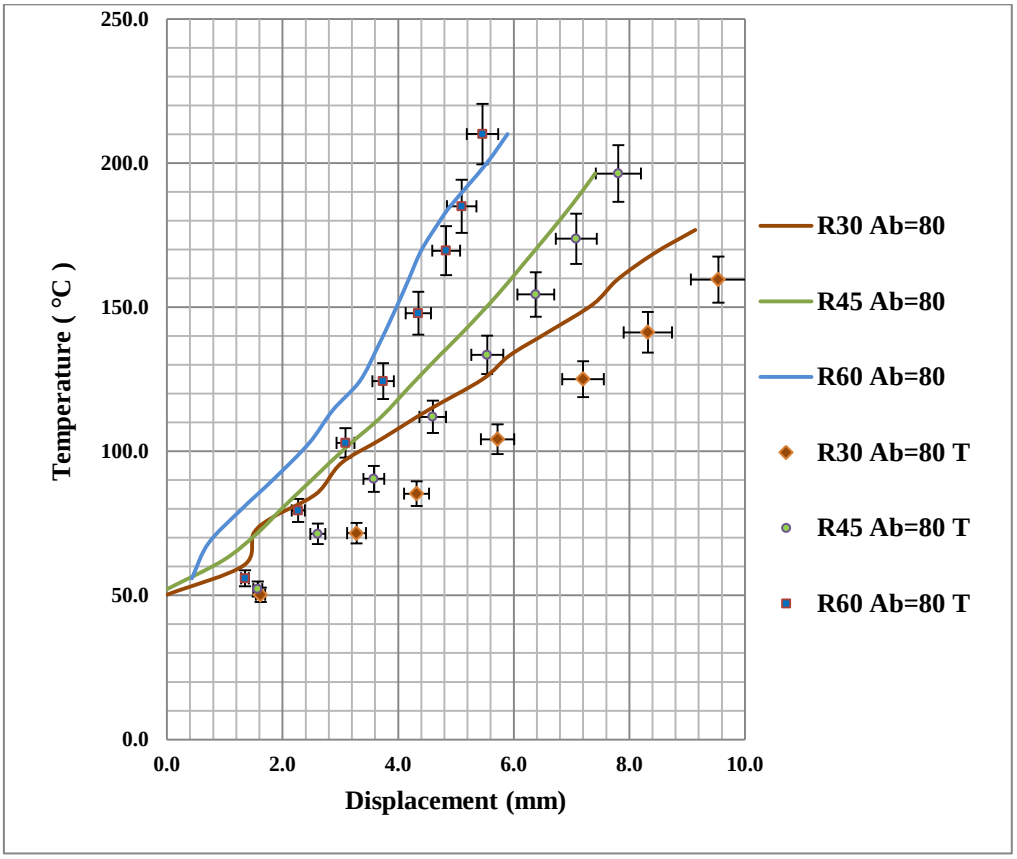

Fig.6-15 Verification of Temperature with Displacement for Ab = 80mm

It can be observed that the smaller the radius of curvature coupled with a shorter length Ab, the more the relationship between temperature and displacement becomes non-linear. The opposite is true in that the larger the radius of curvature and the longer length Ab tend to make the relationship more linear in nature. If the radius of curvature is small and the length of strip is large, then the amount of non-linearity will fall between the two extremes previously mentioned.

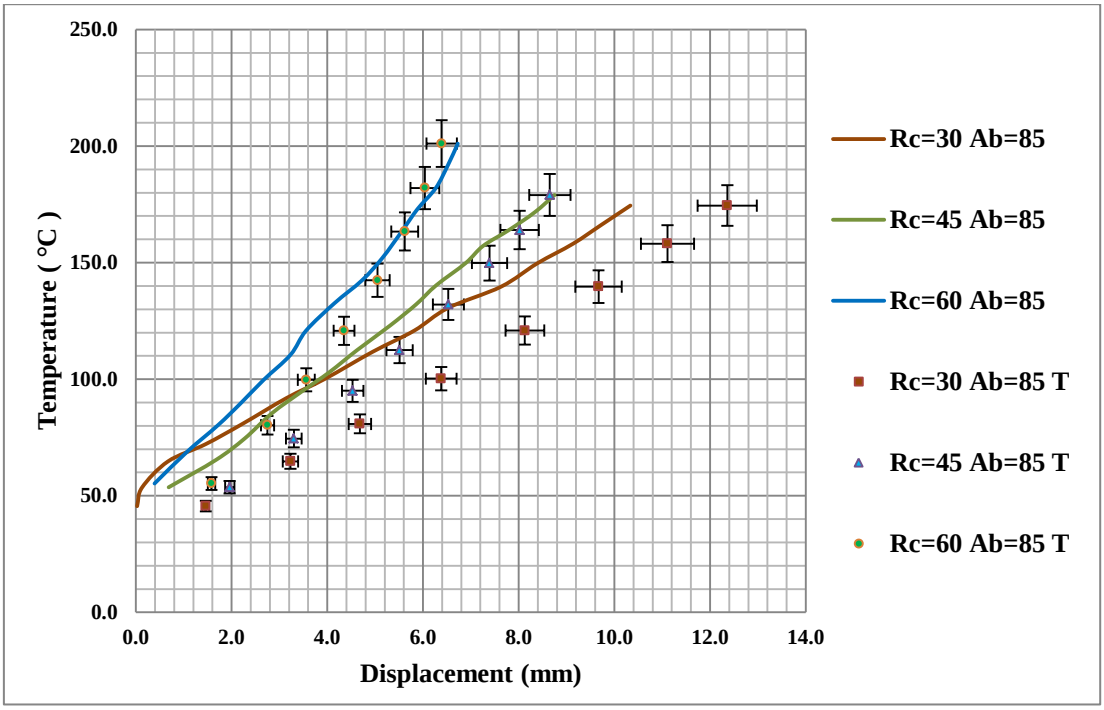

Fig.6-16 Verification of Temperature with Displacement for Ab =85 mm

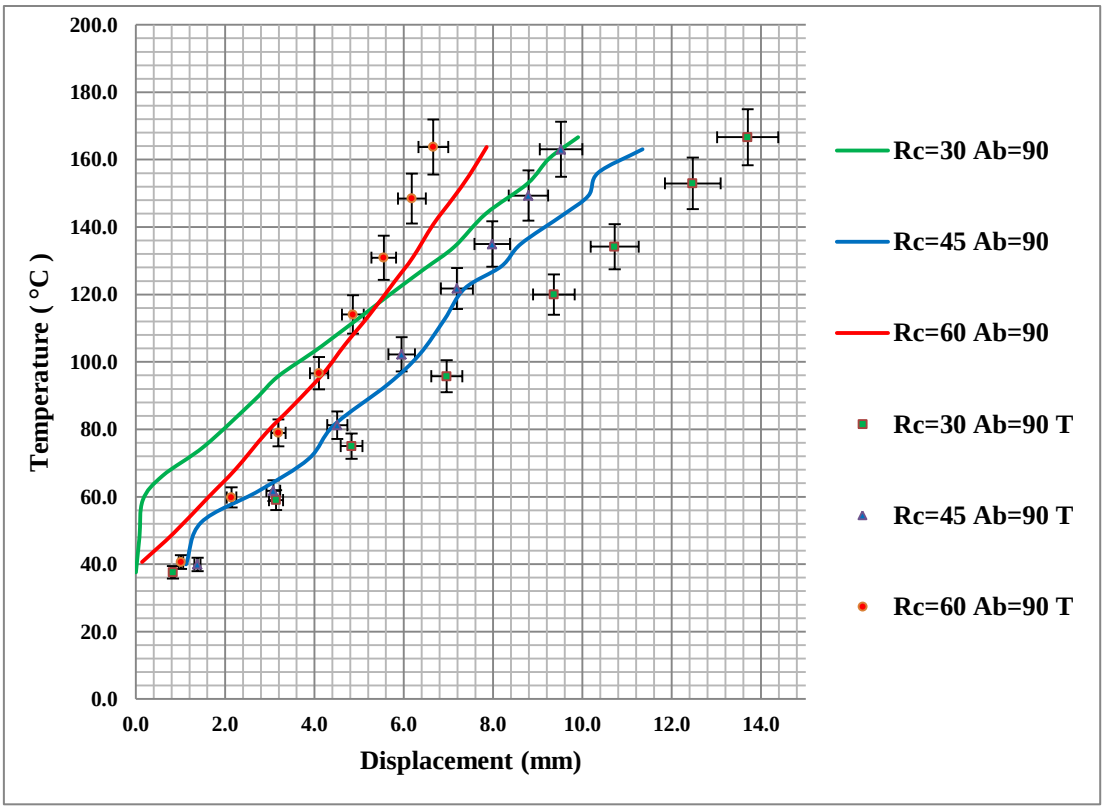

Fig.6-17 Verification of Temperature with Displacement for Ab =90mm

The results overall correlate to within 60 to 70% of the results lie within 10% error band, if 10% error bands are assumed. If the 5% error bands are used then only 26% of the test results were within 5% of the theory. There was a reasonable overall fit of the theory to the test.

That concludes the temperature vs. displacement correlation for bespoke test data.

6.3.6 Load vs. Temperature: Correlation – Fabricated Samples

For the Load vs displacement test set, equation

$$X = \{2\left(\frac{\rho R_c}{\rho - R_c}\right) sin\left(\frac{A_b(\rho - R_c)}{2\rho R_c}\right) - 2R_c\, sin\left(\frac{A_b}{2R_c}\right)\} - \{\frac{2FR^3}{E_a\, I}\left[\frac{\omega}{2} - \frac{3sin(\omega)}{4} + \frac{\omega * cos(\omega)}{4}\right]\}$$

from section 3.5 was used for the generation of theoretical points.

This section provides the correlation between the theory put forward in section 3.6 and the test results. The 5% error bars were used to compare the theory to the test results.

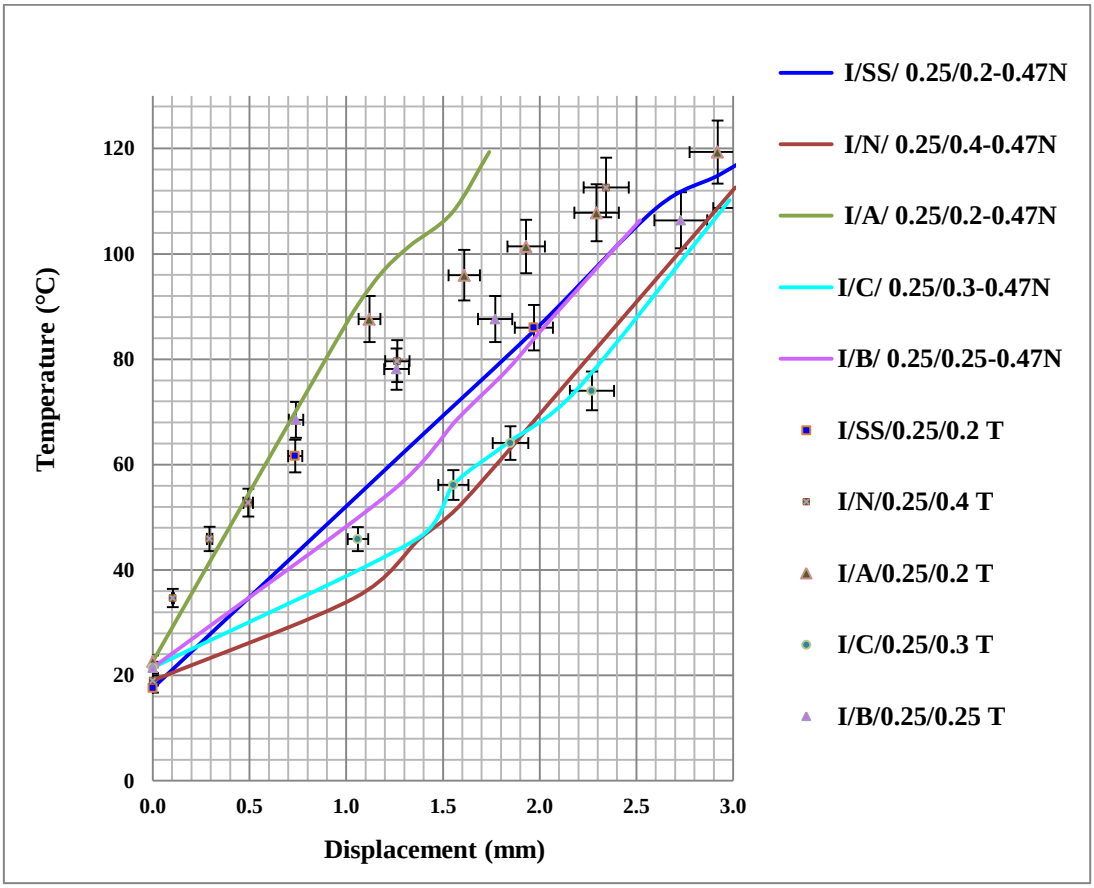

Fig.6-18 Verification of Temperature with Loaded Displacement for fabricated

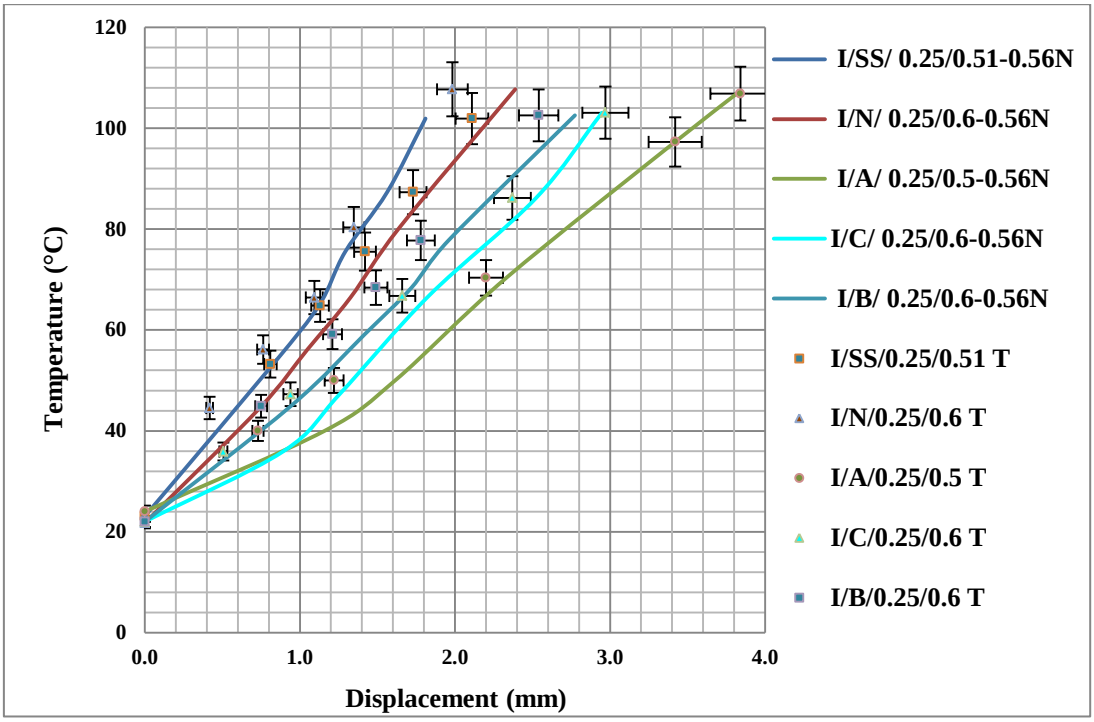

Fig.6-19 Verification of Temperature with Loaded Displacement for fabricated

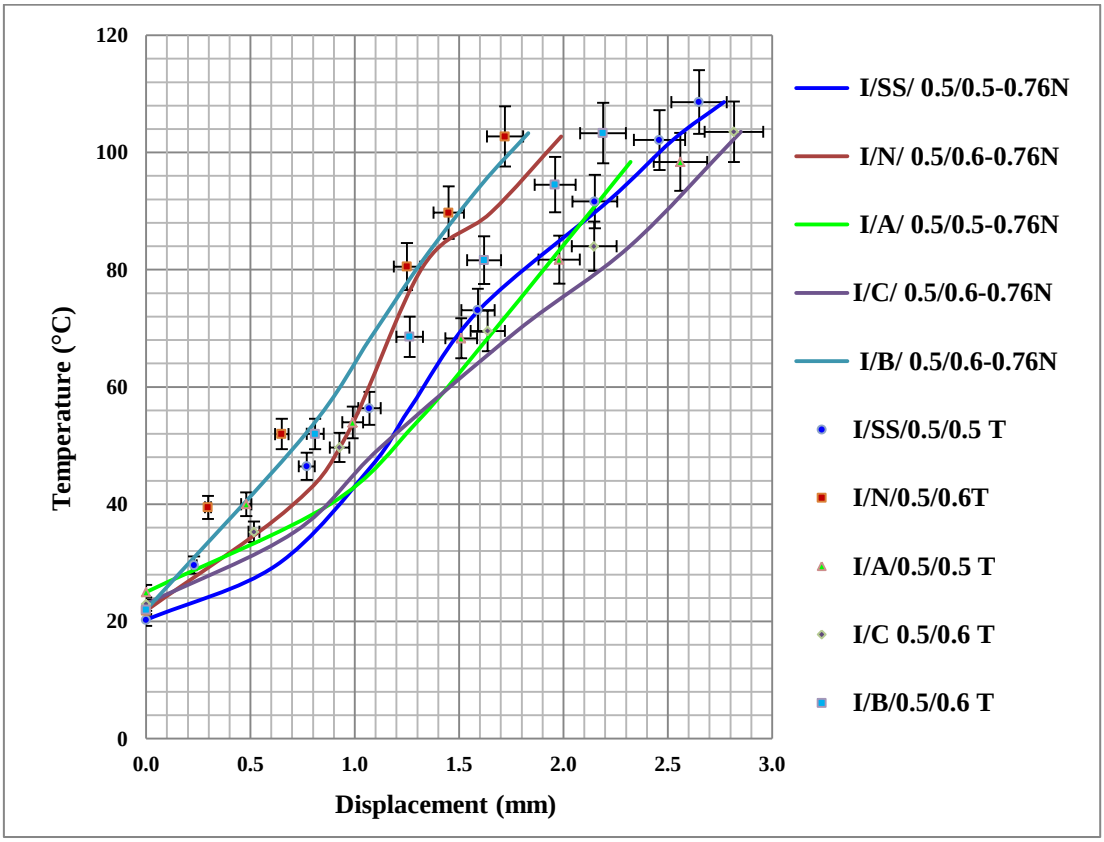

Fig.6-20 Verification of Temperature with Loaded Displacement for fabricated

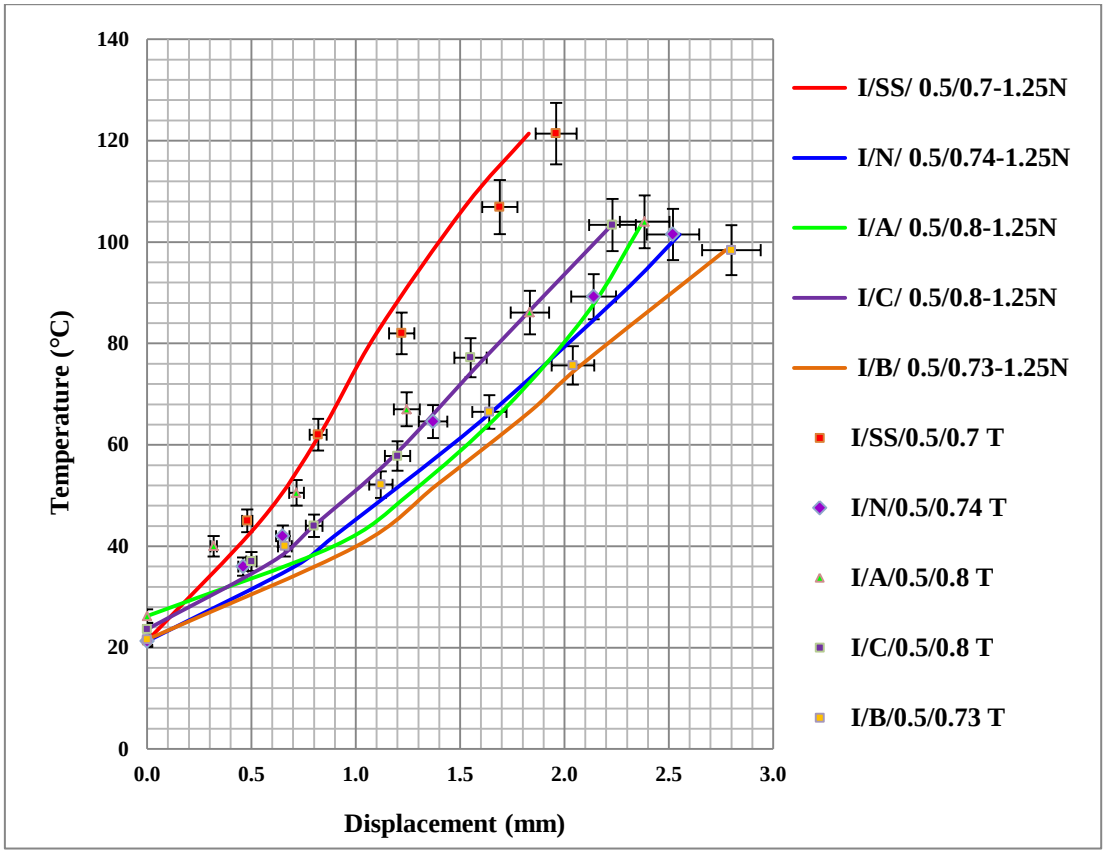

Fig.6-21 Verification of Temperature with Loaded Displacement for fabricated

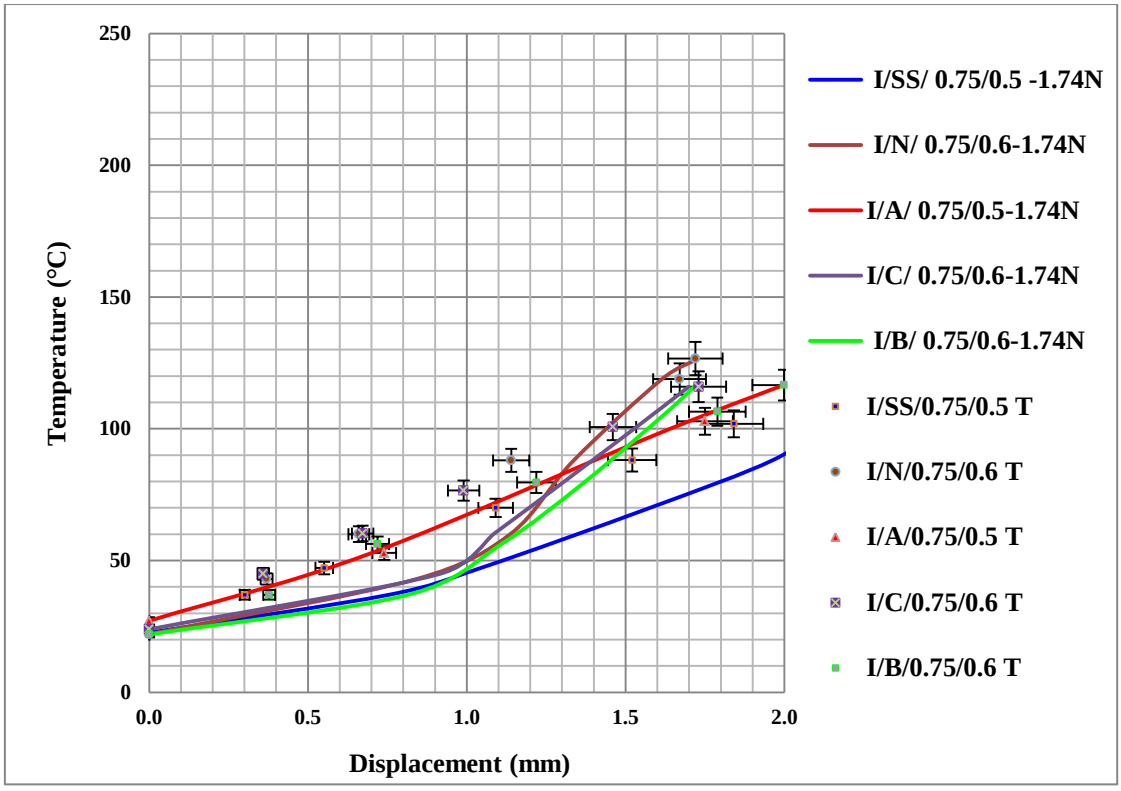

Fig.6-22 Verification of Temperature with Loaded Displacement for fabricated

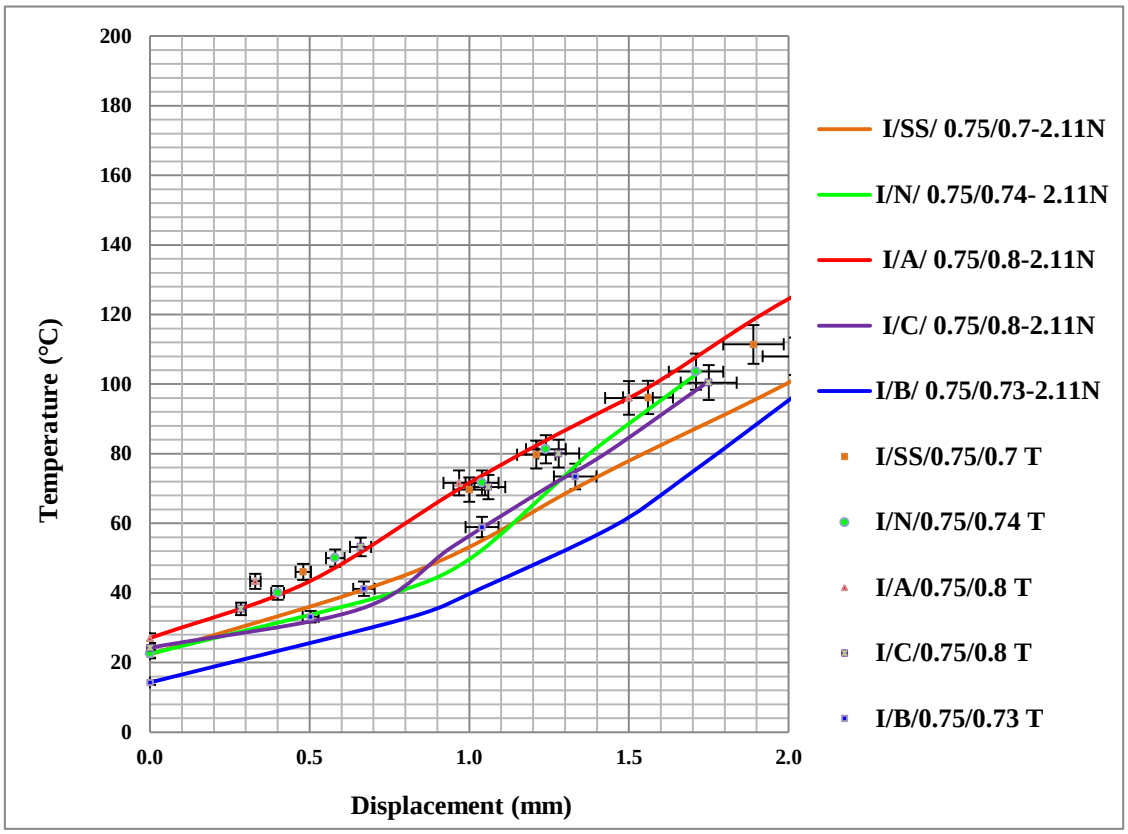

Fig.6-23 Verification of Temperature with Loaded Displacement for fabricated

For Fig.6-18 - 10 points hit 5% of 30 points, 33 % of points are accurate within 5%.

For Fig.6-19 -16 points hit 5% of 30 points, 53% of points are accurate within 5%.

For Fig.6-20 17 points hit 5% of 30 points, 56% of points are accurate within 5%.

For Fig.6-21 - 17 points hit 5% of 30 points, 56 % of points are accurate within 5%.

For Fig.6-22 - 8 points hit 5% of 30 points, 27 % of points are accurate within 5%.

For Fig.6-23 – 9 points hit 5% of 30 points, 30 % of points are accurate within 5%.

Overall average of points that were within 5% error were: 42.5%.The estimate for those points within 10% error was approximately 73%.

The amount of deviation in this test range can be attributed to many factors, some working for the correlation, and some against. For the factors contributing to the success of getting within 10% of the theory, was the consistency of the tests, i.e. the magnetic coupling test rig afforded repeatable test results consistently. For the factors that contributed against the theory to test match, there was a constant frictional load due to the rubbing of the bimetallic test pieces in their mounts during the tests. Additional frictional loads were experienced in the test rig at the mass pulley, and where the magnetic floating assembly touched the PTFE walls of the rig. However, the frictional load contribution was constant since no lubricants were used in the test rig. Other

factors causing the deviation between the test data results and the theory, were down to variability obtained by the published data for the coefficients of linear thermal expansion and the Young's modulus of the metals making up the bimetallic strip. Additionally, the fabricated bimetallic test samples were joined only intermittently and thus the test samples only approximated to theoretical bimetallic strip. Furthermore, due to an early manufacturing problem during the fabrication of the test samples, the last 15mm of each end of the strip were not fixed together at all. All these factors combined have contributed to the percentage error calculated previously.

Whilst a relatively low score of 42.5% of the points were within 5% of the theory, a much higher value of up to 73% was estimated for data points that were within 10% of the theory. The most realistic value is probably about 65% of all data points were within about 7 - 8% error from the theory for this data set.

That concludes the Load vs. Temperature correlation for fabricated samples.

6.3.7 Load vs. Disp. vs. Temperature: Correlation – Bespoke Samples

For the Load vs displacement test set, equation

$$X = \{2\left(\frac{\rho R_c}{\rho - R_c}\right) sin\left(\frac{A_b(\rho - R_c)}{2\rho R_c}\right) - 2R_c\, sin\left(\frac{A_b}{2R_c}\right)\} - \{\frac{2FR^3}{E_a\, I}\left[\frac{\omega}{2} - \frac{3sin(\omega)}{4} + \frac{\omega * cos(\omega)}{4}\right]\}$$

The theory from section 3.6 was used for the generation of theoretical points.

The testing for this test data set was performed on both the Sauter test rig and the vertical lift test rig. As before the 5% error bars were used to correlate the theory to the test data results and as before T denotes theoretically calculated values.

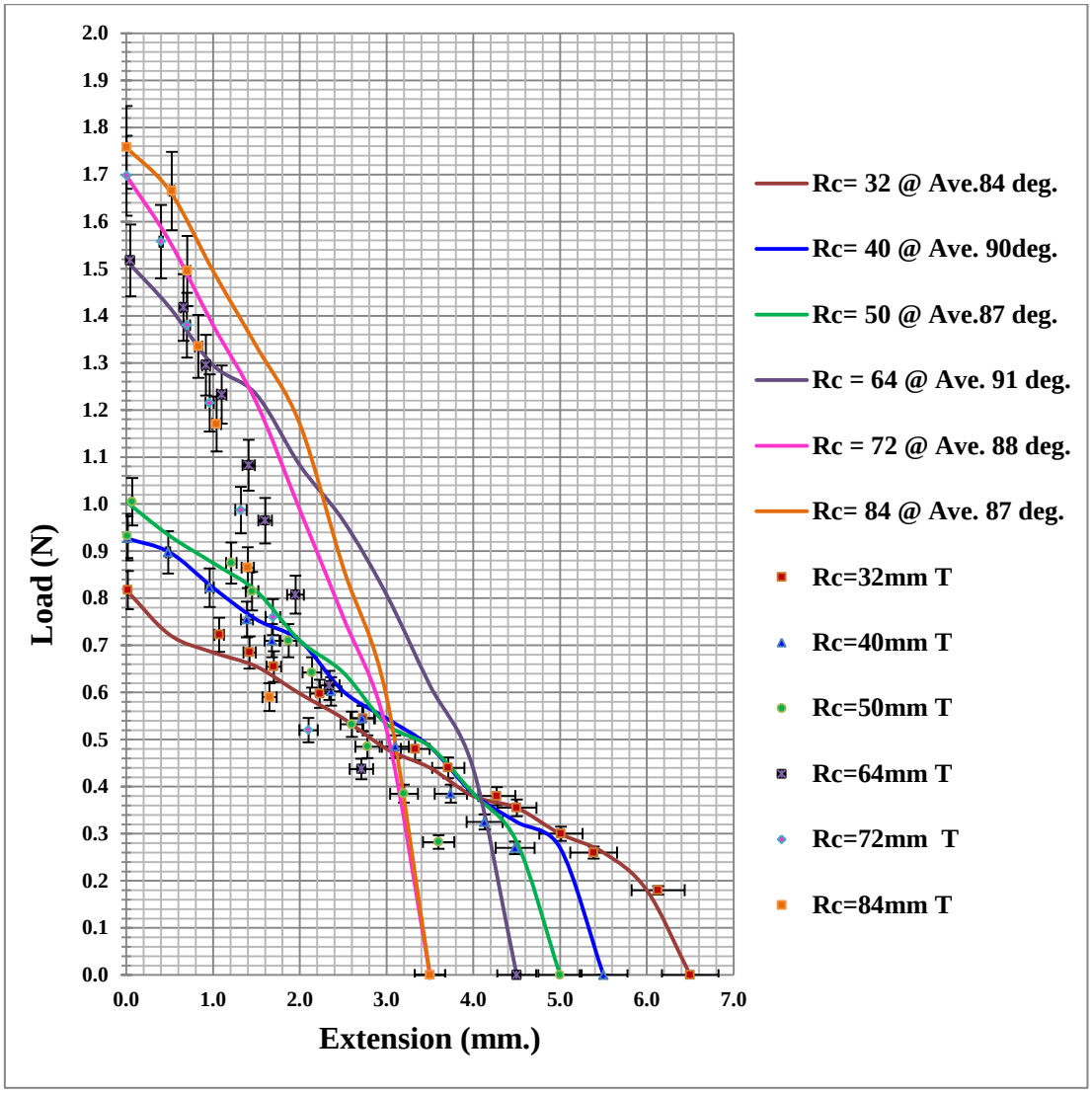

Fig.6-24 Verification of Load with Extension for Constant Temperature

For Fig.6-24 - 41 points hit 5% of 63 points, 65 % of points are accurate within 5%.

As can be observed from graph 23, most of the points that were within 5% were on the smaller radii i.e., Rc=32mm, Rc=40mm test curves. The equations used to generate the theory lines were Timoshenko's formula for obtaining the hot radius of curvature and thus the heated generated maximum displacement of the end of the bimetallic strip. Castigliano's derived formula was used to evaluate the loaded displacement of the free end of the strip. As was discussed earlier, because Castigliano's formula is based upon simple bending theory, the theory applied to the combined heating and loading case just correlated, is limited to quasi-linear displacements. Thus the theory is not as accurate for larger radii of curvature as confirmed in Fig.6-24.

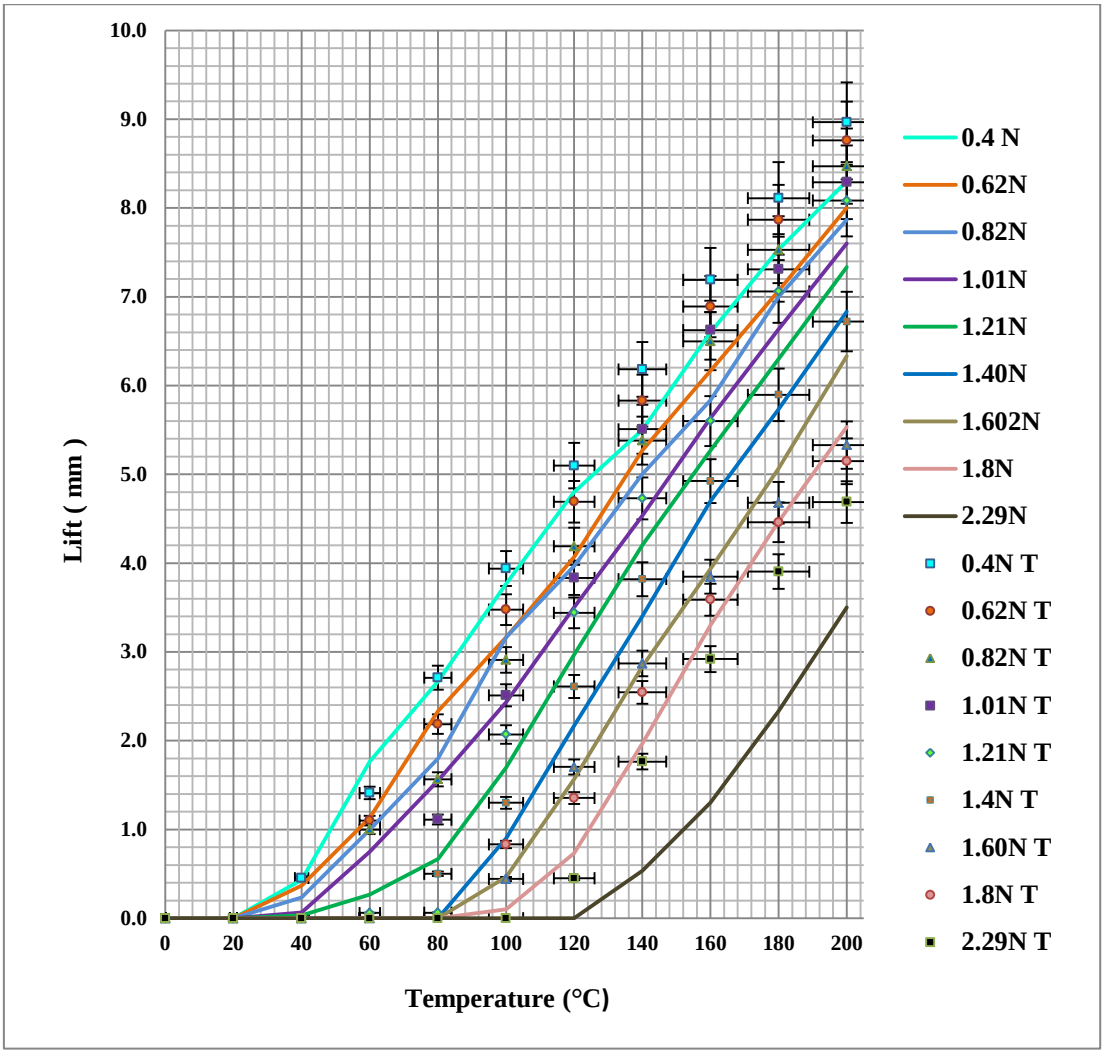

Fig.6-25 Verification of Lift with Temperature for various loading

For Fig.6-25 - 53 points hit 5% of 81 points, 65.4 % of points are accurate within 5% error, but a much higher percentage are within 10% error.

The major contribution for the deviation from the error for this test sample set was a combination of the vertical test rig dry friction plus reading error. This test used a steel rule with a magnifying glass to record the lift displacements. The combination of heat induced lifting plus an applied static loading produced the net loaded lift displacement. From Fig.6-25 it can be seen that the more heavily loaded test samples e.g. for the 1.8N load required a higher temperature 100 °C, to lift the mass from the zero position. Conversely for the less loaded test samples, e.g. 0.4N load, the lift started at a much lower temperature 30°C.

From both tests, on two different test rigs, the average number of theory points hitting the test data generated curves with 5% error was 65.25%.

The value of points within the 10% error was in the region of 75%.

With a 5% error band, 65% of the data matched the theory put forward by this work and a higher up to 75% was within 10% error. From these results it can be concluded with a reasonably high level of confidence, that the theory proposed in section 3.6 adequately describes the net loaded displacement combined heating and loading case.

6.3.8 Spatial End Point Position Correlation – Bespoke Samples

For the spatial end point position correlation, equation's

$x = L_h \cos\left(\frac{A_c}{2}\left(\frac{1}{R_c} - \frac{1}{R_h}\right)\right)$; $y = L_h \sin\left(\frac{A_c}{2}\left(\frac{1}{R_c} - \frac{1}{R_h}\right)\right)$ and Timoshenko's heat bending formula to evaluate R_h were used from section 3.10 to generate the theoretical points. These test results were for the bend to straight test, whereby the pre-curved test bimetallic strip was fixed at one end and the applied heat straightened up the test piece. For Fig.6-26, 24 points hit 5% of 24 points, i.e. 100 % of the points are accurate within 5% error, but as can be seen in Fig.6-26, a fair percentage of points lie within 2 % error.

From Fig.6-26, it can be seen that larger the radius of curvature, the larger the deviation from the theory. For the D128mm plotted points the large error was caused by Hunting, a phenomenon whereby the end of the bimetallic strip was constantly moving due to being alternatively heated and cooled as result of the fixed position of the heat source and the clamped end. The spatial bend test correlation was within 5% for all points, and within 2% or less for many other points.

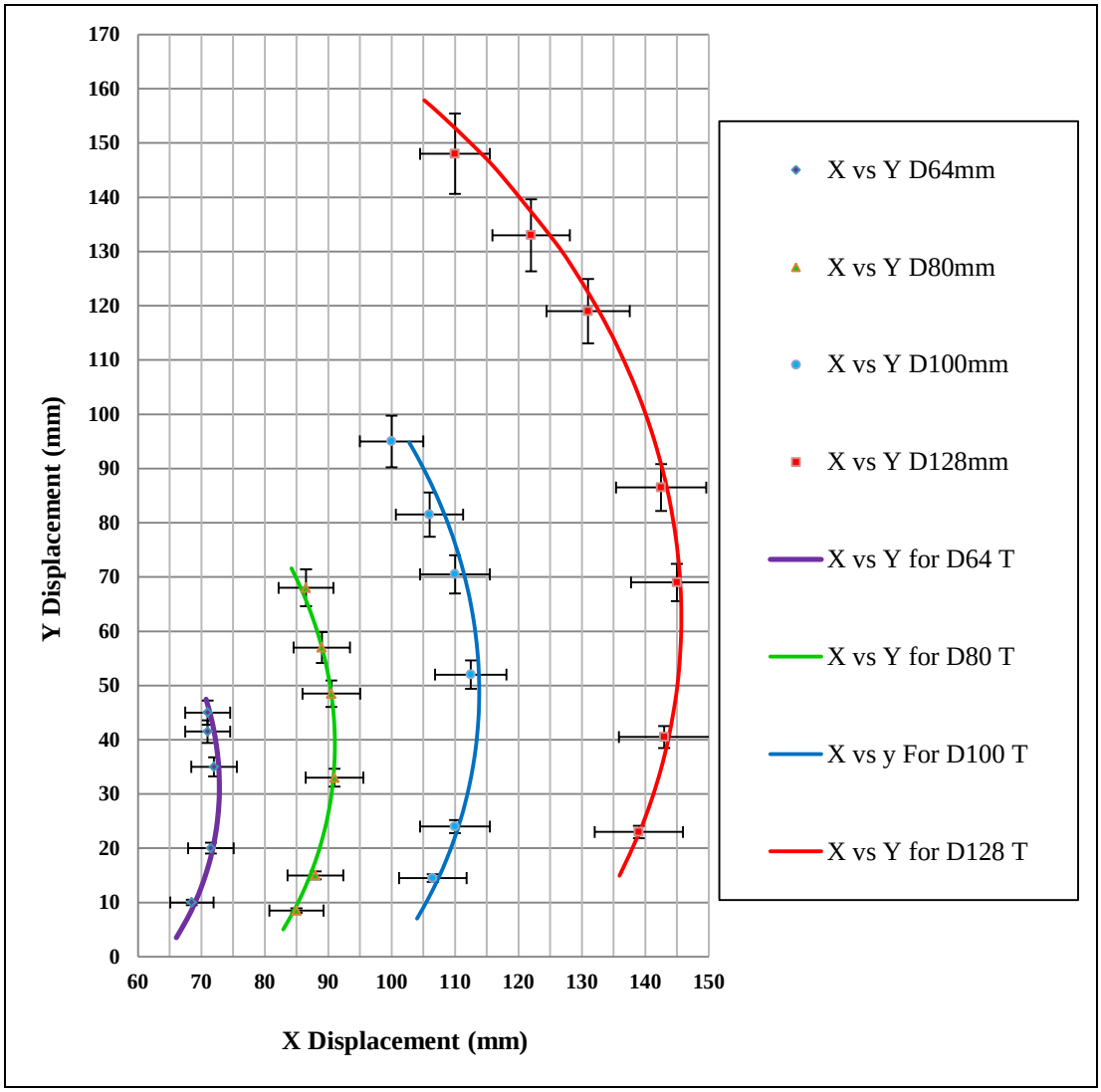

Fig.6-26 Verification of Theory against Test for Straightening Test Data

6.3.9 Time vs. Displacement: Correlation – Fabricated Samples

For the time vs displacement correlation , equation' s $R = \frac{t\Omega}{\Delta T}$, where $\Omega = \frac{(\alpha_2 - \alpha_1)^2}{(\alpha_2 + \alpha_1)\,\alpha_2^{\,2}}$, were used instead of the Timoshenko formula to evaluate the radius of curvature as a function of heating. $R_t = \frac{(m_1+m_2)(c_{p1}+c_{p2})\,t_b\,\Omega}{2Q\,t_{tm}}$ was used to evaluate the radius of curvature from flat strip as a function of time. $\mathrm{R_h} = \frac{R_c R_t}{R_t - R_c}$ was then used to evaluate the hot radius of curvature from R_c.

The displacement was evaluated as previously using $x_d = L_h - L_c$ and the supporting equations$L_h = 2R_h \sin\left(\frac{A_b}{2R_h}\right)$ and$L_c = 2R_c \sin\left(\frac{A_b}{2R_c}\right)$ all stated previously.

The object, as originally stated in section 1.2 was to find the theory that could predict the time to displace a pre-curved bimetallic strip along its chord line axis as defined

previously. The theoretical equations derived in section 3.12 were used in the correlation. Fig's 6-27, 6-28, 6-29, 6-30, and 6-31 are the correlation plots. As before, T denotes the theoretical time calculated by the theory from section 3.12.

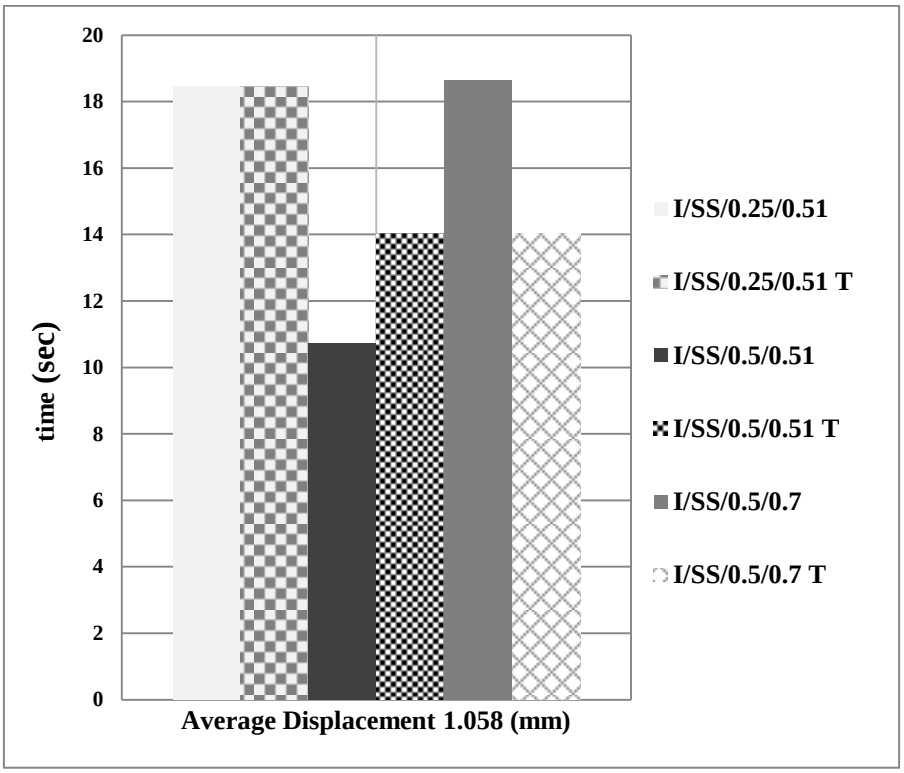

Fig.6-27 Verification of Time with Distance over a fixed distance

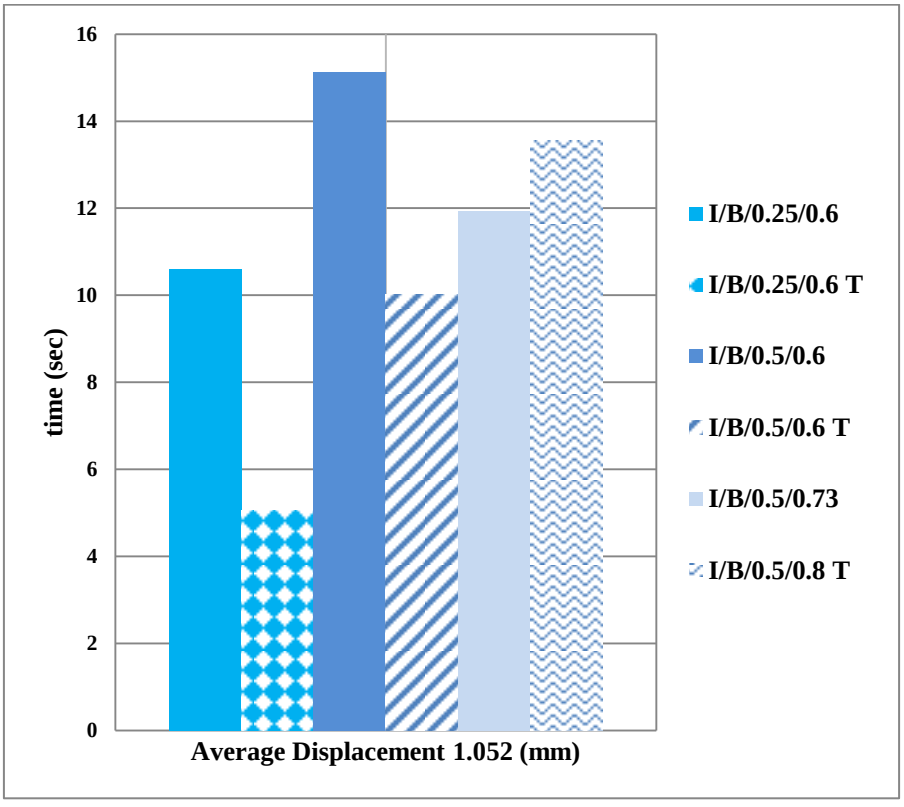

Fig.6-28 Verification of Time with Distance over a fixed distance

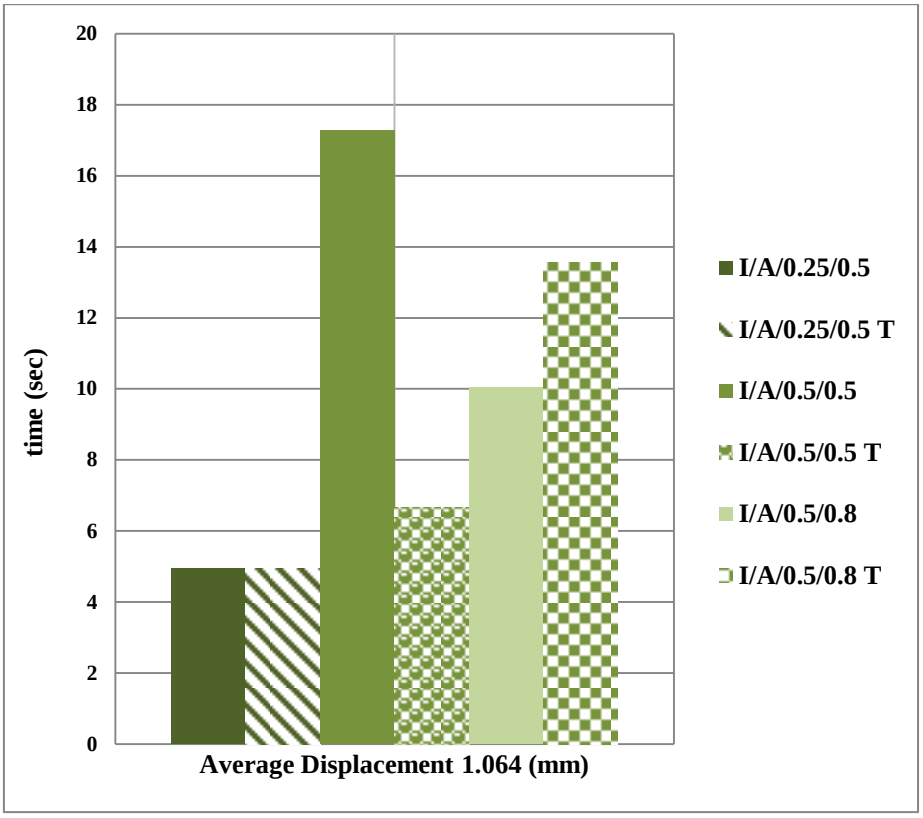

Fig.6-29 Verification of Time with Distance over a fixed distance

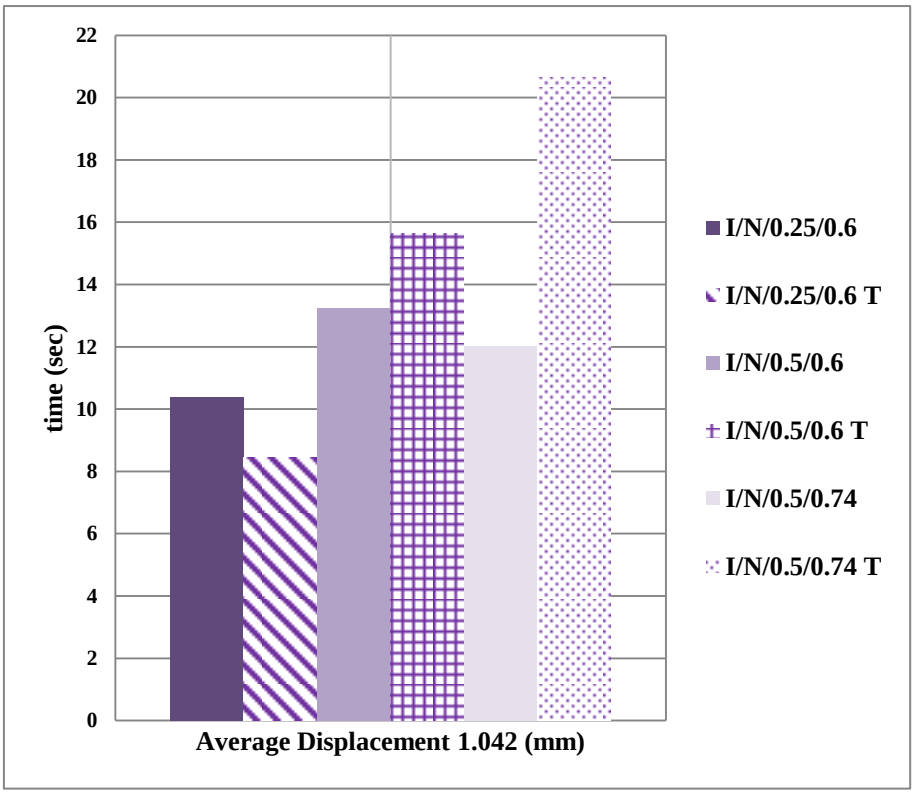

Fig.6-30 Verification of Time with distance over a fixed distance

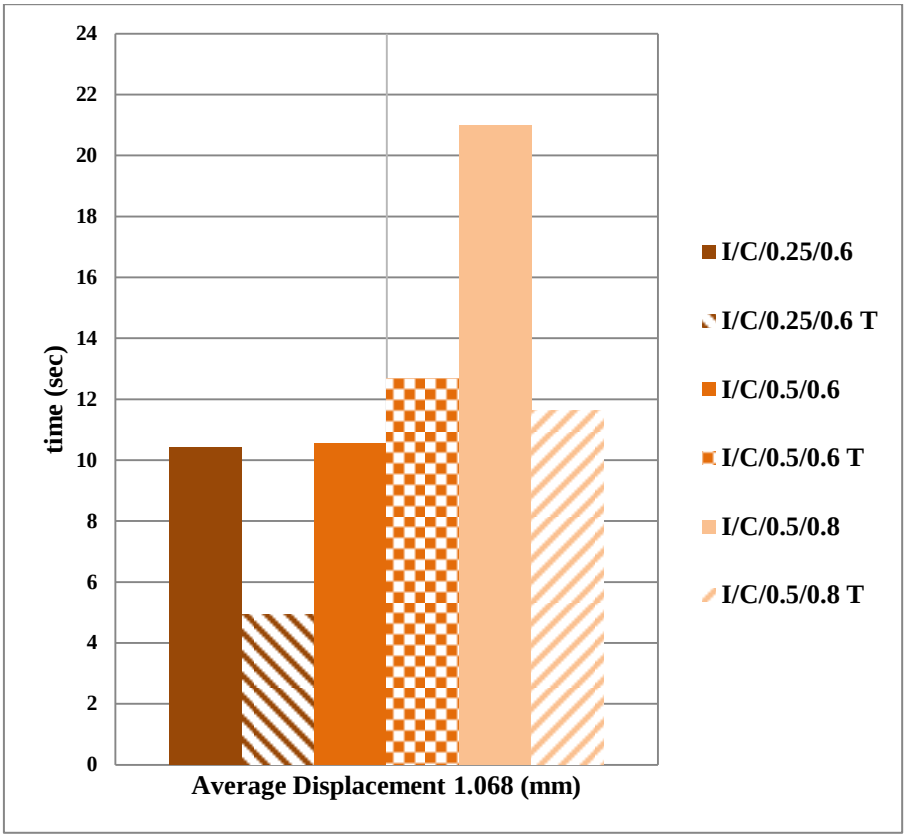

Fig.6-31 Verification of Time with distance over a fixed distance

For the correlation, the theory time calculated was divided by the test time to displace each test sample 1mm in theory, or an average of 1.058mm for the test samples. The ratio of theory to test time provides the correlation of how close the theory time relates to the actual test time. For the 15 test sample plots the average ratio of theory to test results was 0.96285, or in error terms 100% - 96.285% = 3.715%, which was the overall average error.

As per test procedure of section 5.7.5, each test piece was suddenly exposed to a controlled hot air flow by the opening the heat gate. The sudden opening of the heat gate exposed the test sample to a steady state hot air gun temperature of 300 °c. The time to make electrical contact over a fixed distance of 1mm was recorded.

The major contribution of the error came from the manual method of synchronising the heat gate opening, and simultaneously recording of the time to make contact. This operation was performed manually, and could have erred by 1sec or more. Although the sensing system worked well, i.e. as the 1mm displacement was reached a light came on, the human response to interpretation of the light signal and the recording of the value of displacement was not instantaneous. The human errors in operation of the test would have contributed to the deviation between the theory and the test results.

Despite the possible additive errors in recording the time to displace 1mm in 15 separate fabricated test samples, the overall average percentage error was 3.715%.
From the correlation value of 3,715% error between the theory proposed by this investigate and the test results, it can be inferred that the theory matches the test data with a reasonable confidence level.

6.4 Discussion of Overall Correlation of Test Results

This chapter has provided the correlation between the theory proposed in chapter 3 and the actual test data provided in this chapter in accordance with objectives 1 to 8, as set out in section 1.2. An overall correlation table is shown in Table 9.

From Table 9, the average correlation of all tests performed, was that 66% of the tests results were within 5% of error.

Table 9 Overall correlation results

Type of test	Conditions	Rig Used	Loading	Type of Bimetallic	Correlation results
Load vs. Displacement	Ambient Temperature	Magnetic Assembly	Horizontal	Fabricated Bimetallic Strip	**40.96% within 5%**
Load vs. Displacement	Ambient Temperature	Sauter Force Displacement	Horizontal	Bespoke Bimetallic Strip	**98% within 5%**
Temperature vs. Displacement	Varying Temperature, No Load	Magnetic Assembly	Horizontal	Fabricated Bimetallic Strip	**58% within 5%**
Temperature vs. Displacement	Varying Temperature, No Load	Sauter Force Displacement	Horizontal	Bespoke Bimetallic Strip	**26% within 5%**
Combined Heating and Loading	Varying Mass Load & Temperature	Magnetic Assembly	Horizontal	Fabricated Bimetallic Strip	**42.5% within 5%**
Combined Heating and Loading	Varying Mass Load & Temperature	Vertical Gravity	Vertical Lifting	Bespoke Bimetallic Strip	**65% and 65.4% within 5%**
Straightening Test	Varying Temperature, No Load	Bench Fixed One End	Horizontal	Bespoke Bimetallic Strip	**100% within 5%**
Time vs. Displacement	Temperature Constant, No Load	Magnetic Assembly	Horizontal	Fabricated Bimetallic Strip	**98.285% within 5%**

A conservative value of between 67% and 75% were within 10% error. The testing of the pre-curved bimetallic test samples took the form of both pre-fabricated and bespoke test samples, both types of bimetallic strip test samples were subjected to the same methods of test, albeit on separate test rigs. The overall correlation results provide reasonable confidence in the correctness of theory proposed by this investigation.

6.5 Conclusions of the Test Results and Correlation to Theory

In section 6.2, the factors affecting the accuracy of the correlation of the theory to the test results, were listed. There were many contributing error factors that have heavily influenced the outcome of the accuracy of the test results.

Despite the many possible errors that incurred during testing, a reasonably good overall correlation exists between the theory introduced by this work, and the physical test data. The results have shown that 66% of all tests are within 5% error, and up to 75% of all tests are within 10% error.

Therefore objectives 1 to 8 as set out in 1.2 of this investigation, have all been completed. With the realisation of the objectives, the aims of this study from section 1.2 have also been addressed in full.

CHAPTER 7 Discussion, Conclusion and Further Work

Summary

This chapter discusses additional formulae, general conclusions and further work. New formulae and geometric proofs are provided.

7.1 Introduction

The new knowledge introduced by this work addresses the objectives set-out in section 1.2, namely to characterise the behaviour of a pre-bimetallic strip that is loaded as follows:

1) Load vs. Displacement
2) Temperature vs. Displacement
3) Load vs. Temperature

The early chapters employed Timoshenko for the theoretical bending formula and Castigliano energy theorem to evaluate the chord line force displacement relationships.

The following sections address the main objectives and provide further, additional understanding of the relationships of chord line forces of pre-curved bimetallic strip.

A new chord line force versus displacement formula was introduced that improves upon the Castigliano derived expression, by accommodating larger displacements for shallow arc bimetallic strip. A simpler, more immediate alternative to the Timoshenko temperature induced bending formula was introduced. A new net loaded position for pre-curved bimetallic strip straightening case was introduced.

This study has produced a variety of new formulae and geometric relationships pertaining to arcs of a circle, and relationships between adjoining and overlapping arcs of circles. The geometric relationships were either discovered, or derived from first principles, and proven to hold true for all combinations of the values tested. The relationships were found during the geometry simulation of a pre-curved bimetallic strip using Catia Dassault (2014) software. It should be noted that the level of accuracy of the Catia software is precise to greater than six decimal places, which enabled the validation of the new formula with a high confidence to the exactness of the resulting relationships. Catia was programmed with the chord length formula, Eqn.7, page 44, using the built in Catia formula facility. The formula capability of Catia facilitated the validation of angles and distances that were calculated by the relationships and equations introduced in this section. Catia screenshots of the arc validation geometry are shown in the Appendices.

7.2 Various Proven Derived Relations

This section provides derived, or discovered relationships that have all been exhaustively tested using Catia geometry simulation, and found to hold true for all values tested.

Fig. 7-1 shows the idealised model of the generic pre-curved bimetallic geometry of two thin strips in two states of heating. State 1 as denoted by subscript 1, is when the strip is at ambient temperature. State 2, is when the strip has been heated and increased its radius of curvature denoted by subscript 2. The increase in radius of curvature results in the extension of the strip along its chord line to length L_2.

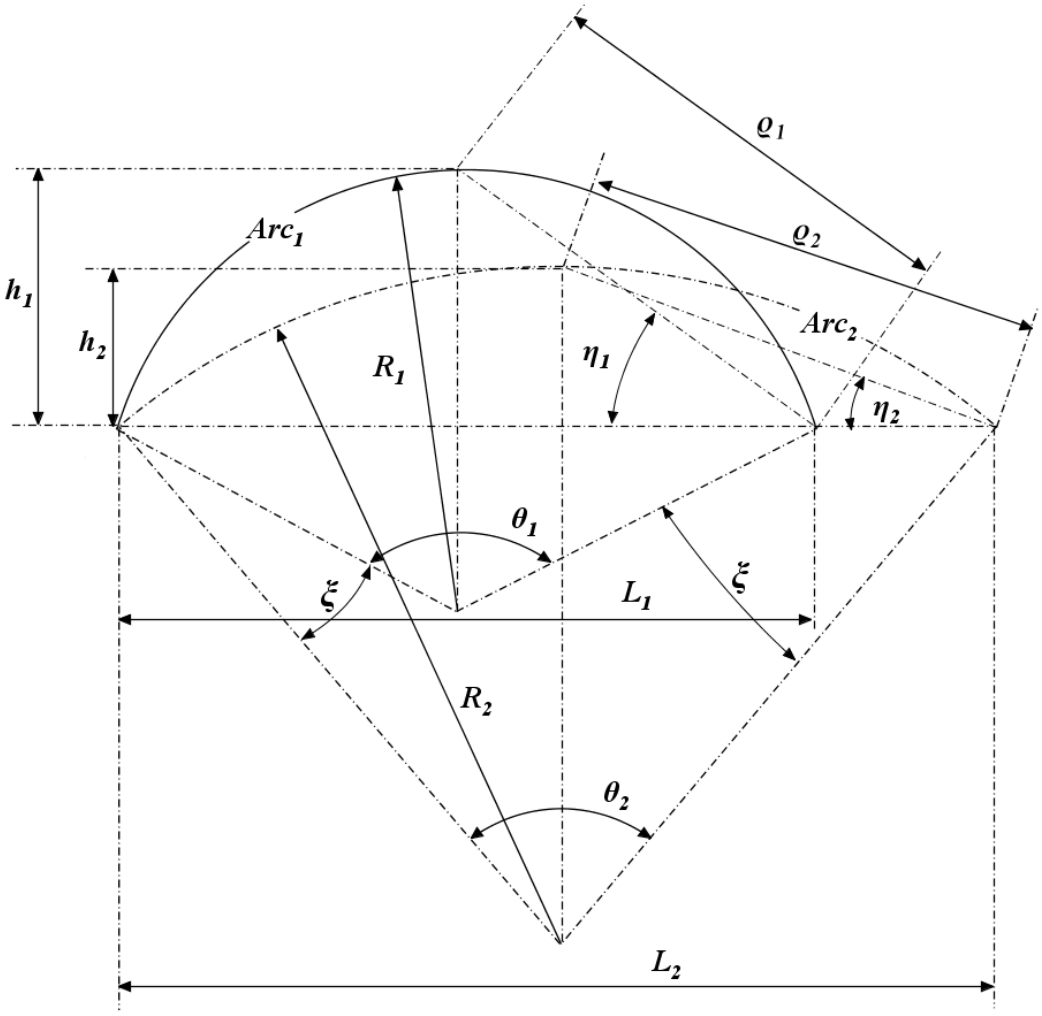

Fig.7-1 Various arc geometry

By derivation: $R_1 = \frac{1}{2\,h_1}\left(\left(\frac{L_1}{2}\right)^2 + {h_1}^2\right)$ Eqn. 86

Same for R_2. $R_2 = \frac{1}{2\,h_2}\left(\left(\frac{L_2}{2}\right)^2 + {h_2}^2\right)$

Derivation:

By Pythagoras: $(\frac{L_1}{2})^2 + (R_1 - h_1)^2 = {R_1}^2$

This expands to with re-arrangement and simplifying; $(\frac{L_1}{2})^2 = 2\,R_1 - {h_1}^2$

Hence $R_1 = \frac{1}{2\,h_1}(\left(\frac{L_1}{2}\right)^2 + {h_1}^2)$ same for R_2

Eqn. 90 can be alternatively expressed: $R_1 = (\frac{{L_1}^2}{8\,h_1} + \frac{h_1}{2})$ Eqn. 87

Same for R_2. $R_2 = (\frac{{L_2}^2}{8\,h_2} + \frac{h_2}{2})$

The radius to sector angle ratio relationship is as follows:

$$\frac{R_2}{R_1} = \frac{\theta_1}{\theta_2} = \frac{\eta_1}{\eta_2} \qquad \text{Eqn. 88}$$

Derivation:

From Fig.6-3 in general terms; $\frac{R-h}{R} = \cos(\frac{\theta}{2})$

This becomes after re-arranging;

$$h = R\left(1 - cos\left(\frac{\theta}{2}\right)\right) \qquad \text{Eqn. 89}$$

Noting that; in general, $\eta = \frac{\theta}{4}$

thus $h = R\big(1 - cos(2\eta)\big)$

Using the Mathematical book $\sin(x)^2 = \frac{1}{2}(1 - \cos(2x))$, substituting and re-writing in general terms;

$$R = \frac{h}{2\,sin^2\eta} \qquad \text{Eqn. 90}$$

Additionally :

$$R_1 = \frac{L_1}{4}(\tan(\eta_1) + \frac{1}{\tan(\eta_1)})$$

And thus; $R_2 = \frac{L_2}{4}(\tan(\eta_2) + \frac{1}{\tan(\eta_2)})$ Eqn. 91

Height relationships at mid-span of the chord are as follows:

$$h_1 = \frac{L_1}{2}\tan(\frac{A_b}{4R_1})$$

Likewise: $h_2 = \frac{L_2}{2} \tan(\frac{A_b}{4R_2})$ Eqn. 92

And also $h_1 = \frac{A_1}{2\eta_1} sin^2\eta_1$

Likewise: $h_2 = \frac{A_2}{2\eta_2} sin^2\eta_2$ Eqn. 93

Alternatively: $h_1 = R_1\left(1 - cos\left(\frac{A_1}{2\,R_1}\right)\right)$

Also $h_2 = R_2\left(1 - cos\left(\frac{A_2}{2\,R_2}\right)\right)$ Eqn. 94

7.3 Angle ξ as a Function of η_1, η_2

A new relationship linking angle ξ and the difference between η_1, η_2 was established in the Catia geometry simulation presented earlier.

It was proven to hold true for all values that:

$$\xi = 2(\eta_1 - \eta_2) \quad \text{Eqn. 95}$$

Also that: $\xi = \frac{(\theta_1 - \theta_2)}{2}$ Eqn. 96

Equating Eqn.99 & Eqn.100;

$$4((\eta_1 - \eta_2) = (\theta_1 - \theta_2)$$

Individually can be expressed as: $\eta_1 = \frac{\theta_1}{4}$

And thus: $\eta_2 = \frac{\theta_2}{4}$ Eqn. 97

A further definition of general angle η, is that it can be expressed as a function of the arc length divided by four times the radius of curvature in radians.

Thus in general: $\eta = \frac{Arc}{4R}$ Eqn. 98

7.4 Ratios of Short Chords of Arcs as a Function of Radii

The following relationship was discovered in the Catia Simulation and holds to be true for all values that in general:

$$\frac{\boldsymbol{\psi_1}}{\boldsymbol{\psi_2}} = \frac{\boldsymbol{R_1}}{\boldsymbol{R_2}} = \frac{\boldsymbol{\theta_2}}{\boldsymbol{\theta_1}} = k \quad \text{Eqn. 99}$$

where *k* is a constant.

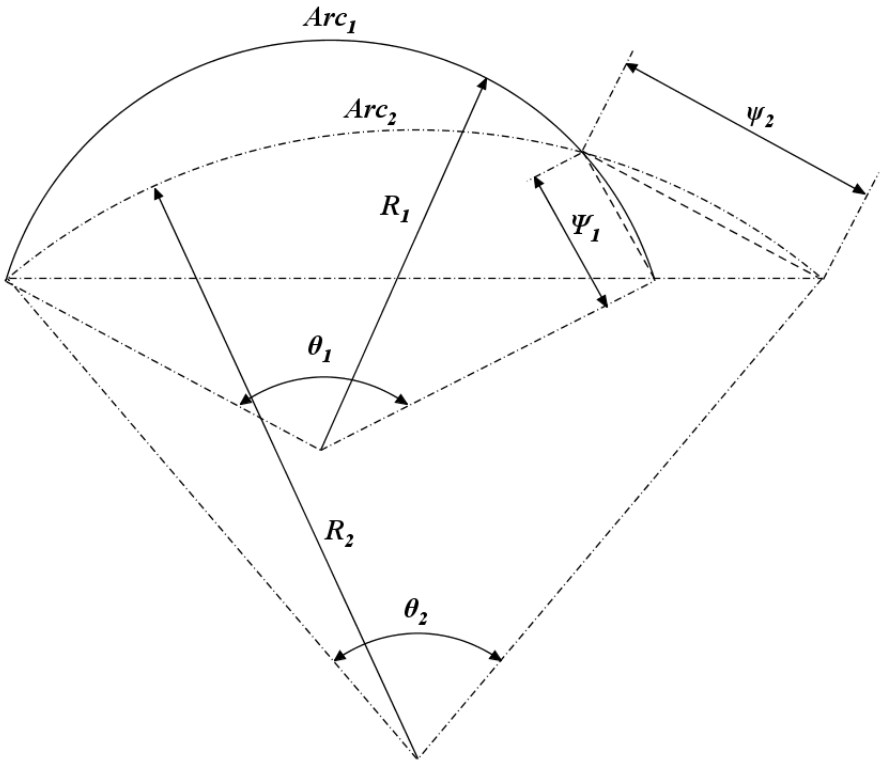

Fig.7-2 Ratios of short chord of arcs and radii

From Fig.7-2, the short chord lengths ratio of ψ_1 divided by ψ_2 is proportional to the ratio of the radii; R_1 divided by R_2, that is further inversely proportional to the angles of the sectors θ_2 divided by θ_1, of the adjoining arcs.

The relationships hold true for any combination of values provided that the lengths of both arcs are the same, i.e. $Arc_1 = Arc_2$.

7.5 *"x"* and "*y*" Positions as a Function of ω and θ and R.

Using Catia Dassault (2014) in the Design Sketcher environment, a relationship was established by graphical means, that links angle β to angle ω and angle θ . This relationship was tested for a variety of values of arc $A_{b,}$ angle β, and angle ω, and it was found to hold true for all values tested that in general:

$$\beta = \frac{\omega - \theta}{2} \quad \text{Eqn. 100}$$

The proof is as follows:

From Fig.7-3, in triangle Δcbe, $\rho + \beta + \alpha + \theta = 180°$, and also $\rho = \beta + \alpha$

Thus by substitution and tidying up: $2\beta + 2\alpha + \theta = 180°$

From triangle Δabe, $2\alpha + \omega = 180°$,

Hence by substitution and tidying up

$$\beta = \frac{\omega - \theta}{2} \quad \text{proven}$$

This is the angle between line τ and *x* axis, line *a* to *b*, see Fig.7-3.

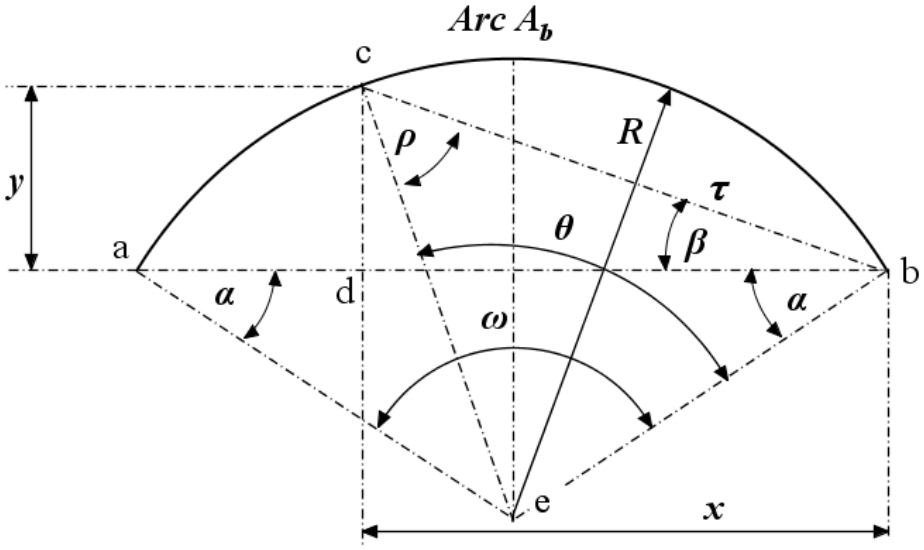

Fig.7-3 *x* and *y* positions as a function of ω and θ and *R*

A further relationship between line τ and angle θ is also derived.

From Fig.7-3, the chord line *ab* was earlier described by length: $L = 2Rsin(\frac{\omega}{2})$, thus chord line *cb,* length τ, can also be written as : $\tau = 2R\ sin(\frac{\theta}{2})$.

From the standard trigonometric identity for half-angles chords; Abramowitz (1964)

$sin(\frac{\theta}{2}) = \sqrt{\frac{1-\cos\theta}{2}}$, if each side of this equation is multiplied by $2R$ and then squared thus; $4R^2\ sin^2\ \frac{\theta}{2} = 2R^2(1 - cos\ \theta)$, But from before, the LHS of the equation is equal to τ^2, then ;

$$\tau = \sqrt{(2R^2\big(1 - cos(\theta)\big))} \quad \text{line } cb$$

For the curved geometry as shown in Fig. 6-3, the new geometric relationships were established:

$$y = \sqrt{(2R^2\big(1 - cos(\theta)\big))}\ sin\ (\frac{\omega - \theta}{2})$$

$$x = \sqrt{(2R^2\big(1 - cos(\theta)\big))}\ cos\ (\frac{\omega - \theta}{2}) \quad \text{Eqn. 101}$$

7.6 Finding the Angular Ratio k_n as a Function of Temperature

This section establishes the constant ratio k_n as a function of temperature which is specific to a particular bimetallic strip.

It was stated in an earlier section that as a bimetallic strip is heated above ambient temperature, it must obey Hooke's law and remain within the material's elastic limit during heating. To conform to linear elastic behaviour, upon cooling, it must return to the same shape or form, found originally at ambient temperature. Therefore, if a bimetallic strip exhibits linear thermal characteristics, then a linear thermal relationship must exist between the temperature of the bimetallic strip and its radius of curvature, in temperature induced bending.

Therefore this section introduces new formulae that provide the mathematical link between the heating, and the geometry of the arc of the bimetallic strip.

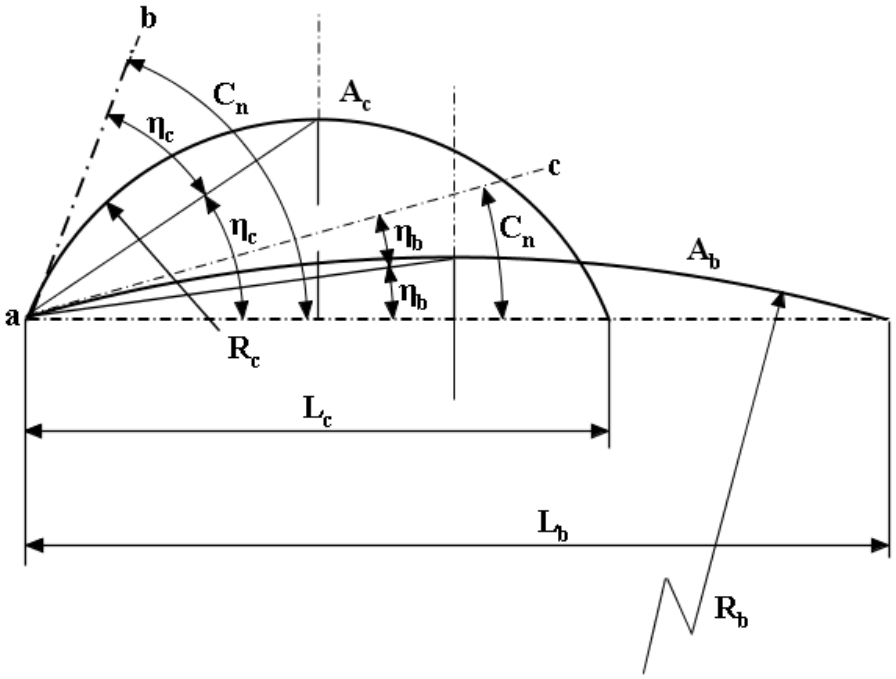

Fig.7-4 Geometry of angular ratio k_n

Assuming a linear thermal relationship exists as a function of the geometry, therefore one possible derivation of this relationship is as follows:

From Fig.7-4, line *ab* is tangent to arc A_c supporting radius of curvature $R_{c,}$ and like wise, line *ac* is tangent to arc A_b supporting radius of curvature $R_{b,}$ where in fact: A_c = A_b, both arcs are the same length of the same bimetallic strip.

Using the simplified, more immediate radius of curvature formula, introduced earlier in this study, thus from before:

$R = \frac{t(\alpha_2-\alpha_1)^2}{\Delta T(\alpha_2+\alpha_1)\alpha_2{}^2}$ which can be simplified to $R = \frac{t\Omega}{\Delta T}$ where $\Omega = \frac{(\alpha_2-\alpha_1)^2}{(\alpha_2+\alpha_1)\alpha_2{}^2}$.

Note: Timoshenko's radius of curvature formula ρ can also be used in this derivation, but as stated earlier, it is a more complex formula, and thus harder to integrate with other formulae. Assuming that $C_n = k_n \Delta T$ is a linear thermal relationship linking the angle of the tangent line *ab*, or *ac*, to an arc of radius of curvature R. The change in temperature, ΔT is due to the heating of a flat straight bimetallic strip to form arc A_b. From Fig.7-4, it can be seen that the internal angle to the midpoint of the arc A_b, and the external angle tangent to the arc are both equal to angle η_c, and the same for η_b. The equivalence of the internal angle to external angle exists for all arcs.

Let $C_n = 2\,\eta_c$ or in general, let $C_n = 2\ \eta$ Eqn. 102

where C_n is the angle between the tangent to the arc and the chord line axis.

From earlier work it was generally stated that $\eta = \frac{A_b}{4\,R}$ in radians.

Thus by simple manipulation it can be shown that the constant k_n can be expressed by various relationships:

$$k_n = \frac{2\eta}{\Delta T} \qquad \text{Eqn. 103}$$

or

$$k_n = \frac{A_b}{2\,R\,\Delta T} \qquad \text{Eqn. 104}$$

or $$k_n = \frac{A_b}{2\,t\,\Omega} \qquad \text{Eqn. 105}$$

Eqn.103 requires the evaluation of angle η, which is a function of R or ρ, if Timoshenko is used. Eqn.104 requires R plus the arc length A_b. Eqn.105 requires arc length A_b, the thickness t and Ω which is a function of the coefficients of linear thermal (CTE) expansion of the bimetallic strip. Thus Eqn.105 is the most useful since it is relatively easy to find the CTE of the metals, plus the thickness and arc length. Furthermore, Eqn.105 does not require the value of R, or ρ, which needs to be calculated first in the preceding two formulae.

Hence $$C_n = \frac{A_b}{2\,t\,\Omega}\Delta T \quad \text{Eqn. 106}$$

where $\Omega = \frac{(\alpha_2-\alpha_1)^2}{(\alpha_2+\alpha_1)\,\alpha_2{}^2}$ was defined earlier.

t the total thickness of the bimetallic strip.

ΔT and A_b have been defined earlier.

Eqn.106 is the linear thermal expression linking the temperature to the external angle C_n. For the bespoke bimetallic strip SBC206-1, t = 0.4mm thick, and for an arc length

of; A_b= 80mm, a graph of angle C_n vs. temperature ΔT was plotted out see Fig. 7-5.

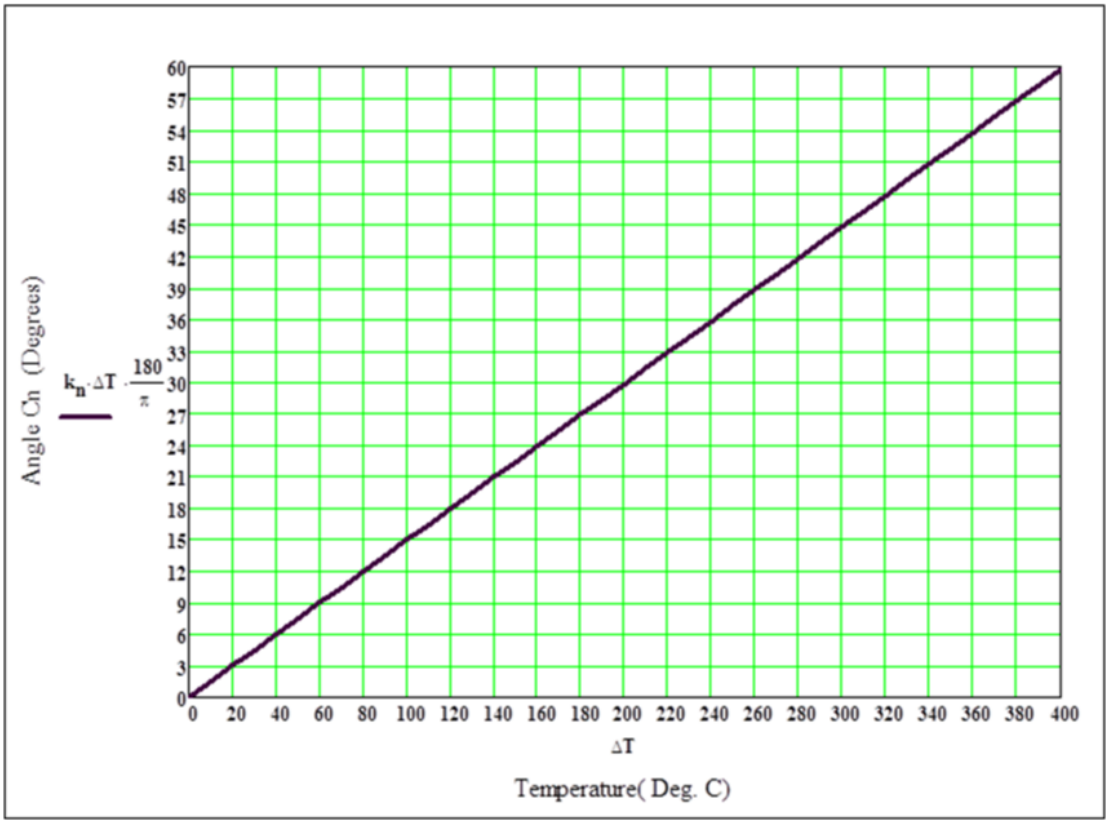

Fig.7-5 Angle temperature relationship for SBC206-1 bimetallic strip

Thus having established the $C_n\ vs.\ \Delta T$ curve, for a specific bimetallic strip, it is possible to find any bend radius R_b as a function of a temperature change, by simply reading off the graph.

Simulation

Therefore for the SBC206-1 bespoke flat un-curved bimetallic strip 80mm long, at 220°C – ambient 20°C, i.e. at 200°C, $C_n \approx 30$ extracted from Fig.7-5. Note the actual calculated value is 29.8627 and $C_n = 2\,\eta$ and also $\eta = \frac{A_b}{4\,R}$ thus:

$C_n = \frac{A_b}{2R}$ or $R_b = \frac{A_b}{2\,C_n}$ and this evaluates to $R_b = 0.0767454$ m.

This value accords well with the Timoshenko value for the same data:

By calculation, Timoshenko radius of curvature ρ = 0.076035 m. Thus using this method it is possible to evaluate the radius of curvature of a bimetallic strip from an initial flat straight condition providing that you know the following parameters:

1) Coefficient of linear thermal expansion for both metals making up the bimetallic strip
2) The arc length or the initial cold length of straight bimetallic strip.

3) The total thickness of the bimetallic strip.
4) The change of temperature experienced by the strip.

A method of evaluating the constant k_n was established for a specific bimetallic strip which enabled the calculation of the bend from flat radius of curvature if the 4 parameters previously shown are known. k_n is the parameter that links the change in temperature to the angle of tangent of the arc with the radius of curvature.

7.7 Finding Constants "a" & "b" in a Parabola

The force displacement curve for a pre-curved bimetallic strip when loaded along its chord line produces a non-linear displacement response. It has been found by testing pre-curved bimetallic strip that the chord force vs. displacement characteristic of a thin pre-curved bimetallic strip, closely matches a parabolic curve. The following method enables the finding of the constants of the force displacement parabola, when two forces and two displacements are known. The general form of a parabola is generally published as $y = ax^2 + bx + c$. See Fig.7-6 for plotted test data and Fig.7-7 for the test data extrapolated to match a parabolic function.

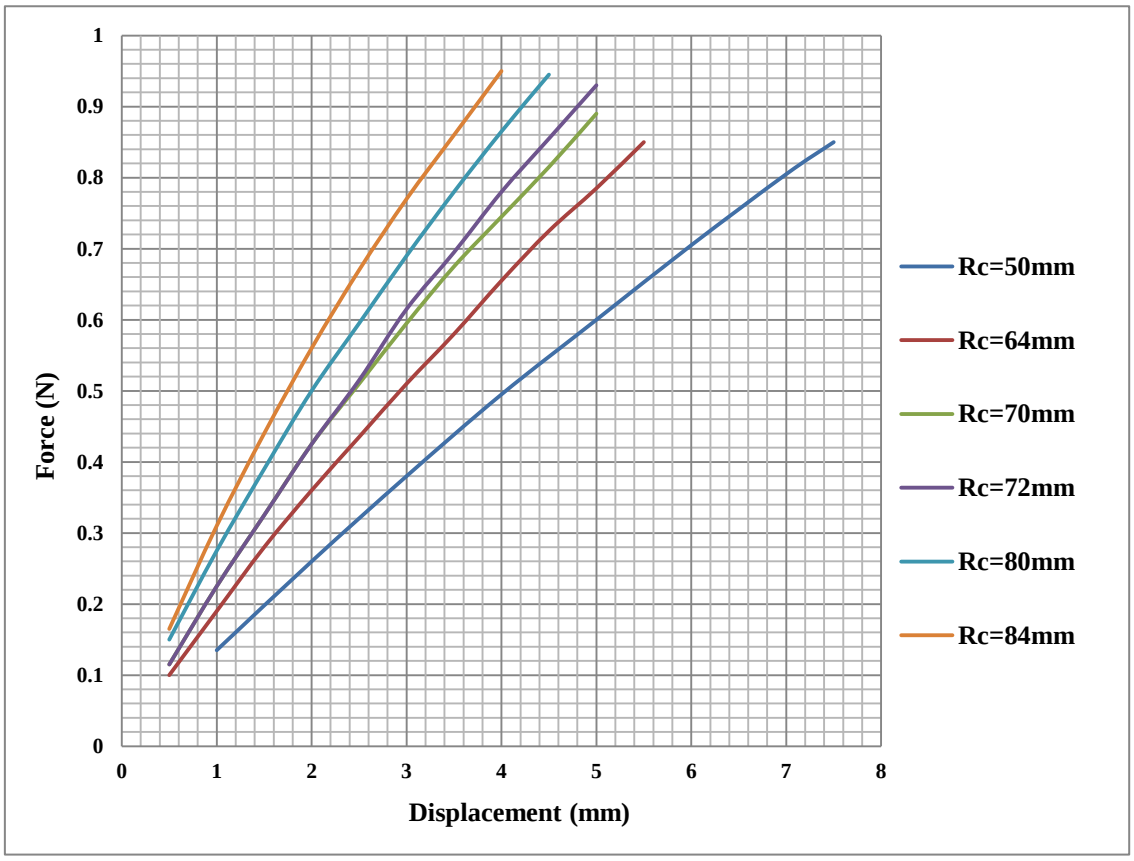

Fig.7-6 Test force vs displacement curves for various radii of curvature

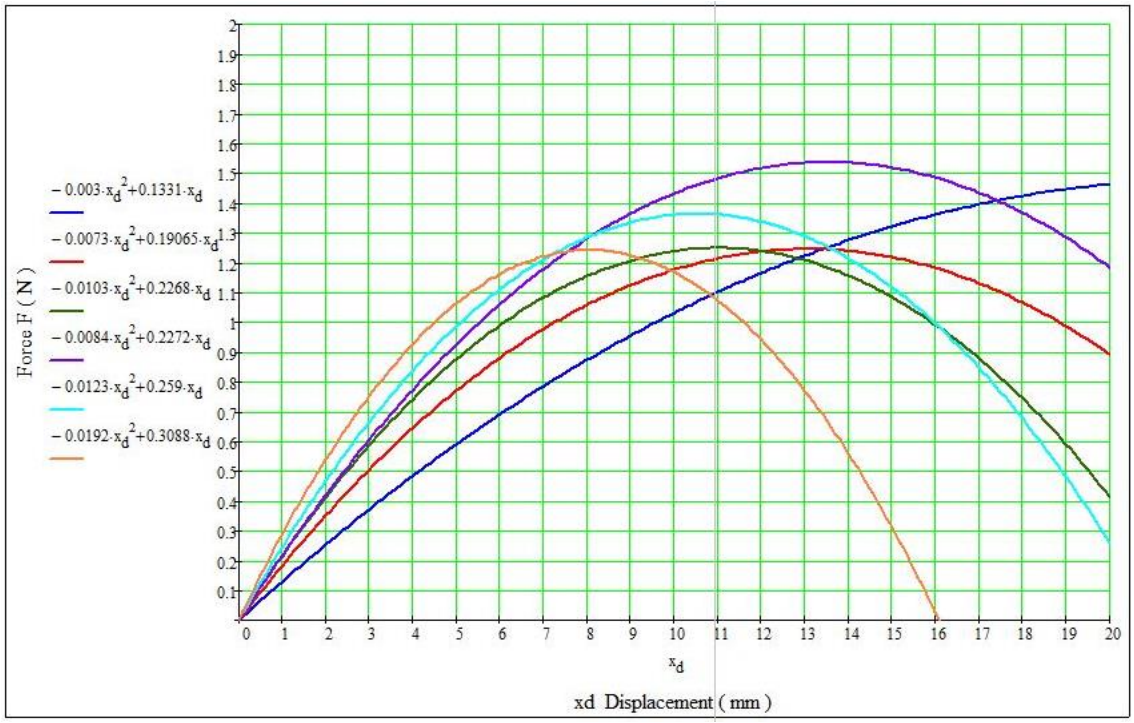

Fig.7-7 Force vs displacement test data - curved fitted and plotted out

Fig.7-7 shows the second order curve fitting and extrapolation of actual force vs. test data from Fig.7-6. Note, only the first half of the parabola up to the maximum is in the useful range in theory, the actual permissible displacement will be limited to and dictated by the yield stress of the pre-curved bimetallic strip. Fig.7-7 has been generated from Fig.7-6 by using the equation fitting facility in the Excel spread sheet. When reviewing the test data curve fitting, the values best fit a parabola of the following form: $F = -ax^2 + bx$, whereby the constant "c" is ignored as the function starts from zero.

Finding the constants *a* and *b* of a parabola. The derivation method is similar two finding the constants in the force displacement expression; *F = k x*, as found in a linear spring.

Let $F_1 = -ax_1^2 + bx_1$ and let $F_2 = -ax_2^2 + bx_2$.

Multiply the first equation by the ratio ε; which equals $\varepsilon = \frac{x_2}{x_1}$

Thus $\varepsilon F_1 = -a\varepsilon x_1^2 + b\varepsilon x_1$

Hence: $F_2 - \varepsilon F_1 = -ax_2^2 + bx_2$ - $[-a\varepsilon x_1^2 + b\varepsilon x_1]$

Substituting $\varepsilon = \frac{x_2}{x_1}$ and re-arranging this simplifies and becomes:

$$a = \frac{F_2 - \varepsilon F_1}{\varepsilon x_1^2 - x_2^2} \qquad \text{Eqn. 107}$$

And hence :

$$b = \frac{F_2 + a x_2^2}{x_2} \qquad \text{Eqn. 108}$$

where: $\varepsilon = \frac{x_2}{x_1}$

$F_2 > F_1$ Forces (N), two input forces.

$x_2 > x_1$ Displacements (mm); two input displacements.

X is the new displacement output (mm).

F is the new Force output (N).

Thus the parabola is equal to: $F = -aX^2 + bX$ Eqn. 109

To use Eqn.109, Eqn.108 & Eqn.109 require two inputted forces and associated displacements; this will enable the evaluation of the constants $a, \& b,$ from whence all other values of force vs displacement can be calculated for that particular bimetallic strip.

Equation 109 check; using the $R_c = 50mm$ curve;

From Fig.7-6, extracting approximate values of forces and associated displacements:

$$F_1 = 0.26N \ \& \ x_1 = 2mm$$

$$F_2 = 0.8N \ \& \ x_2 = 7mm$$

And thus: $\eta = \frac{7}{2} = 3.5$

Evaluating $a = \frac{0.8 - 3.5 * 0.26}{3.5 * 4 - 49}$ = 0.0031 and thus $b = \frac{0.8 + 0.0031 * 49}{7}$ = 0.1360

Hence for $X = 5mm$ inputted ; $F = -0.0031X^2 + 0.1360\ X = 0.6025N$

This can be checked against the $R_c = 50mm$ curve in Fig.7-6, which shows a good correlation between the derivation and the test curve data values.

7.8 Discussions and Conclusions

This work has investigated the special axial, or chord line loading case of a pre-curved bimetallic strip that serves as a bimetallic blade for the harvesting of renewable energy in the application of a thermal motor. From the literary review of patents and work by others in this field, the author could find no other study or references that relate to the special chord line axial case that this work covers. This work introduces new formulae specific to a pre-curved bimetallic strip that is mounted so that it produces forces and displacements along its chord line axis. An extensive set of tests on pre-curved bimetallic strip were conducted to provide test data for correlation of the theory to meet the objectives as defined in section 1.2. The new theoretical relationships and formulae that have been introduced by this study have been correlated to the test data, and thus the general objectives and aims of section 1.2 of this investigation have all been achieved.

As a by-product of this work, a new method of fabricating bimetallic strip has been invented and successfully implemented. The technique of using tabs and cut-outs to affect a local join in the two metals was successfully implemented. Moreover, in addition to joining two metal components, the method can also permanently join polymers to metals and other rigid non-metallic materials. The fabrication techniques employed in this work could also be adopted for development work or short production runs, where, as was shown in the review, there is a significant set up cost and lead time to procure bespoke manufactured bimetallic strip. The tabs and cut-outs method of fabricating bimetallic strip is therefore useful for producing a variety of fabricated bimetallic or bi-material test pieces for research or development purposes.

New relationships and formulae have been derived by this work that characterise the parameters of a pre-curved bimetallic strip subjected to heating and loading. New arc related geometries have been introduced that enable the evaluation of other arcs that have changed as a result of either chord line loading, or heating. The impact of the new set of arc related formulae and special relationships are also useful for other geometry related fields of study. This work establishes the links between the theoretical formulae of arcs and lines, to the properties of the metals that have been formed into the geometries shown.

As part of this study, new geometric relationships between overlapping arcs of circles and their relationships have been introduced. One new relationship enables the evaluation of the y and x ordinates for any arc as a function of an increasing sector angle, as y moves along the chord line. Additionally, a new formula for evaluating the chord line force as function of large displacements has been introduced. A new alternative Timoshenko approximation formula was also introduced by this study, plus a formula for evaluating the combined chord line heating and loading case. The straightening up from bend formulae has an application as a loaded bimetallic sensor, and thus the work introduced here can be used in the field of bimetallic sensors. Therefore in conclusion, the scope of the application of this body work has a much wider appeal and significance, because it introduces new geometric formulae for sensing applications, plus new chord line force displacement formulae that can be utilised in the application of linear thermal actuators, again widening the appeal and relevance of this study. Summarising, this study has introduced many new useful formulae and geometric relationships that can be recommended for any future study in the field of thermal motors, linear thermal actuators, and pre-curved bimetallic sensors.

7.9 Further Work

Further refinement of the temperature induced bending formula that is a function of time, could be developed. The current theory is limited to one dimensional heat flow. If a two-dimensional heat flow formulae was developed, this would improve on the accuracy of the current formula to predict the bend into a radius of curvature as a function of time. See chapter 3; section 3.12, Eqn.75. The assumption of the current theory is that the flow is steady state, this is not the case since the heating and cooling time varies constantly within a short period. Further work could investigate the transient effects and how it influences the accuracy of the time prediction. Future bimetallic strip research could investigate the performance of a hybrid shape memory alloy bimetallic structure. A shape memory alloy such as Nitinol was referred to in a patent by Sandoval (1977), who described Nickel-Titanium alloys as changing their shape upon a heat differential. The temperature induced shape changing properties of Nitinol could be used in a bimetallic strip. Nitinol which is a Nickel-Titanium alloy, rapidly changes shape via the mechanism of a material phase change, due to a temperature difference. Although the bimetallic strip changes shape by a different mechanism to Nitinol, a Nitinol-bimetallic strip may offer a more controlled rate of change in shape that could be tuned via the bimetallic constrained structure. The trigger to change shape could be sensed by the bimetallic aspect of the hybrid structure, and the activation of the shape due to the Nitinol phase change. This research is purely conjecture at this stage and may not offer any benefits and only drawbacks, but it would be interesting to see if such a structure could be made. For a quick evaluation of the proposed Nitinol-bimetallic strip structure, the fabrication method successfully introduced by the current study, could be used to produce the test samples. Research into the effects of different combinations of mating materials with Nitanol could be easily be explored via the fabrication process established by this work. A future bimetallic application of this study could look at a small scale development of the thermal motor which would be driven directly by the Sun's rays. The future work would use a small size motor in the range of 2 to 5 meters in diameter, to be setup and operated in a very hot region for the evaluation of the concept. Dependent upon the detail design, a small scale thermal motor of this size (5 meters) should be able to produce a few hundred watts of useful power, which may be sufficient to pump water up from a well. The future application of the thermal motor could also benefit from a possible Nitinol-bimetallic blade if that research yields positive results.

PUBLICATIONS RELATED TO THIS WORK

A Sustainable Energy Harvesting Machine
G.D. Angel, G. Haritos, I.S. Campbell
Proceedings of the World Congress on Engineering 2013 Vol III,
WCE 2013, July 3 - 5, 2013, London, U.K. *pp2103-2108*
ISBN: 978-988-19252-9-9
ISSN: 2078-0958 (Print); ISSN: 2078-0966 (Online)

Straightening Locus of a Curved Bimetallic Strip Subjected to Heating
G.D. Angel, G. Haritos, I.S. Campbell
Proceedings of the World Congress on Engineering 2013 Vol III,
WCE 2013, July 3 - 5, 2013, London, U.K. *pp2059-2064*
ISBN: 978-988-19252-9-9
ISSN: 2078-0958 (Print); ISSN: 2078-0966 (Online)

Spatial Prediction of a Pre-Curved Bimetallic Strip under Combined Loading.
G.D.Angel, G.Haritos, I.S.Campbell
Transactions on Engineering Technologies - Special Volume of the World Congress on Engineering 2013. ISBN: 978-94-017-8831-1 ; Chapter 17 ; 15 pages
Springer ITET. Accepted for publication March 2014.

Chord Line Force vs. Displacement for Thin Shallow Arc
Pre-Curved Bimetallic Strip
G.D. Angel, G. Haritos, A.Chrythanou, V.Voloshin.
Journal of Mechanical Engineering Science, Proceedings of the I. Mech.E , Part C:
Accepted for publication, March 2014.

An Immediate Formula for the Radius of Curvature of A Bimetallic Strip
G.D. Angel, G. Haritos.
Vol.2 - Issue 12 (December - 2013), International Journal of Engineering Research & Technology (IJERT), ISSN: 2278-0181, www.ijert.org, on line Journal.

REFERENCES

ABRAMOWITZ, M., STEGUN,I. (ed.) 1964. *Handbook of Mathematical Functions* Washington DC 20402 USA: US Government Printing Office.

AFTANDILYANTS, Y. 2007. Manufacturing technology of bimetallic castings by high durability. *Innovations Market for R&D* Hannover: Physico Technological Institute of Metals and Alloys of National Academy Science Ukraine Kiev, *pages 14.*

AISAKA, T., ET.AL. 1980. *Bimetal and method for manufacturing the same*. Japan patent application. USPO 4207381

ANGEL, G. 2013. *A Sustainable Energy Harvesting Machine*, London, IAENG.
Proceedings of the World Congress on Engineering 2013 Vol III,
WCE 2013, July 3 - 5, 2013, London, U.K. *pp2103-2108*
ISBN: 978-988-19252-9-9
ISSN: 2078-0958 (Print); ISSN: 2078-0966 (Online)

ASTM STANDARD B106-08 2008. "Standard Test Methods for Flexivity of Thermostat Metals". ASTM International: West Conshohocken, PA, 2008, DOI: 10.1520/B0106-08, www.astm.org.[Accessed Jan 2013]

ASTM STANDARD B388-06 2006. "Standard Specification for Thermostat Metal Sheet and Strip". ASTM International, West Conshohocken, PA, 2012, DOI: 10.1520/B0388-06R12 , www.astm.org. [Accessed Jan 2013]

ASTM STANDARD B753-07 2007. "Standard Specification for Thermostat Component Alloys". ASTM International, West Conshohocken, PA, 2012, DOI: 10.1520/B0753-07 , www.astm.org. [Accessed Jan 2013]

AVERY 2011. Calibration Certificate. *Weight -Tronix. 5962.* see in Appendix .

BAUCHAU, O. & CRAIG, J. 2009. Euler-Bernoulli beam theory. *Structural Analysis.* Springer.

BLUHM, J. 1946. The Metallurgical Examination of a Japanese Samurai Sword. Watertown Arsenal Labs MA. Department of the Army, United States Army Research Laboratory Aberdeen, ProvingGround, Maryland 210055066
Online www.dtic.mil/100.2/ADB962712 [Accessed June 2014]

BOESSENKOOL, H. W., ET.AL. 1954. *Solid phase bonding of metals*. USA patent application USPO 204346.

BOISSEAU.S. 2012. A bimetal and electret-based converter for thermal energy harvesting *Classical Physics***,** 3.

BROWN, P. 2012. *A layman's understanding of Damascus steel* [Online]. Available: http://www.thearma.org/essays/damascus-steel.html [Accessed Dec.2013]

BS EN 14597 2012. Temperature control devices and temperature limiters for heat generating systems. *temperature sensing control type ASW* BSI Standards Limited 2012.

BS ISO 24213 2008. Metallic materials. Sheet and strip. Method for springback evaluation in stretch bending. *BSI.* UK: BSI.

CHEN, J. L., YANG, J. C., SUN, B. J. & PAN, Y. 2009. Manufacture technique of bronze-iron bimetallic objects found in M27 of Liangdaicun Site, Hancheng, Shaanxi. *Science in China Series E: Technological Sciences,* 52**,** 3038-3045.

CHURCHILL, W. H. et.al 1968. *Heat Motor*. USA patent application.USPO 3404530

CLARK, R. O. 1973. *Thermal Motor and Generator*. USA patent application.USPO US7952239B2

COLE, S. W. 1965. *Thermal Motor for Rotating a Rotisserie Shaft*. USA patent application. USPO 3184914

CREATIVE WATER JET 2012. Water jet cutting cervice. Online http://www.creativewaterjet.co.uk [Accessed Jan 2013].

DALHLBERG.T 2004. Procedure to calculate deflections of curved beams. *Int. J. Eng Ed*.

DASSAULT , S. 2014. Catia V5 R19 CAD Software. *Part Modeller, Sketcher Enviroment.* Dassalt Systemes PLM, www.intrinsys.com [Accessed Jan 2013]

DAVIES, A. 1982. *Mathematical Handbook,* Hatfield Polytechnic, College Lane, Hatfield, Mathematics Group, Hatfield Polytechnic, .

DAVISTOWN, M. 2013. *Glossary of Ferrous metallurgy Terms* [Online]. Available: http://www.davistownmuseum.org/PDFs/GlossaryOfFerrousMetallurgyTerms.pdf [Accessed Jan 2013].

DAYTON, C. S. 1951. *Thermal Motor*. USPO 2539185

DIN 1715-1 1983-01. "Thermostat metals: technical delivery conditions". DIN Deutsches Institut für Normung e. V. Am DIN-Plazt, Burggrafenstabe 6, 10787 Berlin, Germany ,http://www.fnne.din.de/. [Accessed Jan 2013]

DIN 1715-2 1984-01. "Testing the specific thermal curvature". DIN Deutsches Institut für Normung e. V. Am DIN-Plazt, Burggrafenstabe 6, 10787 Berlin,Germany ,http://www.fnne.din.de/. [Accessed Jan 2013]

DMC. 2013. *DetaCLAD® explosion welding process* [Online]. Available: http://dynamicmaterials.com/innovations-technology/explosion-welding-process.html. [Accessed Jan 2013]

DOSSETT, J. L., BOYER,H.E., 2006. *Practical Heat Treating,* Materials Park, OH, 44073-0002.,USA, ASM international.

DURST.G. 1955. *Method and apparatus for cleaning metal strips*. USA patent application. USPO 2713011

EGELHOFF, C. J. 2010 *Application of modern engineering tools in the analysis of the stepped shaft* , 2010 IEEE Frontiers in Education Conference,ISBN 1-4244-6261-4, 978-1-4244-6261-2, DOI 10.1109/FIE.2010.5673504

ENGINEERINGTOOLBOX. 2014. *Metals-Melting Temperatures* [Online]. Available: www.engineeringtoolbox.com [Accessed 2014].

FRAISSE, A. 1998. *Bimetallic Thermal Triggering Apparatus for a Protection Device*. USA patent application USPO 908523.

FREUDENBERGER,J.et.al, 2009. *Materials Science and Engineering*. Springer Handbook of Mechanical Engineering, ISBN 978-3-540-49131-6

GOULDING, J. M. 1947. *Manufacture of Bimetal*. USA patent application USPO 453494.

HAGA, T. 2009. Clad strip casting by a twin roll caster. *World Academy of Materials and Manufacturing Engineering,* 37**,** pages 117-124.

HEIN, L. A. E. A. 1976. *Mechanical Thermal Motor*. USA patent application.USPO 3987630

HIBBELER, R., C, 2006. *Structural Analysis,* Singapore, Pearson Prentice Hall.

HOKE, D. 1989. Product Design and Cost Considerations: Clock, Watch, and Typewriter Manufacturing in the 19th century. *Business and Ecomonic History.* pages 119-128.

HOLBROOK, M. 1992. Bimetallic-Strip Thermometer. *In:* COLLECTIONS, H. M. A. G. (ed.). Glasgow: Universtity of Glasgow. Online http://www.huntsearch.gla.ac.uk/cgi-bin/foxweb/huntsearch/DetailedResults.fwx?collection=all&searchTerm=105657&mdaCode=GLAHM,[Accessed Jan 2013].

HOWARD, E. R. 1942. Thermostatic Bimetal *Engineering and Science,* 5**,** pages 16 -24.

JOHNSON, W. S. 1883. *Electric Tele-Thermoscope*. USA patent application.USPO 281884

KANTHAL, A. B. 2002. *The Kanthal Thermostatic Bimetal Handbook,* Box 502, SE-734 27 Hallstahammar, Sweden, PRIMAtryck,Hallstahammar, Catalogue 3-A-1-3.4.pages 130 Online www.kanthal.com [Accessed Jan 2013]

KEYSER, P. 1992. A new look at Heron's "Steam Engine". *Archive for History of Exact Sciences,* 44**,** pages 107-124.

KINYANJUI, T. W. 2007. *Finite element methods for geometrically linear curved beams.* Masters, TECHNISCHE UNIVERSIT¨AT KAISERLSLAUTERN.pages 79.

KOPELLOVICH,D. 2012. Engine Bearing Materials. Available: http://www.kingbearings.com/. King Engine Bearings, Inc, Online [Accessed Jan 2013]

KRULEVITCH P, J. G. C. 1998. Curvature of a Cantilever Beam Subjected to an Equi-Biaxial Bending Moment. *Materials Research Society Conference.*

LOW, G. M. et. al. 1972. *Solar Energy Powered Heliotrope*. USA patent application. USPO 3663839

MARTINI, W.R.1978. Stirling engine design manual. Washington Univ., Richland (USA). Joint Center for Graduate Study.

MATTHEWS, C. 2005. *Engineers Data Book,* Trowbridge Wilts. UK, Wiley.

MATWEB. 2013. *Online Materials Information Resource* [Online]. WWW. Available: http://www.matweb.com/ [Accessed Nov 2013].

MCLAREN,C.A.B. The search for the holy grail, John Harrlson and the bimetallic strip BARR, A. M., ed. *The history of anaesthesia society proceedings,* 1994 Guernsey. 34 -36. Onine ; http://www.histansoc.org.uk/uploads/9/5/5/2/9552670/volume_15.pdf [Accessed Jan 2013]

MORRISON, W. H. E. A. 1963. *Method for making a bimetallic strip for bearings*. USA patent application. USPO 3093885

MUNDAY, A., J, FARRAR,R,A 1982. *An Engineering Data Book,* London and Basingstoke, The MACMILLAN PRESS LTD.

NASA. 2012. *What is the temperature in space* [Online]. USA: NASA. Available: http://www.nasa.gov/audience/foreducators/topnav/materials/listbytype/What_Is_the_Temperature.html. [Accesssed Jan 2012]

O'HARE, L. R. 1985. *Bimetallic Solar Engine.* USPO 404449.

PETROSKI, H. 1996. Harnessing steam. *American Scientist,* 84**,** 15-19.

POLONI, A., et.al. 2006. *Device and method for the continous casting of a bimetallic strip through a twin roll casting machine*. Eur patent application. EP 1 506 825 B1

PRASAD, K. 1993. Principle and Properties of Thermoststat. *Journal of Materials*.

RIABZEV, R. 2002. *Sterling Cycle Machine* [Online]. RICOR Cryogenic & Vacuum Systems. Available: http://www.scribd.com/doc/92938510/58 Stir-pt [Accessed Dec. 2012].

SANDOVAL, D. J. 1977. *Thermal Motor*. USA patent application.USPO 4010612

SHERBY, O. D. & WADSWORTH, J. 2001. Ancient blacksmiths, the Iron Age, Damascus steels, and modern metallurgy. *Journal of Materials Processing Technology,* 117**,** 347-353.

SHIRZADI, A. A., et.al 2004. Diffusion Bonding *Science and Technology of Welding and Joining,* 9.

SHIVALIK.2013. *Shivalik Bimetal Controls, Ltd.,* [Online]. Available http://www.shivalikbimetals.com [Accessed Jan 2013]

SLONNEGER, J. L. E. A. 1970. *Thermal Motor*. USA patent application.USPO 3495101

SOBEL, D. 1995. *Longitude: The True Story of a Lone Genius Who Solved the Greatest Scientific Problem of His Time,* London, Walker. ISBN 978-0-8027-1529-6; 0-8027-1344-0

SOLAR THERMAL. 2008. *Solar Thermal Energy, an Industry Report* [Online]. Available: http://www.solar-thermal.com/ [Accessed Jan 2013].

TIMOSHENKO, S. 1925. Analysis of Bi-metal Thermostats. *JOSA,* 11**,** 233-255.

TIMOSHENKO, S. P. 1945. Theory of bending, torsion and buckling of thin-walled members of open cross section. *Journal of the Franklin Institute,* 239**,** 249-268.

TOX, P.2013. *TOX PRESSOTECHNIK,* [Online]. Available: http://www.tox-de.com/de/kontakt.html [Accessed Jan 2013].

UHLIG,W, et. al. 2007. *Thermostatic Metal, Manufacture and Application,* Hammerplatz 1, D-08280,Aue/Sachsen, Auerhammer Metallwerk, GMBH. www.auerhammer.com [Accessed Jan 2013] books.google.co.uk/ pages 200

WEISSTEIN, E.W. 2014. Polynomial Discriminant. From MathWorld-A Wolfram Web Resource. http://mathworld.wolfram.com/PolynomialDiscriminant.html [Accessed Jan 2014]

WHITNEY, L. A., et. al. 1945. *Thermal motor*. USA patent application.USPO 2382928

WRIGHT, D. 2013. *MISCELLANEOUS STRENGTH TOPICS - Castigliano's theorem and the deflection of thin curved beams* [Online]. WWW: Edinburgh Engineering Virtual Libruary. [Accessed Nov 2013].

YOUNG, D. H., BANKER J.G. 2004. Explosion Welded, Bi-Metallic Solutions to Dissimilar Metal Joining. *Texas Section of the Society of Naval Architects and Marine Engineers* Houston, Texas Section of the Society of Naval Architects and Marine Engineers

APPENDICES

LIST OF TECHNICAL DRAWINGS

LIST OF FIGURES

Appendix A: Thermal motor technical drawings

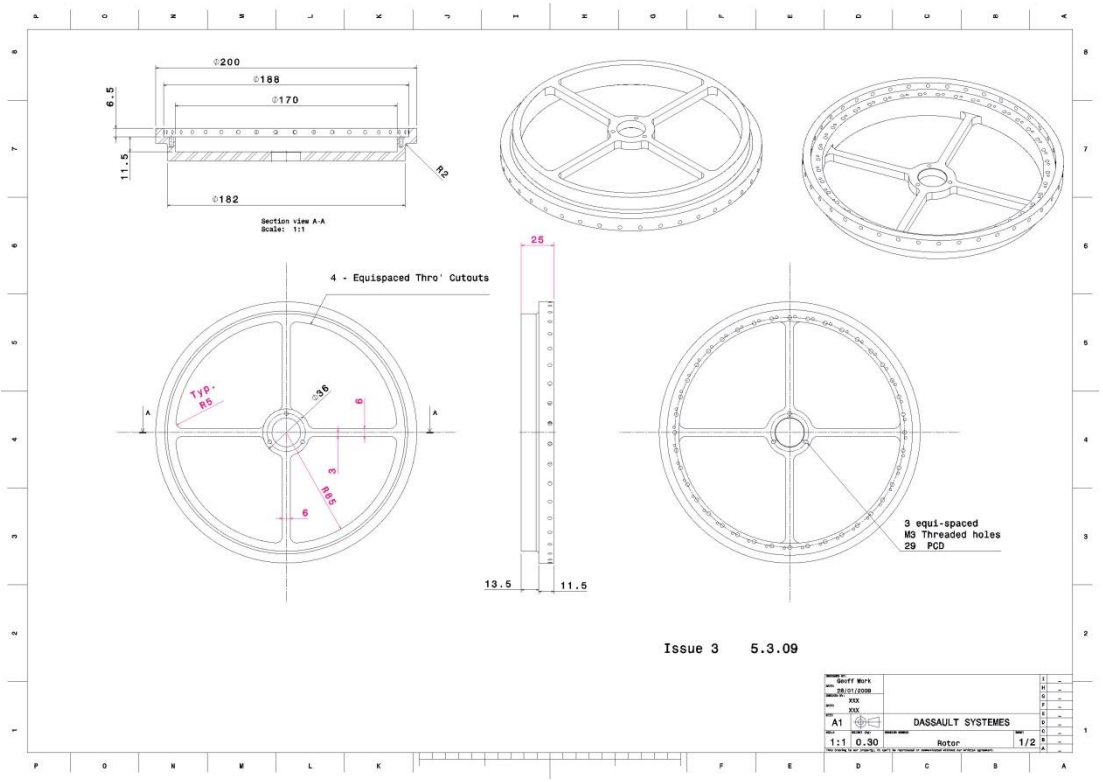

Figure 1A– Rotor Rim: Mark I Thermal Motor

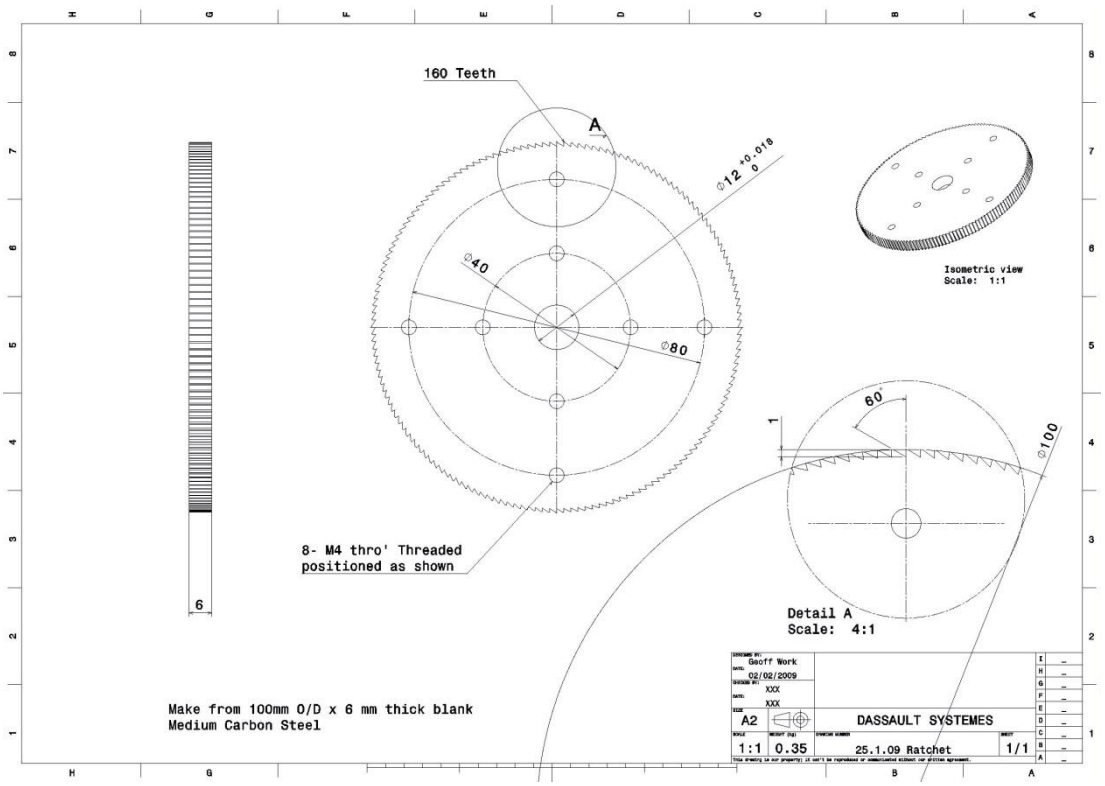

Figure 2A – Fixed Ratchet: Mark I Thermal Motor

Appendix A: Thermal motor technical drawings

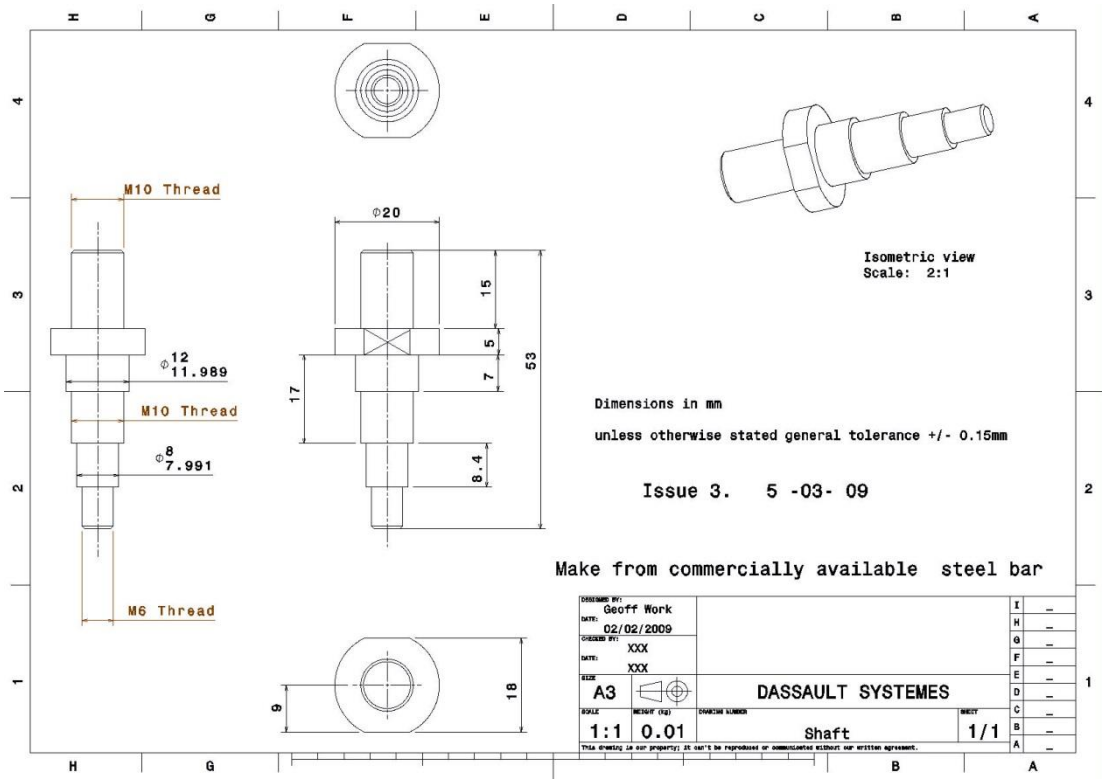

Figure 3A – Shaft: Mark I Thermal Motor

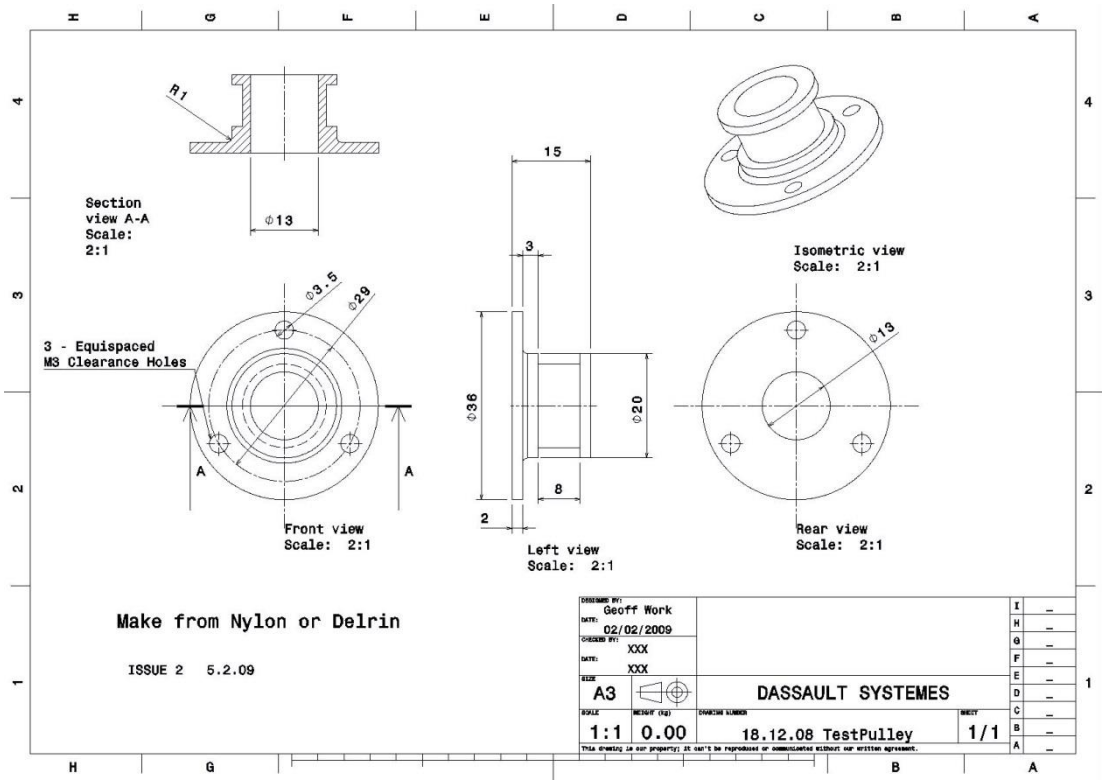

Figure 4A – Test Pulley: Mark I Thermal Motor

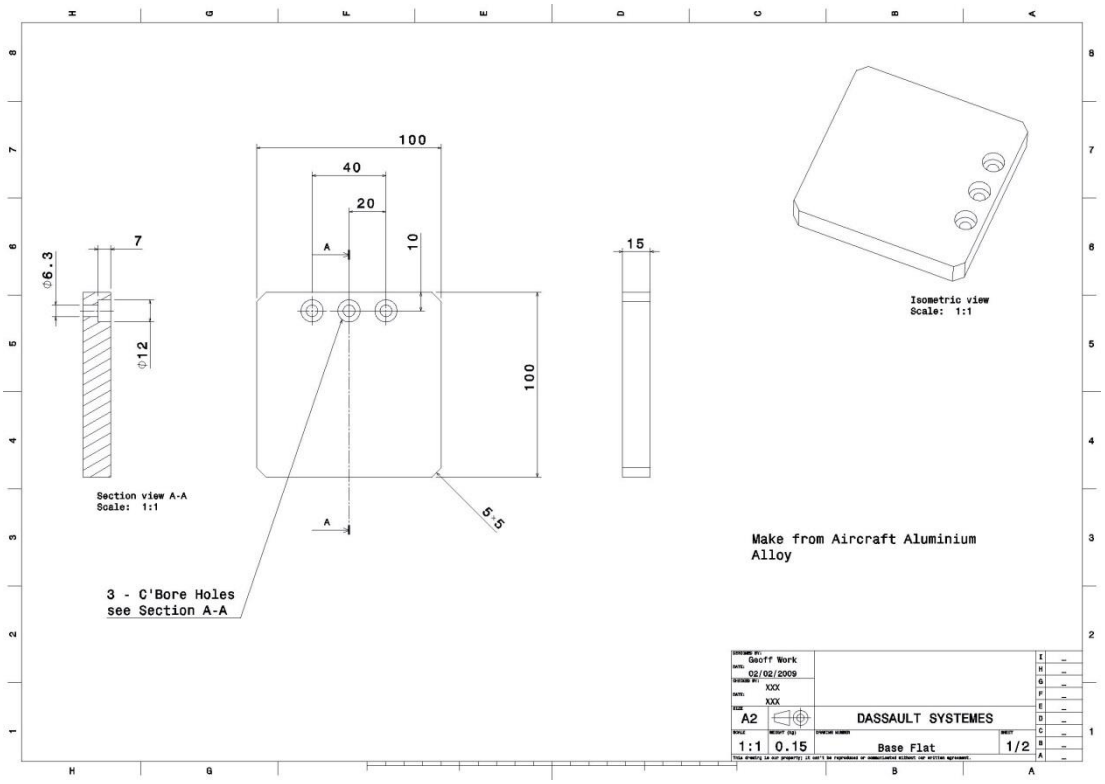

Figure 5A – Base Flat: Mark I Thermal Motor

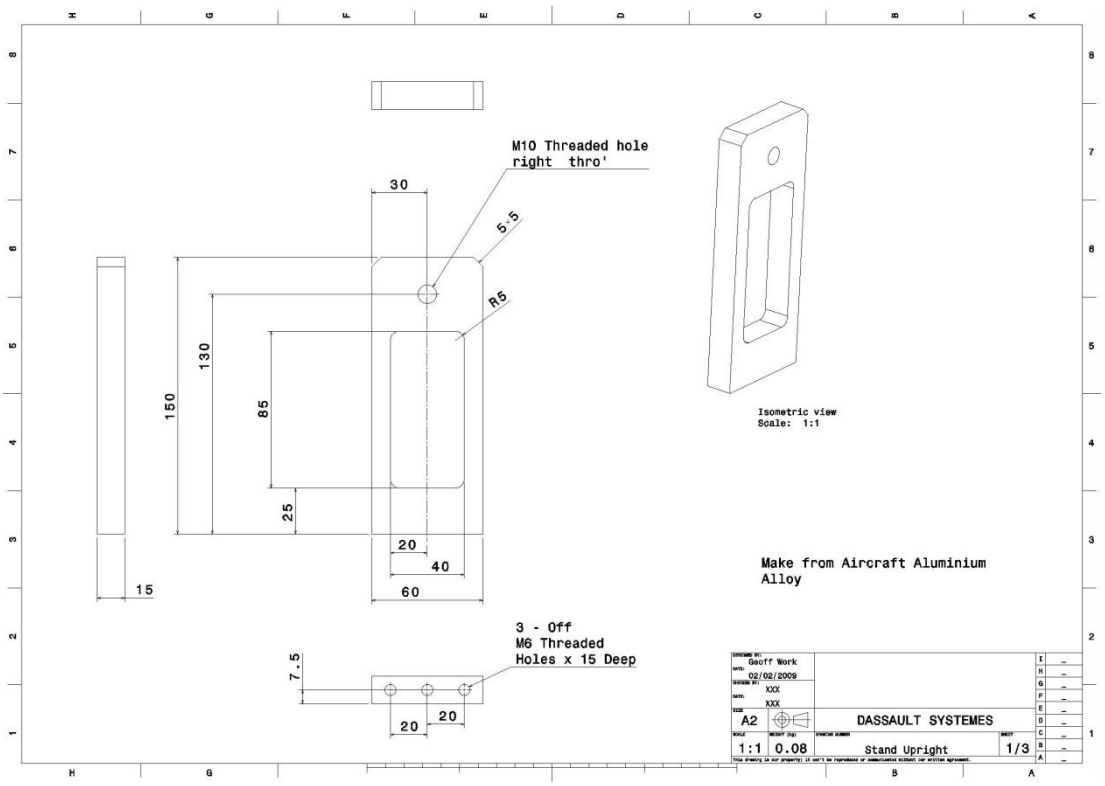

Figure 6A – Stand Upright: Mark I Thermal Motor

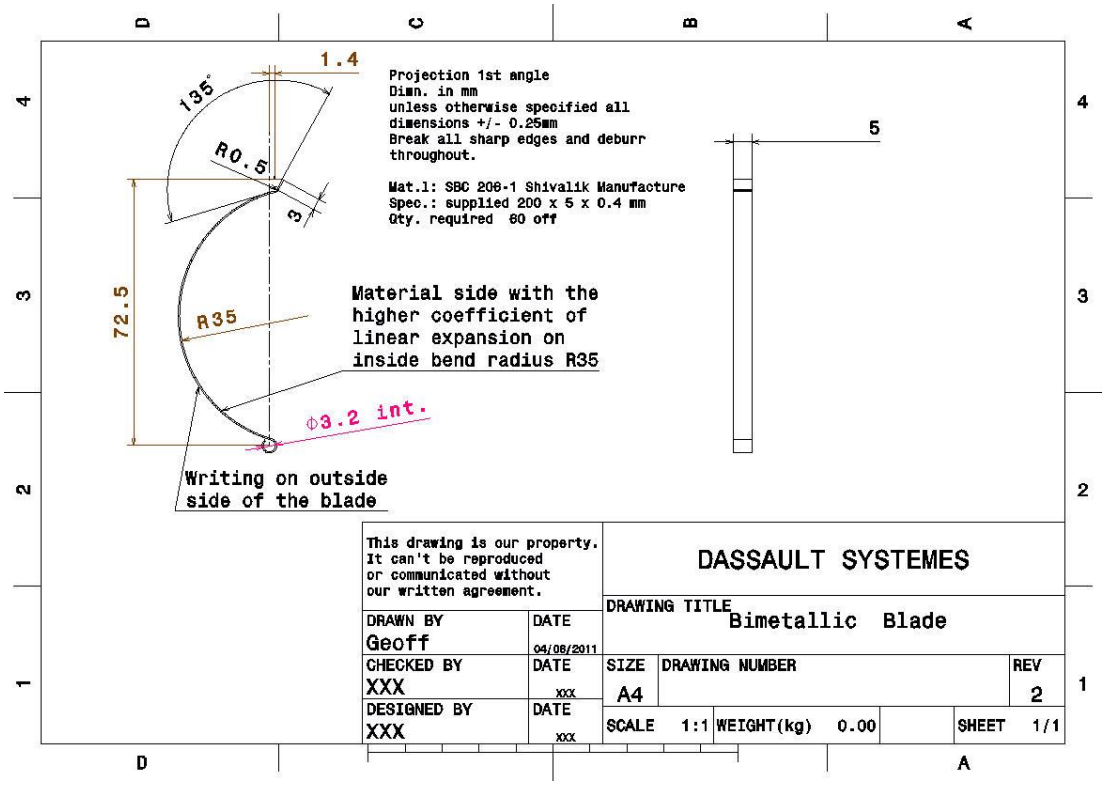

Figure 7A – Bimetallic Blade: Mark I & Mark II Thermal Motor

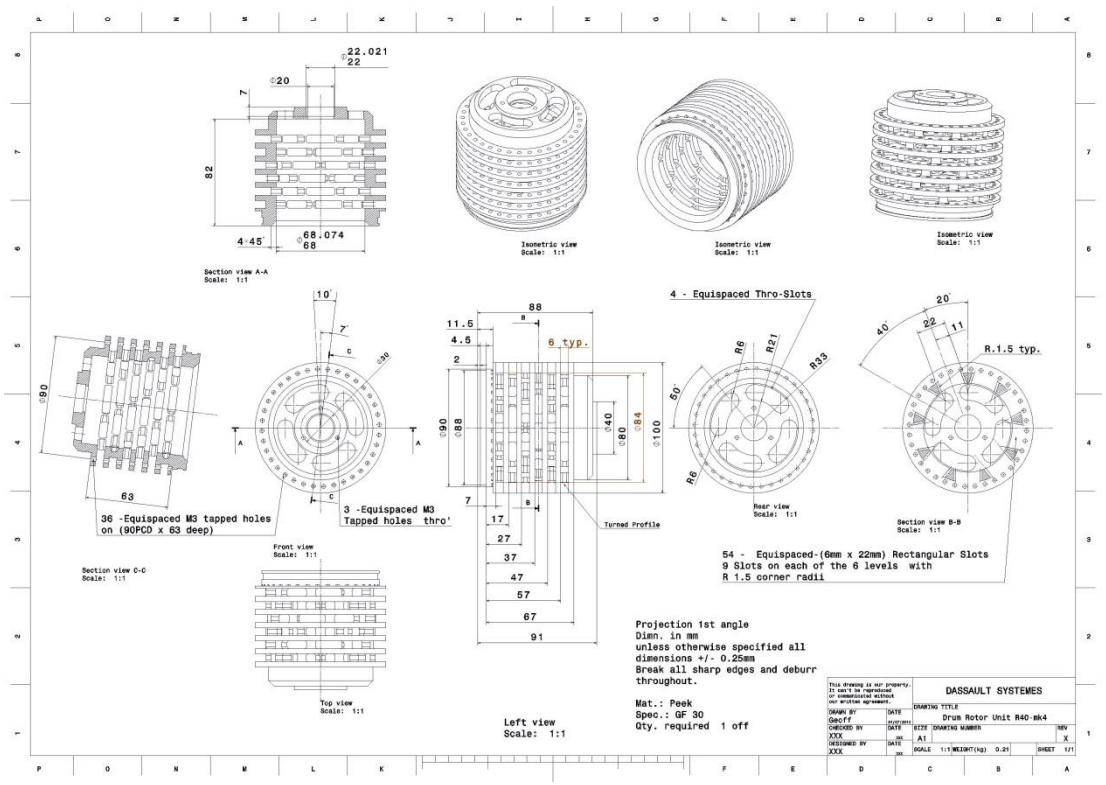

Figure 8A –Drum Rotor Unit: Mark II Thermal Motor

Appendix A: Thermal motor technical drawings

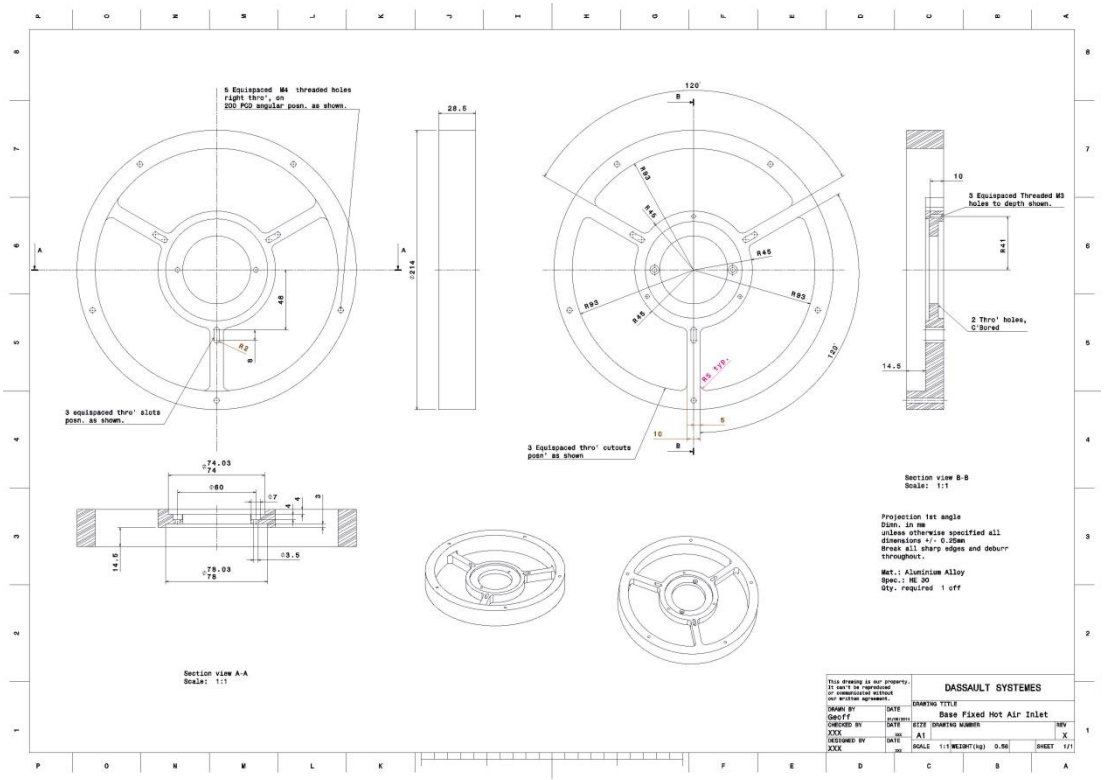

Figure 9A –Base Fixed Hot Air Inlet: Mark II Thermal Motor

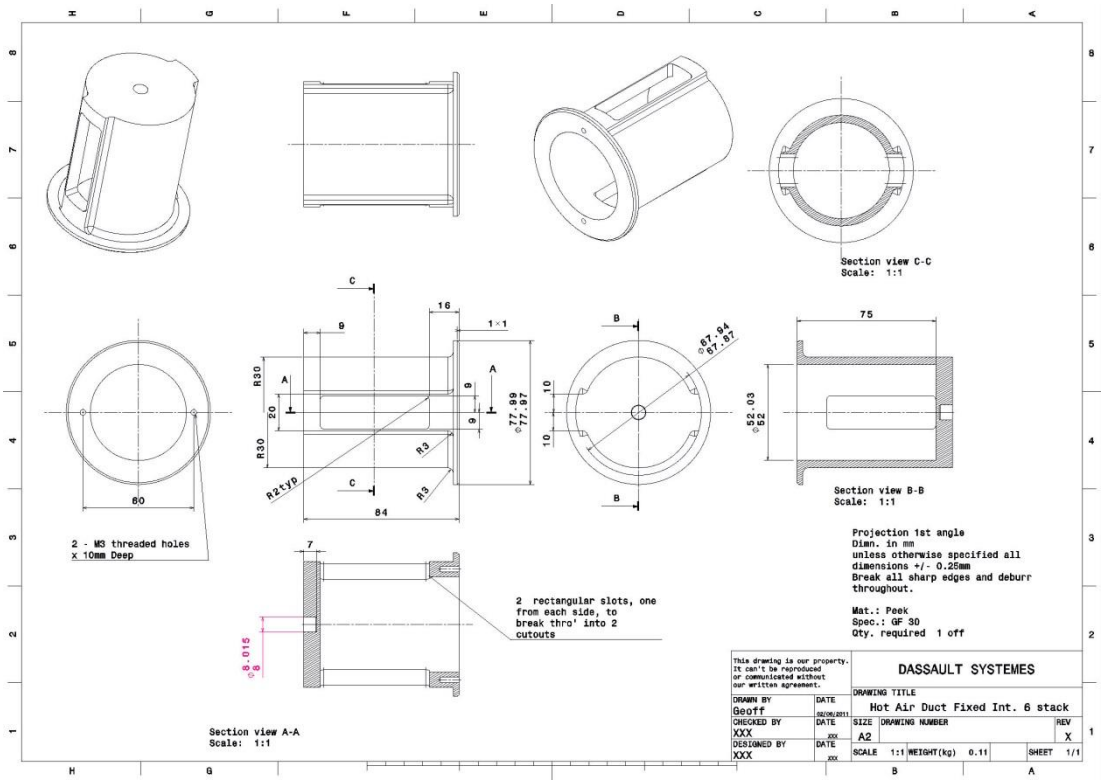

Figure 10A –Hot Air Duct Fixed: Mark II Thermal Motor

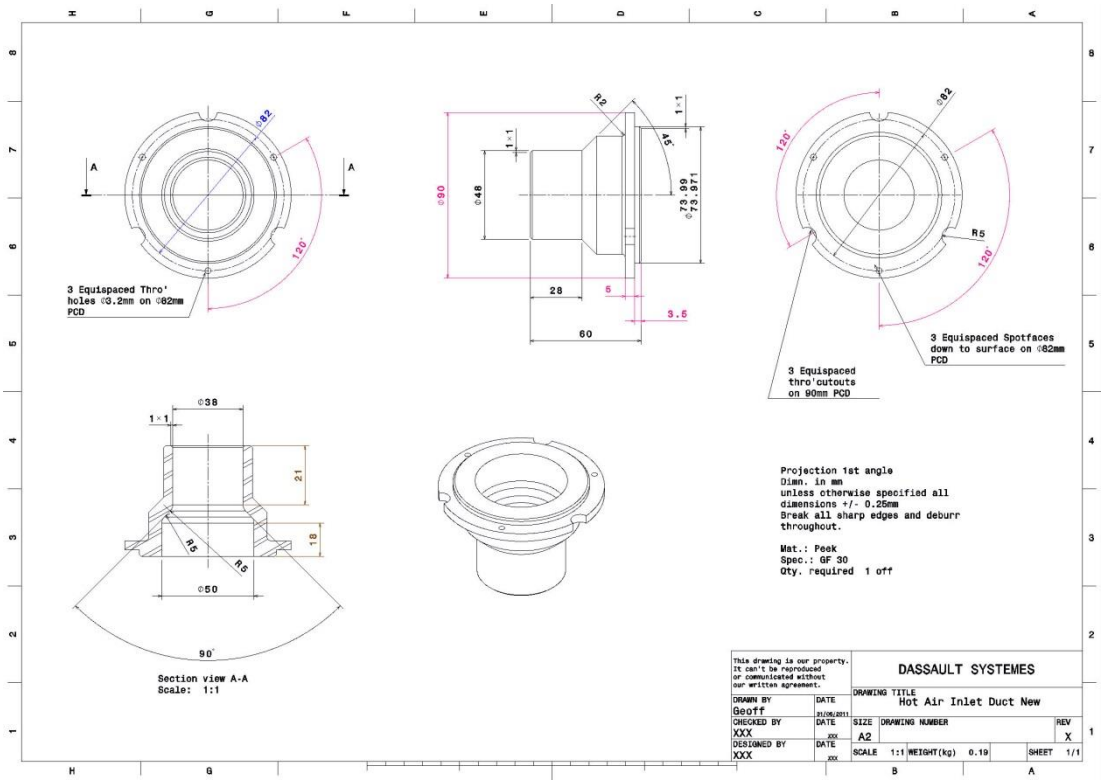

Figure 11A –Hot Air Inlet Duct: Mark II Thermal Motor

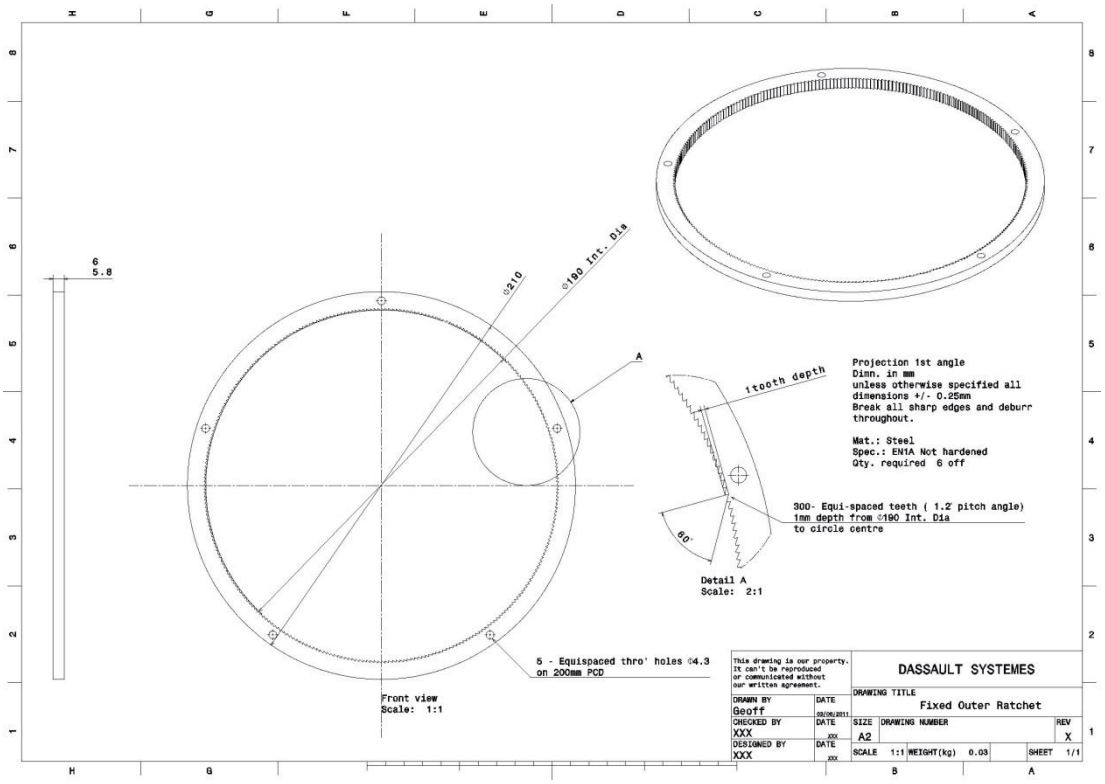

Figure 12A –Fixed Outer Ratchet: Mark II Thermal Motor

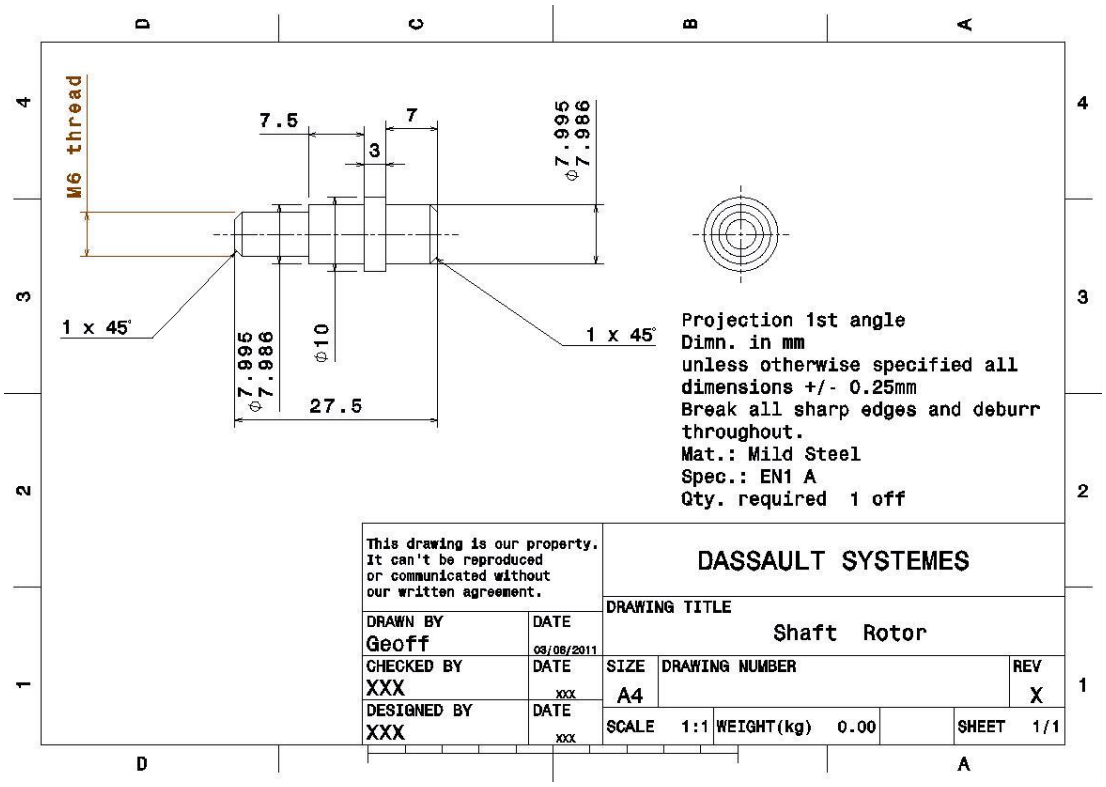

Figure 13A –Shaft Rotor: Mark II Thermal Motor

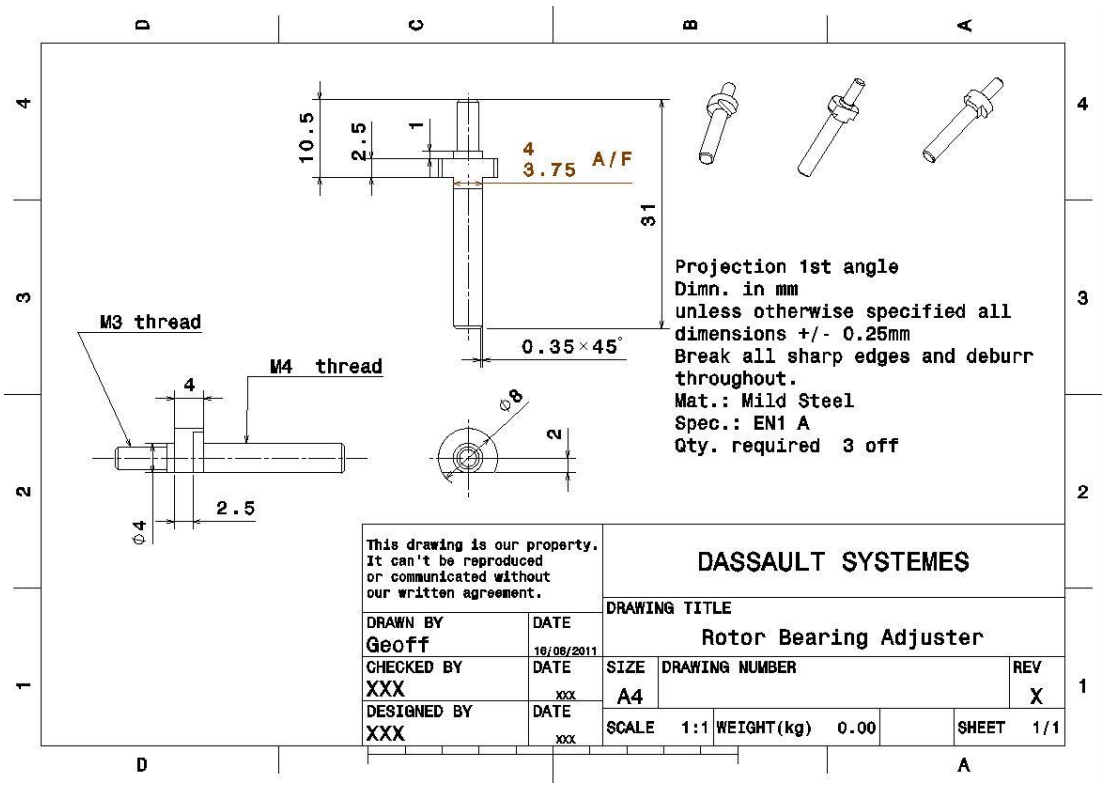

Figure 14A –Rotor Bearing Adjuster: Mark II Thermal Motor

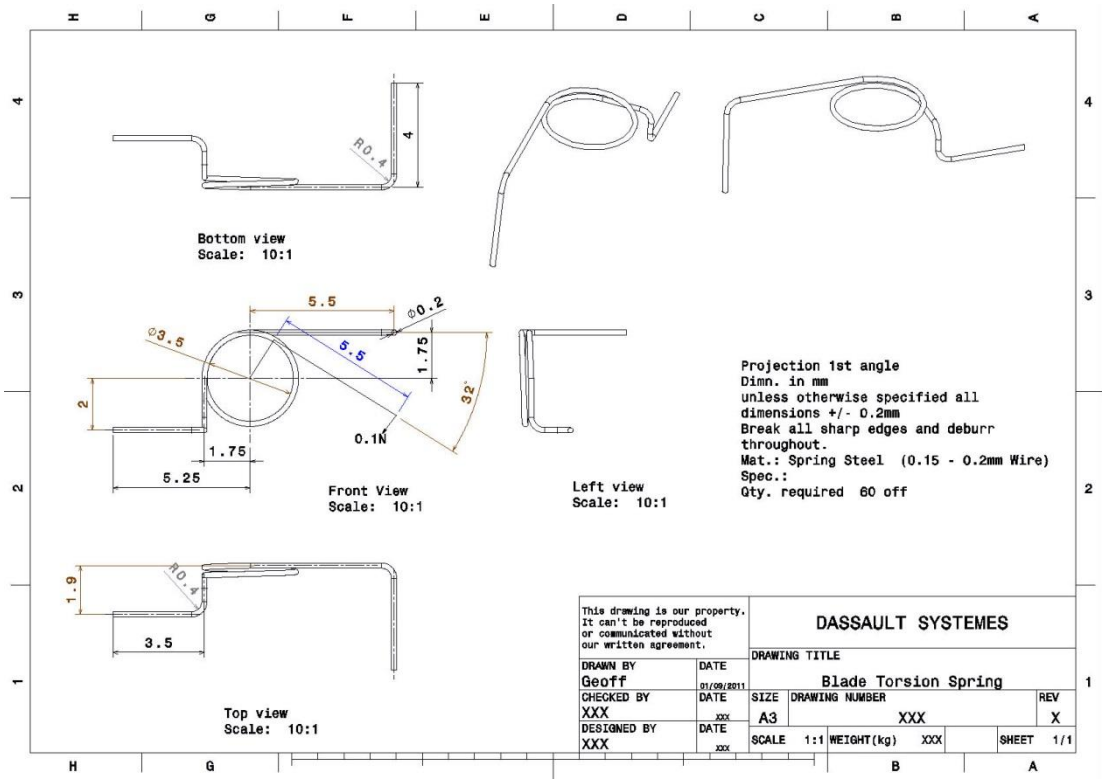

Figure 15A –Blade Torsion Spring: Mark II Thermal Motor

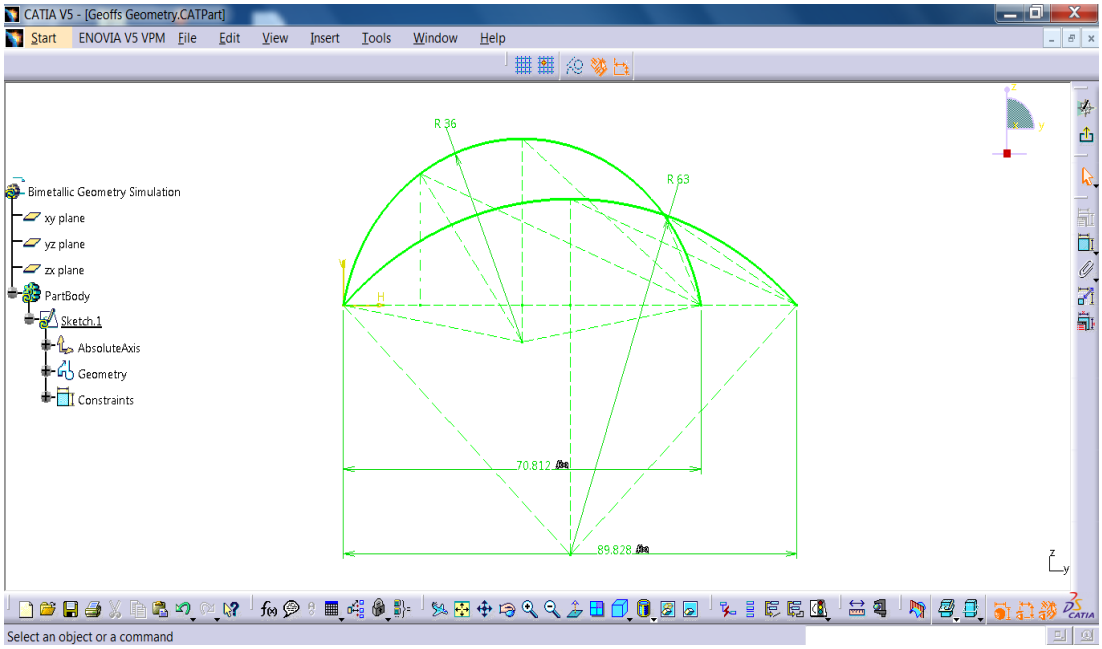

Figure 16A – Catia Sketcher – Bimetallic Strip Geometry- at Ambient Temperature

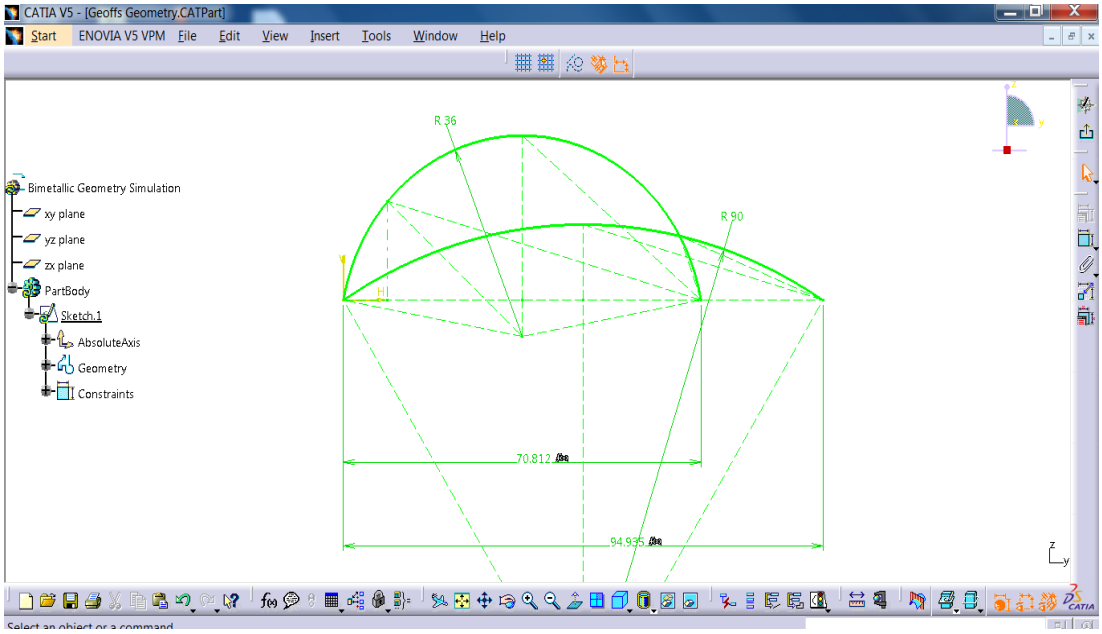

Figure 17A – Catia Sketcher – Bimetallic Strip Geometry – Hot Displaced

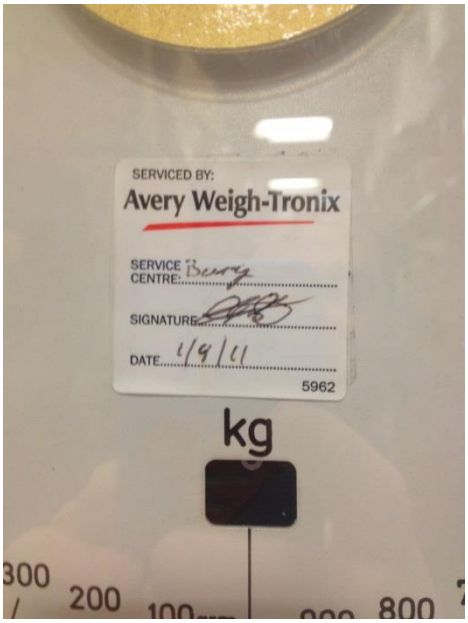

Figure 18A – Calibration Certificate. *Weight -Tronix. 5962.* Avery (2011)